NASA CR-145120

CORRELATION OF AH-1G HELICOPTER FLIGHT VIBRATION DATA AND TAILBOOM STATIC TEST DATA WITH NASTRAN RESULTS

By

James D. Cronkhite, Henry E. Wilson

and Victor L. Berry

Prepared under Contract NAS1-13801

By

Bell Helicopter Textron

Fort Worth, Texas

for

National Aeronautics and
Space Administration

CONTENTS

CONTENTS (Continued)

ILLUSTRATIONS

TABLES

CORRELATION OF AH-1G FLIGHT VIBRATION DATA AND TAILBOOM STATIC TEST DATA WITH NASTRAN ANALYTICAL RESULTS*

By James D. Cronkhite, Henry E. Wilson, and Victor L. Berry

Bell Helicopter Textron

1. SUMMARY

This report includes the results of two studies to correlate a NASTRAN analysis of the AH-1G helicopter airframe structure. The first study is the comparative evaluation of the analysis for calculating level flight airframe vibration at main rotor excitation frequencies. The second is the comparison of a NASTRAN tailboom analysis with test data for evaluation of methods used to determine effective skin in a semimonocoque sheet-stringer structure. These studies are a continuation of two earlier programs in which a NASTRAN airframe model was developed and then compared to static stiffness and vibration tests (References 1 and 2).

The flight vibration correlation involved comparison of level flight vibration for two helicopter configurations: clean wing, at light gross weight and wing stores at heavy gross weight. Vibration response was compared at main rotor two-, four- and six-per-rev frequencies for airspeeds of 60 to 140 knots. There was good agreement of the vertical vibration at two-per-rev, the predominant excitation frequency of the Bell two-bladed rotor. Four- and six-per-rev correlations were fair.

Measured main rotor hub accelerations and control loads were used to excite the NASTRAN model. Some problems that were encountered in the method of applying hub accelerations as excitation are discussed. In particular, the vertical (axial) stiffness modeling of the main rotor pylon in the NASTRAN analysis was found to be very critical.

In the tailboom correlation, deflections and internal loads were compared using static test data and a NASTRAN analysis. An iterative procedure was used to determine the amount of effective skin of buckled panels under compression load. In general, comparison of internal loads and deflections from analysis agreed well with test, the analysis being slightly stiffer. Stresses did not compare as well and were strongly dependent on the appropriate cross sectional area that was used in the analysis.

*The contract research effort which has lead to the results in this report was financially supported by USAAMRDL (Langley Directorate).

2. INTRODUCTION

A NASTRAN model of the AH-1G helicopter airframe was developed under Army Contract DAAF03-73-C-0122. The model was to be suitable for representing the low frequency vibration characteristics of the airframe with complete documentation so that government personnel could independently make changes to the model and use it for in-house analyses. The resulting model is documented in Reference 1 and is shown in Figure 1. Briefly, the fuselage and wing structures are built-up idealizations using primarily rods and shear panels in the bending sections. The tailboom is idealized as an elastic line using bar elements. The main rotor pylon is modeled as an elastic line using bar elements with scalar springs at the elastomeric mount attachments to the fuselage. The number of degrees of freedom in the model was reduced to about 250 by the Guyan reduction to produce an acceptable analysis size for the Givens eigenvalue solution.

Following development of the NASTRAN model, static testing of the AH-1G fuselage, wings, tailboom and vertical fin was done to verify the stiffness modeling that was used. Shake testing was also done in order to verify the vibration response characteristics (including both stiffness and mass effects). The results of the comparison of the analysis with the static and vibration tests is presented in Reference 2. In general, the agreement between the vibration analysis and test was good through main rotor four-per-rev (21.6 Hz). However, there were significant differences in pylon rocking natural frequencies and damping that could be important in the flight vibration correlation where main rotor excitation is used.

This study involves correlation of the AH-1G NASTRAN model with in-flight vibration test data collected under an AH-1G operational load survey (Eustis Contract DAAJ02-73-C-0105). In-flight vibration at main rotor, two-, four-, and six-per-rev excitation frequencies is compared to the NASTRAN analysis. Hub accelerations and control loads are used to excite the model.

In addition to flight vibration correlation, deflection and internal load data from static tailboom tests are compared with a NASTRAN analysis. The purpose of the tailboom test correlation study is to better quantify the effects of buckled skin under compression loading on the stiffness and internal loads of the semimonocoque tailboom structure. Rather than use the elastic line model of the tailboom, a built-up NASTRAN tailboom model was developed for the analysis. This was

considered necessary so that the many load paths that were instrumented in test were represented in the model for direct comparison.

In the previous tailboom static test comparison, the NASTRAN elastic line model agreed well with measured deflections. The tailboom stiffness properties for the elastic line model were calculated by considering the skins as fully effective. This is not totally accurate since the tailboom is of semi-monocoque sheet-stringer design. This type of design compensates for skin buckling and the corresponding reduced element areas at stress levels near the limit design stress. Since this analysis is based on stress levels resulting at 1g level flight conditions rather than 3.5g limit conditions, consideration of the skins as being fully effective is believed accurate. However, better procedures for determining the effective skin should be developed to determine the stiffness of sheet metal panels under various loadings for use in dynamic analysis. This study is a step in that direction since current methods are evaluated by comparison with test.

3. FLIGHT VIBRATION CORRELATION

3.1 FLIGHT VIBRATION TESTS

The flight test data used for correlation of the NASTRAN analysis was taken under the AH-1G operational load survey, Eustis Contract DAAJ02-73-C-0105. Details of that program are given in Reference 3. The helicopter used in the tests is shown in Figure 2.

Level flight vibration data were selected for two configurations: clean wing at aft cg and wing stores at mid cg. The clean wing configuration used was Flight 35A which was 3768 kg (8300 lb) gross weight at aft cg. After selecting Flight 35A, there was found to be a problem in obtaining airframe vibration data for that configuration. Data from Flight 34B (comparable to Flight 43 in Reference 3) was then used. Flight 34B is a clean wing configuration at mid cg and is considered comparable to Flight 35A. The wing store configuration that was selected was Flight 36A which was 4086 kg (9000 lb) gross weight at mid cg. Wing stores used in Flight 36A are shown in Figure 3.

Level flight vibration data were taken at six airspeeds for each configuration. The airspeeds flown were the following:

Configuration	Airspeed (knots)					
	1	2	3	4	5	6
35A Clean wing at aft cg	67	85	101	114	128	142
36A Wing stores at mid cg	61	76	95	108	120	134

Measured hub accelerations and boost cylinder control loads were used as excitation in the NASTRAN analysis. Locations of the hub accelerations and boost cylinder control loads that were instrumented in test are shown in Figure 4. Two-, four-, and six-per-rev hub accelerations and corresponding boost cylinder control loads are tabulated in Appendix A.

Airframe accelerations were recorded and harmonically analyzed for comparison with the NASTRAN analysis. Airframe locations of accelerometers used in the flight tests are shown in Figure 5. Main rotor two-, four-, and six-per-rev harmonics of the acceleration data are presented in Appendix B as plots of magnitude versus fuselage station. The mode shape data that are shown is phase related to the maximum nose responses.

3.2 NASTRAN ANALYSIS

A discussion of the NASTRAN analysis that was used for comparison with flight vibration test data is included in this section. In addition to the forced response analysis, a discussion of two problem areas that were studied is also included. The problem areas were, first, the effect of pylon vertical stiffness on vibration response when using enforced hub accelerations and, second, the effects of pendulum stiffening, elastomeric mount stiffness and pylon mode damping on the isolation of moments into the fuselage.

3.2.1 Forced Response Analysis

The NASTRAN airframe model shown in Figure 1 was used in the forced response analysis. The model useful weights were changed to correspond to the two configurations that were flown. The wing stores for the Flight 36A condition were modeled as rigid bodies with rigid (stiff bar) attachments to the wings. The useful weights for the two configurations are listed in Tables I, II, and III. The airframe natural frequencies are given in Table IV.

Measured hub accelerations and boost cylinder control loads were used to excite the NASTRAN model. The measured data is tabulated in Appendix A. Hub accelerations were applied to

the NASTRAN model using a big hub mass of .454 x 10^7 kg (10^7 lb). The big hub mass was excited with the force required to give the mass the measured 'g' acceleration. For example, a force of 4.448 x 10^7 N (10^7 lb) is required to produce a 1g acceleration of the .454 x 10^7 kg (10^7 lb) hub mass. The size of the mass is arbitrary but must be large enough so that it is not influenced by the airframe response, i.e., the response to the applied input force is the only significant response of the big hub mass.

The boost cylinder control loads were applied to the NASTRAN model at the locations shown in Figure 4. The boost cylinder support beams were modeled using bar elements. The support beams distribute the control loads to the airframe and should not affect the local structural stiffness.

The two-, four-, and six-per-rev responses were computed using the NASTRAN rigid format 8, Direct Frequency Response analysis in NASTRAN. Two percent damping was used. This was input by setting PARAM G equal to .04. The G parameter is considered as two times the percent critical damping at the natural frequency. The analytical results are compared to measured data in Appendix B. The results of the comparison of analysis and test are discussed in Section 3.3.

3.2.2 Effect of Pylon Vertical Stiffness for Applied Hub Accelerations

The vertical hub accelerations were found to be much smaller than the horizontal hub accelerations, about a factor of 40 to 50 at high airspeeds. This is illustrated in the plot of two-per-rev hub accelerations in Figure 6. The difference in hub component accelerations is caused by the stiff vertical load path into the airframe through the mast transmission case and lift link. The pylon rocking motions are reacted by soft elastomeric mounts resulting in the hub being much softer horizontally than vertically. A sketch of the pylon mounting is shown in Figure 7.

When applying the hub accelerations using a big hub mass as described in the preceding section, the hub is essentially pinned to ground. The resulting loads that can develop in the pylon due to response of the airframe are not controlled and could become very large, especially in the vertical direction. The vertical hub response shown in Figure 6 is on the order of .04g to .05g, or about .0001 m (.004 in) deflection at two-per-rev (10.8 Hz). Horizontal deflections are on the order of .005 m (.20 in). A difference of a few ten thousandths of a meter deflection in the vertical direction would have a tremendous effect on the relative vertical response with negligible effect in the horizontal direction.

When coupling the hub accelerations to the NASTRAN model, it was found that the vertical stiffness of the pylon was very important to the computed airframe response. The sensitivity of the two-per-rev airframe response to changes in the axial stiffness of the pylon is shown in Figure 8. The low response condition shown in Figure 8 results from the original rigid modeling of the pylon in the vertical direction. The high response condition was for an arbitrarily soft spring rate of 175×10^5 N/m (10^5 lb/in) to assess the effect of pylon vertical stiffness. The response difference is more than an order of magnitude. After observing this, it was obvious that axial deformations of the pylon which were originally considered negligible were in fact extremely important to the airframe response.

Calculations of the actual pylon axial stiffness were made. The vertical spring rate that was calculated was 770×10^5 N/m (4.4×10^5 lb/in). Two-per-rev response for this spring rate is shown in Figure 8. This spring rate includes the stiffness of the mast, thrust bearing, upper transmission case, side case and lower case. Resulting stiffnesses for the pylon components and a schematic of each is shown in the cutaway sketch in Figure 9. The spring rate was represented in the NASTRAN model by making the axial stiffness of the bar at the top of the mast equal to the calculated pylon spring rate.

The sensitivity of the airframe response to the vertical (axial) stiffness of the pylon results from the method of applying hub accelerations which does not limit the load to the pylon. The load applied at the hub comes from the main rotor and will be limited between a cantilevered (highest load) and a free (zero load) boundary condition on the rotor hub. The use of hub shear loads rather than hub accelerations should be a more representative method of applying excitation in the NASTRAN analysis, at least in the vertical direction.

With helicopter isolation systems that provide vertical isolation as well as horizontal, such as the "nodal beam" (Reference 4), the problem of extreme sensitivity to small deformations is not expected. For these systems, two-per-rev vertical deformations at the hub are the same order of magnitude as the horizontal hub deformations.

For all conditions used in the correlation study and plotted in Appendix B, the 770×10^5 N/m (4.4×10^5 lb/in) spring rate was included.

3.2.3 Effect of Pylon Damping and Stiffness Parameters

The pylon was represented as a linear elastic model with scalar springs representing the translational stiffness of the elastomeric mounts (see Figure 7). Two percent modal damping was selected for all modes since that value was considered representative of the damping of predominant airframe modes of the helicopter. In the vibration testing of Reference 2, it was found that the natural frequencies and damping of the longitudinal and lateral pylon rocking modes were both higher than the NASTRAN analysis. It was therefore surmised that some known stiffening and damping effects should be incorporated into the pylon model in order to evaluate their influence on two-per-rev airframe vibration. Two-per-rev (10.8 Hz) is the most significant rotor harmonic since it is closest to the pylon rocking modes which are below 5 Hz. Effects of near resonance amplification and damping decrease as the forcing frequency becomes further removed.

The known pylon stiffening and damping effects considered are the following:

- pendulum stiffening due to rotor thrust,
- elastomeric mount cocking (rotational) stiffness, and
- 10 percent damping of the pylon rocking modes.

The pendulum stiffening of the pylon is controlled by the rotor thrust at the hub. When the pylon rocks, the 1g rotor thrust at the hub produces a restoring moment. This effect was analyzed in NASTRAN using a DMAP alter. The alter allowed addition of the differential stiffness matrix from a static load condition with 1g rotor thrust to be added to the structure stiffness matrix. The resulting stiffness matrix was then used to determine the pylon natural frequencies and airframe frequency response using rigid format 11.

A simplified model was used for the NASTRAN analysis. The elastic pylon model was attached to a rigid body fuselage to evaluate the differential stiffness effect on pylon isolation at two-per-rev. The fuselage was attached to ground by soft springs in order to perform the static analysis. The springs were soft so as not to affect the pylon rocking frequencies. In addition to the pendulum stiffening, measured cocking spring rates of .113 x 10^5 N-m/rad (10^5 in-lb/rad) were added to the elastomeric pylon mounts which were represented by only the mount translational spring rates in the airframe model. Also, ten percent modal damping was used in the analysis as

indicated from the measured frequency response in Reference 2. This model was then compared to the original pylon model without the stiffening effects and using two percent modal damping. A comparison of pylon rocking frequencies is given below.

Mode	Natural Frequency (Hz)	
	Baseline	Stiffened
Pylon Pitch (Longitudinal)	3.215	3.308
Pylon Roll (Lateral)	3.357	3.621

The comparisons of the frequency response of the fuselage cg are shown in Figure 10. Roll response to a lateral hub shear and pitch response to a longitudinal hub shear are presented. Although the responses are shown to be quite different near the pylon rocking frequencies, the responses at two-per-rev do not differ significantly. Therefore, the stiffness and damping effects discussed in this section are not considered significant in the flight vibration correlation and are not included in the NASTRAN airframe analysis.

3.3 COMPARISON OF TEST AND ANALYSIS

In this section, the results of the comparisons between measured and calculated flight vibrations at main rotor two-, four- and six-per-rev frequencies are discussed. In Appendix B the data from flight test and the NASTRAN analysis is overlayed on plots of acceleration (g's) versus fuselage station. Both maximum amplitudes and "mode shapes" (forced response) are shown. The harmonic, direction, configuration and airspeed for each comparison plot is listed in Table B-1 in Appendix B for reference.

Both qualitative and quantitative methods are used for evaluating the comparisons between measured and calculated flight vibration data. Following the discussion of results in Section 3.3.3, a qualitative assessment of the analysis for design is given. Quantitative comparisons of the vibration data are given in Appendix C.

3.3.1 Guidelines for Evaluating the NASTRAN Analysis

The following criteria are suggested as necessary to evaluate consistency between test and analysis:

1. The frequency range of validity of the NASTRAN model:

   Results of the vibration test comparison in Reference 2 indicate the airframe analysis agrees quantitatively well through four-per-rev (21.6 Hz) but differs significantly in the frequency range proximate to four- and through six-per-rev. The magnitudes and phases of responses at the main rotor harmonics are most important.

2. The accuracy of the test data used for the purposes of correlation:

   No rationale is available to place weighting factors of importance on any of the transducers used in the flight test. Poor locations of accelerometers and their local effects cannot be ascertained.

3. Suspected NASTRAN modeling deficiencies:

   The effect of the noseboom, downwash impingement, simplified modeling of the elevator, pylon dynamics, structural damping and elastomeric nonlinearities are typical influences.

3.3.2 General Comments on Vibration Characteristics of the AH-1G Helicopter

Two-per-rev is the predominant excitation frequency of the Bell two-bladed rotor. The loads are higher and, consequently, the response is normally higher than the four- and six-per-rev harmonics. The loads increase with airspeed and coupling between the in-plane and vertical response becomes more significant. Large percentage errors in low response levels are not considered important. The ability to predict high responses is considered essential if fatigue damage and annoying vibration environments are to be assessed.

3.3.3 Discussion of Results

Comparisons between the calculated flight vibration responses and test are presented in Appendix B. Possible explanations for poor correlation (large percentage errors) are discussed below.

3.3.3.1 Vertical Responses

1. Two-per-rev

   For both the clean wing and wing stores configurations, there is general agreement of the harmonic

amplitudes between analysis and test. The trends of response with airspeed are consistent with exception of the highest airspeed. In these cases the forward fuselage response predictions are significantly lower than test. The vibratory hub shears in the horizontal directions increase more than the vertical hub shears at the higher airspeeds (refer to Figure 6), and the idealized NASTRAN pylon may be isolating pitching moments due to the horizontal shear better than test indicates. Also, the noseboom that was on the test helicopter (see Figure 2) but not in the NASTRAN analysis may be affecting the nose response.

2. Four-per-rev

For both flight test configurations, the NASTRAN response is extremely high compared to flight test. The four-per-rev vertical resonance introduced by the big hub mass is a possible source for these large differences. This big hub mass constrains the hub and produces a vertical bounce mode of the fuselage on the pylon axial spring. The resulting vertical hub shear at the top of the mast is 14233 N (3200 lb). The expected vertical load, using the in-flight vertical vibration at the hub and the indicial vertical hub response from Reference 2, is 1388 N (312 lb). This ratio of applied vertical load to expected vertical load reduces the response by a factor of ten. The reduced responses agree much better with test. This supports the hypothesis discussed in Section 3.2.2 that hub shears instead of hub accelerations are a more practical means of exciting the model in the vertical direction.

NOTE: The expected vertical load was calculated as follows:

Vibration test vertical hub response (Reference 2, page 117)	=	.000045 g/N (.0002 g/lb)
Vertical hub response at 142 knots	=	.077g = .75 m/s^2

Rotor weight = 430 kg (947 lb)

$$\text{Vertical load} = [.077g \div .000045\ g/N]$$
$$- [430\ kg \times .75\ m/s^2]$$
$$= 1388\ N\ (312\ lb)$$

Assuming that the method for reducing the NASTRAN responses is feasible, the following comments apply. Although the percentage error is not small, the predicted responses are the same order of magnitude as the measured response with better agreement at the higher airspeeds. The trend with airspeed for the clean wing configuration is poor as indicated by the apparent scatter in the data. For the wing stores configuration, the overall trends of response with airspeed agree well, with analysis being somewhat higher at the high airspeeds.

The frequency response data of Reference 2 indicates some degradation of correlation near four-per-rev. The method of applying hub excitations introduces an artificial vertical resonance. For these reasons, the lessened degree of correlation at the four-per-rev main rotor harmonic may have been expected. Additional analyses and ground tests appear necessary to confirm these suspected deficiencies.

In general, the four-per-rev response levels are significantly lower than the two-per-rev responses. For purposes of design these differences between analysis and test may be of little consequence.

3. Six-per-rev

The overall predicted response levels are the same order of magnitude as test. The most significant differences occur along the tailboom and the vertical fin. The higher measured elevator response is controlled by the elevator natural frequencies. The NASTRAN elevator model is a simplified elastic line representation with very few degrees of freedom remaining in the analysis after the Guyan reduction. The calculated elevator natural frequencies are 42 Hz for the symmetric bending mode and 47 Hz for the asymmetric bending mode. The test data indicate this mode to be closer to six-per-rev. Improved correlation may be possible by a more detailed representation of the elevator model in NASTRAN.

The frequency response data of Reference 2 indicate significant differences at the six-per-rev main rotor harmonic. Consequently, any agreement for this flight vibration correlation study is difficult to assess. The six-per-rev responses are, in general, lower than the two-per-rev responses except along the tailboom. Although the percentage errors are large, the trend in terms of response magnitude was predicted. These differences between analysis and test may not be important for design.

3.3.3.2 Lateral Responses

1. Two-per-rev

The correlation between analysis and test is poor, especially at the tail. The predicted responses are considerably lower than test. These significant differences are important in design since NASTRAN underestimates the order of magnitude and trend characteristics necessary to structural fatigue and vibration isolation assessments.

The large differences may result from main rotor downwash exciting the tail fin laterally. In addition, the idealized NASTRAN pylon may be isolating rolling moments due to in-plane hub shears better than test indicates.

The frequency response data of Reference 2 is insufficient for excitation at the main rotor hub and suspect. Additional analysis and test is necessary to resolve this problem.

2. Four-per-rev

While the two-per-rev responses were underestimated, the predicted four-per-rev responses are significantly higher than test. Strong coupling between the lateral response and the artificial vertical pylon bounce mode resonance that was discussed earlier may explain these differences for the clean wing configuration. However, this trend is not present for the wing stores configuration, indicating the vertical pylon bounce mode has shifted between the two configurations. The data of Reference 2 indicate NASTRAN is consistently higher than test. Additional analysis and test is required to properly assess these differences. It is considered an

important design requirement to predict low responses as well as high responses if fatigue damage and vibration isolation are to be properly assessed.

3. Six-per-rev

For the clean wing configuration the predicted responses are generally higher than test except at mid and high airspeeds where the measured elevator and tail responses are higher. An elevator asymmetric mode near six-per-rev is suspected. This mode produces torsion in the tailboom which in turn causes high lateral responses at the tail.

For the wing stores configuration the vibration levels are much lower for both test and analysis.

The frequency response data of Reference 2 indicates significant differences between NASTRAN and test for six-per-rev. Consequently, any agreement for this main rotor harmonic may be fortuitous.

3.3.4 Qualitative Assessment for Design

The following table presents an overall qualitative assessment of the aforementioned flight vibration correlation results. The impact of this study on design is emphasized. The results are considered adequate if response magnitude and trends appear reasonable. The results are considered inadequate if the response magnitude and trends cannot be assessed because of insufficient data.

SUMMARY TABLE OF QUALITATIVE ASSESSMENT

Condition	Direction	Harmonic	Correlation	NASTRAN Problem area	Explanation
CW	V	2	adequate	nose at 142 kt, low	pitch isolation, noseboom
WL	V	2	adequate	nose at 134 kt, low	same
CW	L	2	inadequate	response low esp. at tail	roll isolation, main rotor downwash on fin
WS	L	2	inadequate	same	same
CW	V	4	adequate	response was reduced by a factor of 10 based on loads	artificial resonance due to big mass used for hub accelerations
WS	V	4	adequate	response high, trend good with airspeed	none
CW	L	4	inadequate	response very high esp. at tail	lateral coupling with artificial vertical mode in resonance
WS	L	4	adequate	nose higher, tail lower	none
CW	V	6	inadequate	mast higher, elevator, tail lower	suspect elevator mode near 6/rev in test
WS	V	6	inadequate	same	same
CW	L	6	inadequate	same	same
WS	L	6	inadequate	same	same

CW = clean wing
WS = wing stores
V = vertical
L = lateral

4. TAILBOOM STATIC TEST - NASTRAN CORRELATION

4.1 INTRODUCTION

The objectives of this study were the following:

1. Static tests were to be conducted and stresses measured for comparison to stresses calculated using a NASTRAN model of an AH-1G attack helicopter tailboom.
2. A NASTRAN model was to be made and the effects of effective skin on the internal load distribution and deflections investigated.
3. The stresses calculated by the NASTRAN model were to be compared with those measured from test.

4.2 STRUCTURAL DESCRIPTION OF AH-1G TAILBOOM AND VERTICAL FIN

The tailboom and vertical fin structure are shown in Figure 11. The tailboom is bolted to the fuselage at four attachment fittings located at the four main longerons of the tailboom and the four main beam caps of the fuselage.

The tailboom is of semimonocoque construction having aluminum skins, stringers and longerons. The longerons and stringers are supported by bulkhead frames spaced down the length of the boom. A typical cross section of the tailboom is shown in Figure 11. The hinged tail rotor drive shaft cover on top of the boom is assumed nonstructural.

The vertical fin has a two-cell cambered airfoil section with two spars and a trailing edge strip. The hinged tail rotor drive shaft cover on the front of the fin is assumed nonstructural as well as the top portion of the fin which extends above the 90-degree gearbox. A typical fin cross section is shown in Figure 11.

4.3 STATIC TAILBOOM TEST

The test was conducted with the tailboom cantilevered from a support fixture with the tailboom centerline horizontal as shown in Figure 12. Three separate shear loads were applied at the ends of the tailboom: lateral right, lateral left, and vertical down. Strain gages were installed in three different bays near the forward end of the tailboom. Figure 14 and Table V show the location of the gages. Some typical skin panel strain gage installations are shown in Figure 13. Gages were installed on stringers, longerons and skin panels. Load-stress data were taken using an automated data recording system. All reference to direction in this report is with respect to a forward facing position in the helicopter.

4.3.1 Test Specimen

The tailboom and fin assembly used in this test is from an AH-1G helicopter, Ship No. 68-15048, obtained from Rock Island Arsenal in Illinois, and is the same specimen used in a previous load-deflection test, (Reference 2). The tailboom installation is Part No. 209-030-800-7, (Reference 9). The flight history of the tailboom is unknown but no obvious structural defects were present. All cargo and inspection covers were in place and secured for the test. The driveshaft and cover were removed.

4.3.2 Test Loads

Three separate loads were applied perpendicular to the tailboom centerline at Boom Sta. 227. Lateral right and lateral left loads of 5604 N maximum were applied at Boom Sta. 227, W.L. 61.10. A vertical down load of 4448 N maximum was applied at Boom Sta. 227, B.L. 0.0. The lateral right and left loads were applied in thirteen increasing increments with four decreasing increments. The vertical down load was applied in ten increasing increments with four decreasing increments.

4.3.3 Test Fixtures

The tailboom was cantilevered from a support fixture with the tailboom centerline horizontal as shown in Figure 12. The fixture was bolted to the floor of the BHT Engineering Test Building with the tailboom mounted to the test fixture at the four production fuselage attachment fittings.

Test loads were applied to the tailboom using a hydraulic cylinder and hand pump with a calibrated pressure gage. A contour fitting frame was attached to the tailboom at Boom Sta. 227 and load was applied through the frame. The applied load was cycled from 0 to maximum at least three times before data were measured. Data were then recorded for three separate test runs for each load condition.

4.3.4 Instrumentation

Single active arm strain gages were installed at various locations on the tailboom with the axis of the gage parallel to the tailboom centerline. Table V indicates the location of the gages. Figure 14 shows typical gage installations for a

skin panel. Other gages were installed inside the tailboom on stringers and longerons.

Data were recorded automatically with a Hewlett Packard 9830A data acquisition system. The strain level for each gage was converted to stress using a conversion factor for aluminum based on a Young's modulus of E = 7.240 x 10^{10} N/m2. It should be noted that no correction was made to the indicated stress due to changes in indicated strain caused by Poisson effects. Results were printed out for each increment of load.

4.3.5 Test Results

Data were taken during three separate load applications for each load condition. There was no significant difference between results from each load application. The third load application was selected for plotting, since any settling in the joints of the structure would have most likely occurred during the first and second loadings. Plots of load vs. stress for the tests are given in Appendix C.

4.4 NASTRAN ANALYSIS

To study the effects of effective skin and have an analysis to compare to the test data, a NASTRAN model of the AH-1G tailboom was made. The test load cases were simulated with the model.

The results for the maximum test loads are given in Tables VI, VII, VIII and IX.

4.4.1 Modeling Philosophy

The objective of the modeling of the tailboom was to provide an analysis for evaluating the test data. To achieve good comparison between the test and analysis, the structural load paths must be correctly represented. These paths are a function of geometry and sectional properties of the structural members. To meet this primary objective it is important that the stiffness of the structure be accurately represented. Some guidelines used in modeling are the following:

1. In the built-up modeling of the tailboom, grid points are located at the intersection of panels. This is done because the axial members (rods) are generally easier to relocate to the grid point than shear panels.
2. Skin panels are modeled with shear panels and are assumed to carry no axial load. If the skin is unbuckled or has some of its material effective, the

area of the stringer or longeron is increased to reflect the effective skin. The method used is discussed in section 4.4.2.

3. The longerons and stringers are modeled with rod elements that carry only tension or compression axial loads, since their own bending stiffness is assumed negligible compared to the section.
4. The ring bulkheads do not significantly affect the bending stiffness of the overall tailboom. These bulkheads are modeled with bending bars, with stiffness in the plane of the bulkhead to preserve the location of the axial members around the periphery.

4.4.2 Effective Skin

As disucssed in the previous section, the primary objective of the NASTRAN model is to provide an analysis to accurately compare to the test data. To do this, effective axial load carrying skin was accounted for by adding area to the stiffener's cross sectional areas. Each load case was run several times to iterate to the correct amount of effective skin. The method used for determining the portion of the skin panels which are effective in resisting axial loads follow the procedure outlined in Reference 5, page 374, but with two notable exceptions.

These exceptions are:

1. The bending analysis of Reference 5 uses the classical approach based upon the assumption that plane sections remain plane while resisting bending loads. The method contained herein uses a finite element technique for the bending analysis and as such assumes equilibrium and continuity at the model element joints only. Sections which were originally plane in the unloaded state do not necessarily remain plane while resisting bending loads.
2. The bending analysis of Reference 5 includes some effective skin in the first iteration and adds additional effective skin for each successive iteration. The method used in this study assumes no effective skin for the initial iteration but progressively adds the skin areas which are calculated to be effective for each succeeding iteration.

To calculate the effective skin for each iteration, the following methods were used:

1. The skin elements on the tension side of the neutral axis are considered 100% effective in resisting axial load. The area of these skins is distributed equally to adjacent longerons or stringers. Also, at the longeron locations where skin overlap occurs, the skins between the longeron-to-skin attachments are assumed to be 100% effective in both tension and compression.
2. An effective width of skin, W, centered on the line of skin-to-stringer attachments can carry the same compression stress as the stringer. Effective skin widths W_1, W_2, W_3, etc., are shown on the typical tailboom cross section in Figure 16 and can be calculated by:

$$W = (2)(.85)\ t\sqrt{\frac{E}{\sigma_{axial}}}$$

where W is the effective skin width on both sides of a stringer, t the skin thickness, σ_{axial} the applied axial stress of the attached longeron or stringer and E is the modulus of elasticity of the skin material.
3. The remainder of the curved skin between axial members carries a maximum compressive stress of:

$$\sigma_{critical} = \frac{.3Et}{R} \text{ for } \upsilon = .3 \text{ and } \frac{R}{t} < 500 \quad \text{(Reference 6 page 389)}$$

$$\sigma_{critical} = E\left[9\left(\frac{t}{R}\right)^{1.6} + 0.16\left(\frac{t}{L}\right)^{1.3}\right] \text{ for } 500 < \frac{R}{t} < 3000 \text{ and } 0.1 < \frac{L}{R} < 3000$$

$$\sigma_{critical} = KE\left(\frac{t}{b}\right)^2 \text{ for flat sheet } (R = \infty)$$

where $\sigma_{critical}$ is the buckling stress of the skin element, R the radius of curvature of the skin element, L is the tailboom bay depth, K is a constant and is 3.62 minimum and b is the distance between axial members.

Thin curved skin between the axial members normally buckles at a compressive load less than that required to buckle the axial members. In this analysis, the curved skin is treated as an element with varying effective area which depends on the ratio of the curved skin's buckling stress, $\sigma_{critical}$, to the axial member's stress, σ_{axial}. Hence, the effective skin area, A_{eff}, for the buckled skin panels can be written,

$$A_{eff} = b't\ (\sigma_{critical}/\sigma_{axial})$$

where b' is the width of the curved skin between the effective skin widths W_1, W_2, W_3, etc., as shown in Figure 16.

4.4.3 NASTRAN Internal Loads Analysis

The first eight tailboom bays were examined using the NASTRAN model. Since the test loads were applied to the bulkhead just forward of the fin attachment, only the skins and stiffeners forward of that point were considered in the determining of the correct amount of effective skin.

The load cases first examined using the NASTRAN model were the maximum loads obtained during the test. The load cases are:

1. 5604 N(1260 lb) to the right
2. 5604 N(1260 lb) to the left
3. 4448 N(1000 lb) down

The loads were all applied at tailboom station 227. The axial loads calculated for the stiffeners of the first eight tailboom bays for the first and final iterations along with the initial and final stringer areas are given in Tables VI, VII and VIII.

Variation in effective skin (stiffness) can result in a change in the stringer loads. For lateral loading, a difference of 7% is found on the compression side, but for the down load, a 20% difference is shown on element 5 in bay 2. Figure 15 gives the stringer numbering convention.

As the compression stresses in the skins increase, less skin is effective. To study the behavior of the tailboom as the stress levels approach the material yield (advanced stages of post buckling), an 35584 N right load was applied to the NASTRAN model. However, this was not examined in test. The results are given in Table IX.

4.5 COMPARISON OF TEST AND ANALYSIS

4.5.1 Stress Comparison

A comparison between the stresses measured in the test and the stresses calculated in the NASTRAN analysis will full effective skin is given in Table X. Each test load was applied three times. The average of three readings are given as the test stress.

In reviewing the comparison of the test and analysis stresses, good correlation as well as poor correlation can be shown. For the right load, a difference of 35% is shown for element 4, the

compression side, of bay 4 while a 37% difference is shown for the tension side, element 10 of bay 4. Similar discrepancies are observed for the left loading. The down loading had generally better correlation with the exception of the bottom stringer, element number 6, which show a difference of 38% for bay 2, 0% for bay 3, and 26% for bay 4.

For this analysis, the skin was assumed to carry a constant load equal to the buckling load after buckling occurs. Upon examining the strain behavior of the buckled panels, an assumption of the buckled panels carrying no load might give better correlation between test and analysis.

4.5.2 Deflection

A comparison between the calculated and measured deflections is shown in Figures 17 and 18 for vertical and lateral load conditions. Measured deflections are taken from Reference 2. Deflections with and without effective skin are given. The effective skin analysis for the vertical deflection agrees well with the test results. The lateral load case shows the NASTRAN analysis to be stiffer than test. Figure 19 illustrates the load-stress behavior for a buckled panel. The solid line shows the load in the panel as it was assumed to behave for this analysis, constant load equal to the buckling load after buckling occurs. The dashed line curve shows the post buckling behavior of the panel more realistically, with the stress falling off with load. Using the method of calculating effective skin presented in this report, a model that is too stiff may result. This is probably why deflections for the lateral loading do not agree with the test results. Little buckling occurred for the vertical loading while there was considerable buckling for lateral.

5. CONCLUSIONS AND RECOMMENDATIONS

5.1 FLIGHT VIBRATION CORRELATION

Test data from an AH-1G operational loads survey (Eustis Contract DAAJ02-76-C-0105) were compared to a NASTRAN analysis. Measured vibration responses of the airframe for level flight conditions were compared to a NASTRAN vibration model. Measured hub accelerations and control loads were used to excite the analytical model. The correlation was based on comparing vibration amplitude and mode shape curves at three main rotor harmonics: two-, four- and six-per-rev. Guidelines used for evaluating the correlation were discussed and used in judging the correlation.

Conclusions from the flight vibration correlation study are as follows:

1. There was good agreement between calculated and measured vertical two-per-rev vibration. This predominant excitation frequency of the Bell two-bladed rotor produces vibration levels that are normally higher than those at the higher harmonics.

2. Lateral two-per-rev vibration levels were calculated to be much lower than those measured in test, primarily at the tail. Poor prediction of roll isolation from the main rotor pylon or main rotor downwash excitation on the fin are suspect.

3. Vertical stiffness of the main rotor pylon was extremely important in the vibration analysis. This problem was caused by using hub accelerations without control of the applied load. Since the applied vertical hub acceleration was very small, vertical deflections on the order of a few thousandths of an inch had a significant effect on the applied load. Pylon designs with vertical isolation, such as the nodal beam, should not be as sensitive to vertical deflections of the mast and transmission.

4. Pendulum stiffening due to rotor thrust, elastomeric mount rotational stiffness, and increased pylon modal damping were analyzed to determine the effect on two-per-rev isolation of the main rotor pylon. The results of the analysis showed there was not a significant effect at two-per-rev.

5. Except for a resonance of an artificial mode at four-per-rev caused by the method of applying hub accelerations, calculated and measured four- and six-per-rev vibration responses agreed fairly well. It is not surmised that the accuracy of the analysis at these frequencies can be judged, however, since the vibration response at these frequencies was not strongly influenced by modes in close proximity to the forcing frequency. From the results of the vibration testing in Reference 2, the airframe vibration prediction was quantitatively accurate through four-per-rev, but deviated from measured results significantly at six-per-rev. In addition, when exciting at the main rotor hub through the pylon, the correlation obtained was poorer than that obtained when exciting directly on the airframe. Considering these factors, the agreement of four- and six-per-rev may have been coincidental. More information is needed in order to judge the NASTRAN analysis for prediction of airframe vibration at these frequencies.

This study was a continuation of an organized program by the Army to develop, document, correlate and evaluate a NASTRAN analysis of the AH-1G helicopter airframe and determine its validity for predicting low frequency vibration response produced by rotor and weapon firing excitations. The results to date are documented in References 1 and 2 and this report.

Recommendations for further investigations are as follows:

1. Investigate the effect of pylon dynamics on airframe vibration by a combined analytical and test correlation program.

2. Investigate the main rotor two-per-rev downwash environment on the AH-1G fin.

3. Investigate validity of current rotor analyses for prediction of two-, four- and six-per-rev excitation for pylon/airframe NASTRAN analysis. A valid analytical model of the airframe will not accurately predict the vibration response of the airframe if the excitation is not accurate. In addition, a convenient method for measuring hub shears should be developed.

5.2 TAILBOOM STATIC TEST CORRELATION

The tailboom of the AH-1G Attack Helicopter was tested to determine the effect of buckled skin panels on the stress

distribution in the tailboom. Stresses were measured and compared with stresses calculated using a NASTRAN finite element model. The loads on the model were used to calculate effective areas of buckled panels. These areas were then introduced back in the model and loads recalculated. This iteration and procedure was repeated until the effective skin areas had converged.

Conclusions from the study are the following:

1. The built-up model with effective skin gives good deflection correlation.

2. Proper effective skins are needed to determine internal loads accurately.

3. Stress correlation is fair, but can be improved by better representation of discontinuities and effective skin areas.

As different effective skin calculations are investigated, the deflection correlation should improve. The method used in this study was slightly stiffer than test. In the analysis presented, a panel was assumed to maintain its critical buckling load after buckling occurred. After buckling, however, the load in the panel probably decreases as the applied load increases. This would tend to soften the tailboom.

As indicated by comparing the test results with the analysis, better correlation in certain areas of the tailboom can be achieved. Discontinuities such as doors and shelves along with incorrect effective skin attribute to the areas of poor correlation.

As a continuing study, two recommendations are offered.

1. Obtain test data from the tailboom for loads that cause stresses in the tailboom to approach the material yield point. This will allow for examination of the behavior well within the post-buckled region.

2. Investigate alternate effective skin equations. Better correlation between the analysis and test must be achieved before drawing any definitive results as to the importance of effective skin in performing a stress analysis of the tailboom.

APPENDIX A

MEASURED HUB ACCELERATIONS AND CONTROL LOADS

This appendix contains tables of measured main rotor hub accelerations and boost cylinder control loads that were used in the flight vibration correlation study for excitation in the NASTRAN analysis. The data were measured under an AH-1G operational loads survey (Eustis Contract DAAJ02-73-C-0105) for level flight conditions. The data were reduced so that accelerations and loads at main rotor excitation harmonics (two-, four- and six-per-rev) were obtained. Amplitude and phase harmonics of the accelerations and control loads are tabulated for six airspeed conditions and two configurations, clean wing and wing stores. Airspeeds corresponding to each flight condition are listed below.

Configuration	Airspeed (kt)					
	1	2	3	4	5	6
Clean wing at aft cg	67	85	101	114	128	142
Wing stores at mid cg	61	76	95	108	120	134

TABLES

TABLE A-1. TWO-PER-REV HUB ACCELERATIONS

Gross weight configuration/ true airspeed	Hub accelerations					
	Fore-and-aft		Lateral		Vertical	
	Amp (g)	Phase (deg)	Amp (g)	Phase (deg)	Amp (g)	Phase (deg)
3768 kg (8300 lb) - clean wing aft cg						
67 kt	0.839	217.2	0.763	121.1	0.057	30.7
85 kt	0.968	224.5	0.863	122.3	0.055	32.6
101 kt	1.014	227.3	1.026	126.1	0.057	30.8
114 kt	1.281	215.6	1.284	120.1	0.043	31.4
128 kt	1.538	208.8	1.557	110.7	0.051	20.7
142 kt	2.063	216.1	2.193	118.4	0.039	48.7
4086 kg (9000 lb) - wing stores mid cg						
61 kt	0.771	341.3	0.685	254.5	0.031	147.8
76 kt	0.865	329.6	0.704	242.4	0.055	137.6
95 kt	0.993	329.4	0.984	231.6	0.022	145.5
108 kt	1.119	320.3	1.212	227.5	0.016	102.4
120 kt	1.434	315.4	1.451	225.2	0.037	119.3
134 kt	1.893	307.0	1.972	211.9	0.014	126.8

TABLE A-2. TWO-PER-REV BOOST CYLINDER LOADS

Gross weight configuration/ true airspeed	Boost Cylinder Loads					
	Fore-and-aft Cyclic		Lateral Cyclic		Collective	
	Amp N (lb)	Phase (deg)	Amp N (lb)	Phase (deg)	Amp N (lb)	Phase (deg)
3768 kg (8300 lb) - clean wing aft cg						
67 kt	1499 (337)	37.2	2197 (494)	132.1	1308 (294)	308.1
85 kt	1526 (343)	56.6	2531 (569)	159.5	1681 (378)	333.9
101 kt	1788 (402)	87.8	2598 (584)	196.5	2491 (560)	0.9
114 kt	1984 (446)	167.2	2816 (633)	264.2	3487 (784)	77.1
128 kt	2393 (538)	225.3	3149 (708)	312.9	4088 (919)	139.3
142 kt	3167 (712)	343.6	3536 (795)	69.8	4270 (960)	263.1
4086 kg (9000 lb) - wing stores mid cg						
67 kt	1557 (350)	269.6	1962 (441)	14.8	1232 (277)	205.1
76 kt	1472 (331)	334.8	2420 (544)	79.9	1610 (362)	269.3
95 kt	1979 (445)	335.8	2460 (553)	83.6	2175 (489)	254.7
108 kt	2104 (473)	336.5	2736 (615)	74.7	2953 (664)	253.2
120 kt	2166 (487)	340.1	3185 (716)	76.3	3665 (824)	262.4
134 kt	2842 (639)	44.5	3581 (805)	134.5	3990 (897)	329.8

TABLE A-3. FOUR-PER-REV HUB ACCELERATIONS

Gross weight configuration/ true airspeed	Hub Accelerations					
	Fore-and-aft		Lateral		Vertical	
	Amp (g)	Phase (deg)	Amp (g)	Phase (deg)	Amp (g)	Phase (deg)
3768 kg (8300 lb) - clean wing aft cg						
67 kt	0.304	156.4	0.245	47.1	0.041	216.2
85 kt	0.269	92.3	0.373	28.2	0.021	102.5
101 kt	0.498	130.8	0.494	57.6	0.076	125.2
114 kt	0.753	160.6	0.431	67.6	0.074	128.5
128 kt	0.950	154.9	0.418	41.0	0.090	69.8
142 kt	1.193	168.8	0.867	43.9	0.077	59.0
4086 kg (9000 lb) - wing stores mid cg						
61 kt	0.249	89.2	0.077	0.3	0.050	23.7
76 kt	0.286	93.5	0.079	225.6	0.038	73.4
95 kt	0.436	217.2	0.347	225.9	0.024	242.9
108 kt	0.448	303.2	0.564	231.7	0.053	284.8
120 kt	0.365	352.7	0.469	247.1	0.069	252.0
134 kt	0.564	318.0	0.539	196.6	0.076	218.9

TABLE A-4. FOUR-PER-REV BOOST CYLINDER LOADS

Gross weight configuration/ true airspeed	Boost cylinder loads					
	Fore-and-aft cyclic		Lateral cyclic		Collective	
	Amp N (lb)	Phase (deg)	Amp N (lb)	Phase (deg)	Amp N (lb)	Phase (deg)
3768 kg (8300 lb) - clean wing aft cg						
67 kt	102(23)	310.1	360(81)	65.8	142(32)	299.0
85 kt	351(79)	5.2	632(142)	149.3	80(18)	11.0
101 kt	503(113)	97.9	703(158)	238.5	196(44)	351.6
114 kt	374(84)	247.7	485(109)	22.5	311(70)	144.2
128 kt	383(86)	347.4	311(70)	145.4	276(62)	267.2
142 kt	280(63)	251.8	236(53)	115.0	200(45)	163.8
4086 kg (9000 lb) - wing stores mid cg						
61 kt	98(22)	183.6	209(47)	173.7	142(32)	50.8
76 kt	222(50)	218.5	498(112)	339.9	120(27)	230.9
95 kt	374(84)	249.6	609(137)	12.9	76(17)	101.9
108 kt	427(96)	252.5	431(97)	19.4	200(45)	132.9
120 kt	418(94)	246.0	423(95)	20.6	200(45)	150.8
134 kt	360(81)	8.8	276(62)	168.1	196(44)	267.9

TABLE A-5. SIX-PER-REV HUB ACCELERATIONS

Gross weight configuration/ true airspeed	Hub accelerations					
	Fore-and-aft		Lateral		Vertical	
	Amp (g)	Phase (deg)	Amp (g)	Phase (deg)	Amp (g)	Phase (deg)
3768 kg (8300 lb) - clean wing aft cg						
67 kt	0.177	337.5	0.128	307.5	0.063	241.3
85 kt	0.339	23.4	0.256	356.3	0.042	203.2
101 kt	0.263	60.1	0.285	351.3	0.049	145.1
114 kt	0.068	353.2	0.207	301.1	0.035	168.0
128 kt	0.197	7.2	0.387	268.2	0.025	13.0
142 kt	0.210	42.7	0.485	305.9	0.039	15.1
4086 kg (9000 lb) - wing stores mid cg						
61 kt	0.059	336.4	0.127	226.0	0.035	12.6
76 kt	0.292	247.8	0.289	248.2	0.098	106.6
95 kt	0.199	4.8	0.361	251.2	0.053	23.4
108 kt	0.217	50.7	0.247	241.0	0.070	40.7
120 kt	0.114	41.6	0.338	226.3	0.022	31.0
134 kt	0.124	4.9	0.587	203.8	0.029	201.8

TABLE A-6. SIX-PER-REV BOOST CYLINDER LOADS

Gross weight configuration/ true airspeed	Boost cylinder loads					
	Fore-and-aft cyclic		Lateral cyclic		Collective	
	Amp N (lb)	Phase (deg)	Amp N (lb)	Phase (deg)	Amp N (lb)	Phase (deg)
3768 kg (8300 lb) - clean wing aft cg						
67 kt	67(15)	345.6	196(44)	334.2	22(5)	187.4
85 kt	289(65)	105.8	436(98)	92.3	62(14)	207.1
101 kt	463(104)	177.3	120(27)	201.3	67(15)	254.2
114 kt	347(78)	35.6	93(21)	252.8	169(38)	86.1
128 k6	396(89)	190.6	356(80)	35.5	205(46)	271.0
142 kt	222(50)	229.9	476(107)	75.0	320(72)	282.5
4086 kg (9000 lb) - wing stores mid cg						
61 kt	120(27)	238.4	116(26)	248.4	116(26)	150.2
76 kt	276(62)	227.9	387(87)	170.0	173(39)	315.1
95 kt	334(75)	188.5	129(29)	301.5	138(31)	273.6
108 kt	245(55)	181.2	182(41)	8.8	222(50)	258.0
120 kt	325(73)	196.0	231(52)	39.5	351(79)	287.3
134 kt	418(94)	40.3	414(93)	251.7	378(85)	144.0

APPENDIX B

FLIGHT VIBRATION COMPARISON OF TWO-, FOUR- AND SIX-PER-REV RESPONSE

This appendix contains AH-1G helicopter flight vibration comparisons of measured and calculated data. The measured vibration data were taken under an AH-1G operational loads survey (Eustis Contract DAAJ02-76-C-0105). The calculated data came from the NASTRAN airframe vibration analysis. Acceleration amplitudes and mode shapes are plotted in the figures for main rotor two-, four- and six-per-rev excitation frequencies at six airspeed conditions and for two helicopter configurations: clean wing and wing stores. Comparisons are made of vibration responses in the vertical and lateral directions. The .05g band indicated on the figures represents a minimum error band for the measured data. The error band is 1 percent of full scale. Full scale was 5g or higher for the airframe measurements recorded in the flight tests. Measurements within the .05g band are not considered highly accurate for correlation purposes.

The measured and calculated amplitudes can be compared directly but the mode shapes can be misleading. The mode shapes are phase-referenced to a selected location on fuselage and all responses are not generally at maximum value at the same phase angle as the referenced station. The mode shapes are presented for comparison of the predominant shape in which the airframe is vibrating.

The comparison figures are listed in Table B-1. Figure number, harmonic, direction, configuration and airspeed for each comparison figure are tabulated to facilitate locating any particular condition.

TABLE B-1. FLIGHT VIBRATION DATA COMPARISONS

Figure Number	Main Rotor Harmonic	Response Direction	Configuration	Airspeed (Knots)
B-1	Two-per-rev	Vertical	Clean Wing	67
B-2	↓	↓	↓	85
B-3	↓	↓	↓	101
B-4	↓	↓	↓	114
B-5	↓	↓	↓	128
B-6	↓	↓	Clean Wing	142
B-7	↓	↓	Wing Stores	61
B-8	↓	↓	↓	76
B-9	↓	↓	↓	95
B-10	↓	↓	↓	108
B-11	↓	↓	↓	120
B-12	↓	Vertical	Wing Stores	134
B-13	↓	Lateral	Clean Wing	67
B-14	↓	↓	↓	85
B-15	↓	↓	↓	101
B-16	↓	↓	↓	114
B-17	↓	↓	↓	128
B-18	↓	↓	Clean Wing	142
B-19	↓	↓	Wing Stores	61
B-20	↓	↓	↓	76
B-21	↓	↓	↓	95
B-22	↓	↓	↓	108
B-23	↓	↓	↓	120
B-24	Two-per-rev	Lateral	Wing Stores	134
B-25	Four-per-rev	Vertical	Clean Wing	67
B-26	↓	↓	↓	85
B-27	↓	↓	↓	101
B-28	↓	↓	↓	114
B-29	↓	↓	↓	128
B-30	Four-per-rev	Vertical	Clean Wing	142

TABLE B-1. FLIGHT VIBRATION DATA COMPARISONS (Continued)

Figure Number	Main Rotor Harmonic	Response Direction	Configuration	Airspeed (Knots)
B-31	Four-per-rev	Vertical	Wing Stores	61
B-32				76
B-33				95
B-34				108
B-35				120
B-36		Vertical	Wing Stores	134
B-37		Lateral	Clean Wing	67
B-38				85
B-39				101
B-40				114
B-41				128
B-42			Clean Wing	142
B-43			Wing Stores	61
B-44				76
B-45				95
B-46				108
B-47				120
B-48	Four-per-rev	Lateral	Wing Stores	134
B-49	Six-per-rev	Vertical	Clean Wing	67
B-50				85
B-51				101
B-52				114
B-53				128
B-54			Clean Wing	142
B-55			Wing Stores	61
B-56				76
B-57				95
B-58				108
B-59				120
B-60		Vertical	Wing Stores	134
B-61	Six-per-rev	Lateral	Clean Wing	67

TABLE B-1. FLIGHT VIBRATION DATA COMPARISONS (Concluded)

Figure Number	Main Rotor Harmonic	Response Direction	Configuration	Airspeed (Knots)
B-62	Six-per-rev	Lateral	Clean Wing	85
B-63	↓	↓	↓	101
B-64	↓	↓	↓	114
B-65	↓	↓	↓	128
B-66	↓	↓	Clean Wing	142
B-67	↓	↓	Wing Stores	61
B-68	↓	↓	↓	76
B-69	↓	↓	↓	95
B-70	↓	↓	↓	108
B-71	↓	↓	↓	120
B-72	Six-per-rev	Lateral	Wing Stores	134

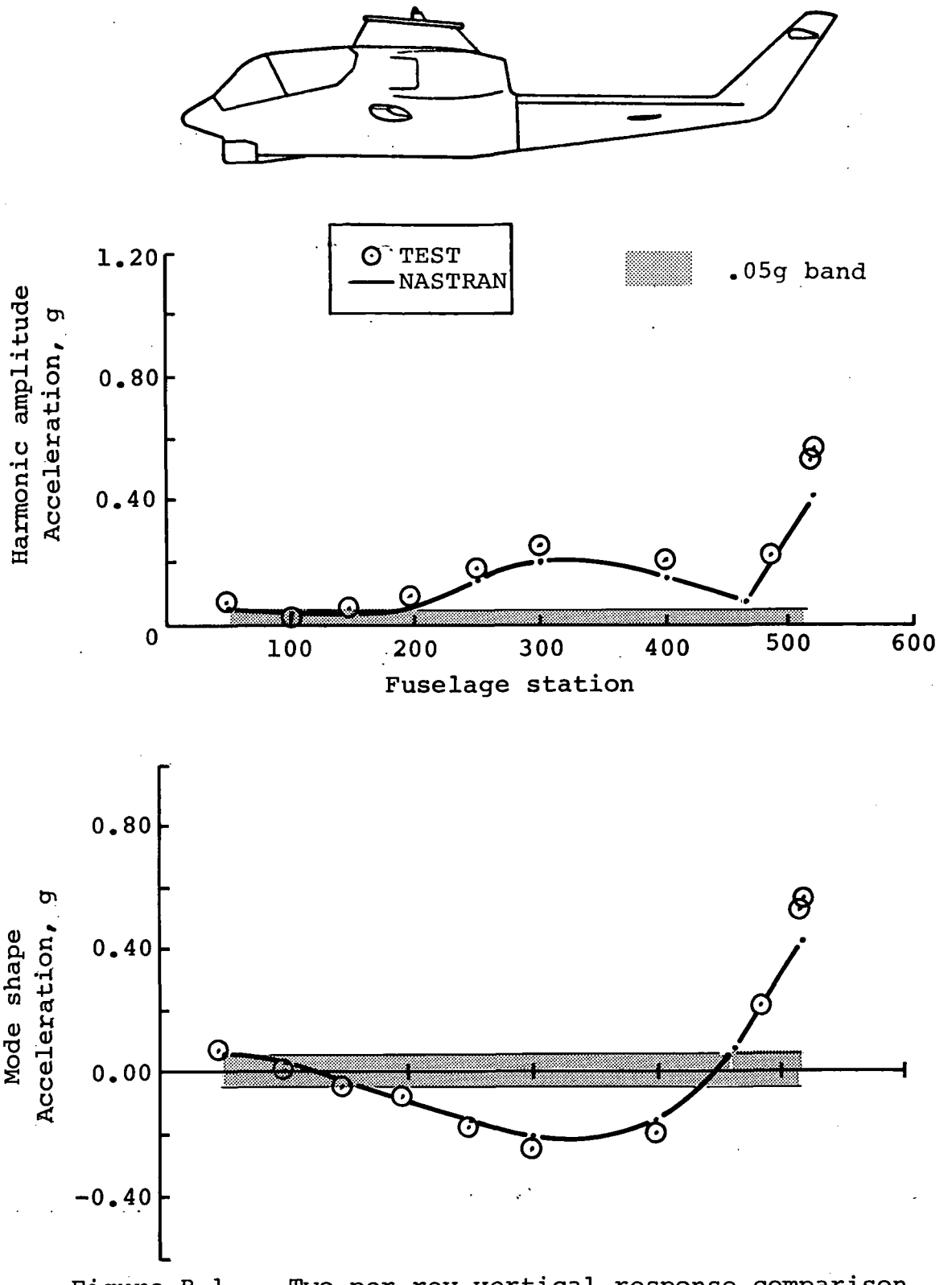

Figure B-1. - Two-per-rev vertical response comparison at 67 knots - clean wing.

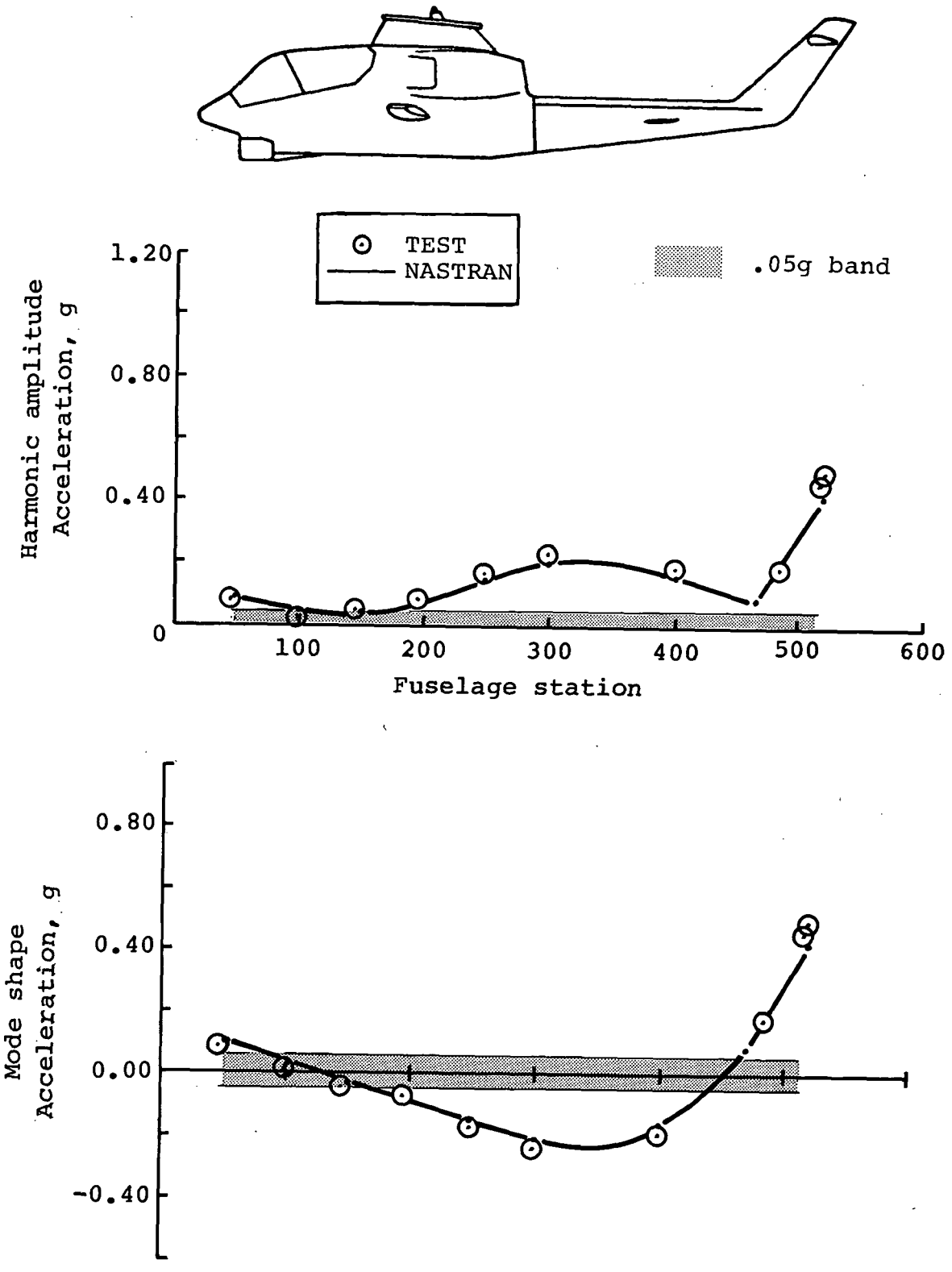

Figure B-2. - Two-per-rev vertical response comparison at 85 knots - clean wing.

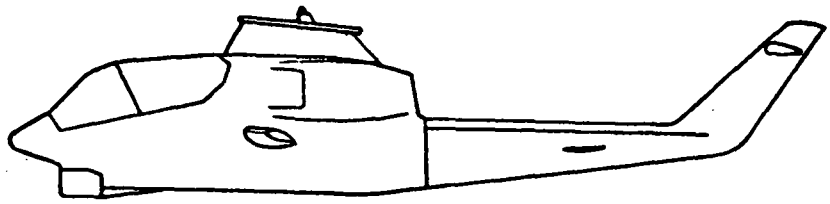

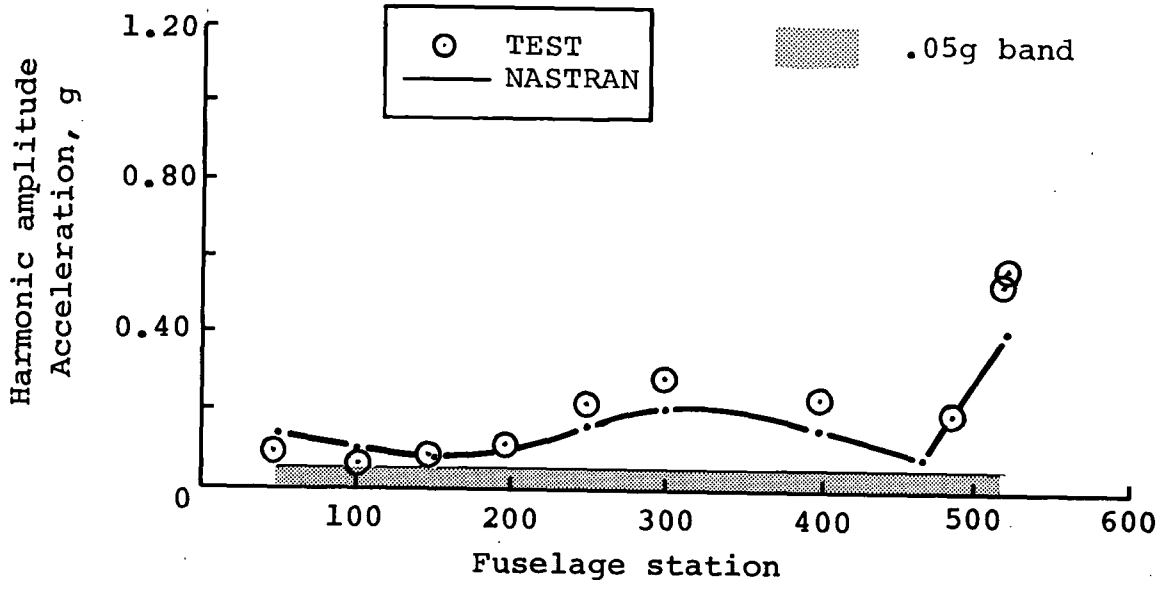

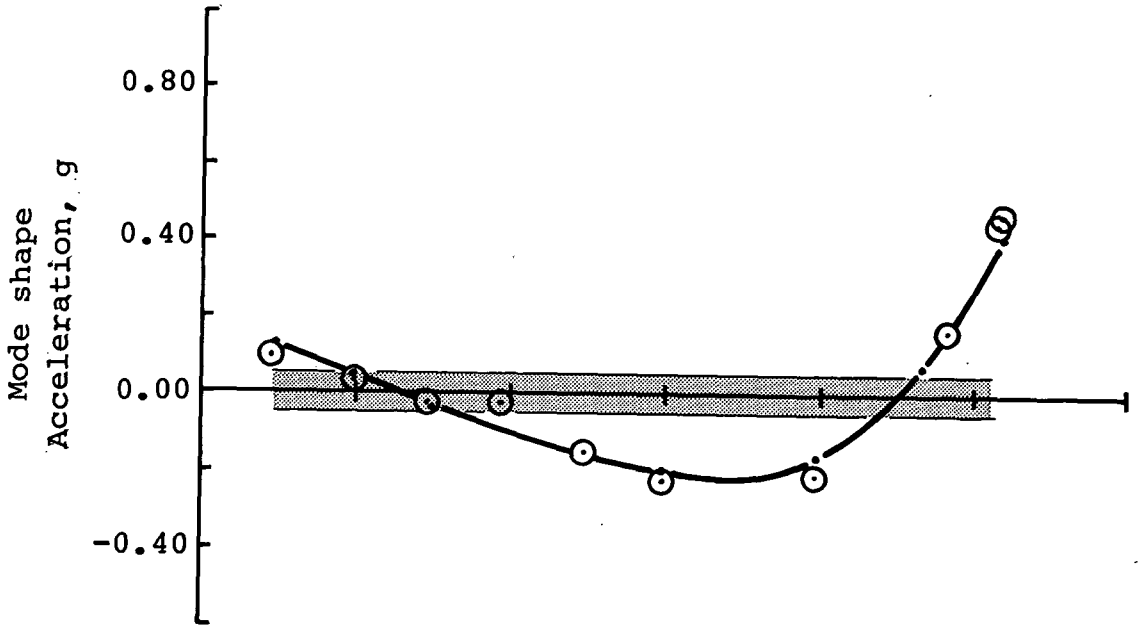

Figure B-3. - Two-per-rev vertical response comparison at 101 knots - clean wing.

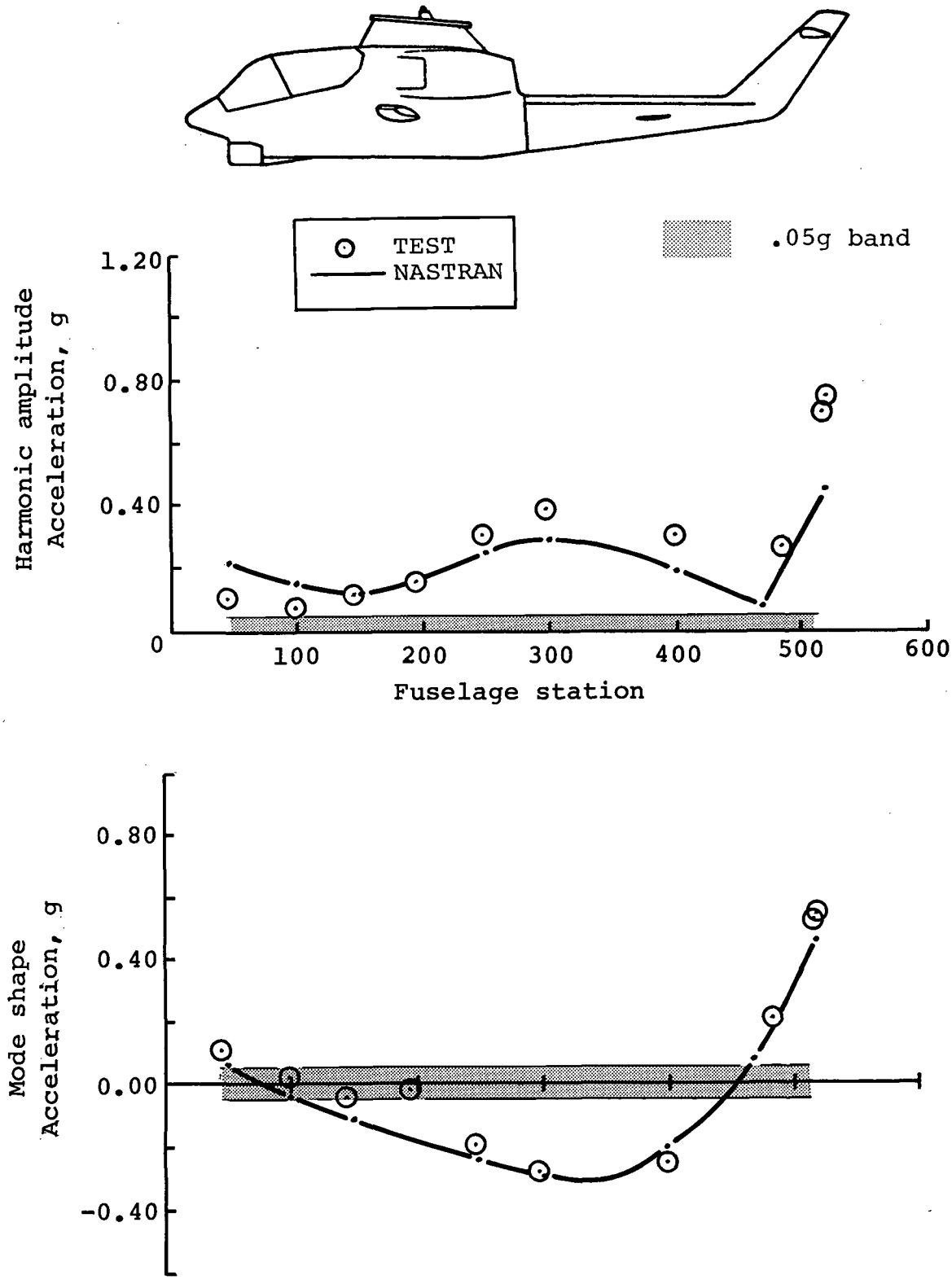

Figure B-4. - Two-per-rev vertical response comparison at 114 knots - clean wing.

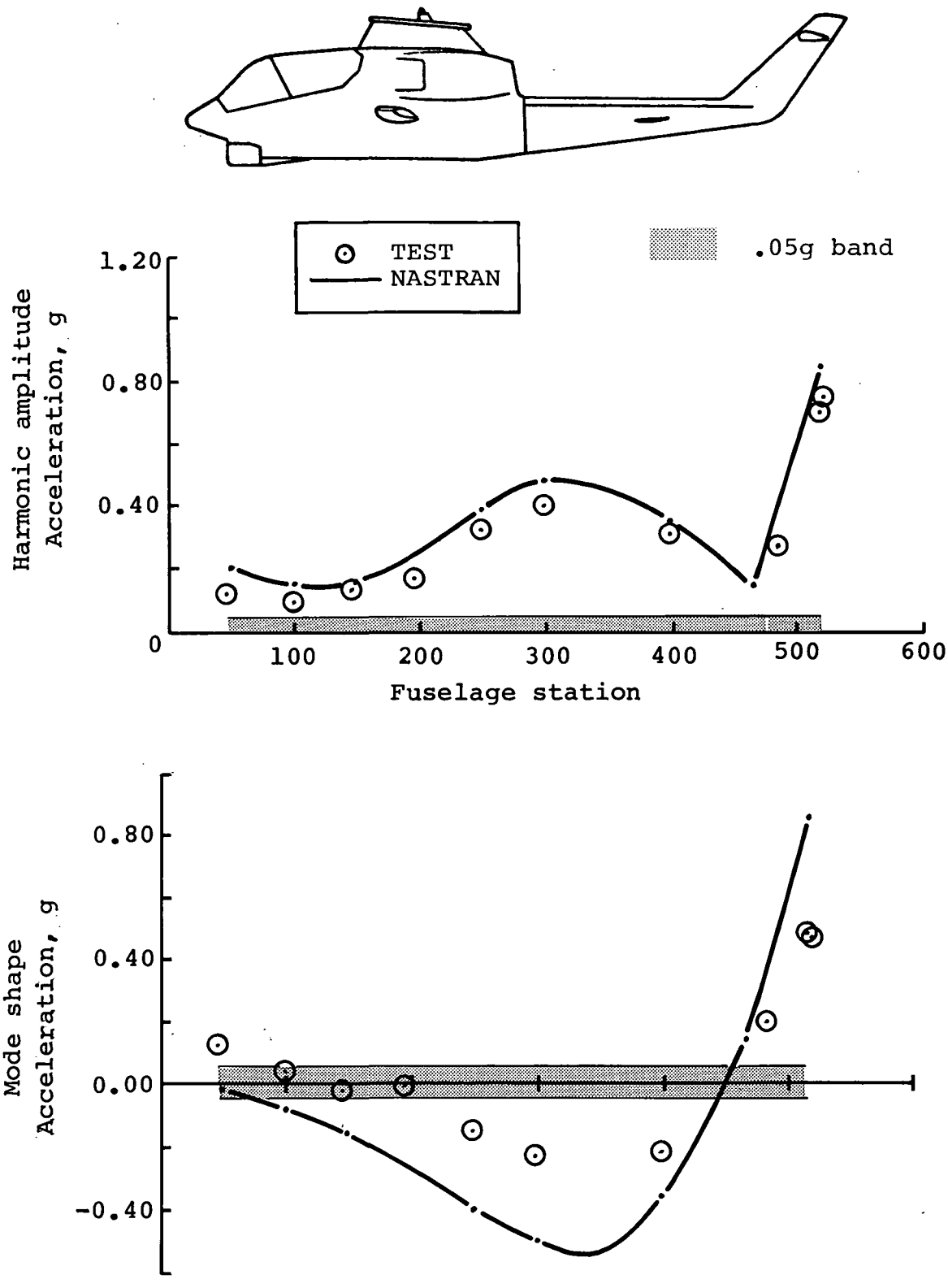

Figure B-5. - Two-per-rev vertical response comparison at 128 knots - clean wing.

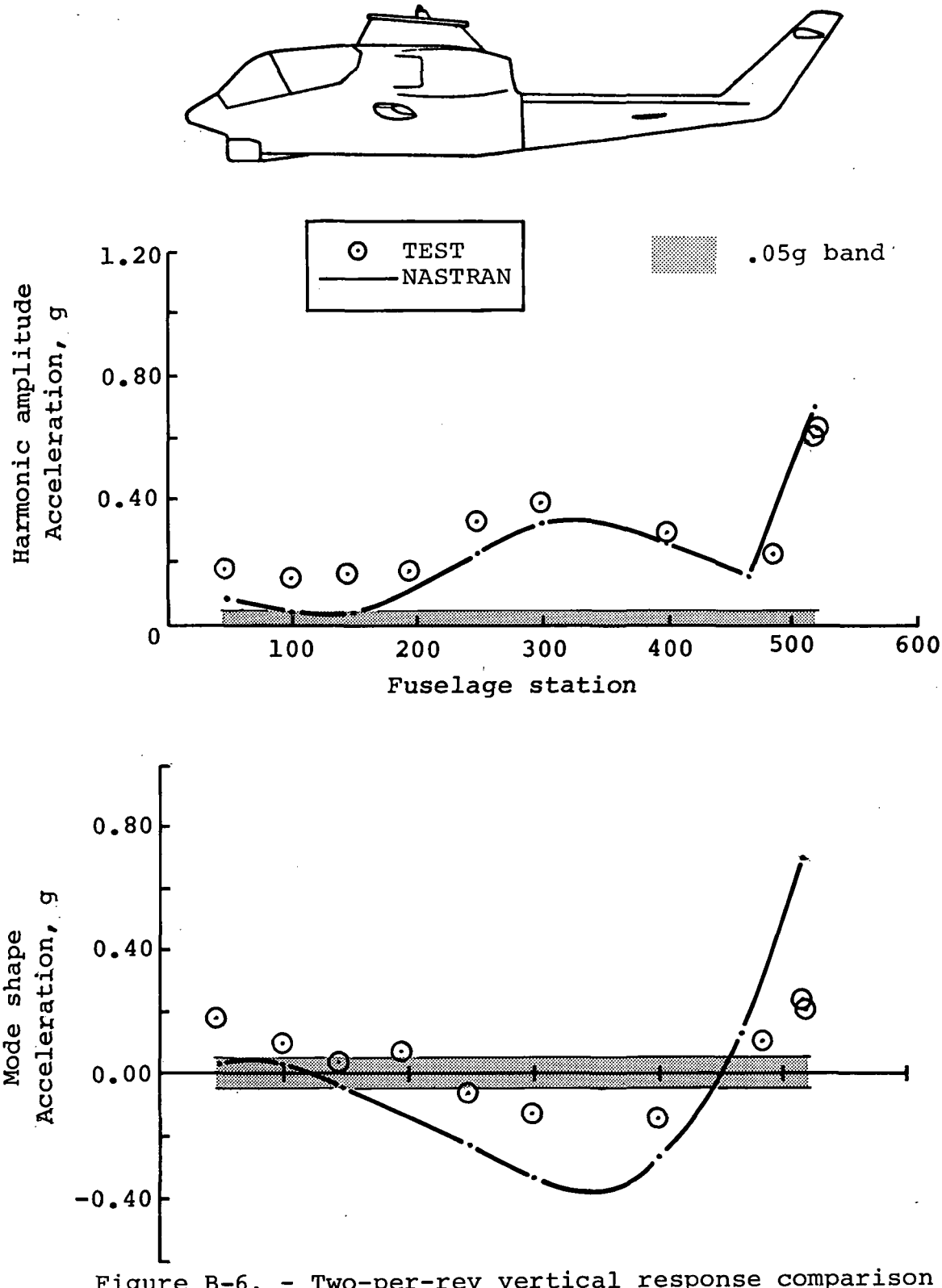

Figure B-6. - Two-per-rev vertical response comparison at 142 knots - clean wing.

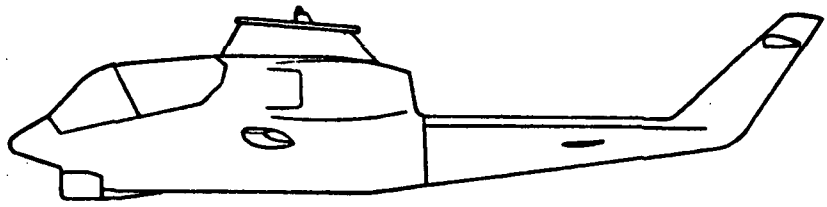

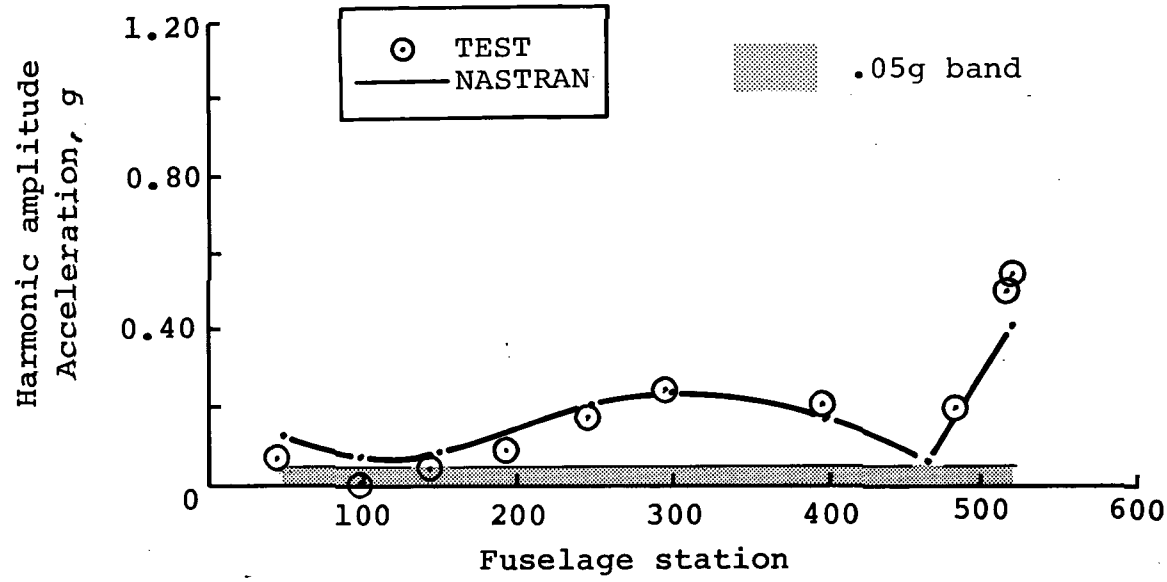

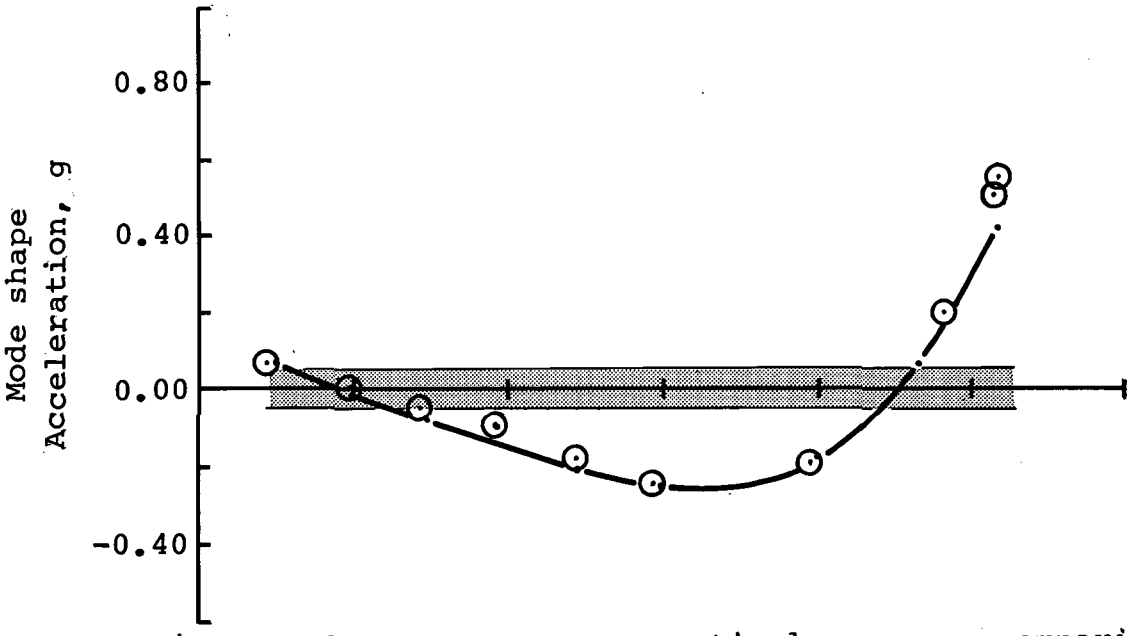

Figure B-7. - Two-per-rev vertical response comparison at 61 knots - wing stores.

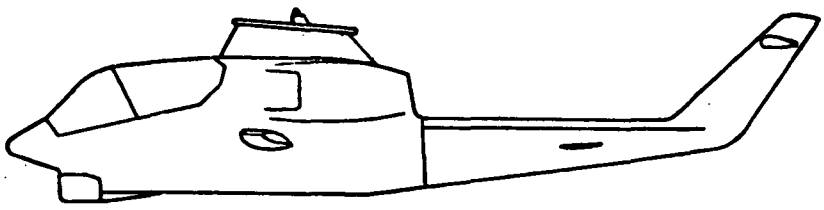

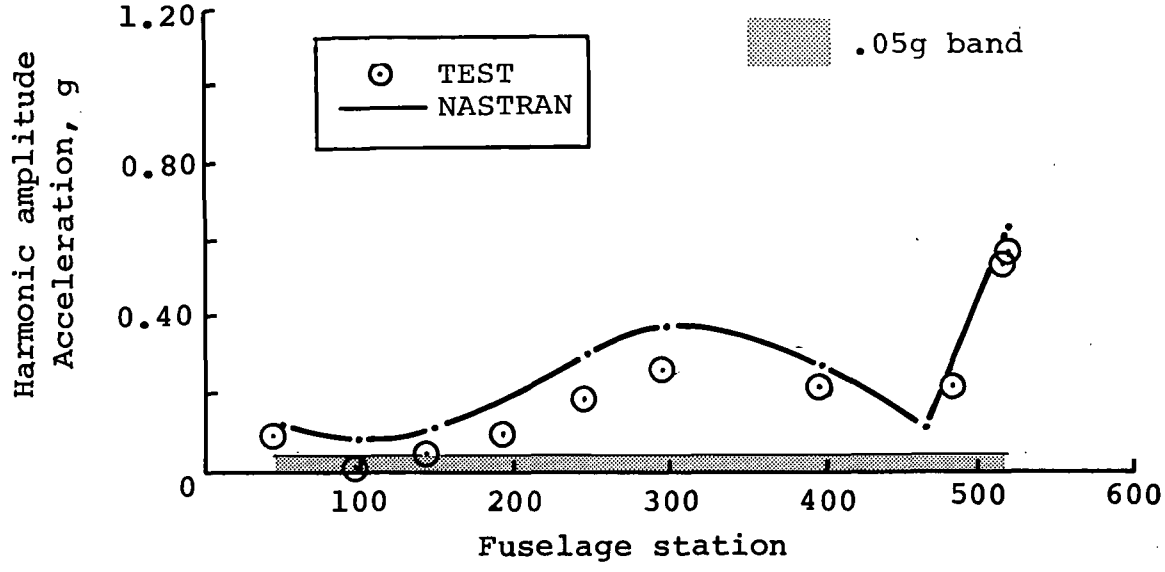

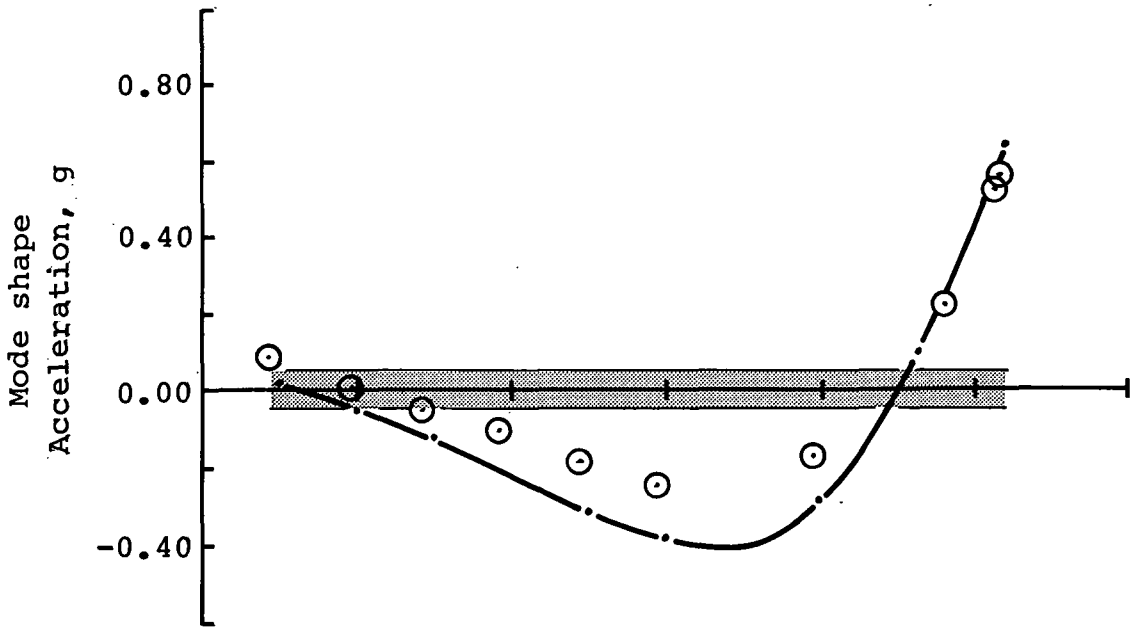

Figure B-8. - Two-per-rev vertical response comparison at 76 knots - wing stores.

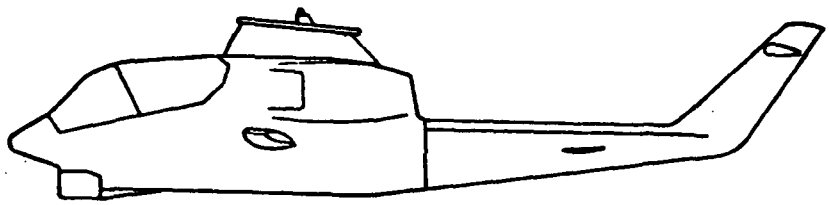

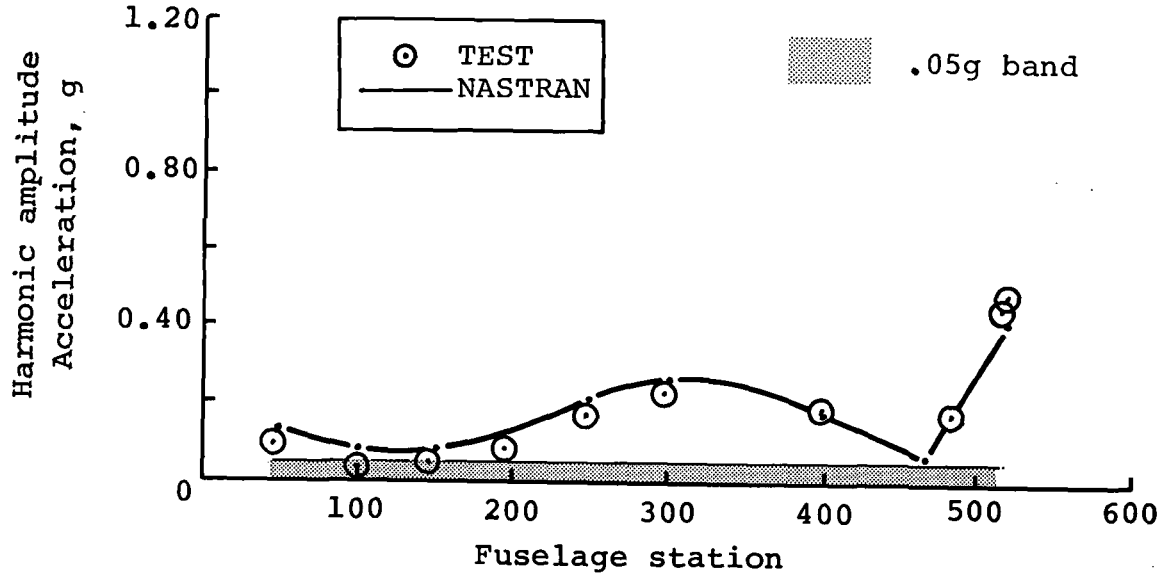

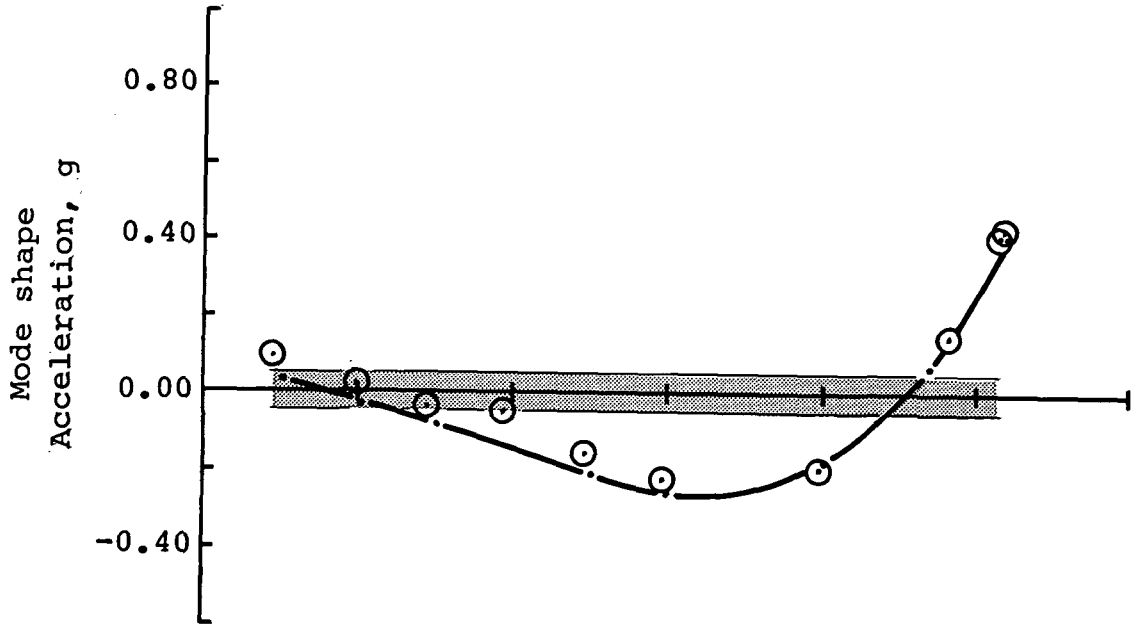

Figure B-9. - Two-per-rev vertical response comparison at 95 knots - wing stores.

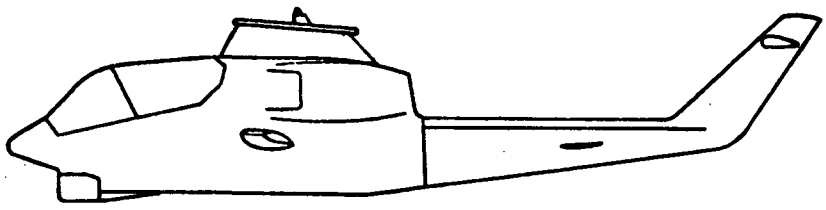

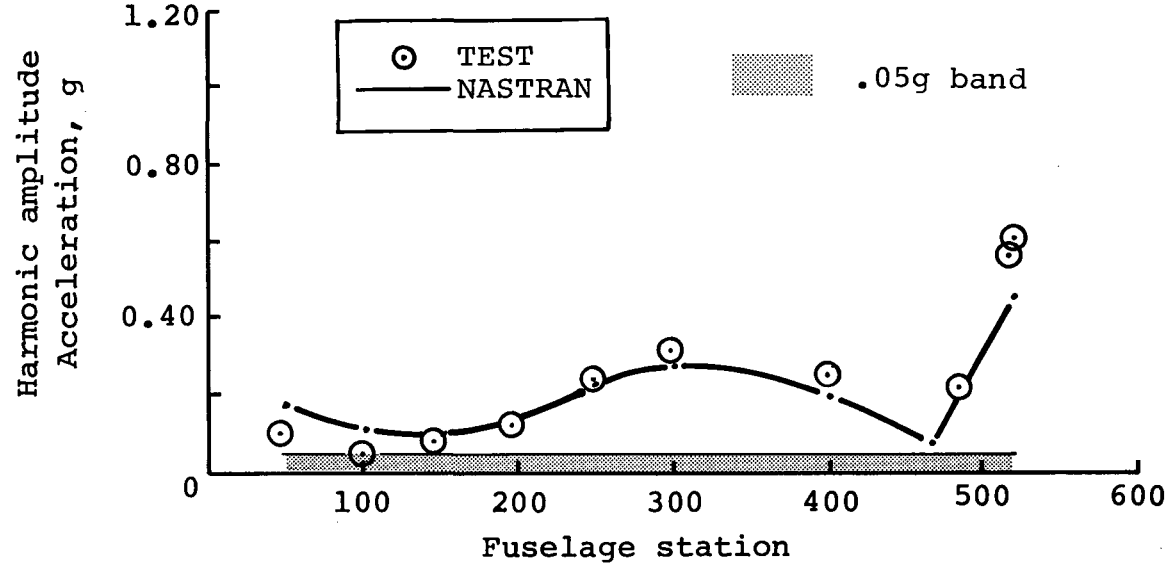

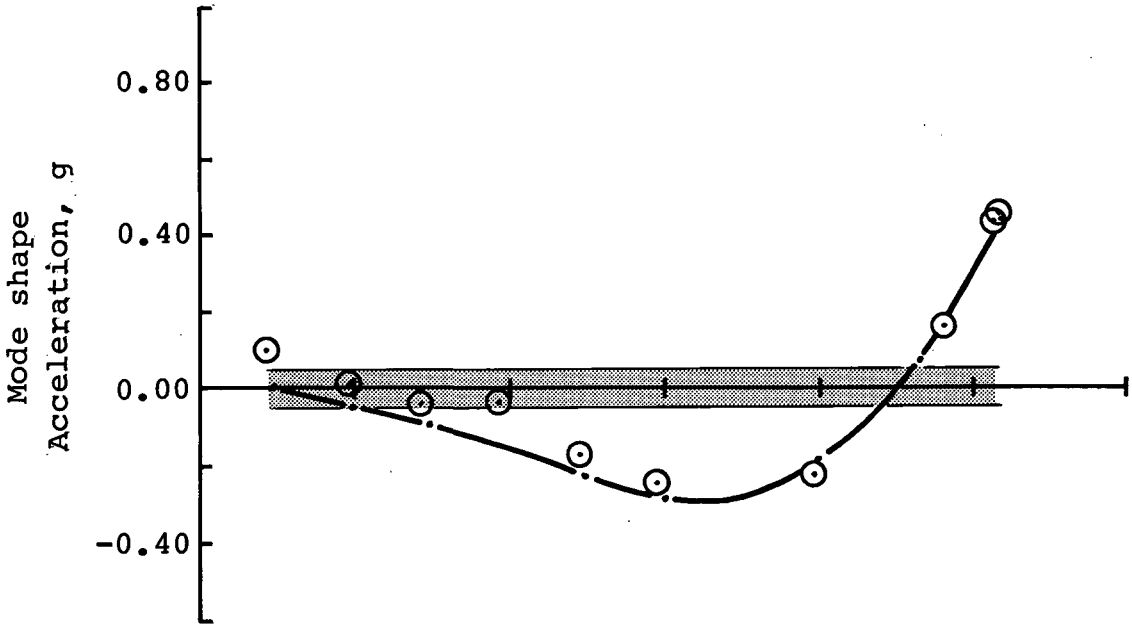

Figure B-10. - Two-per-rev vertical response comparison at 108 knots - wing stores.

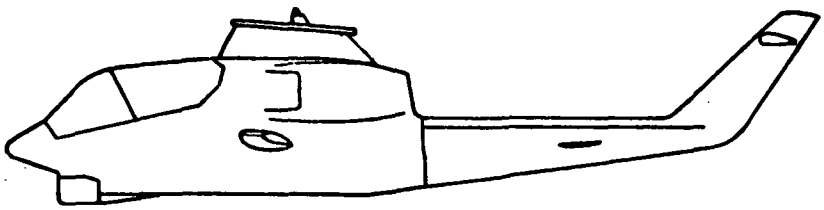

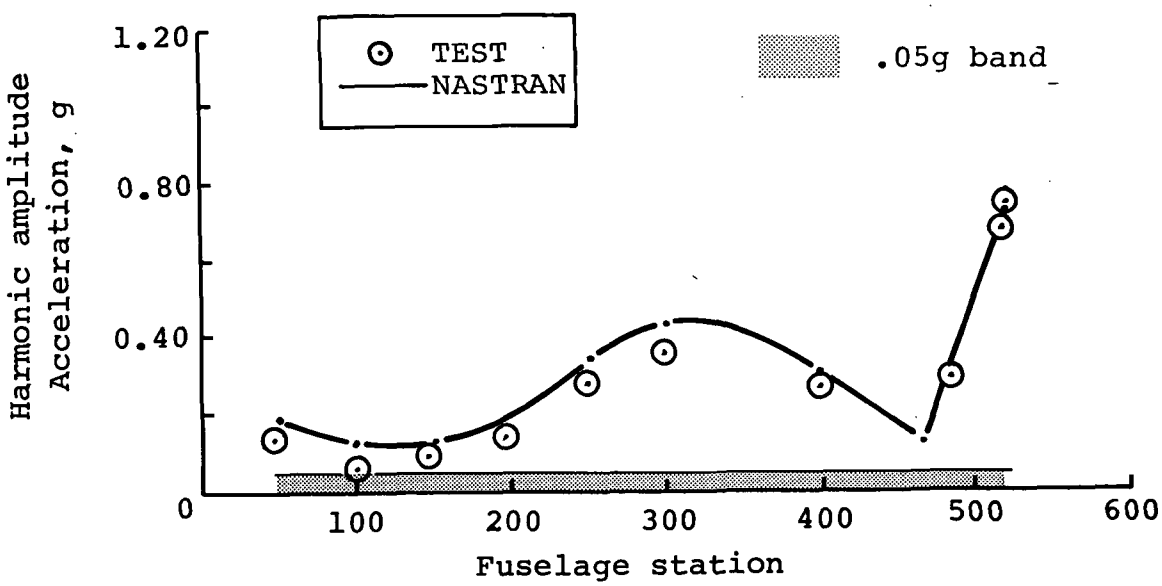

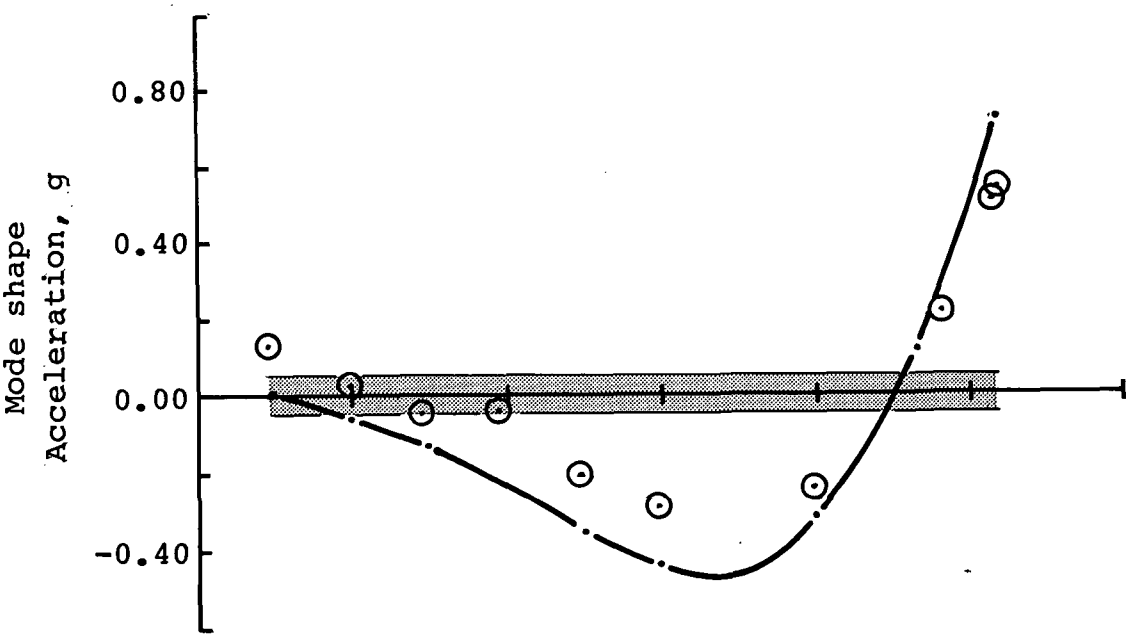

Figure B-11. - Two-per-rev vertical response comparison at 120 knots - wing stores.

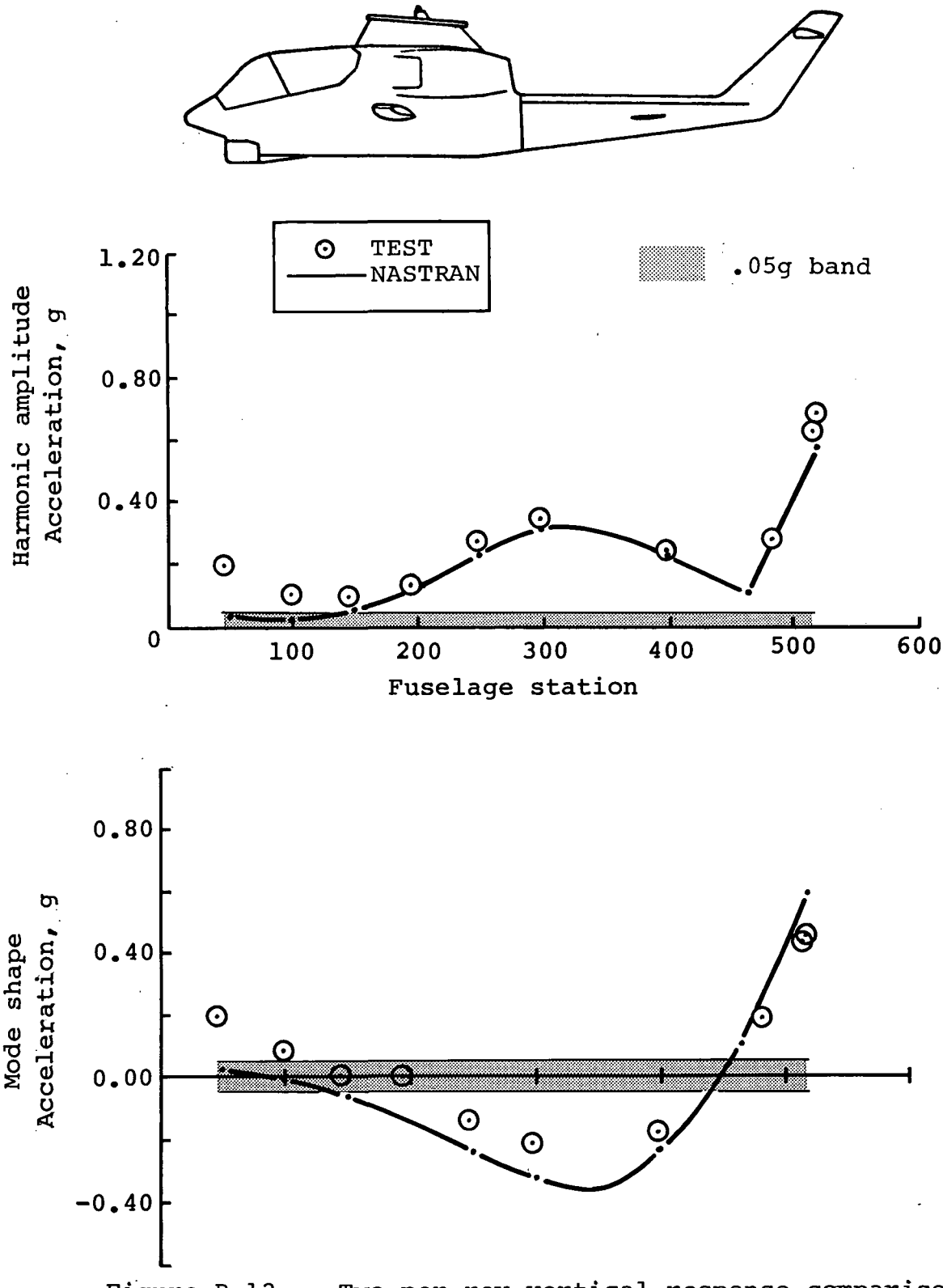

Figure B-12. - Two-per-rev vertical response comparison at 134 knots - wing stores.

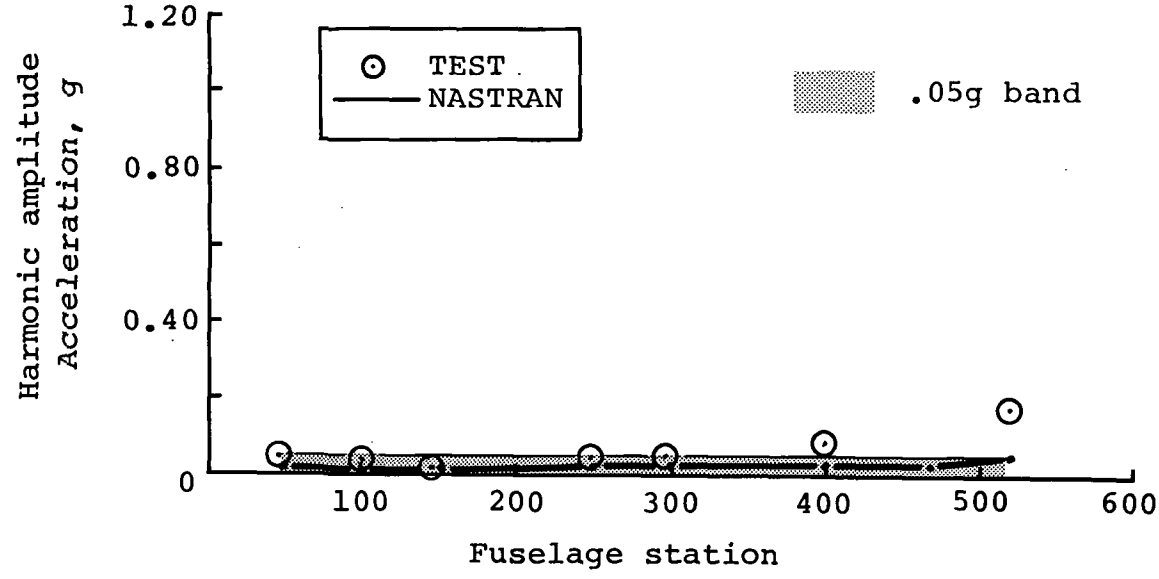

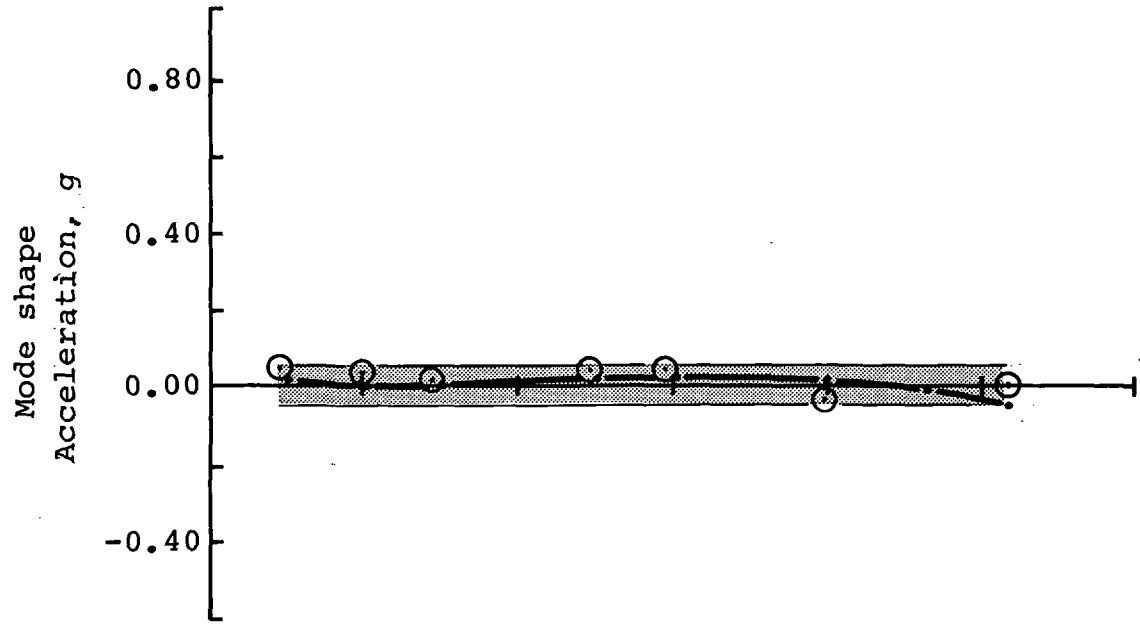

Figure B-13. - Two-per-rev lateral response comparison at 67 knots - clean wing.

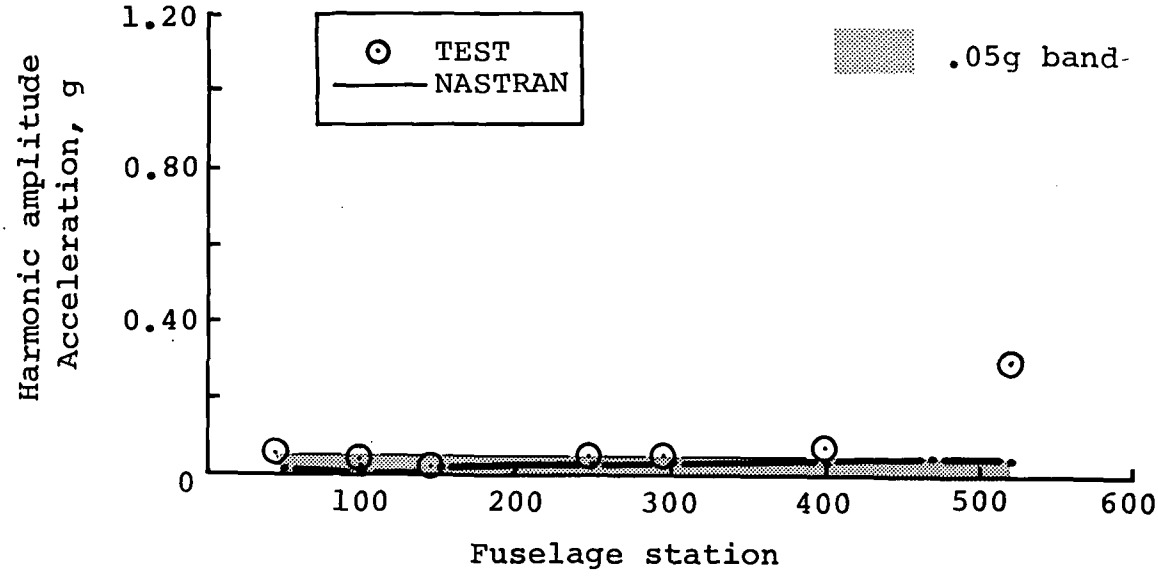

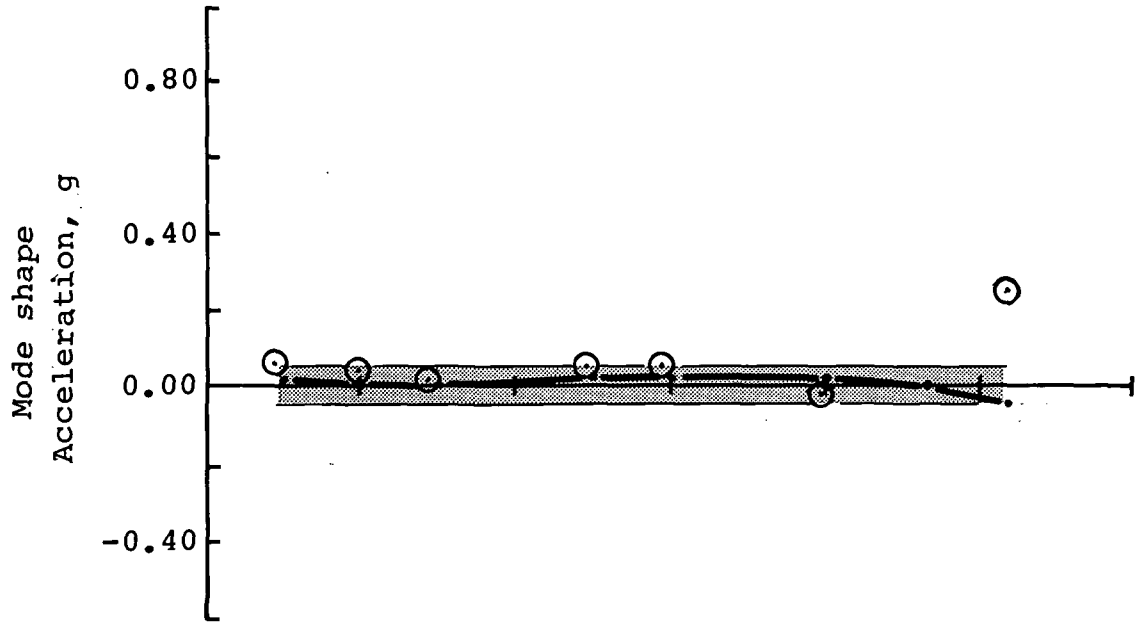

Figure B-14. - Two-per-rev lateral response comparison at 85 knots - clean wing.

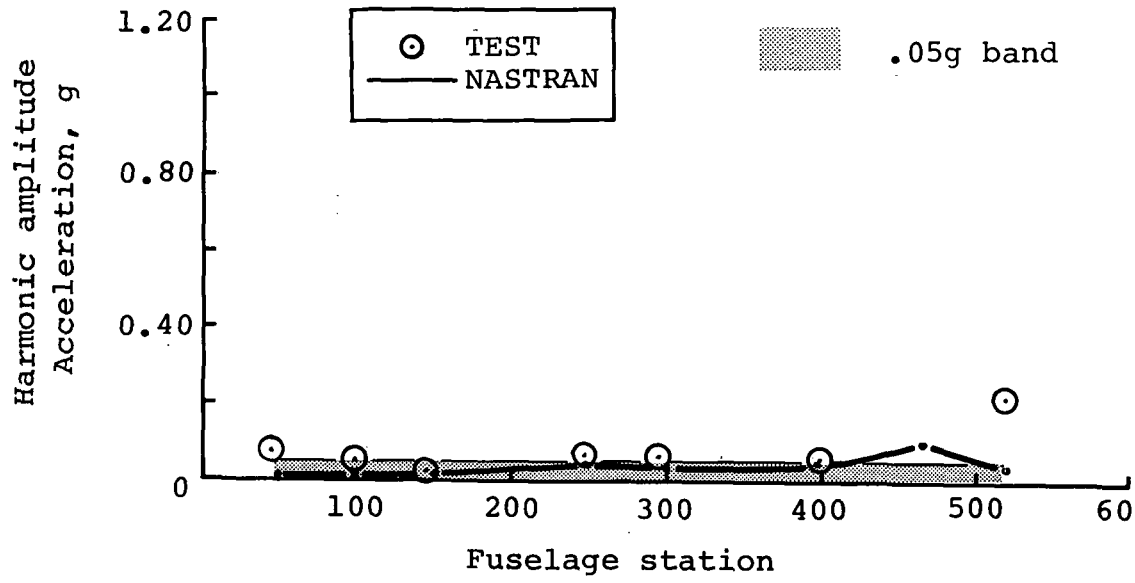

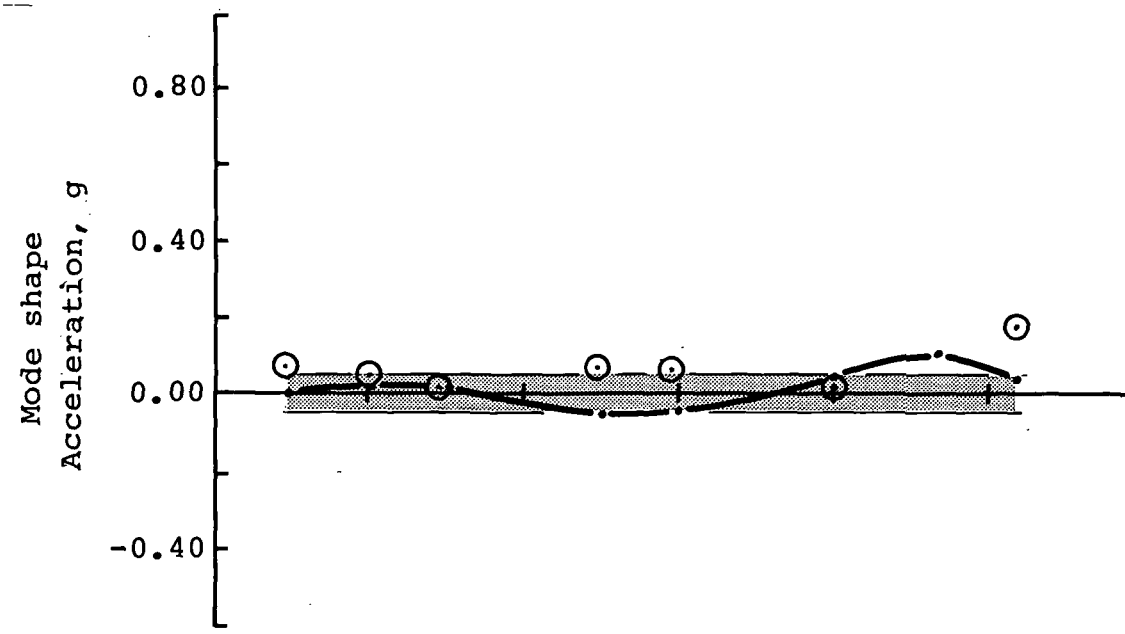

Figure B-15. - Two-per-rev lateral response comparison at 101 knots - clean wing.

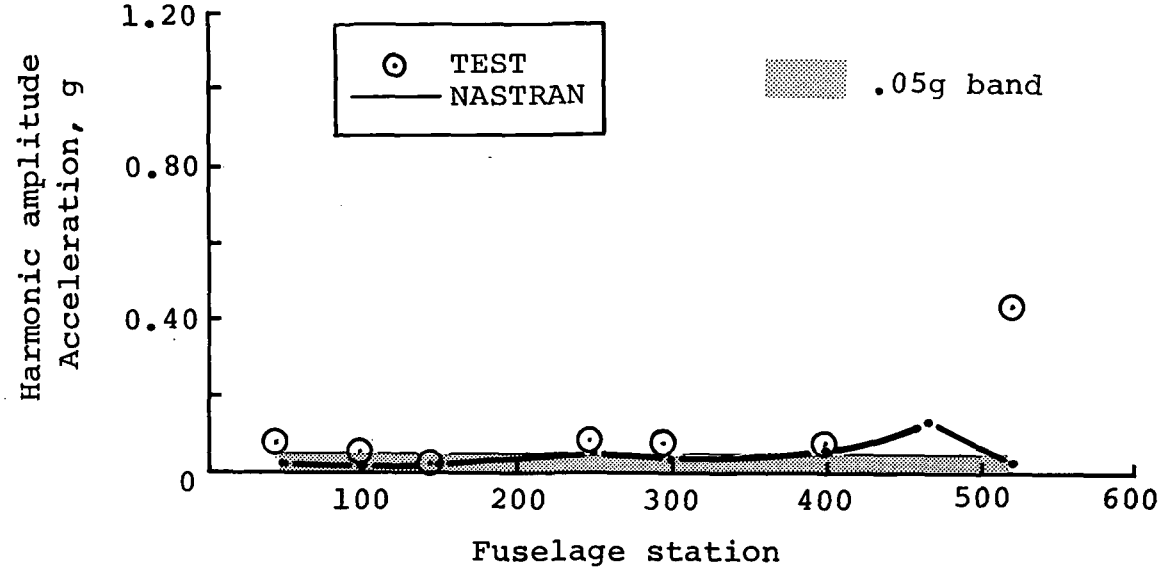

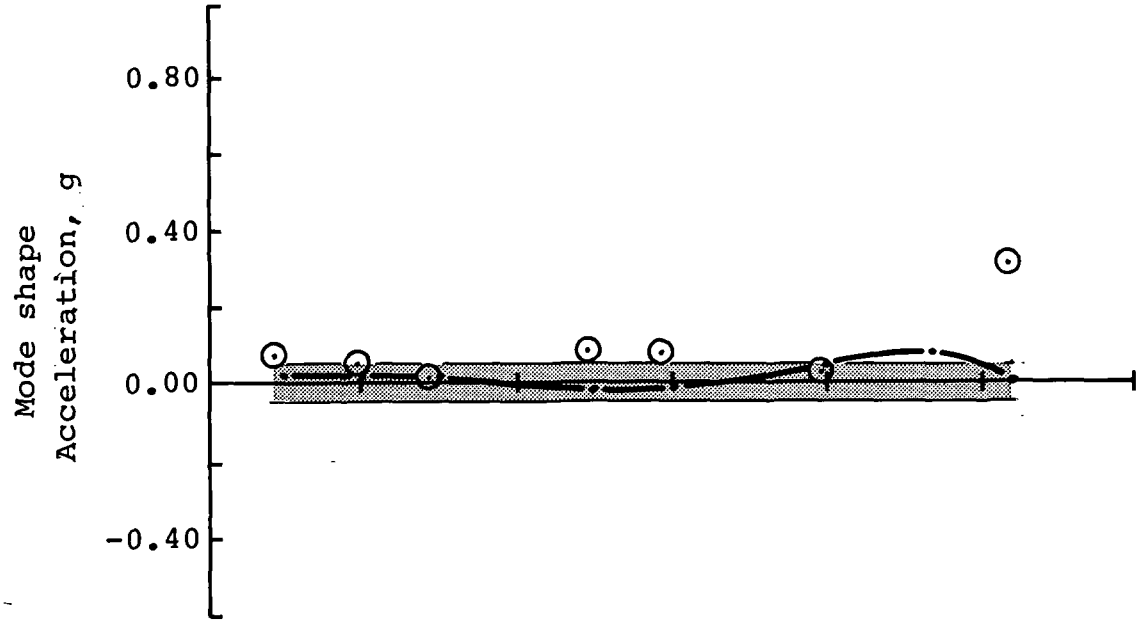

Figure B-16. - Two-per-rev lateral response comparison at 114 knots - clean wing.

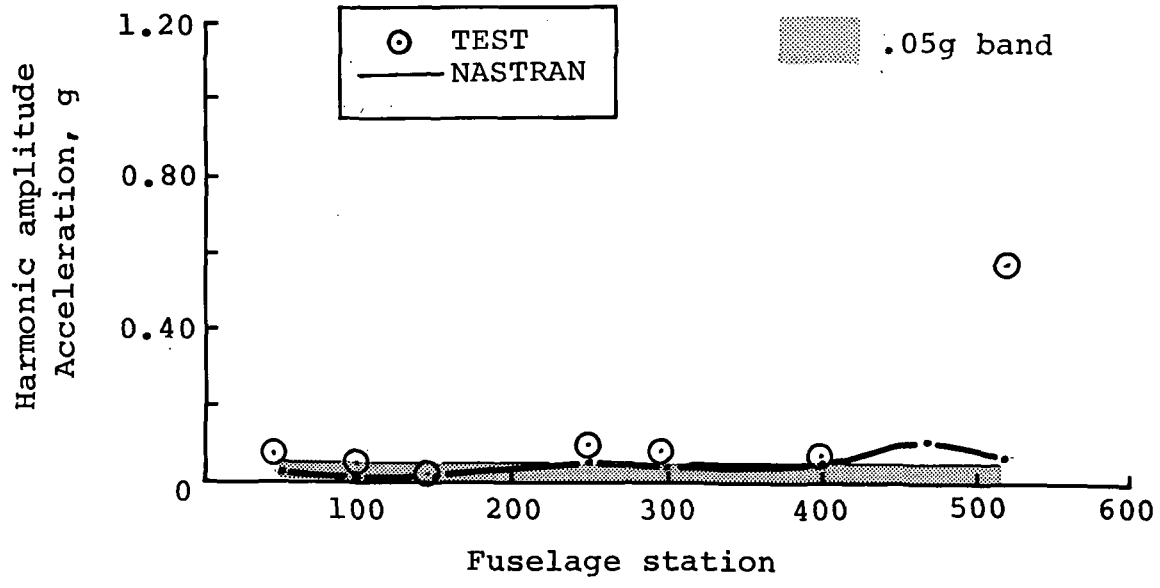

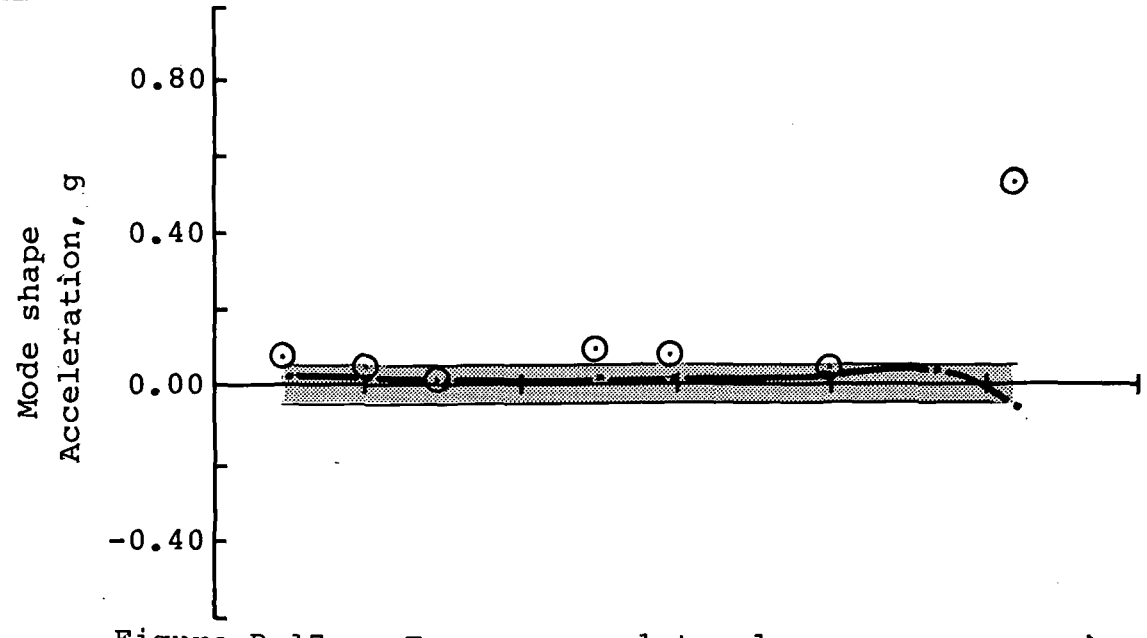

Figure B-17. - Two-per-rev lateral response comparison at 128 knots - clean wing.

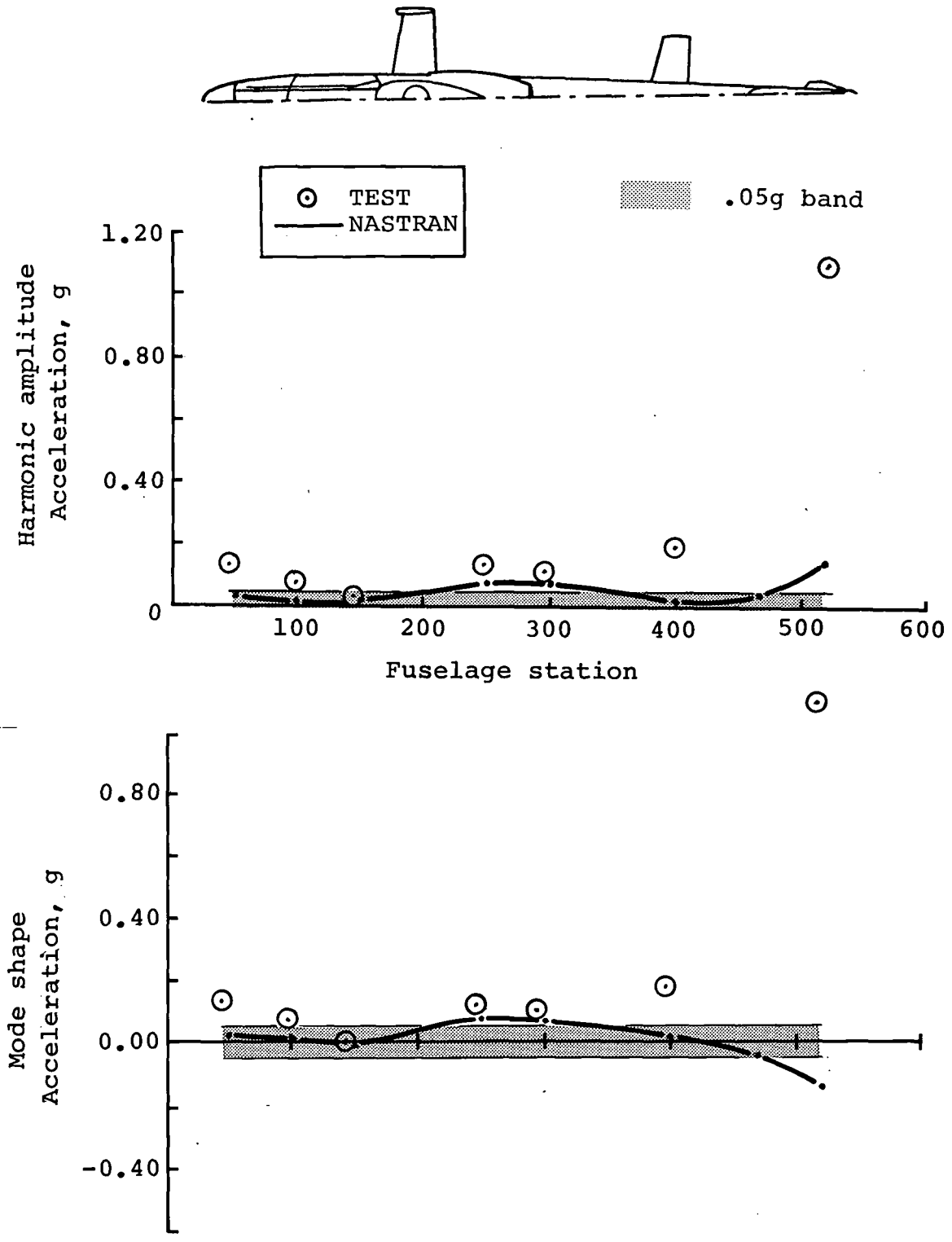

Figure B-18. - Two-per-rev lateral response comparison at 142 knots - clean wing.

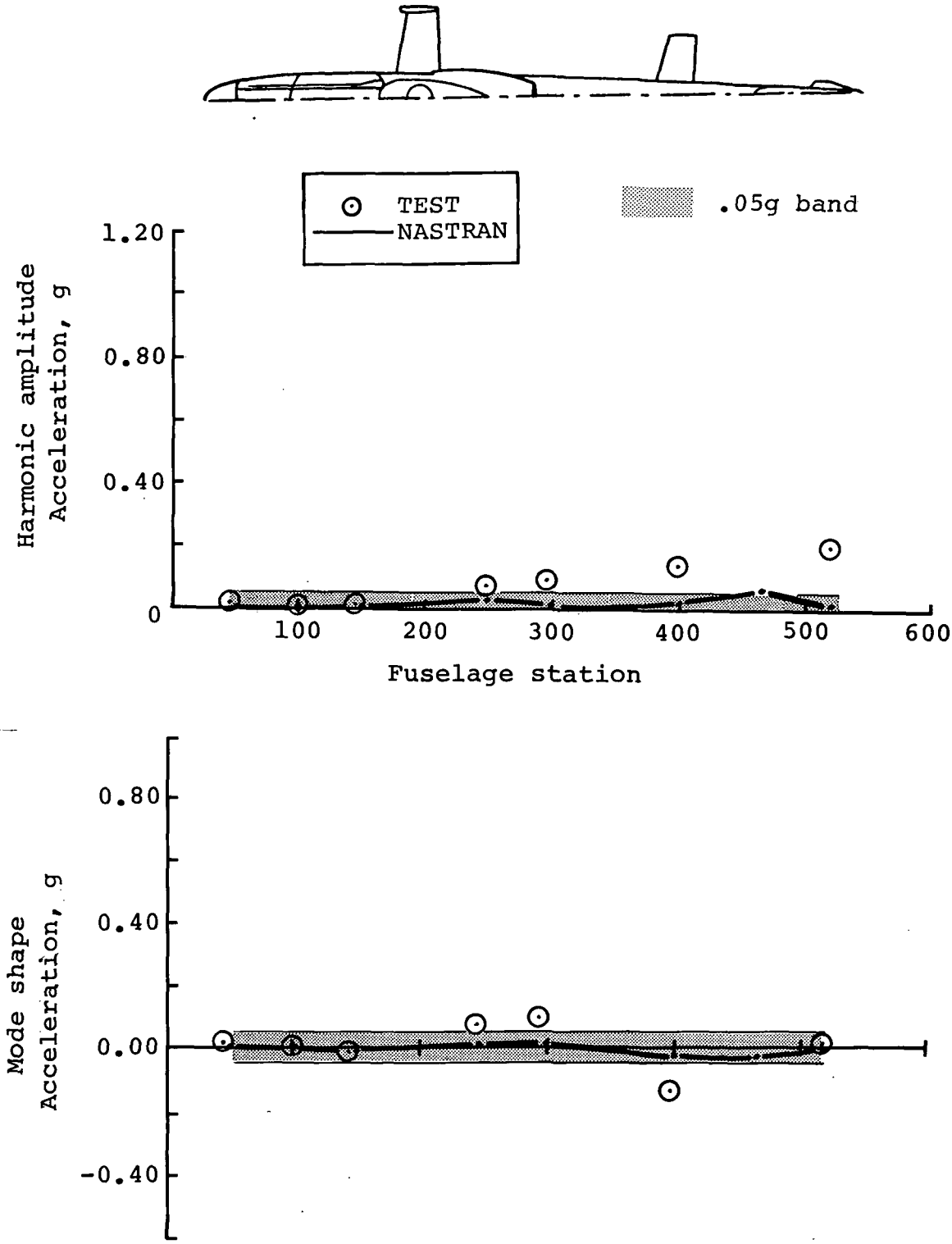

Figure B-19. - Two-per-rev lateral response comparison at 61 knots - wing stores.

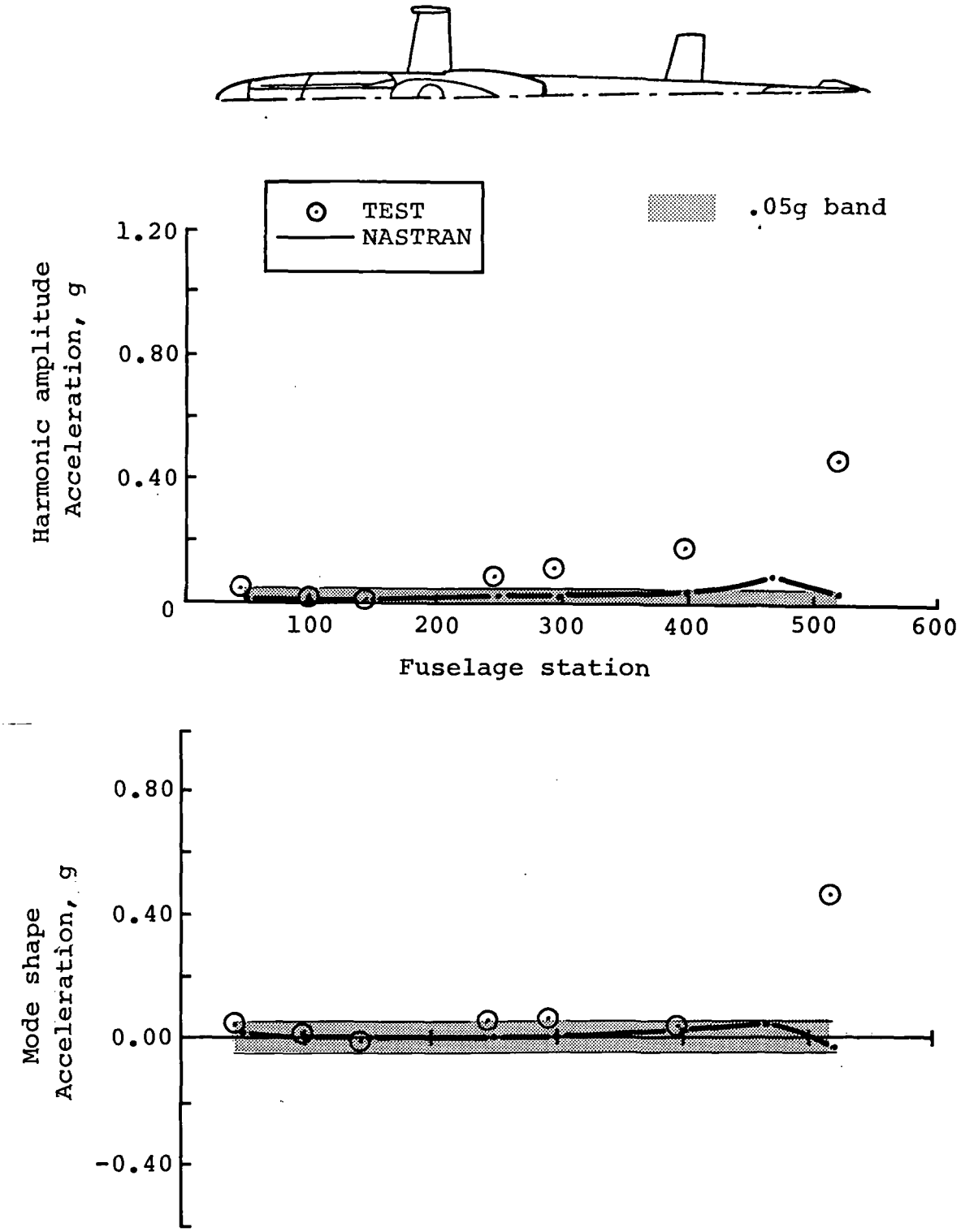

Figure B-20. - Two-per-rev lateral response comparison at 76 knots - wing stores.

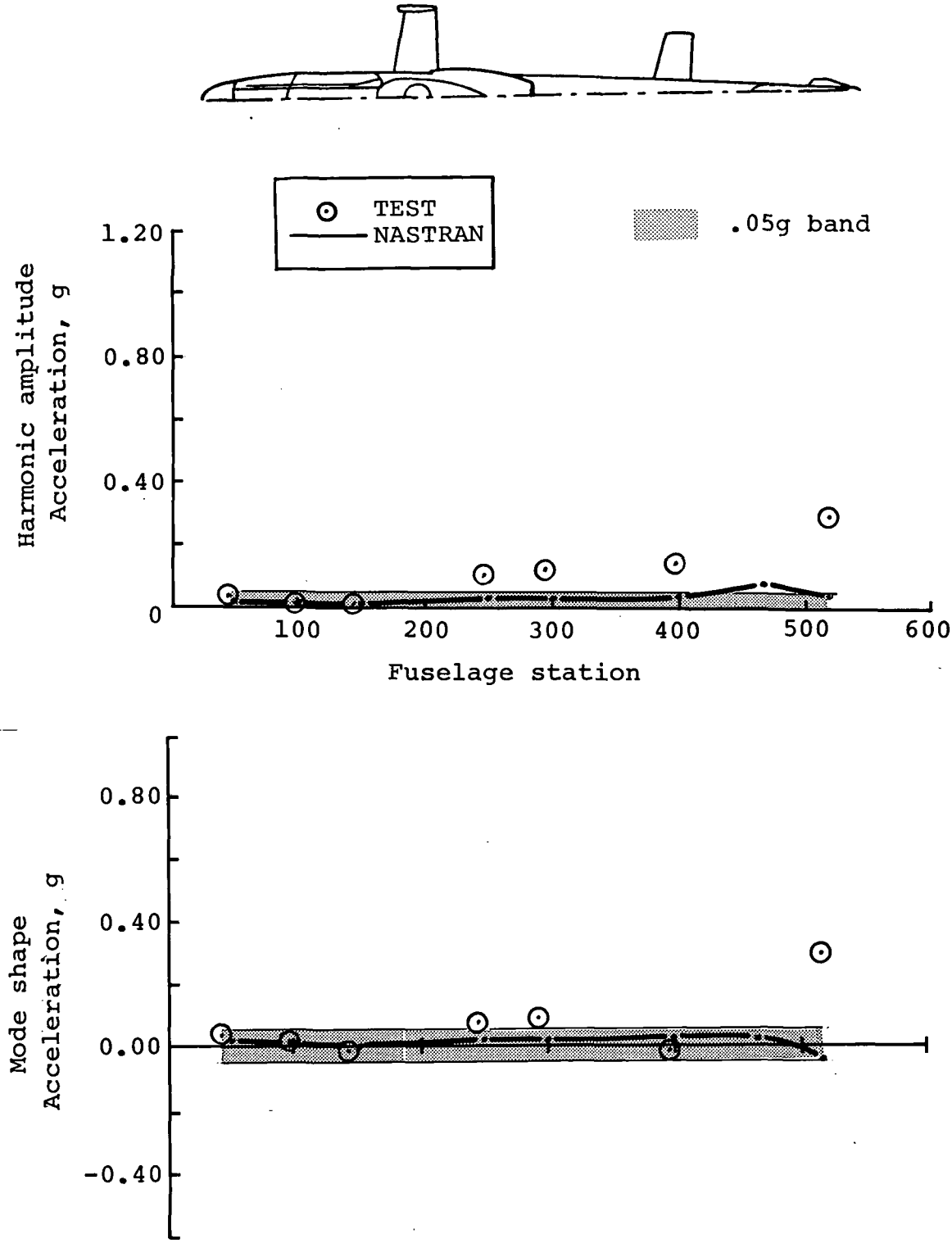

Figure B-21. - Two-per-rev lateral response comparison at 95 knots - wing stores.

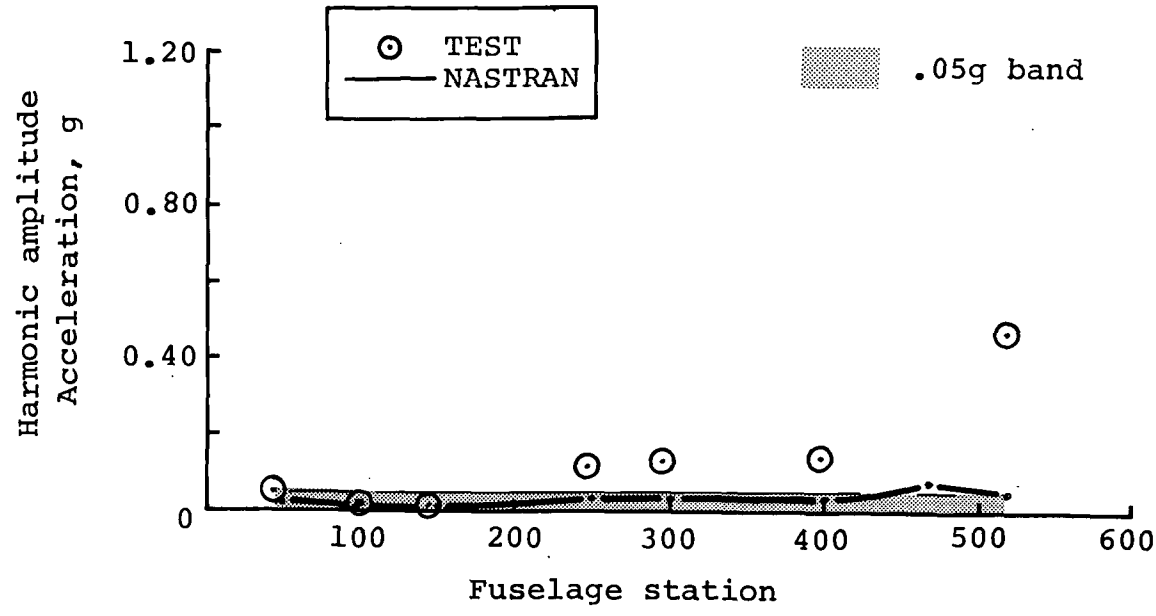

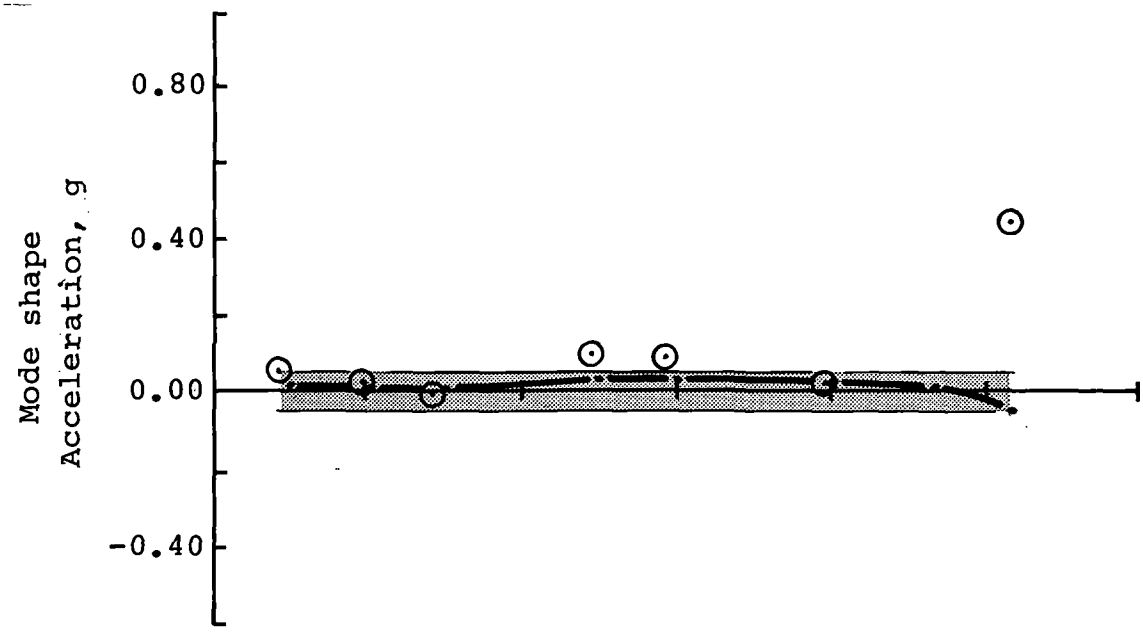

Figure B-22. - Two-per-rev lateral response comparison at 108 knots - wing stores.

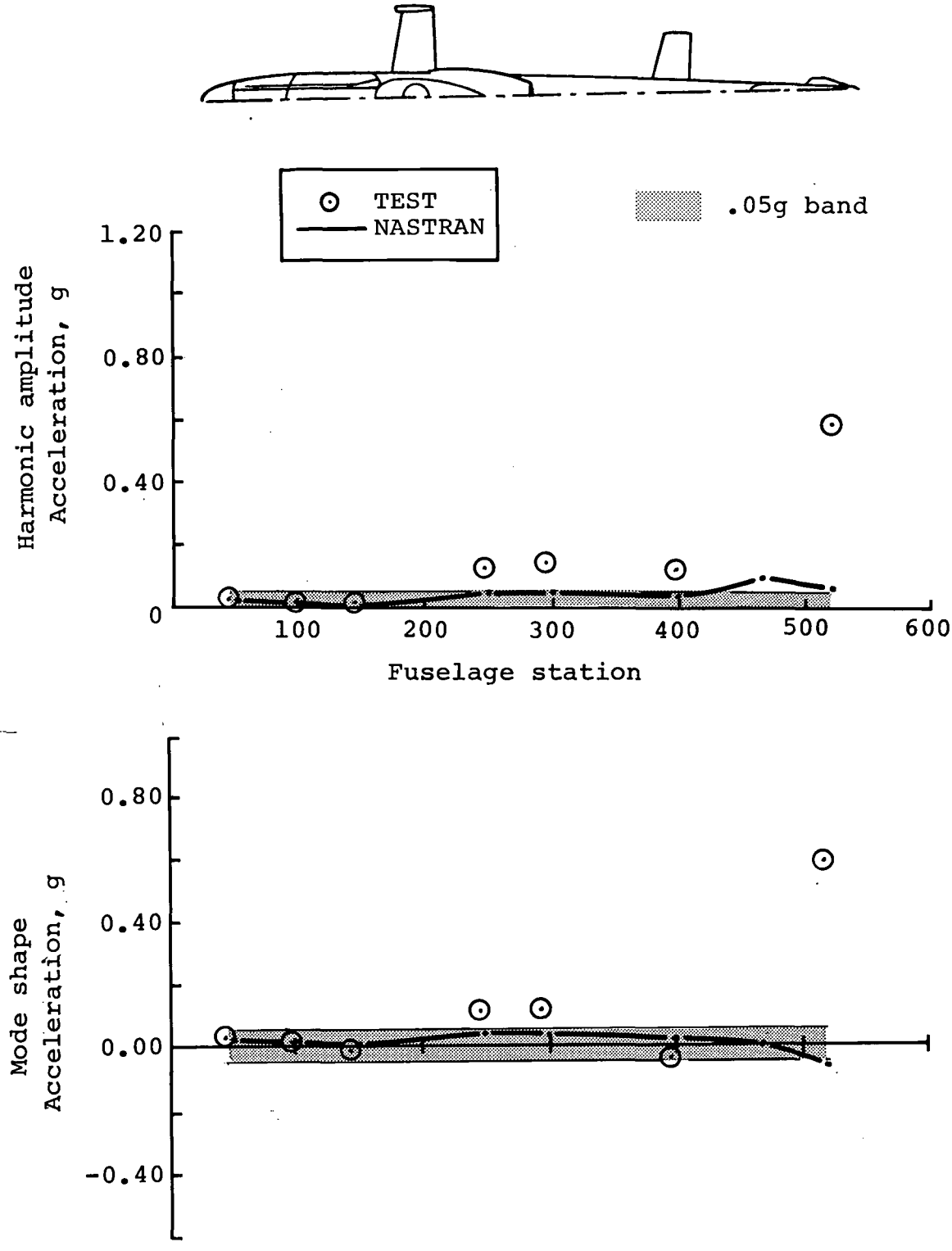

Figure B-23. - Two-per-rev lateral response comparison at 120 knots - wing stores.

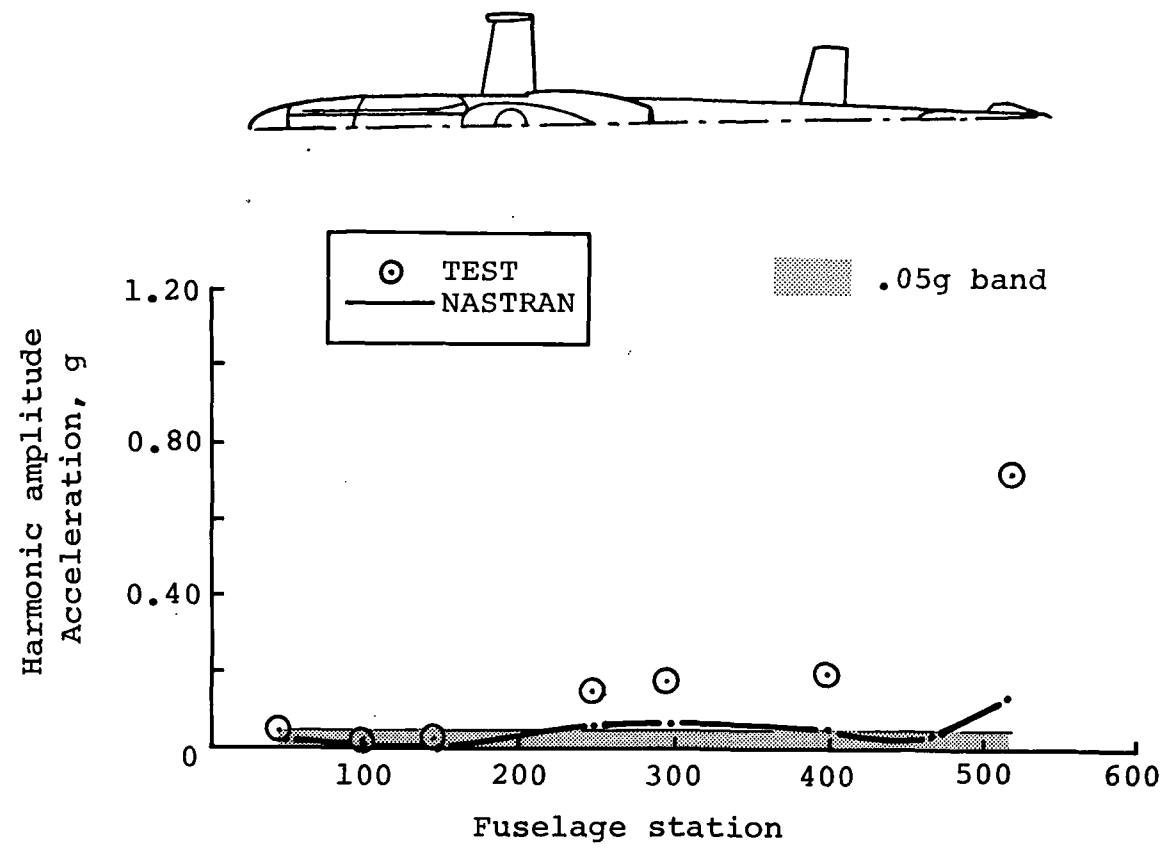

Figure B-24. - Two-per-rev lateral response comparison at 134 knots - wing stores.

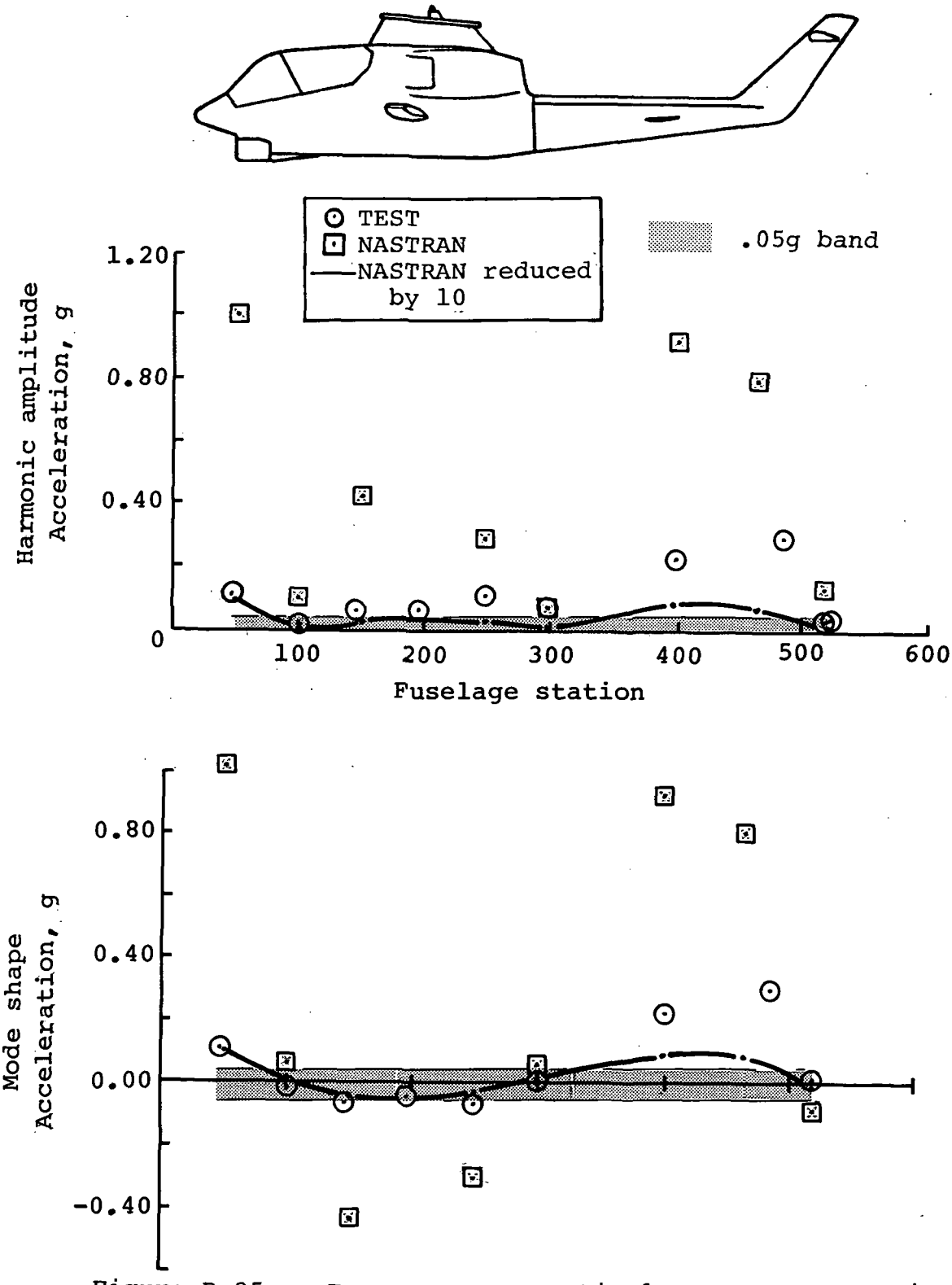

Figure B-25. - Four-per-rev vertical response comparison at 67 knots - clean wing.

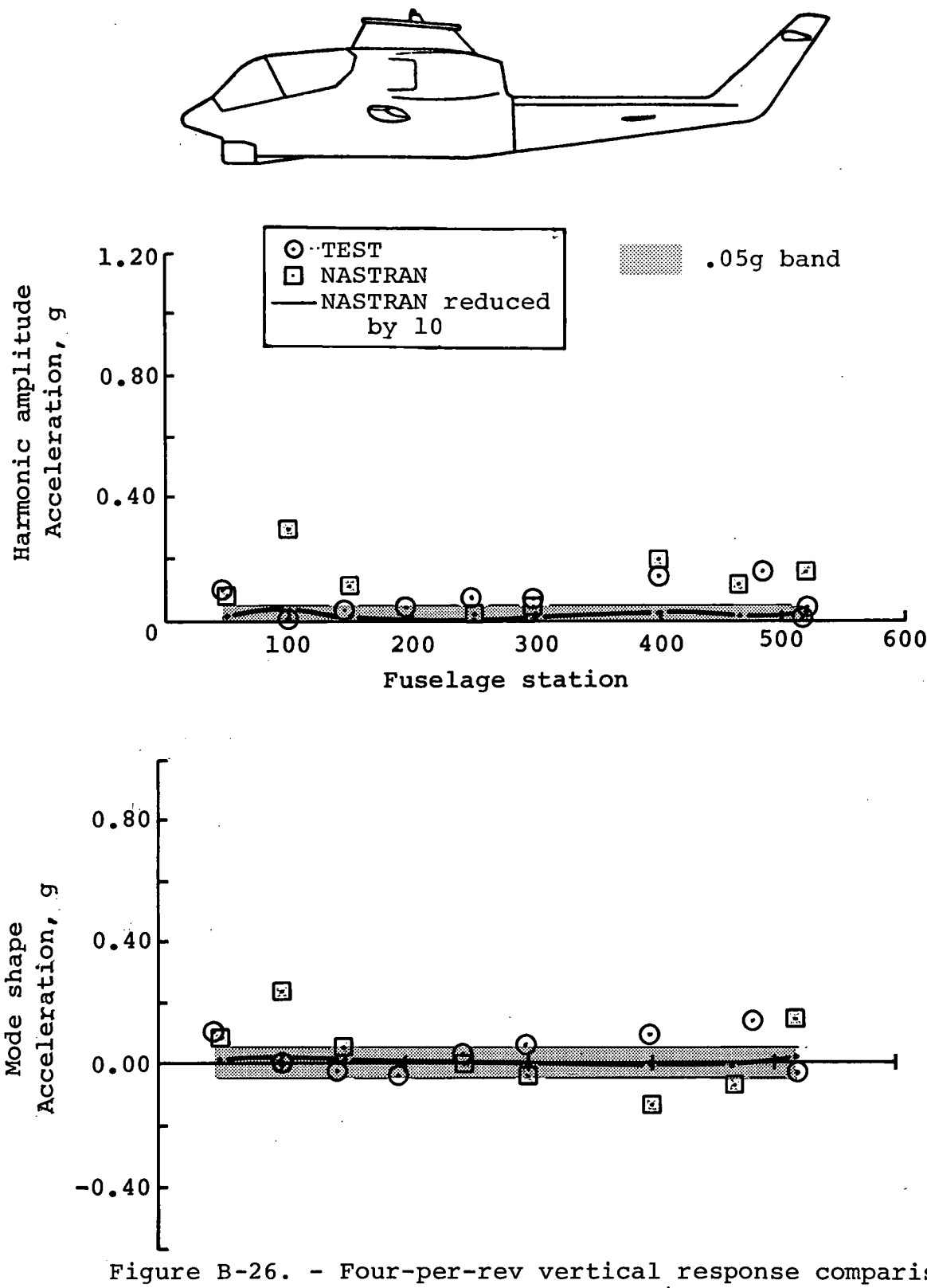

Figure B-26. - Four-per-rev vertical response comparison at 85 knots - clean wing.

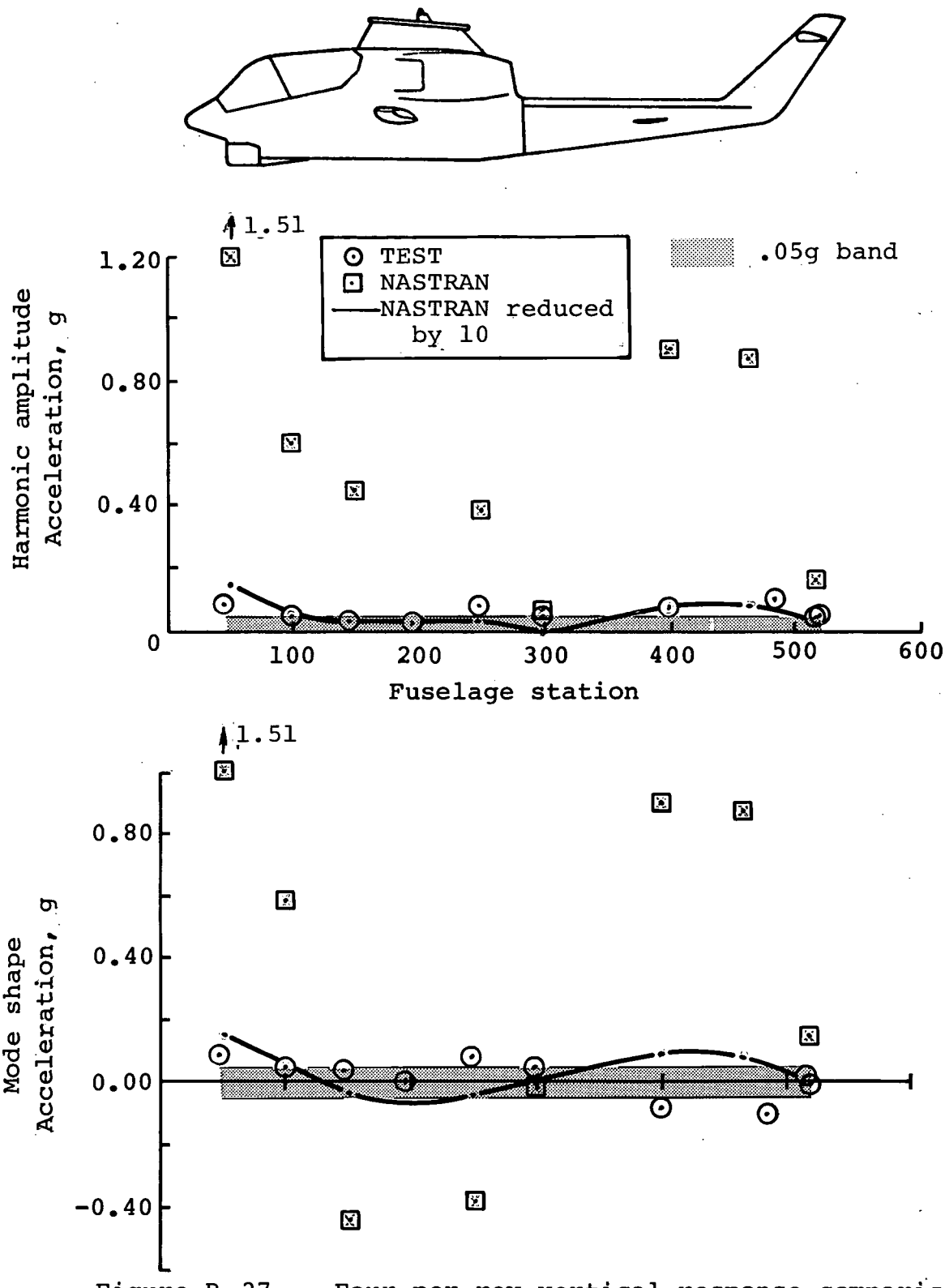

Figure B-27. - Four-per-rev vertical response comparison at 101 knots - clean wing.

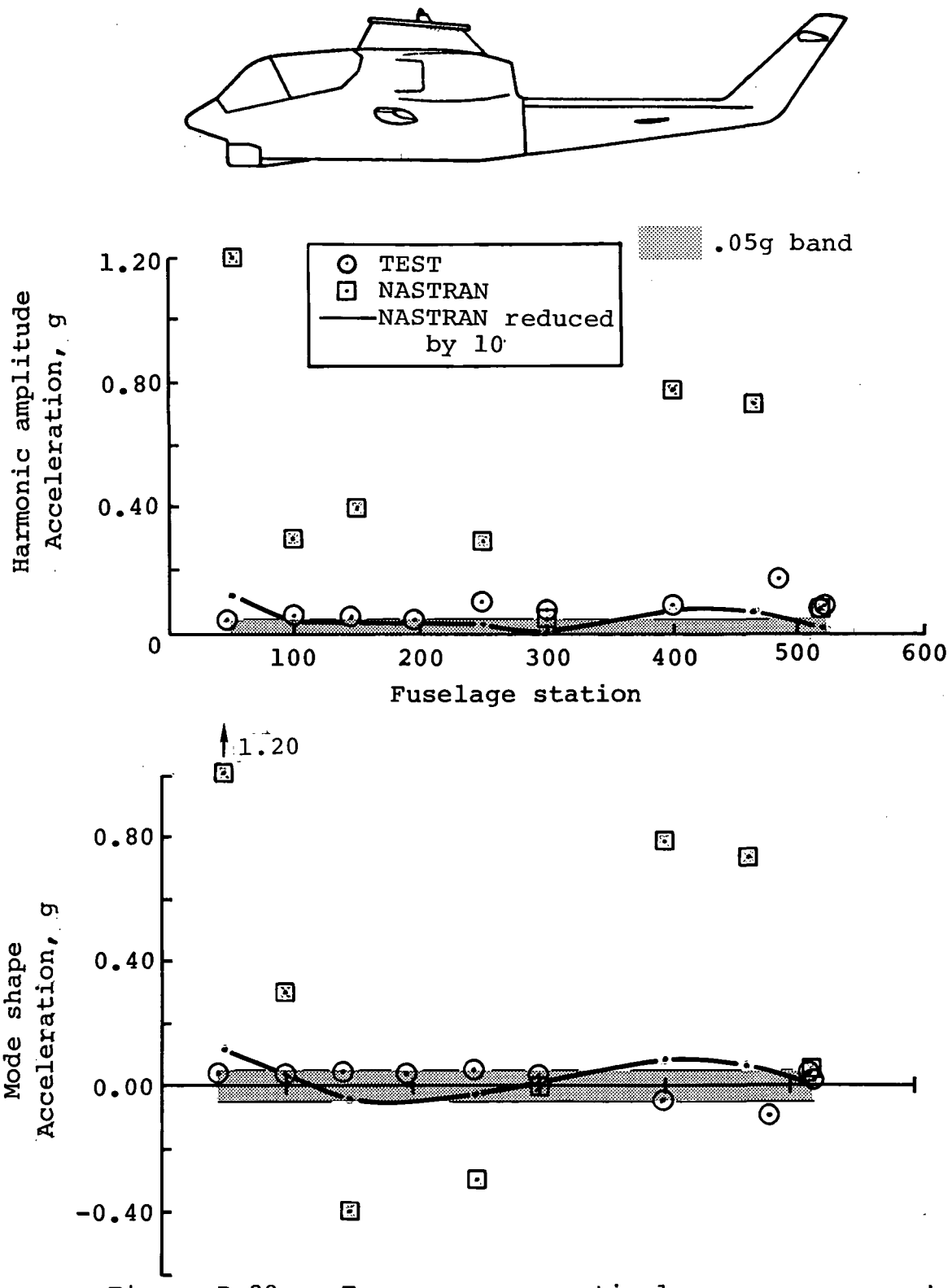

Figure B-28. - Four-per-rev vertical response comparison at 114 knots - clean wing.

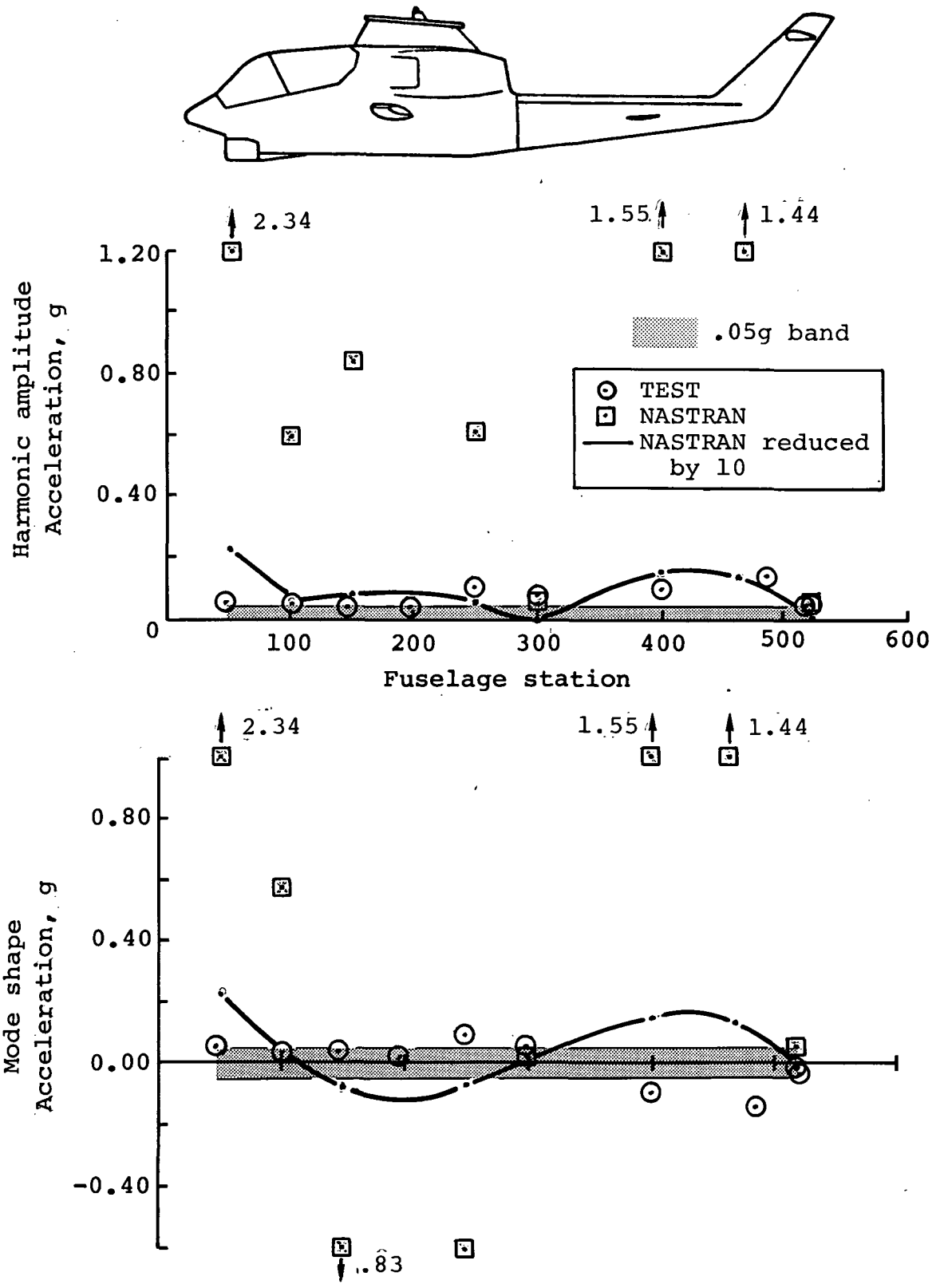

Figure B-29. - Four-per-rev vertical response comparison at 128 knots - clean wing.

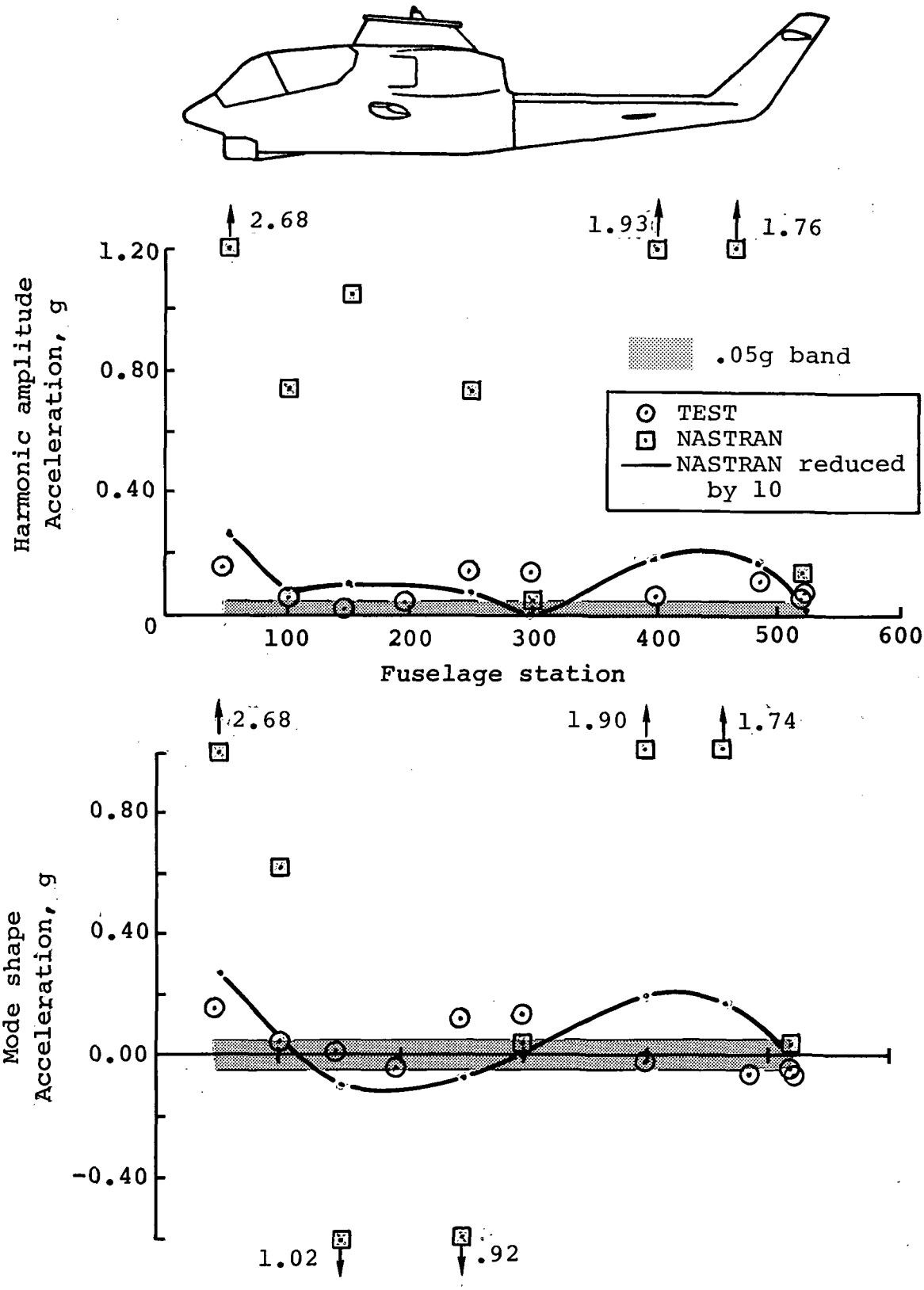

Figure B-30. - Four-per-rev vertical response comparison at 142 knots - clean wing.

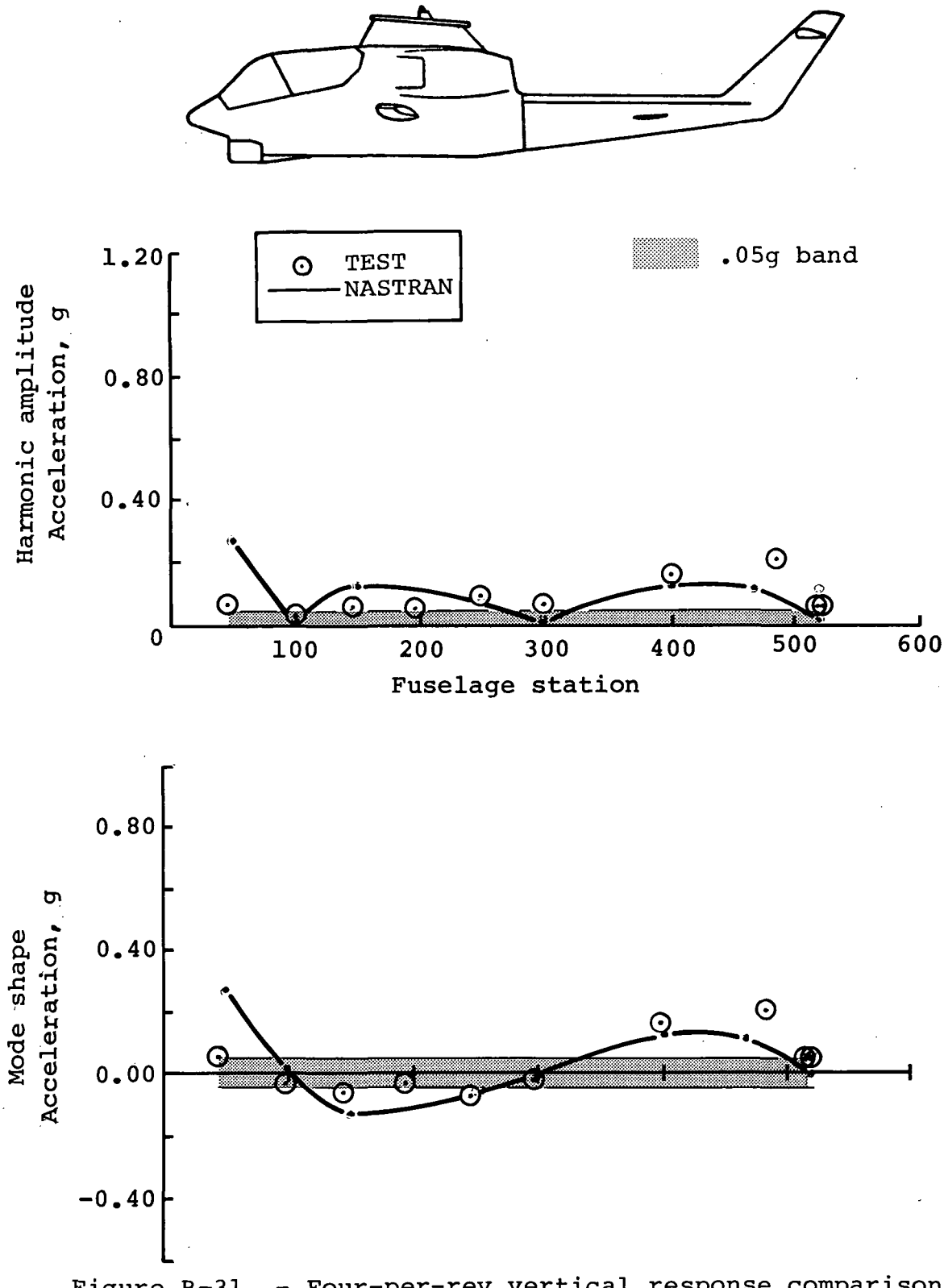

Figure B-31. - Four-per-rev vertical response comparison at 61 knots - wing stores.

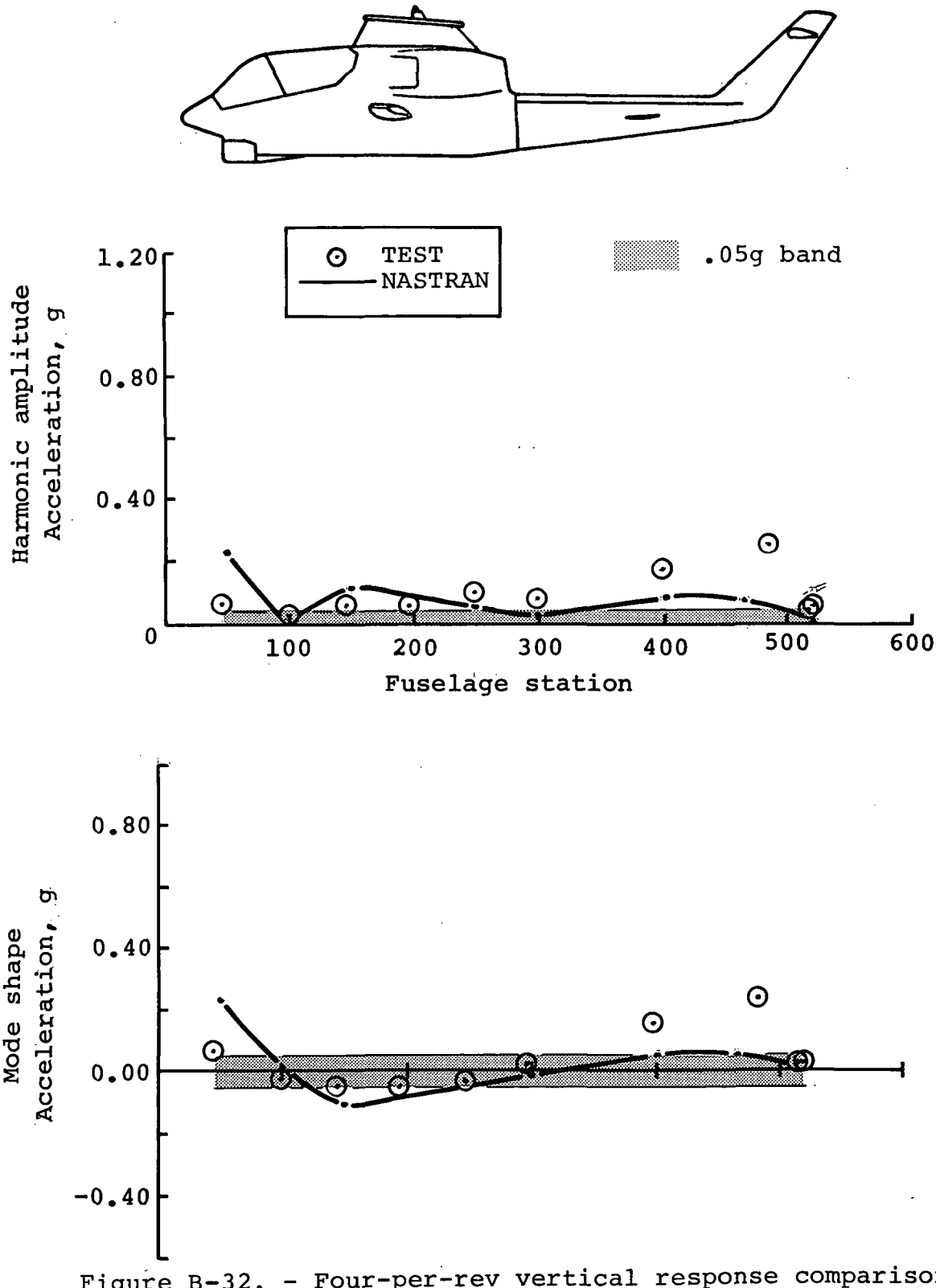

Figure B-32. - Four-per-rev vertical response comparison at 76 knots - wing stores.

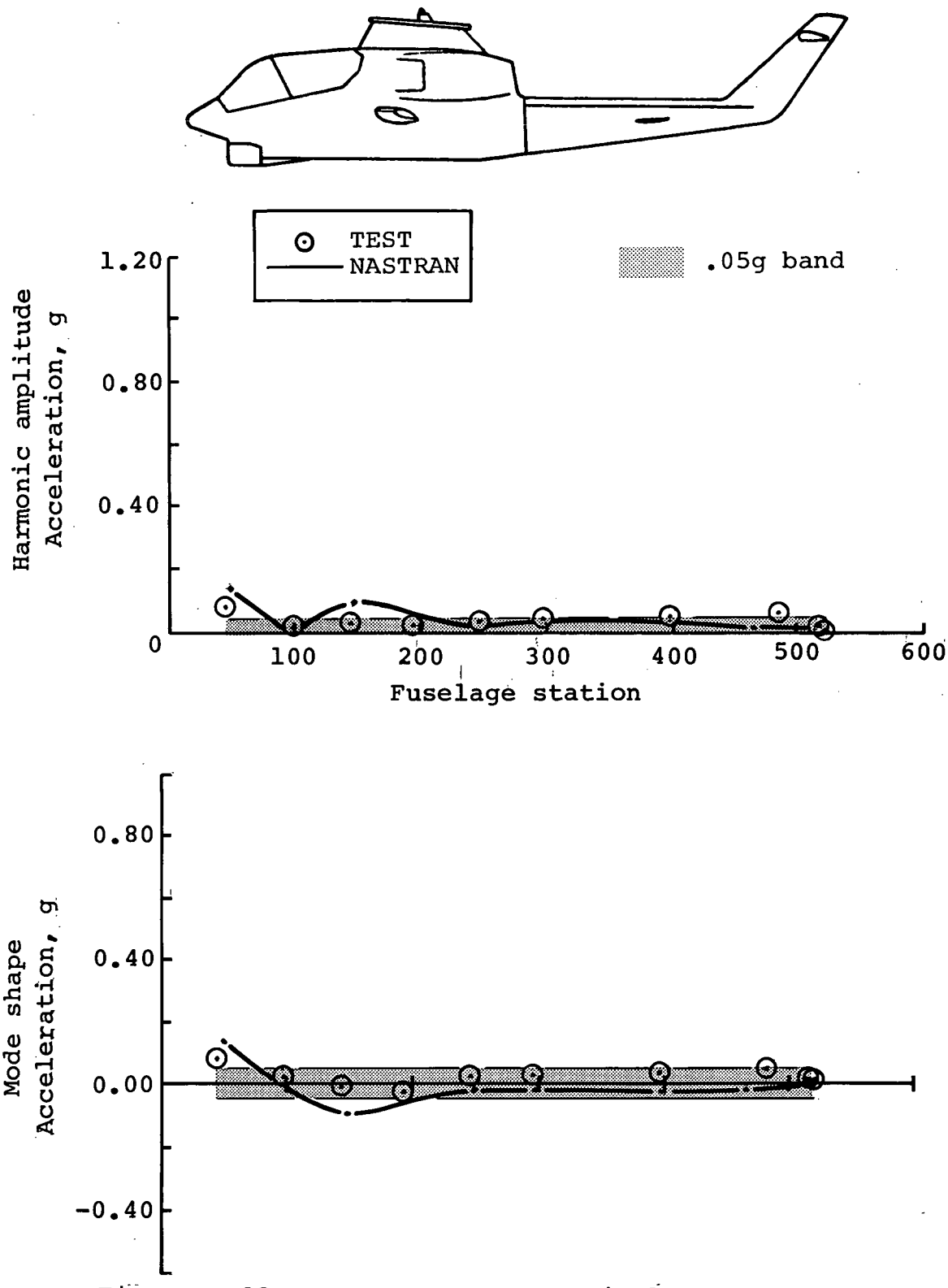

Figure B-33. - Four-per-rev vertical response comparison at 95 knots - wing stores.

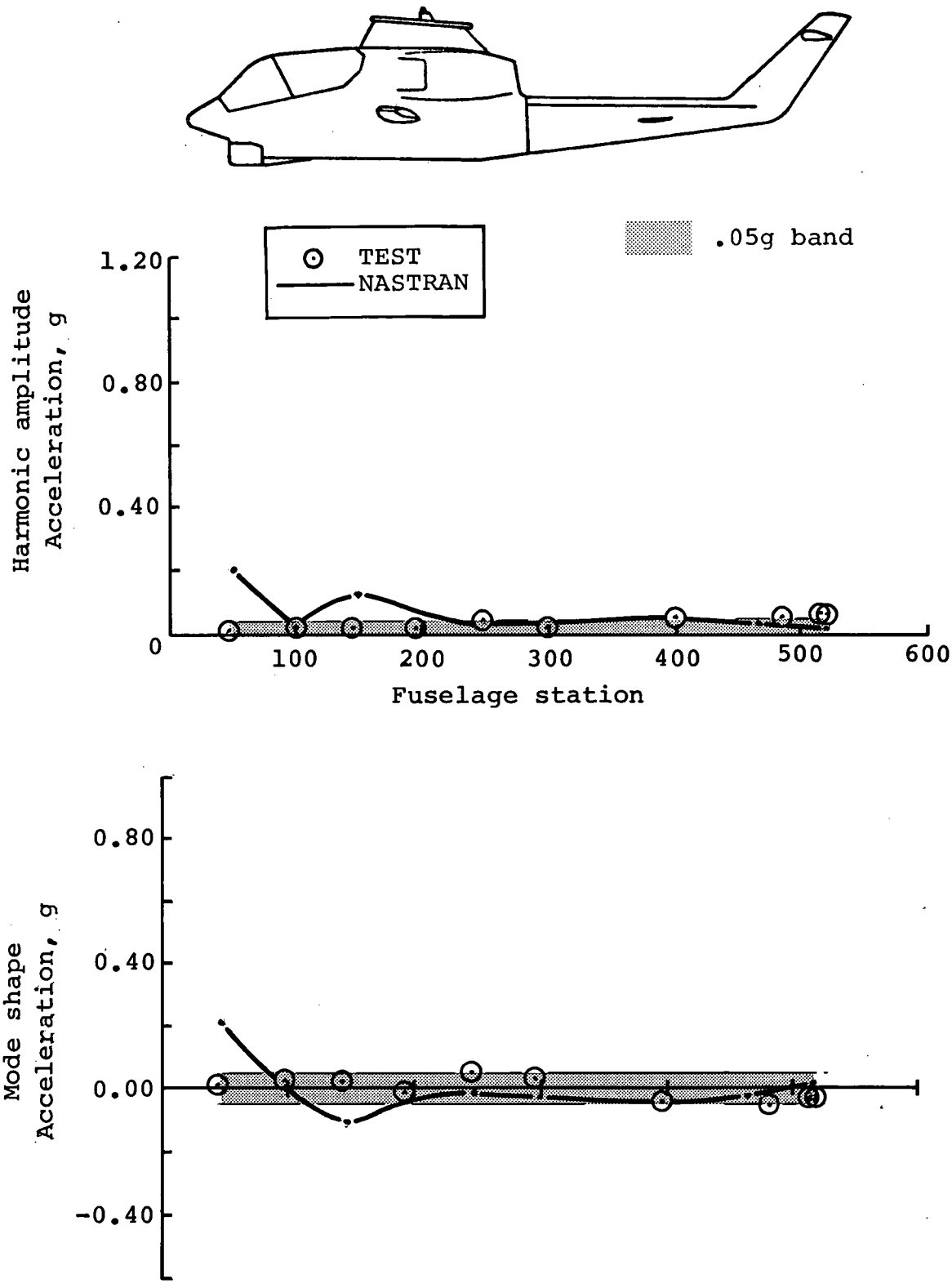

Figure B-34. - Four-per-rev vertical response comparison at 108 knots - wing stores.

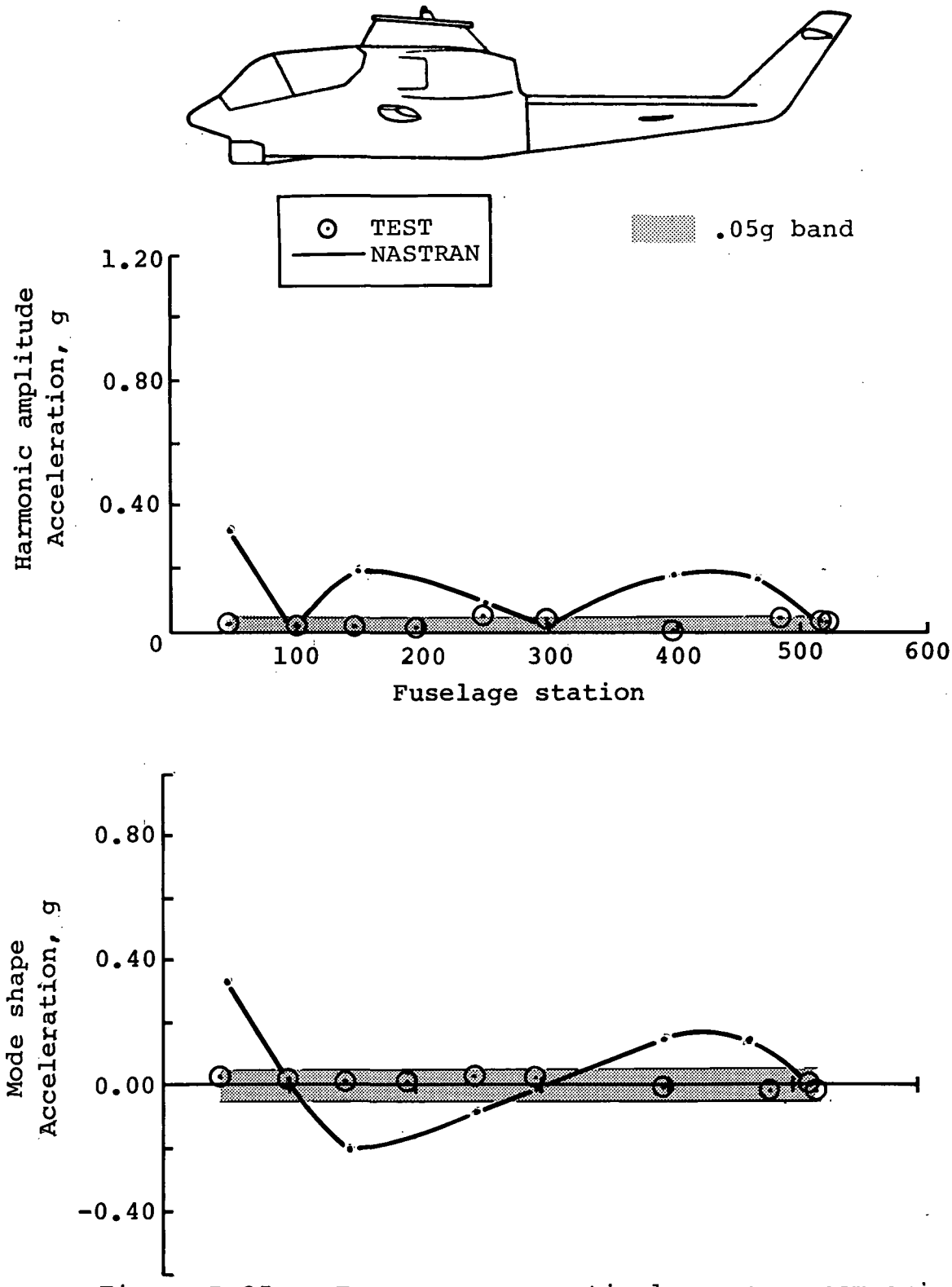

Figure B-35. - Four-per-rev vertical response comparison at 120 knots - wing stores.

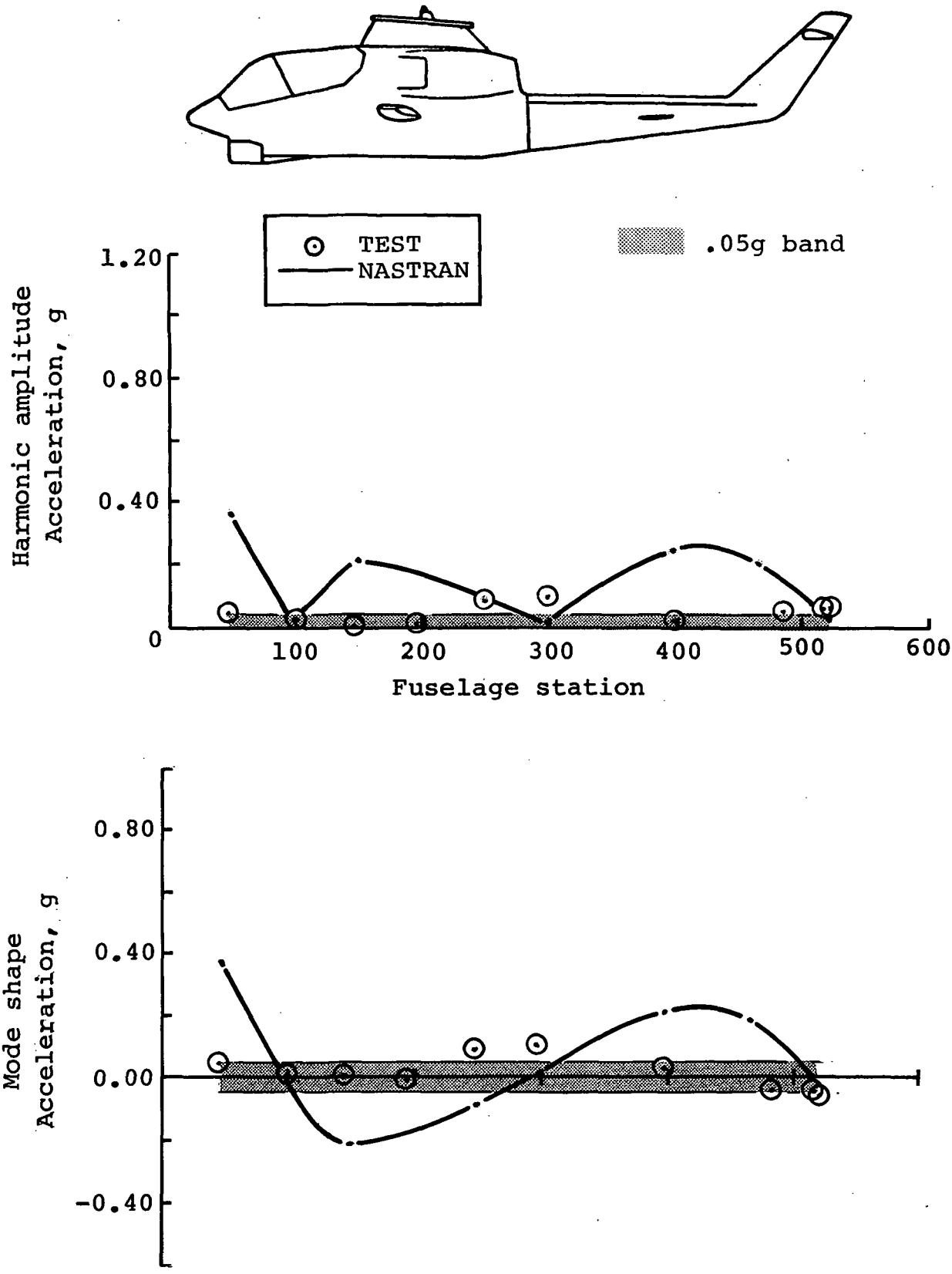

Figure B-36. - Four-per-rev vertical response comparison at 134 knots - wing stores.

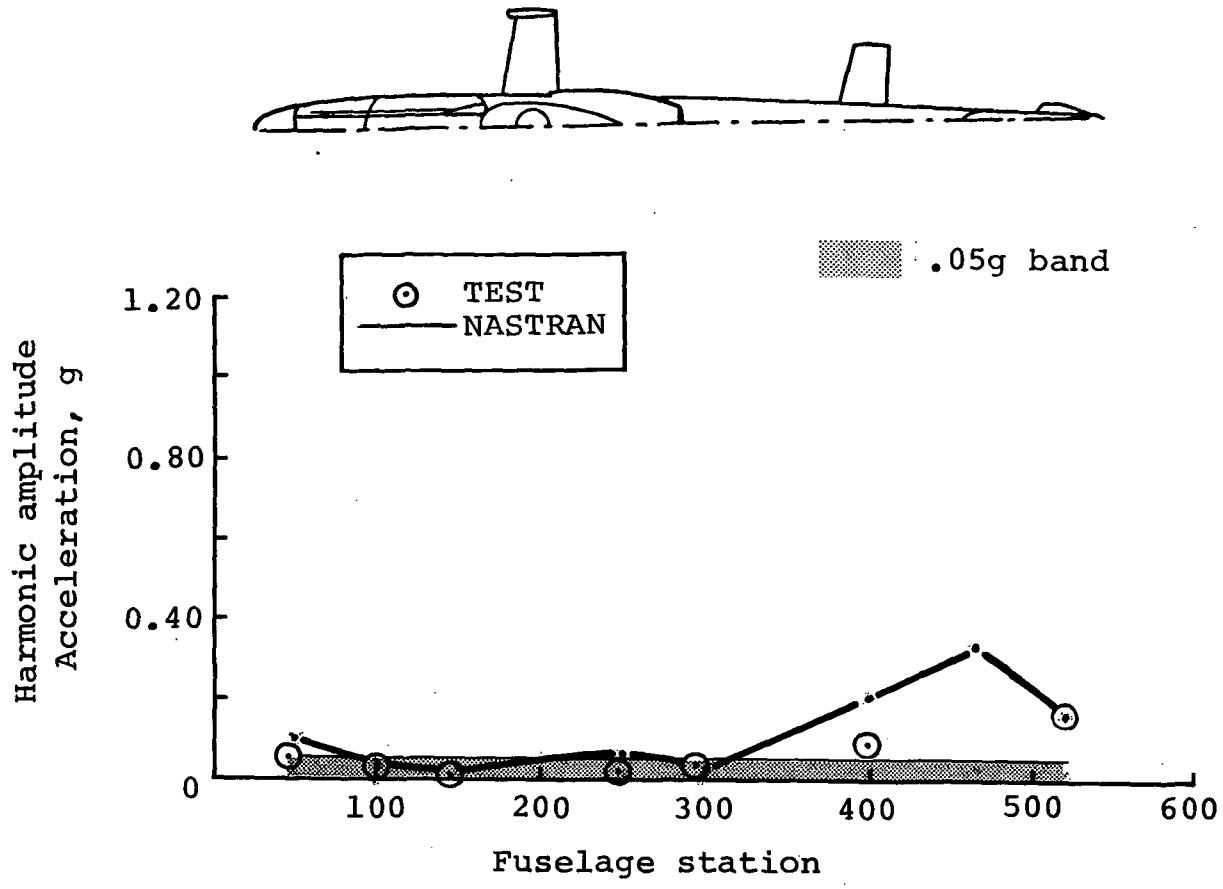

Figure B-37. - Four-per-rev lateral response comparison at 67 knots - clean wing.

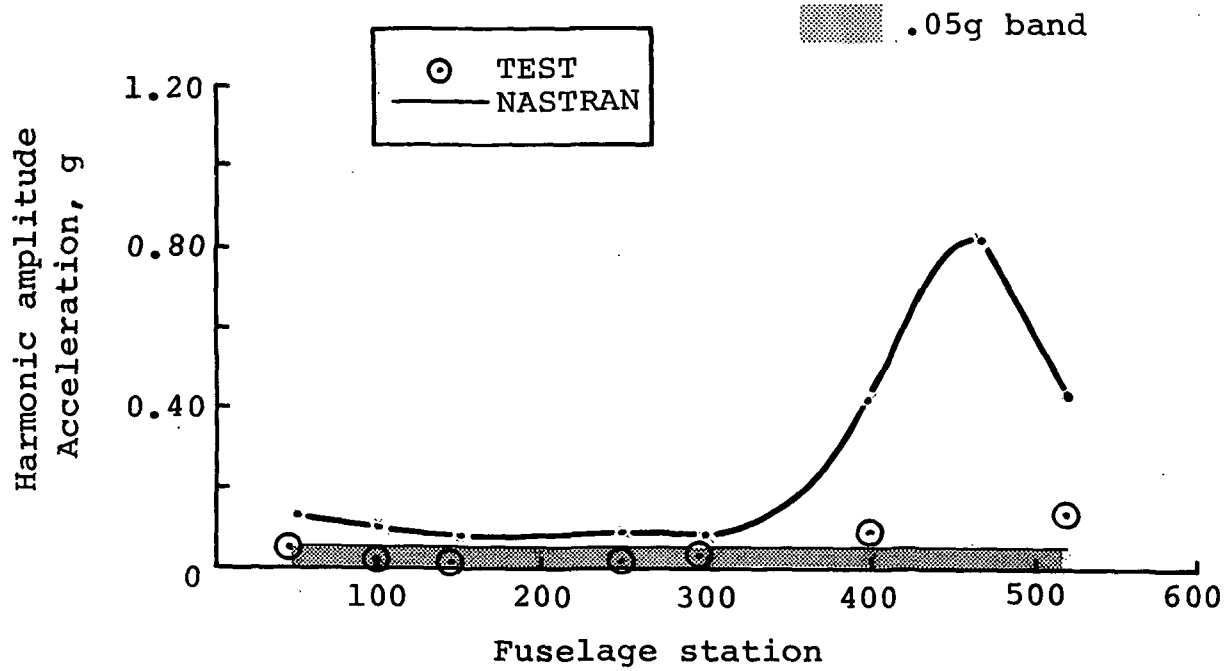

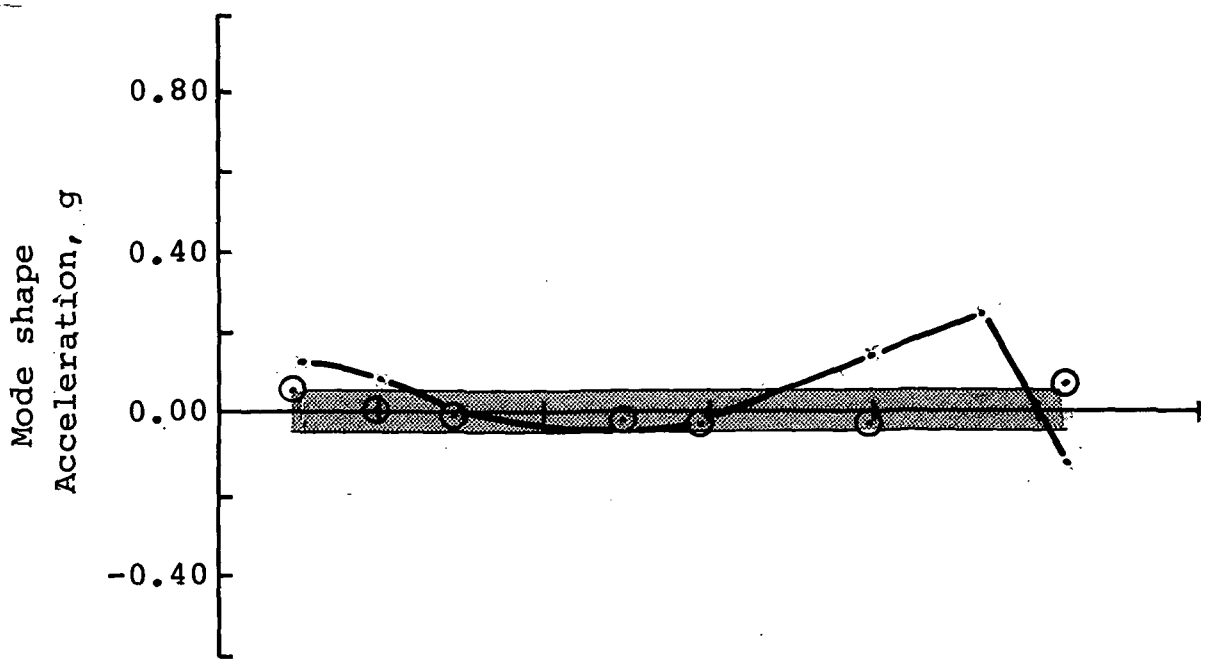

Figure B-38. - Four-per-rev lateral response comparison at 85 knots - clean wing.

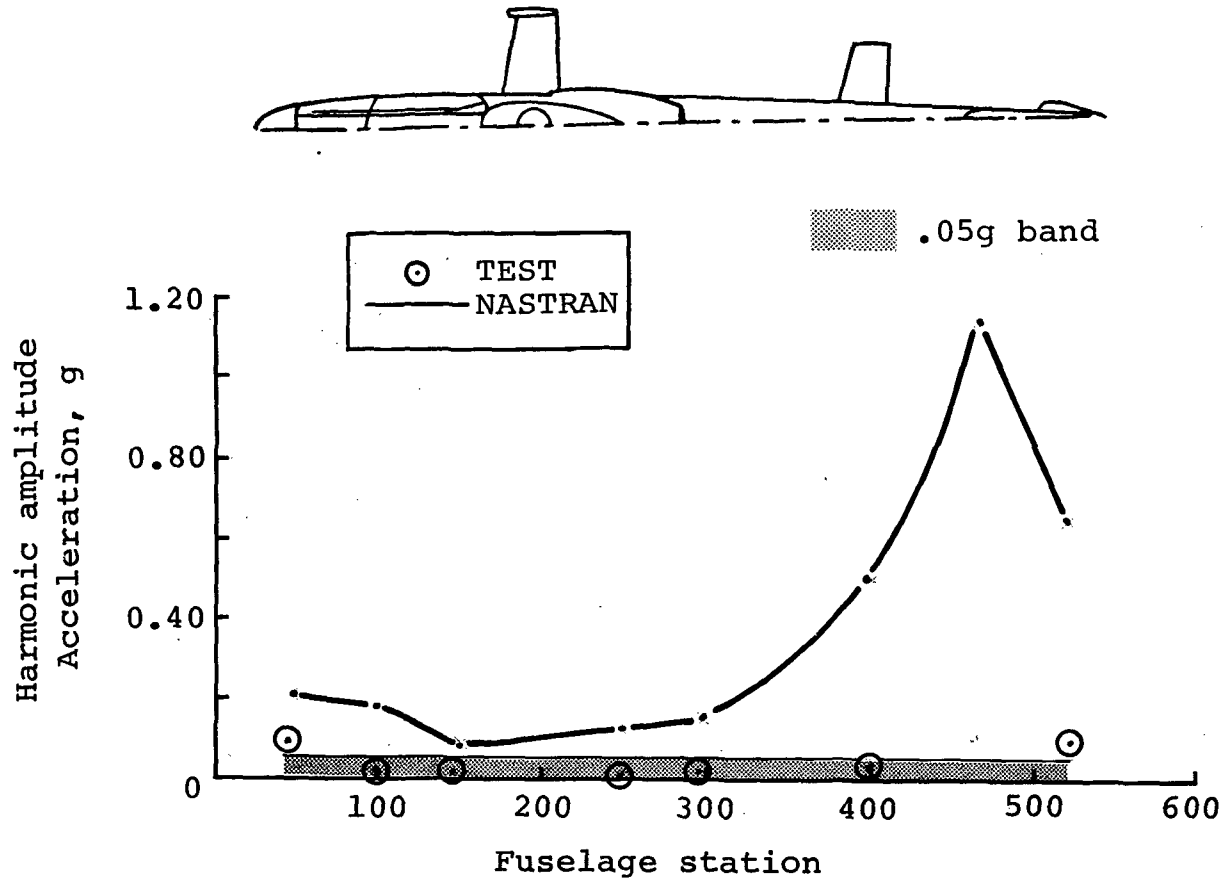

Figure B-39. - Four-per-rev lateral response comparison at 101 knots - clean wing.

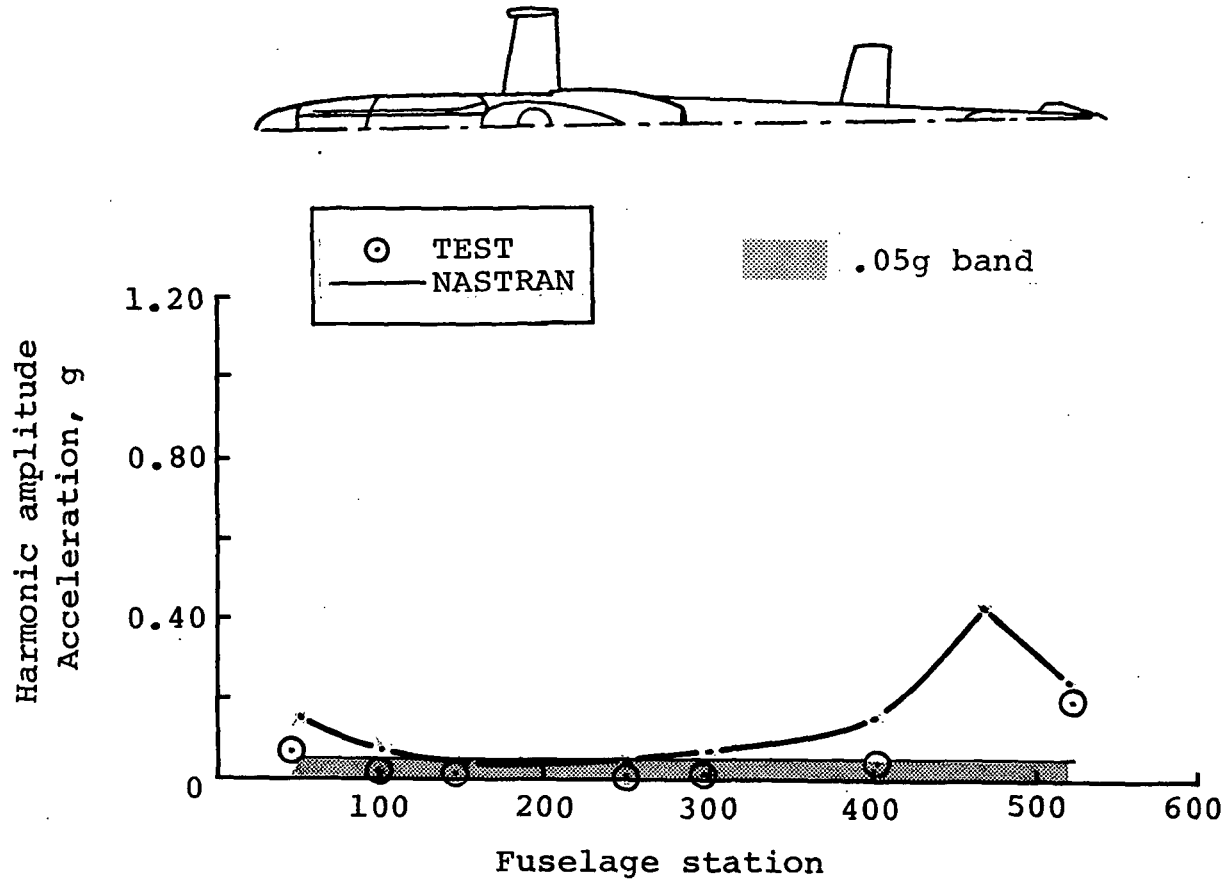

Figure B-40. - Four-per-rev lateral response comparison at 114 knots - clean wing.

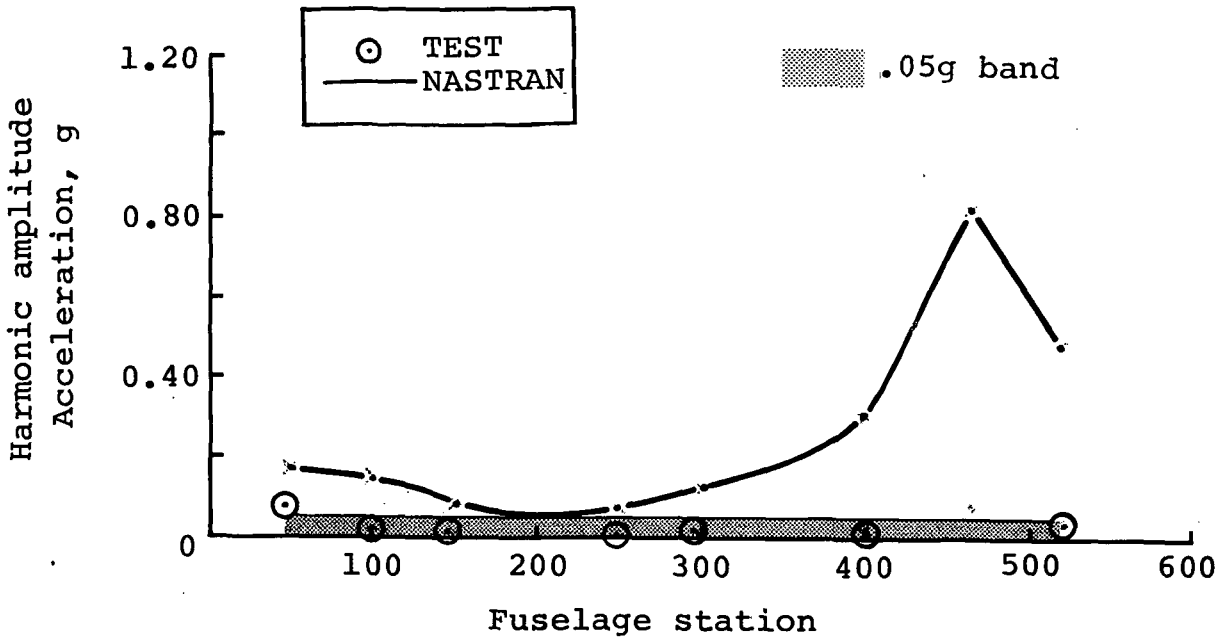

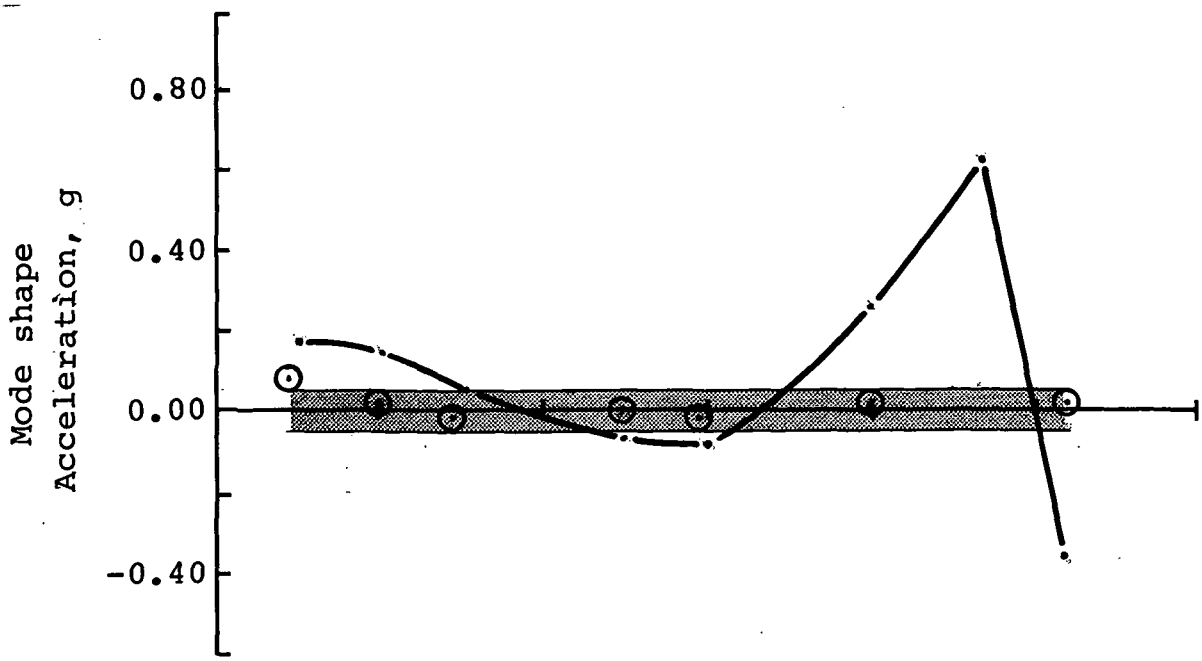

Figure B-41. - Four-per-rev lateral response comparison at 128 knots - clean wing.

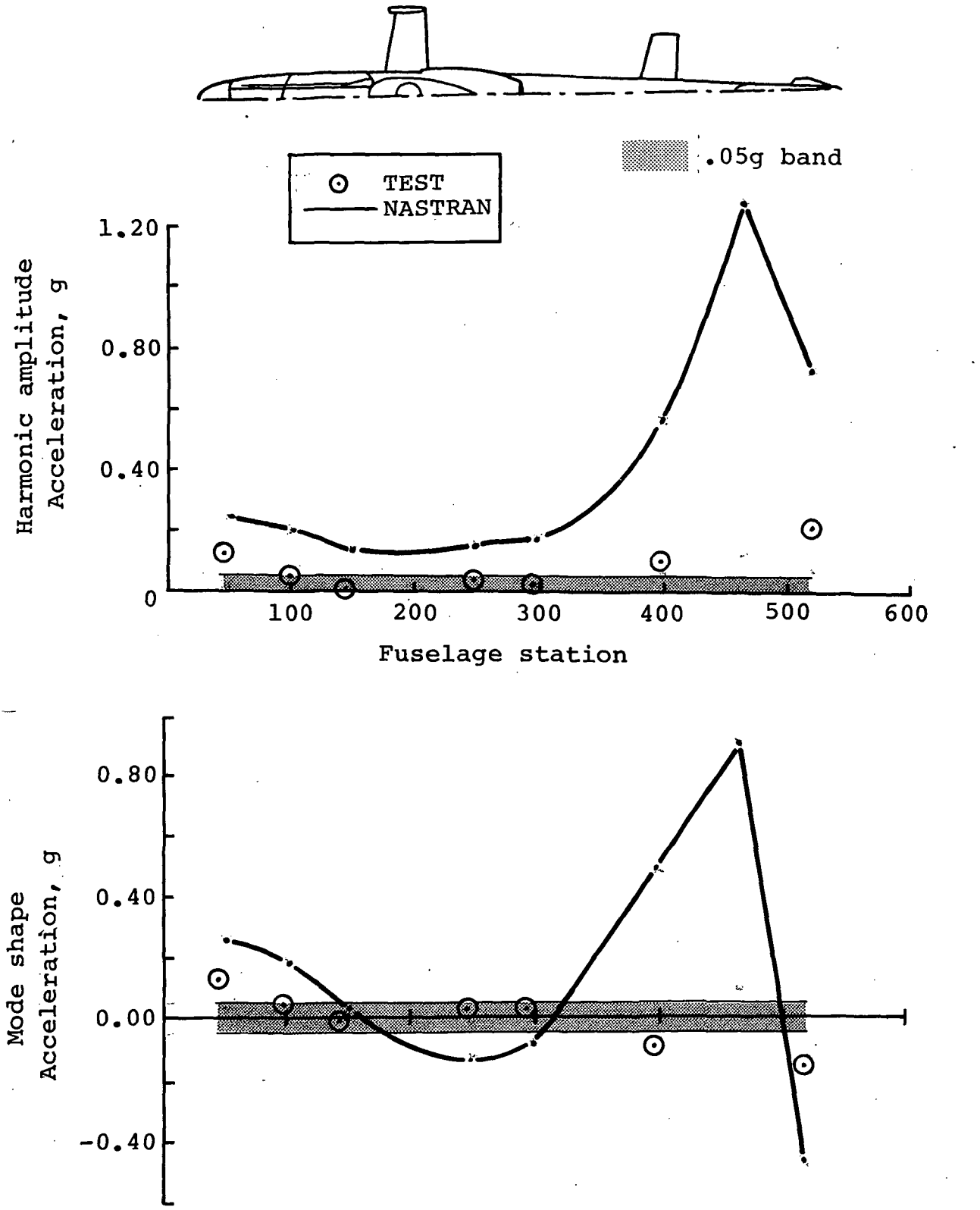

Figure B-42. - Four-per-rev lateral response comparison at 142 knots - clean wing.

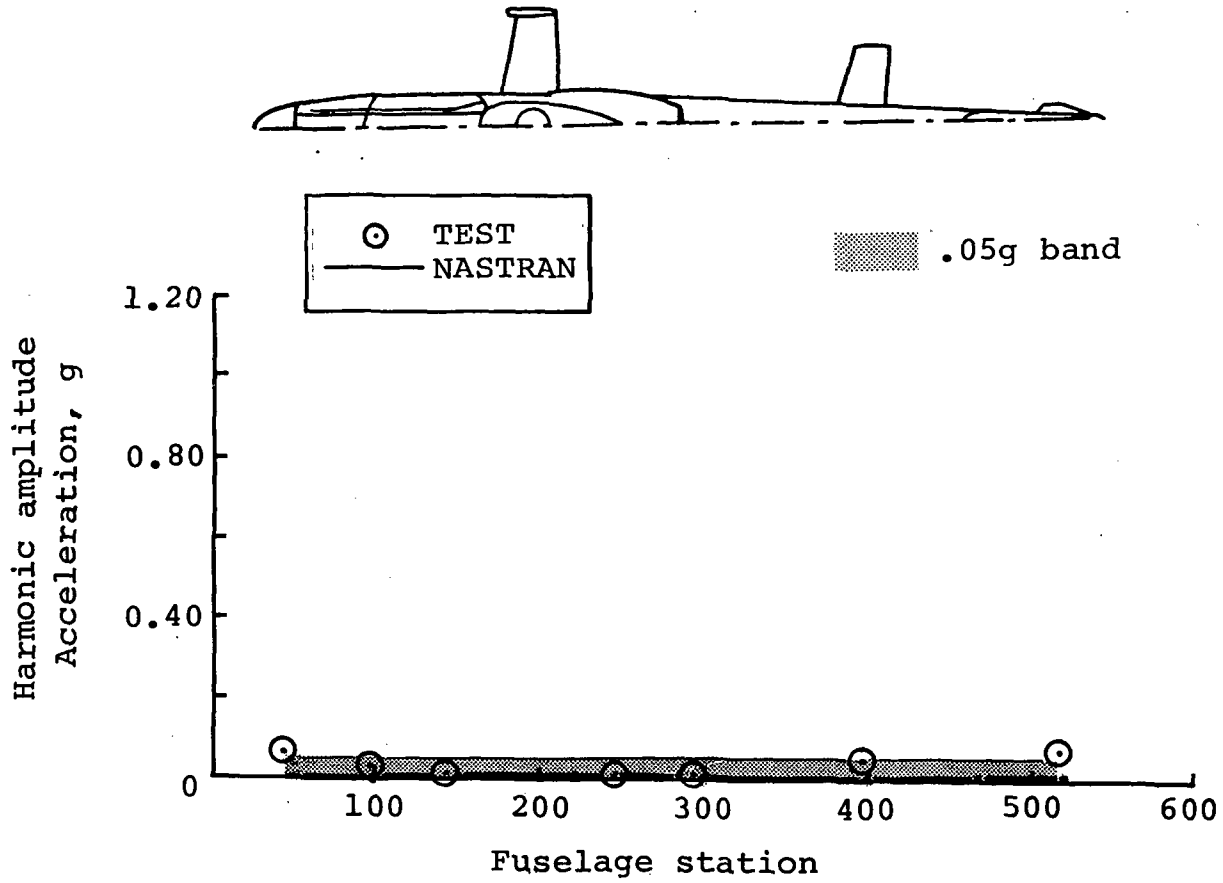

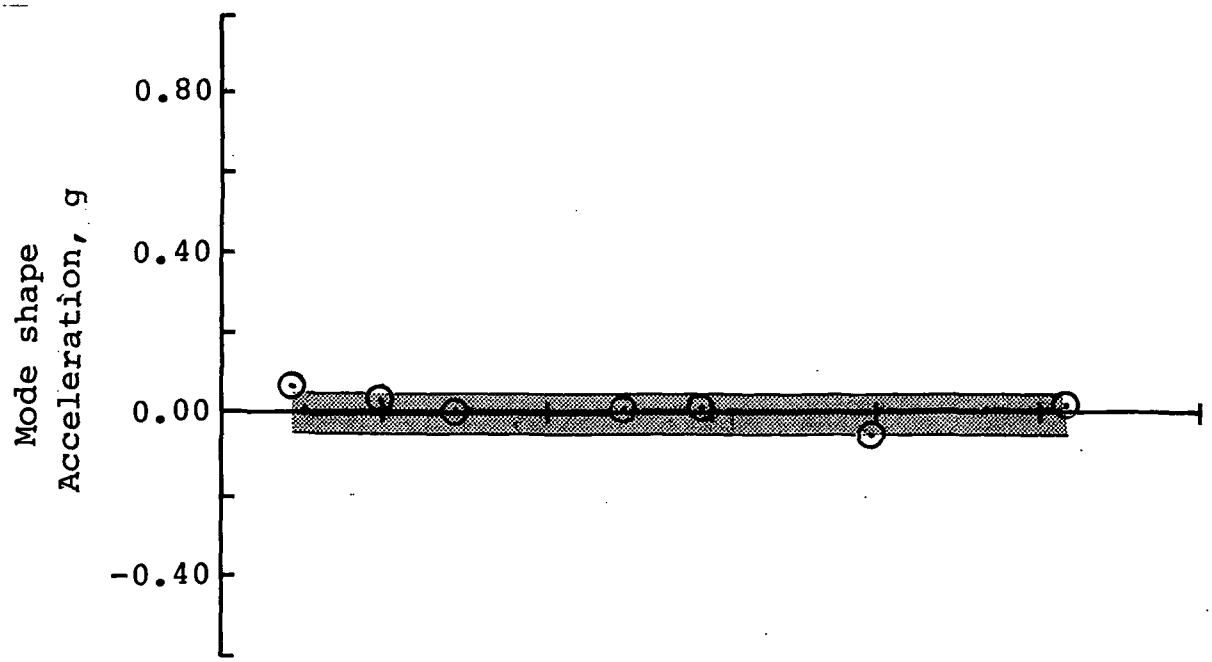

Figure B-43. - Four-per-rev lateral response comparison at 61 knots - wing stores.

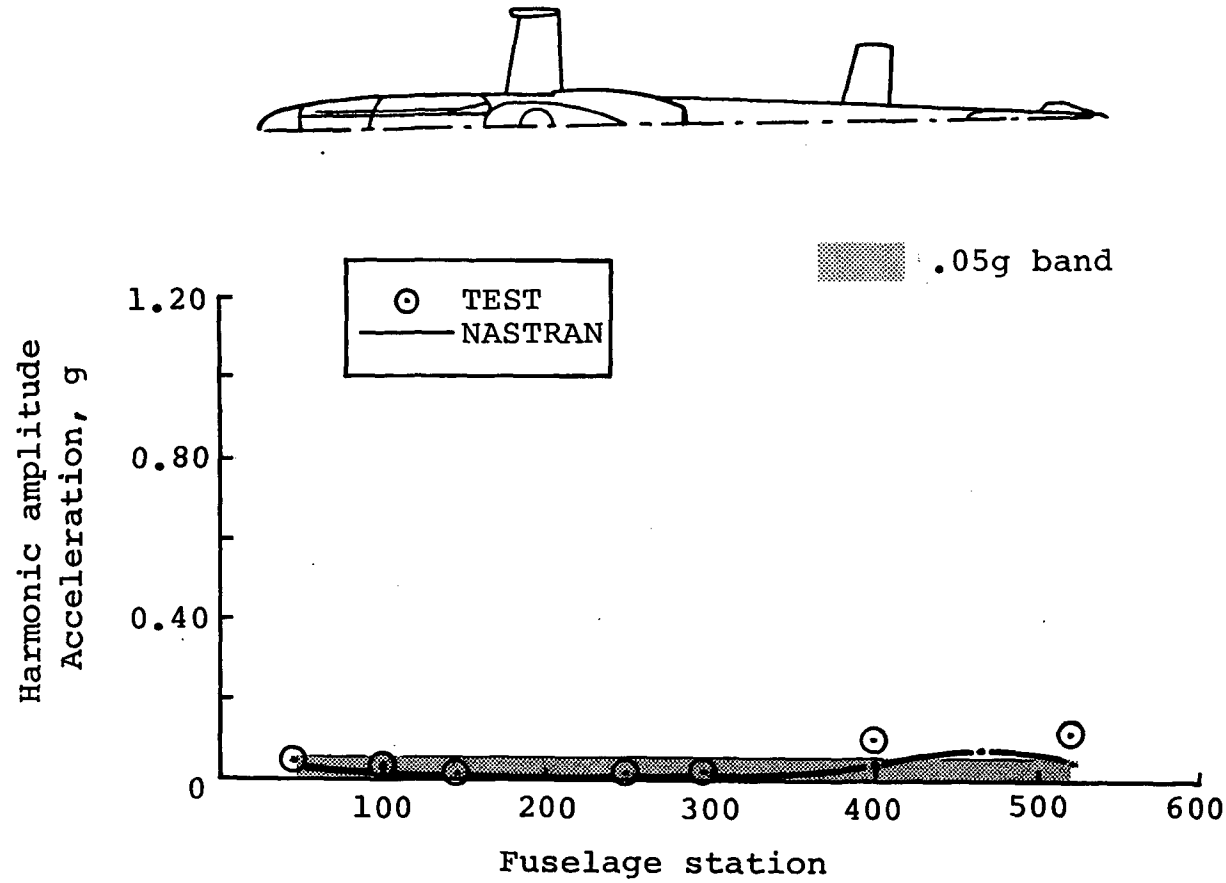

Figure B-44. - Four-per-rev lateral response comparison at 76 knots - wing stores.

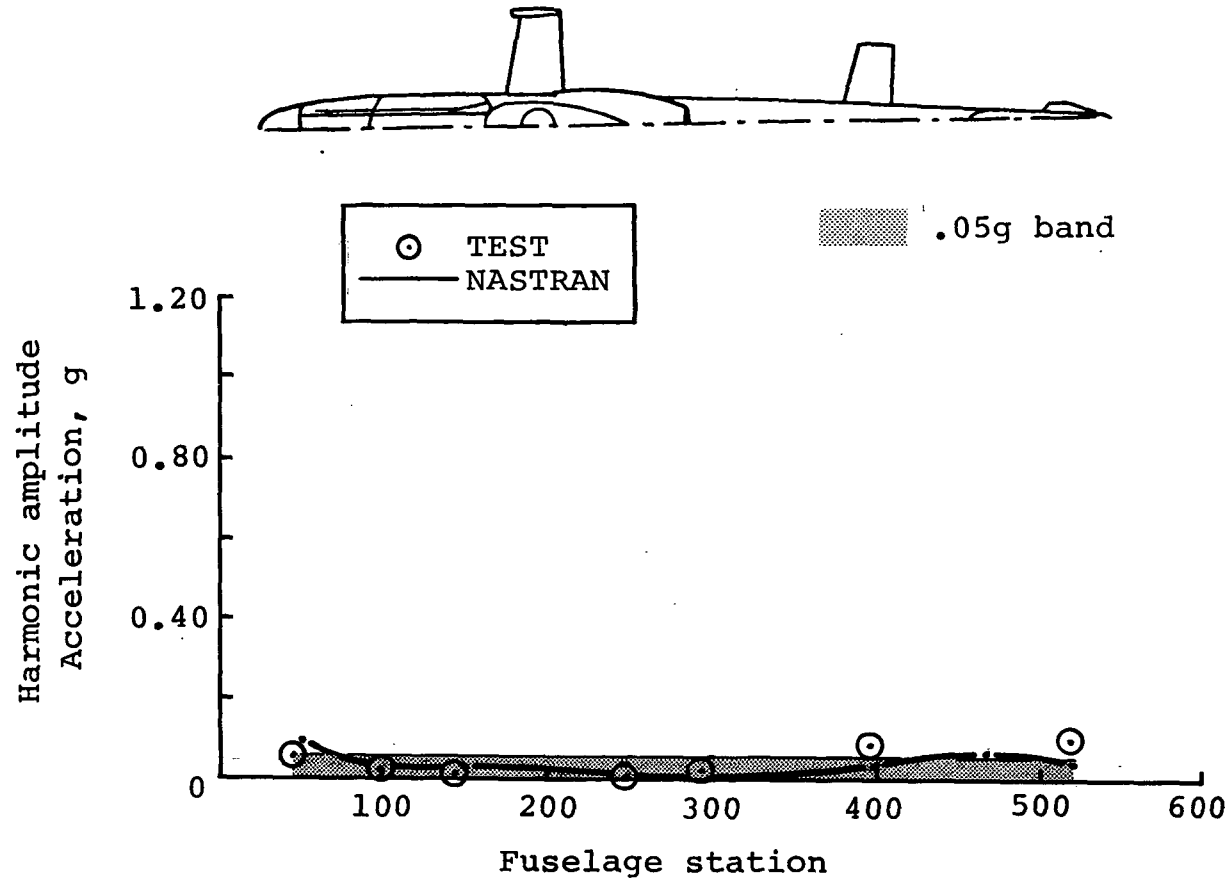

Figure B-45. - Four-per-rev lateral response comparison at 95 knots - wing stores.

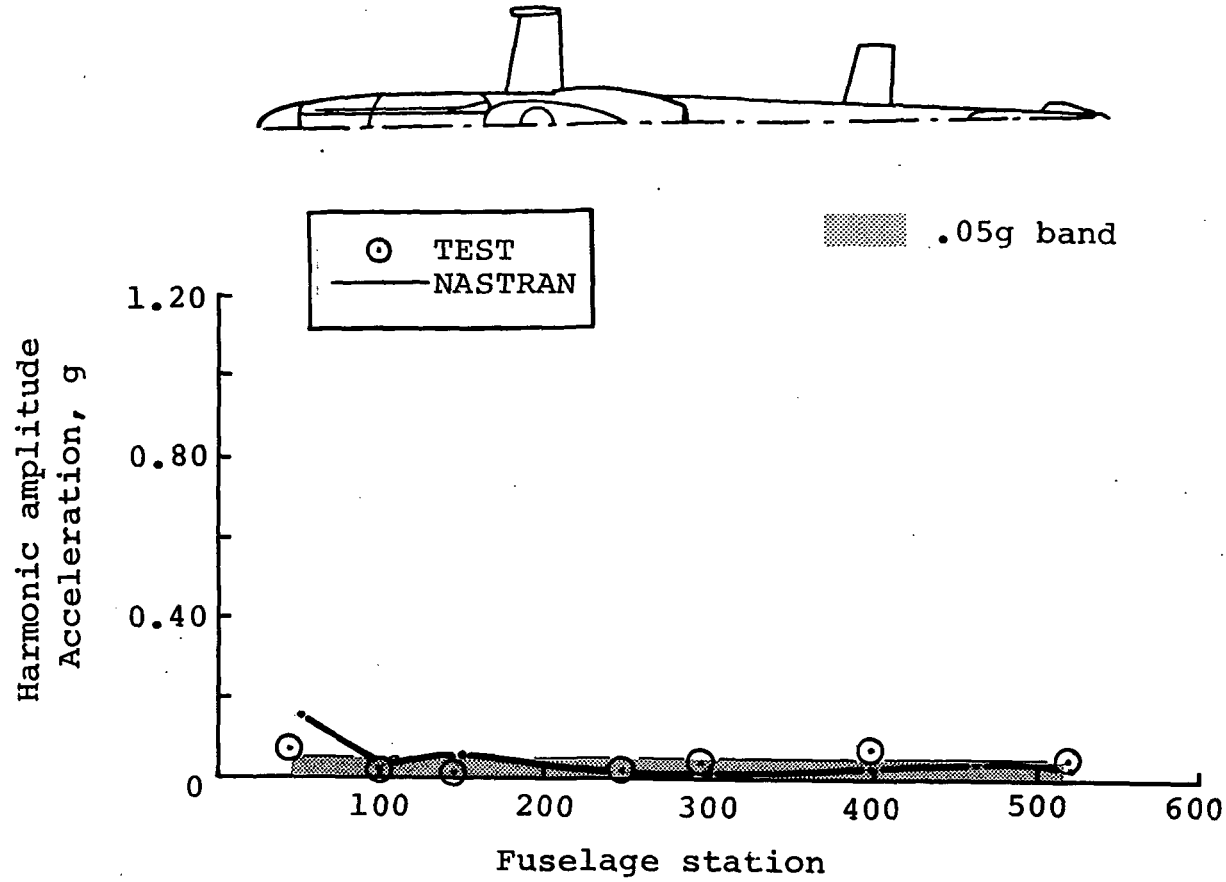

Figure B-46. - Four-per-rev lateral response comparison at 108 knots - wing stores.

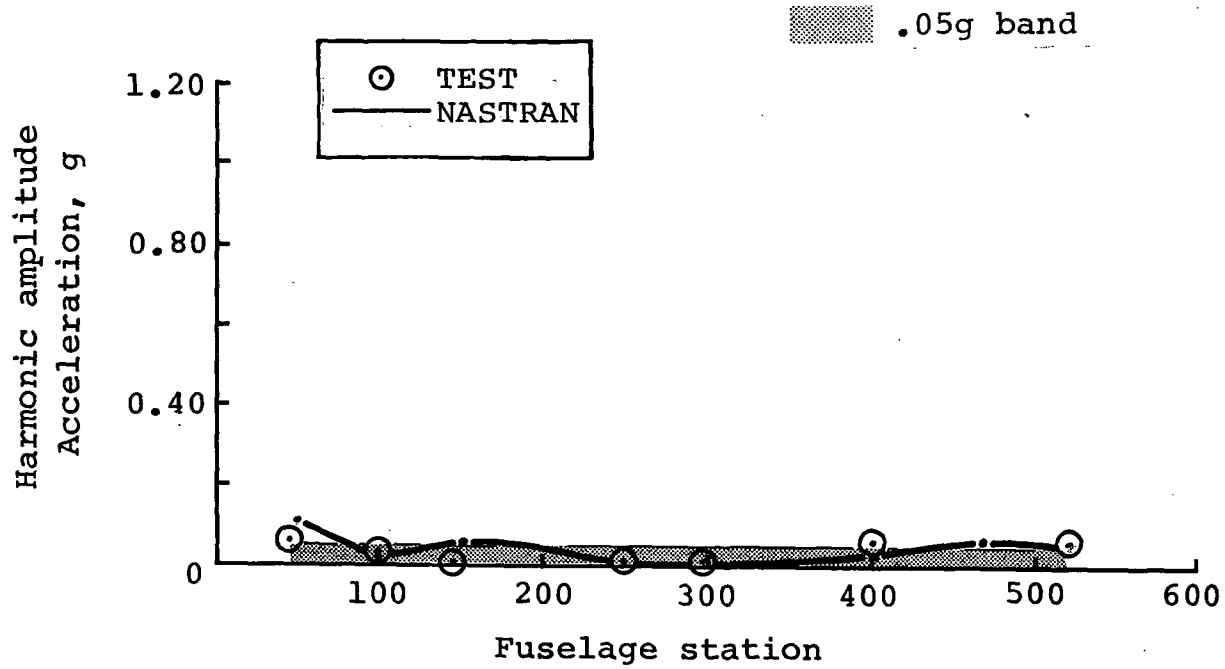

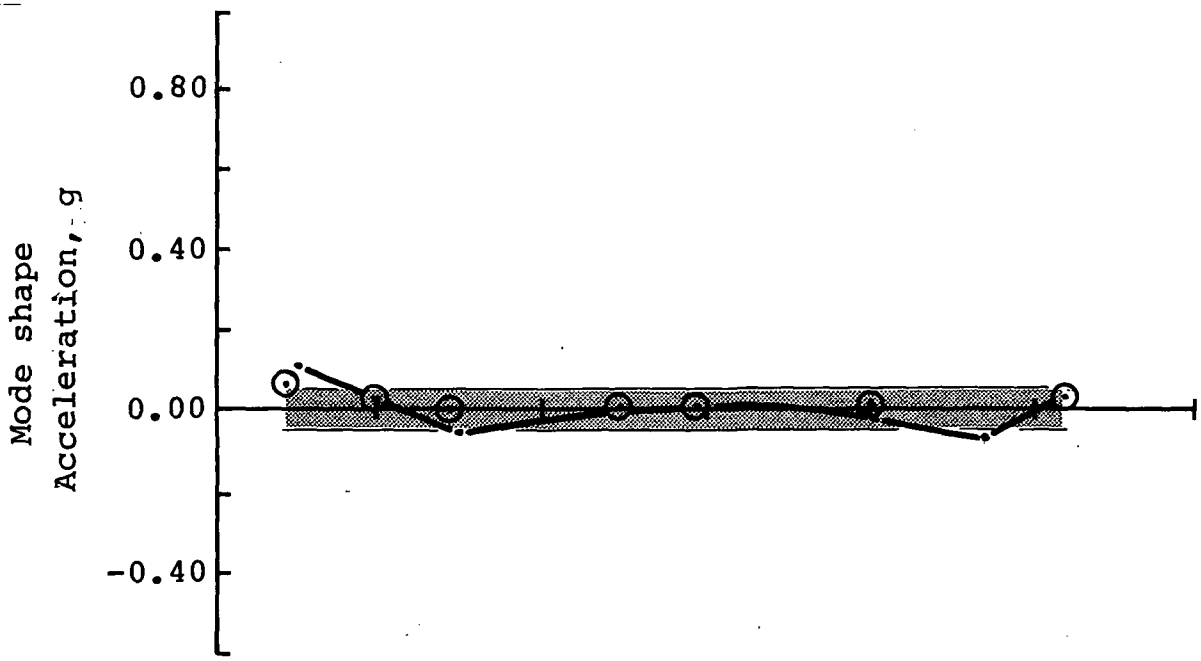

Figure B-47. - Four-per-rev lateral response comparison at 120 knots - wing stores.

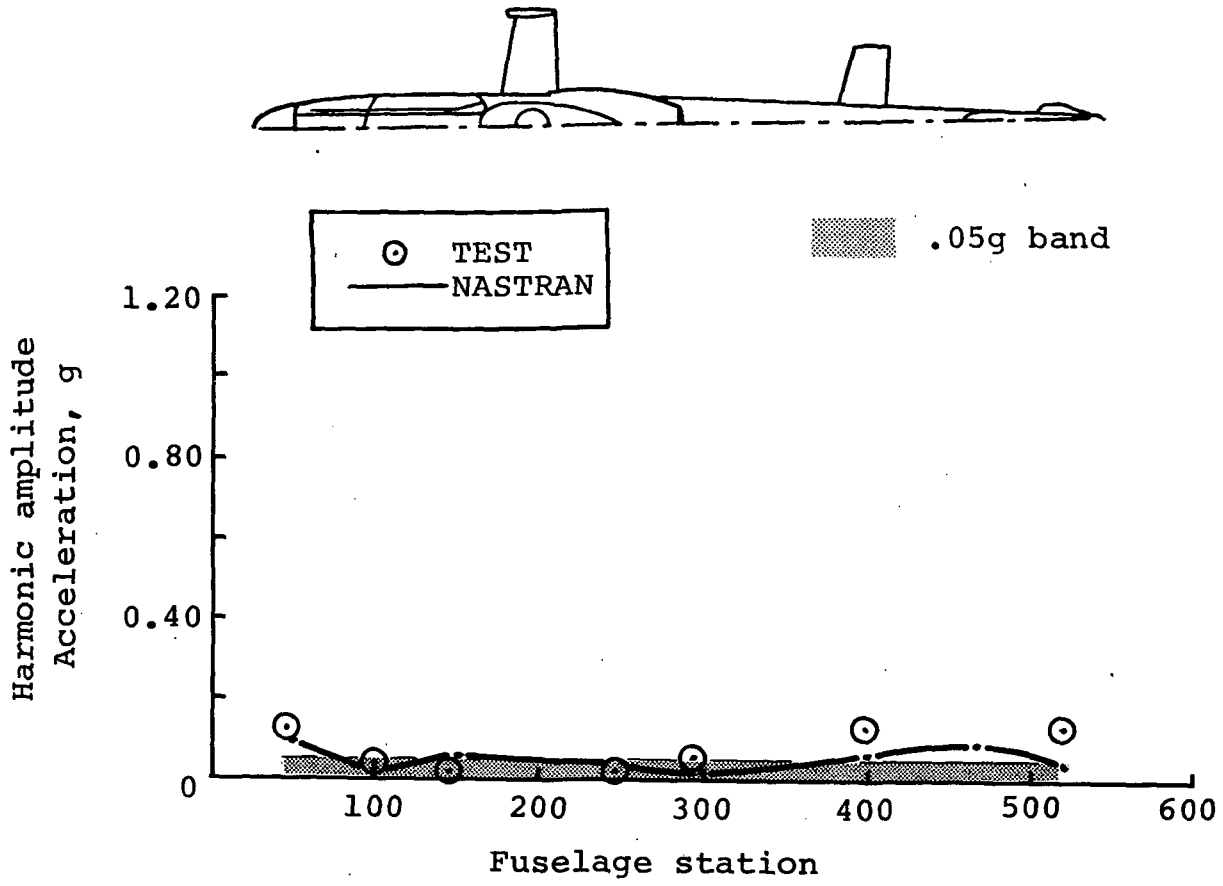

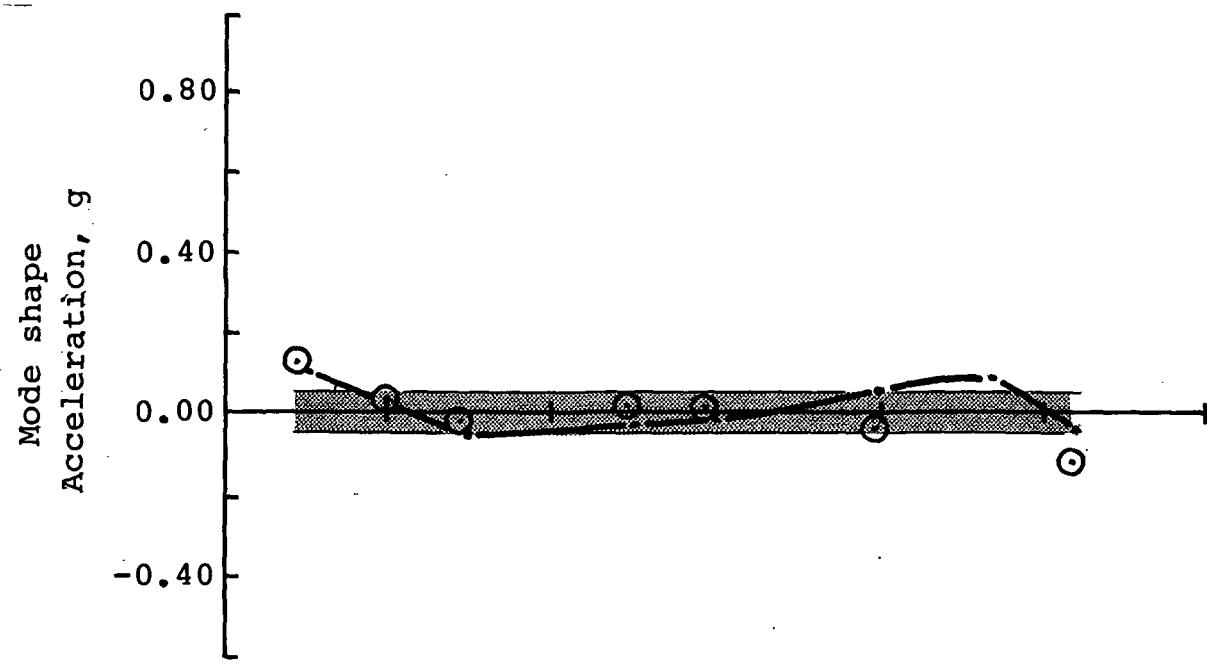

Figure B-48. - Four-per-rev lateral response comparison at 134 knots - wing stores.

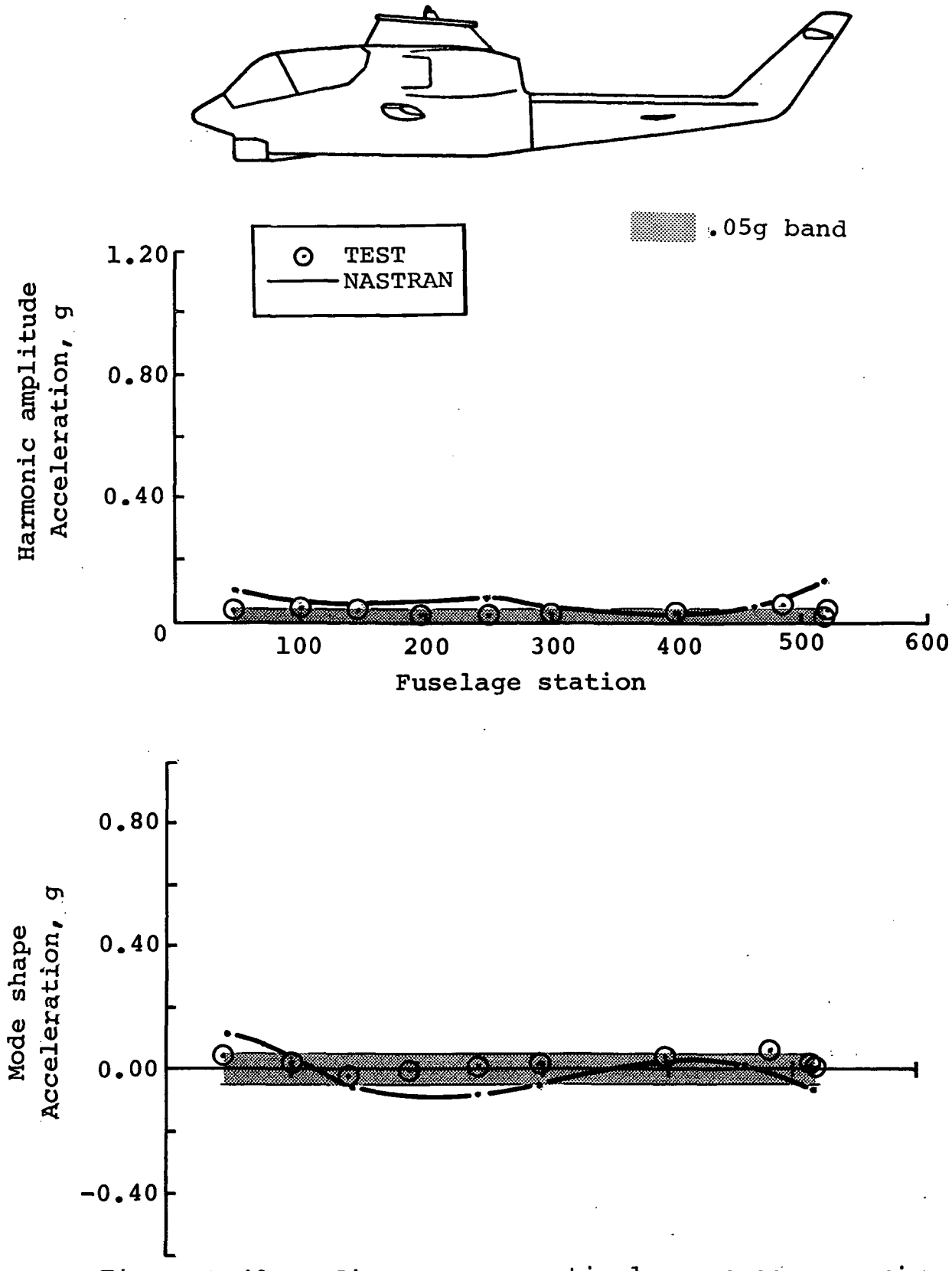

Figure B-49. - Six-per-rev yertical response comparison at 67 knots - clean wing.

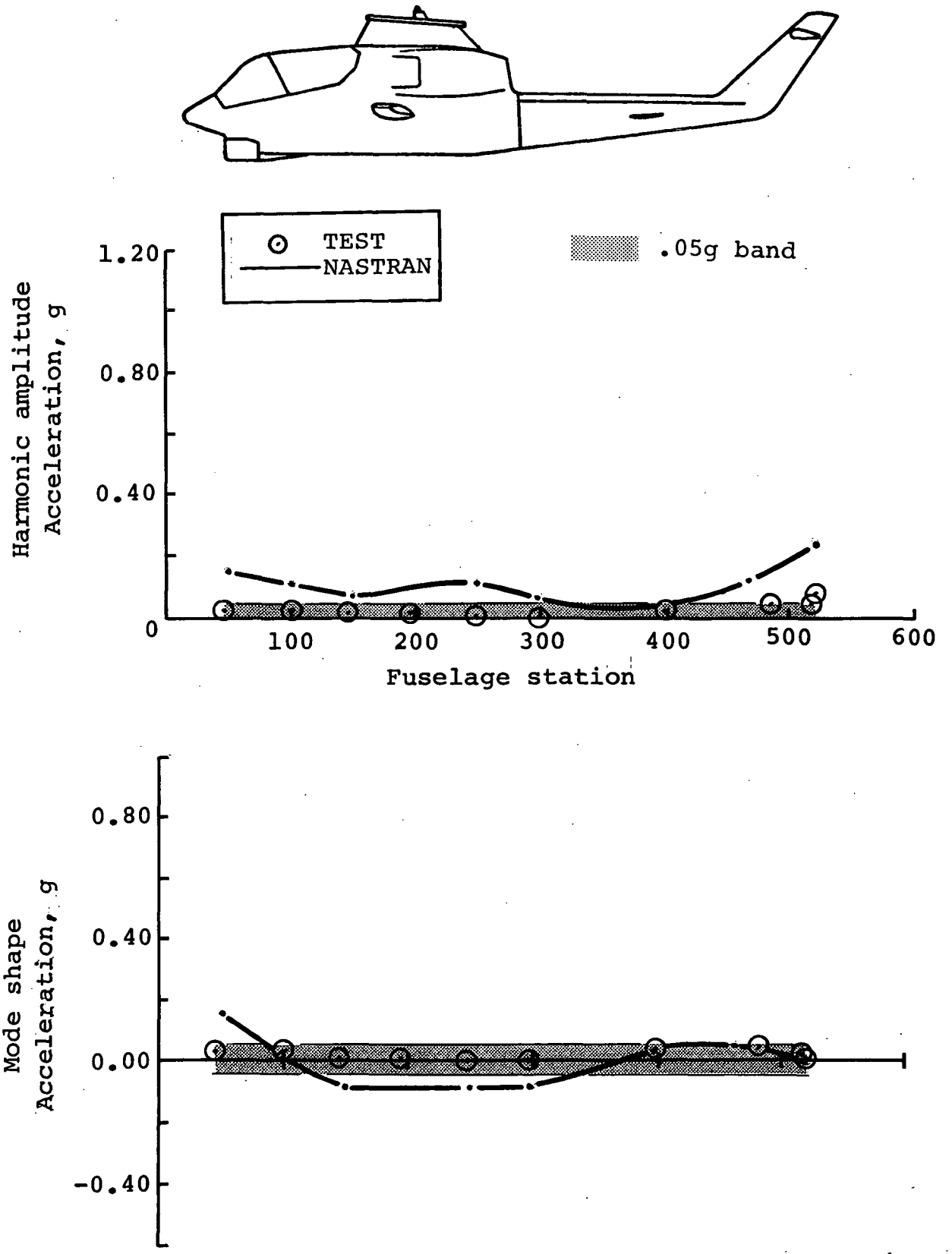

Figure B-50. - Six-per-rev vertical response comparison at 85 knots - clean wing.

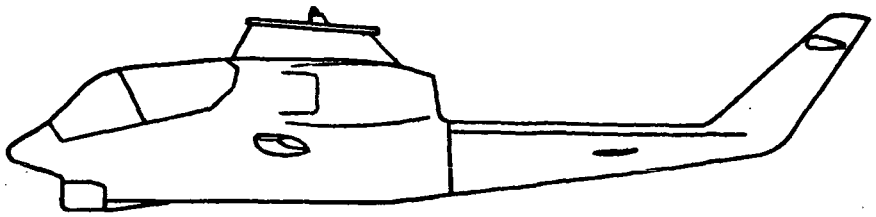

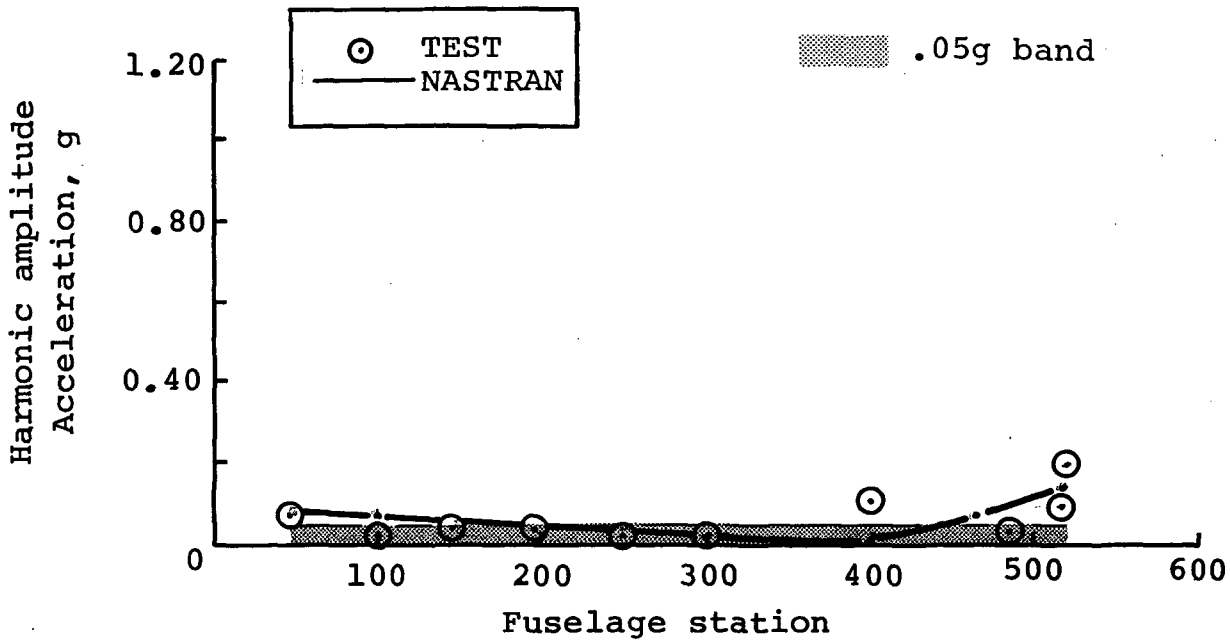

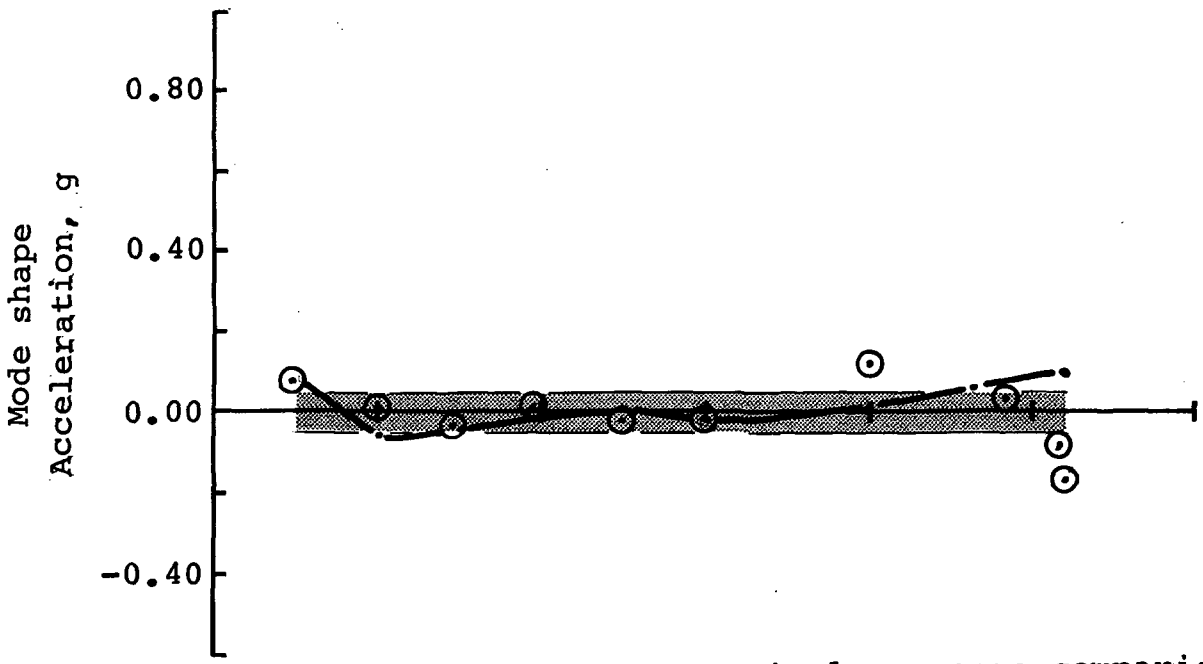

Figure B-51. - Six-per-rev vertical response comparison at 101 knots - clean wing.

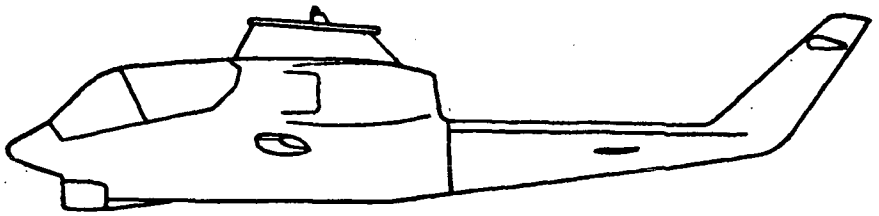

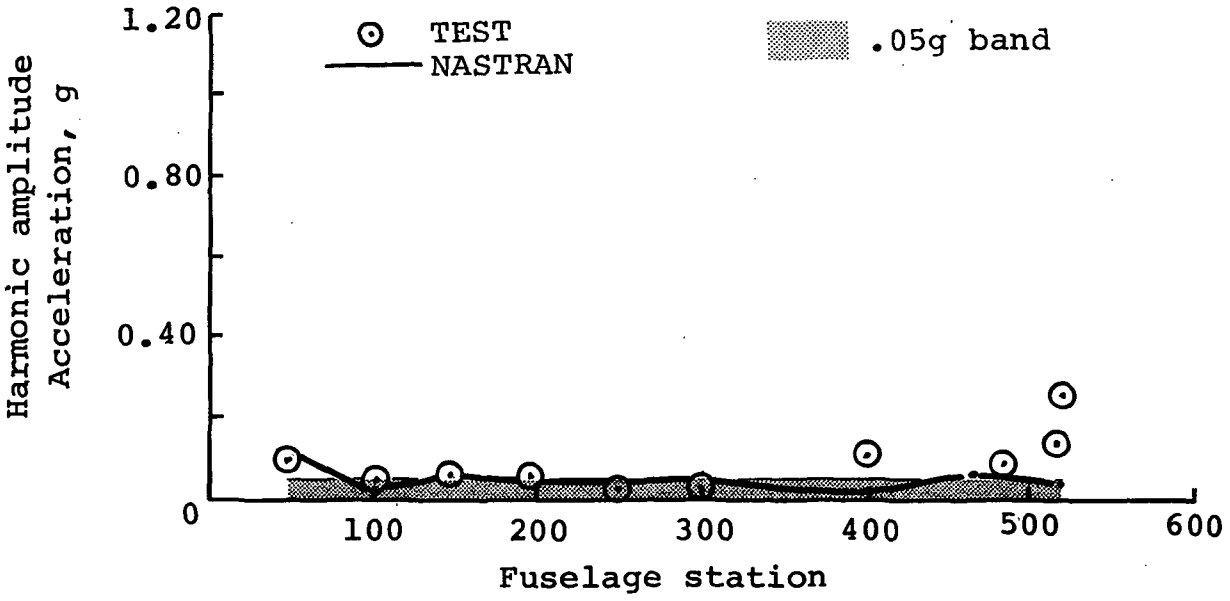

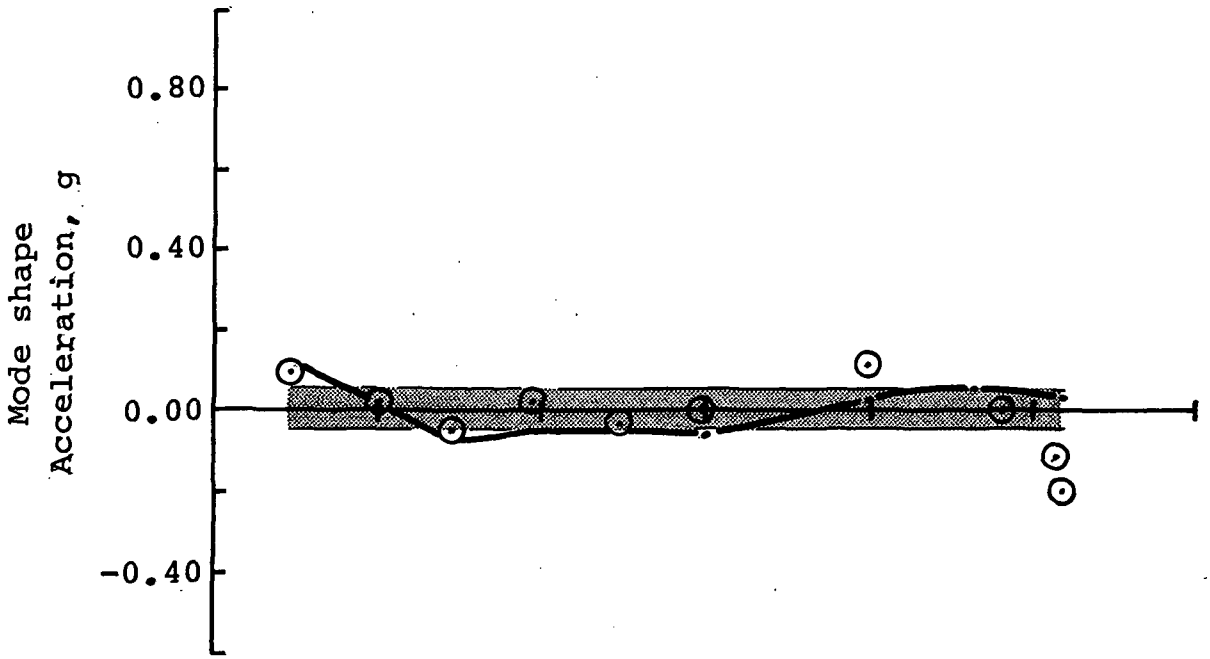

Figure B-52. - Six-per-rev vertical response comparison at 114 knots - clean wing.

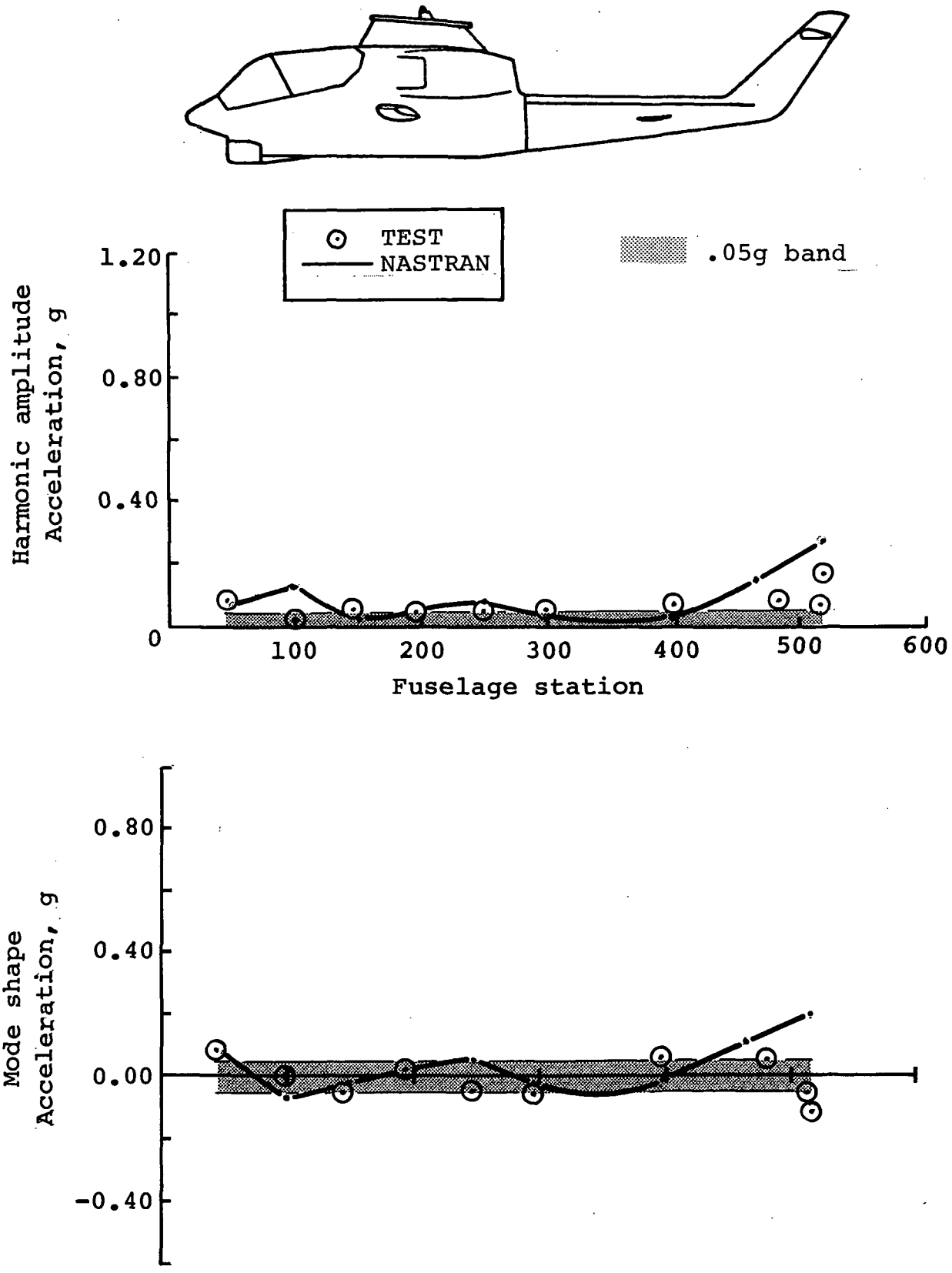

Figure B-53. - Six-per-rev vertical response comparison at 128 knots - clean wing.

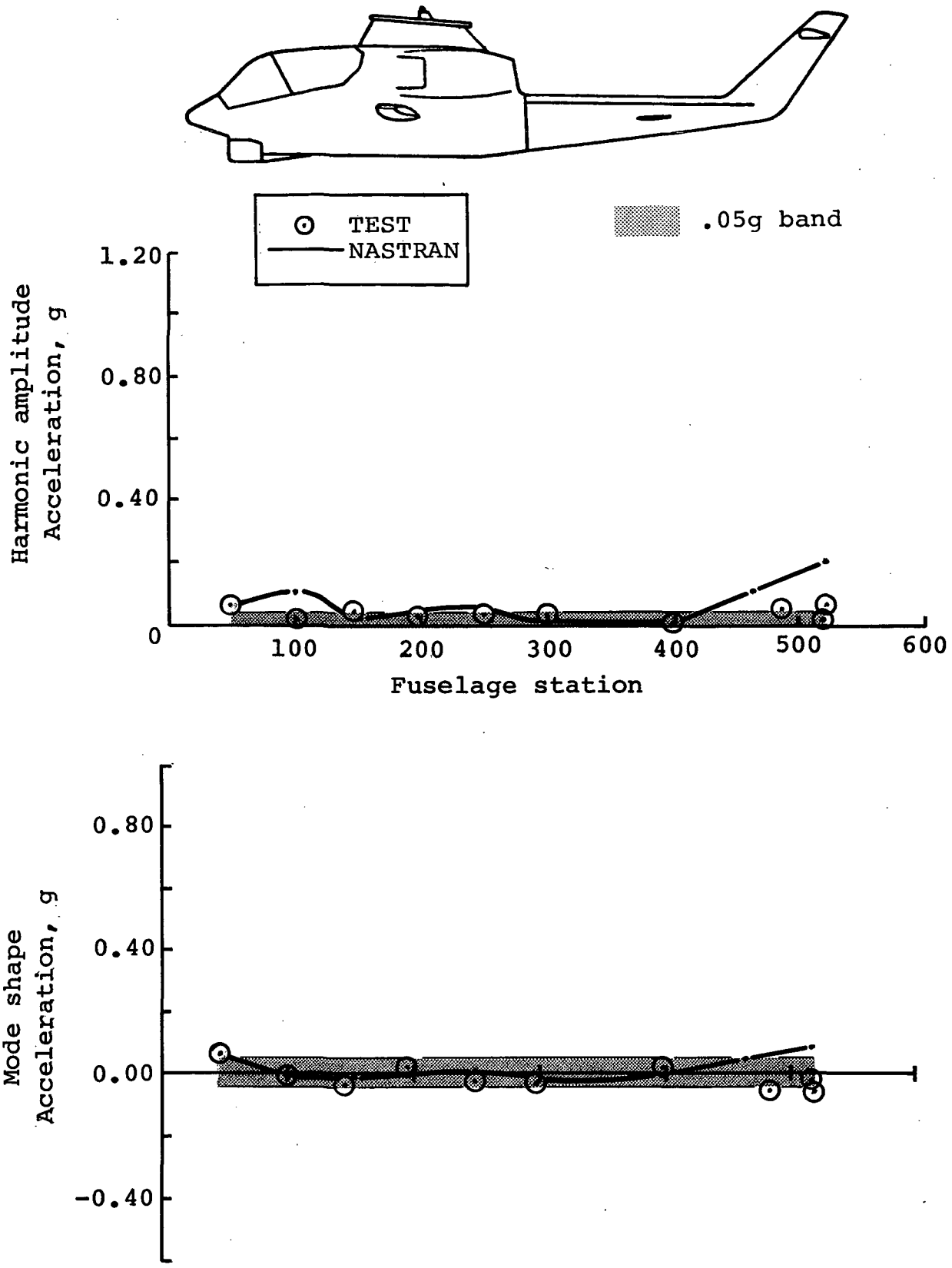

Figure B-54. - Six-per-rev vertical response comparison at 142 knots - clean wing.

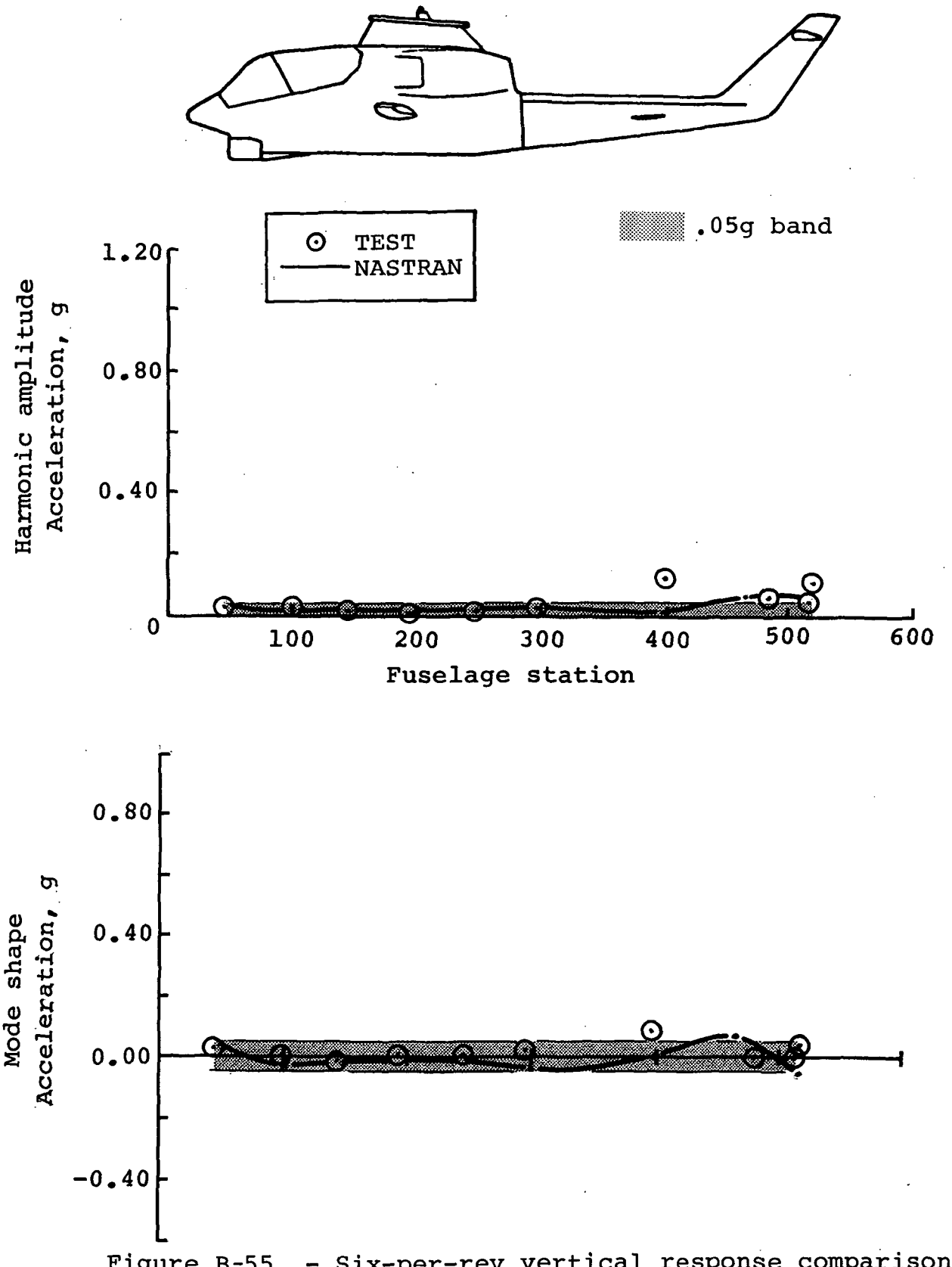

Figure B-55. - Six-per-rev vertical response comparison at 61 knots - wing stores.

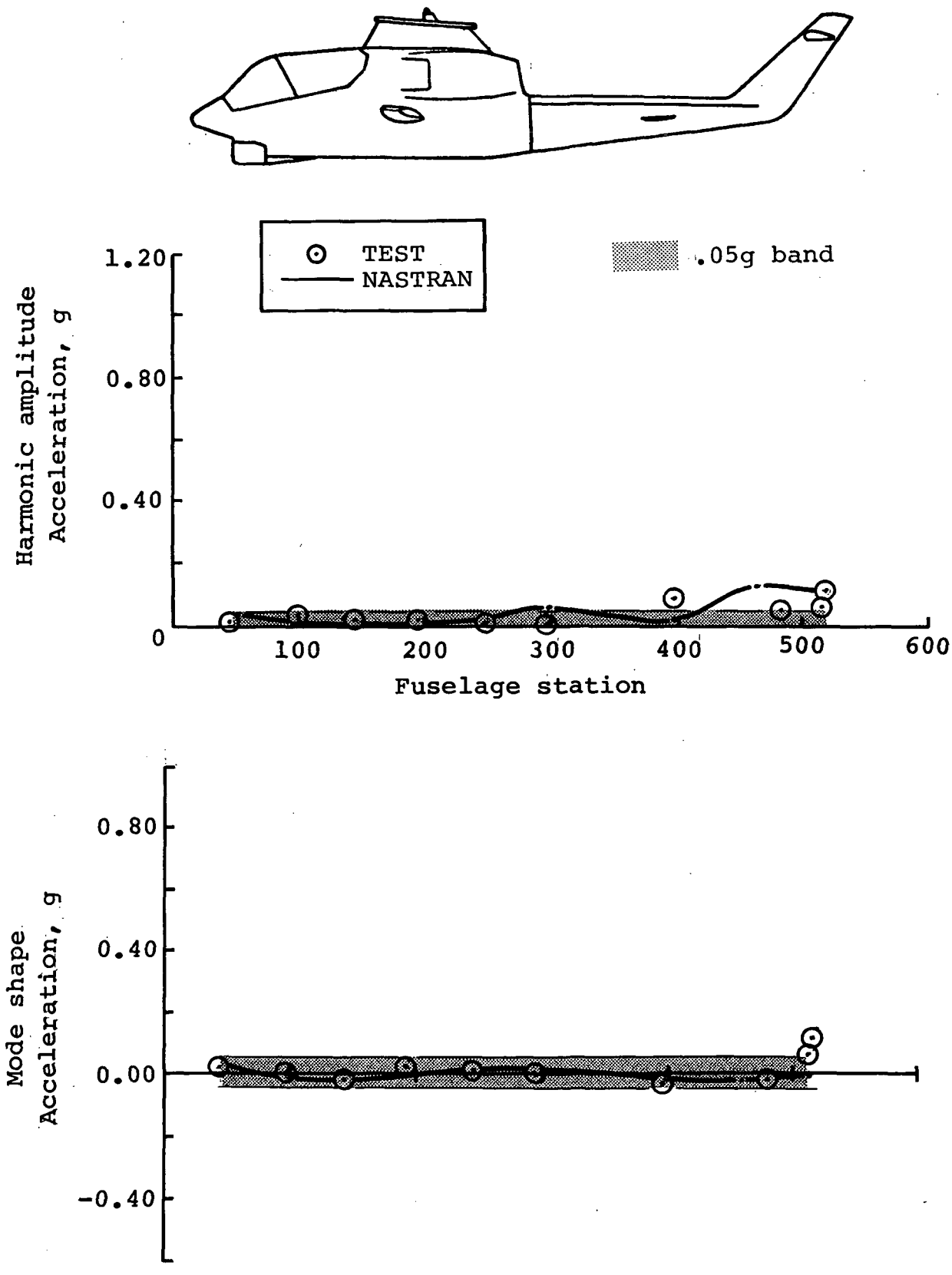

Figure B-56. - Six-per-rev vertical response comparison at 76 knots - wing stores.

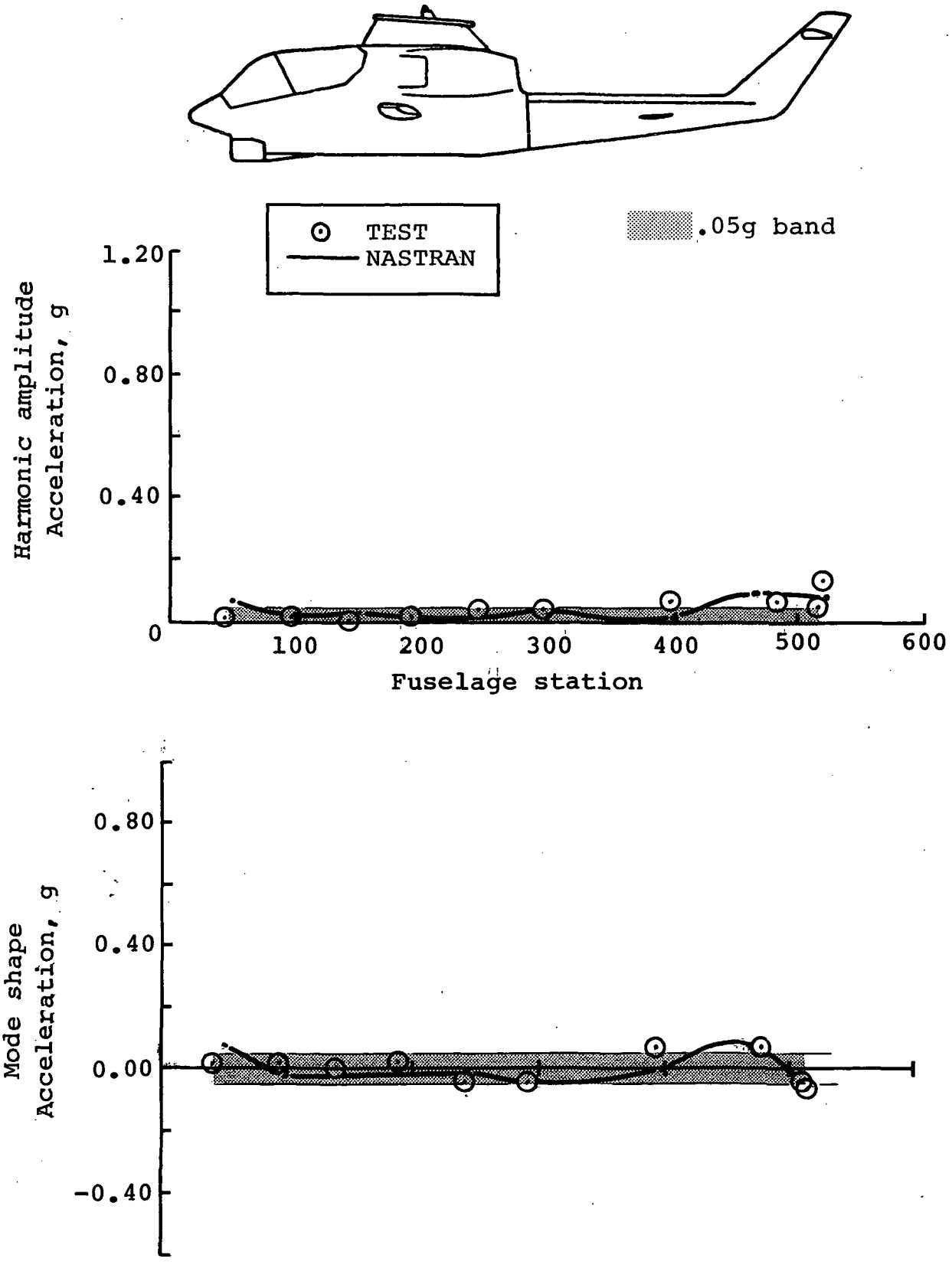

Figure B-57. - Six-per-rev vertical response comparison at 95 knots - wing stores.

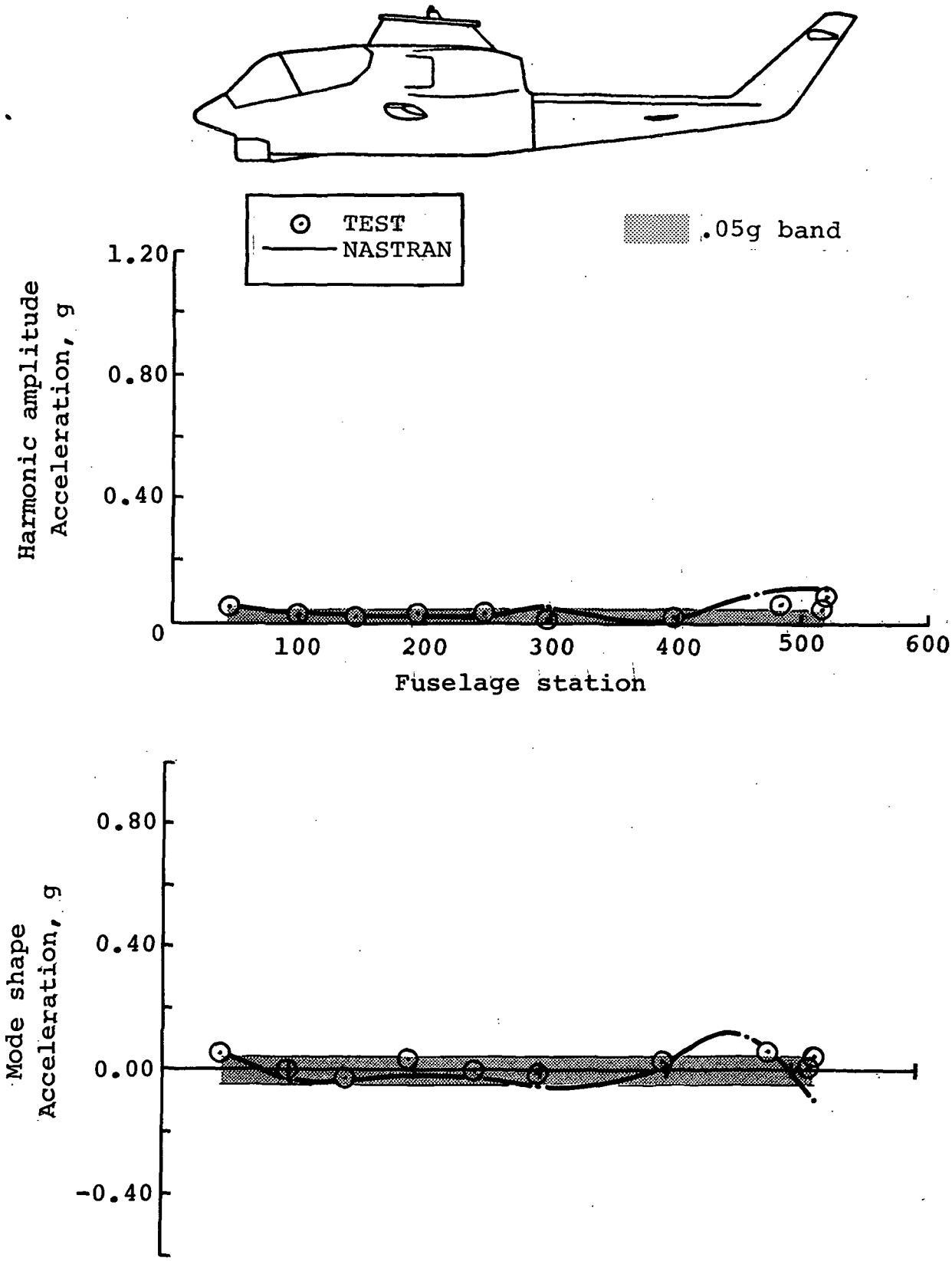

Figure B-58. - Six-per-rev vertical response comparison at 108 knots - wing stores.

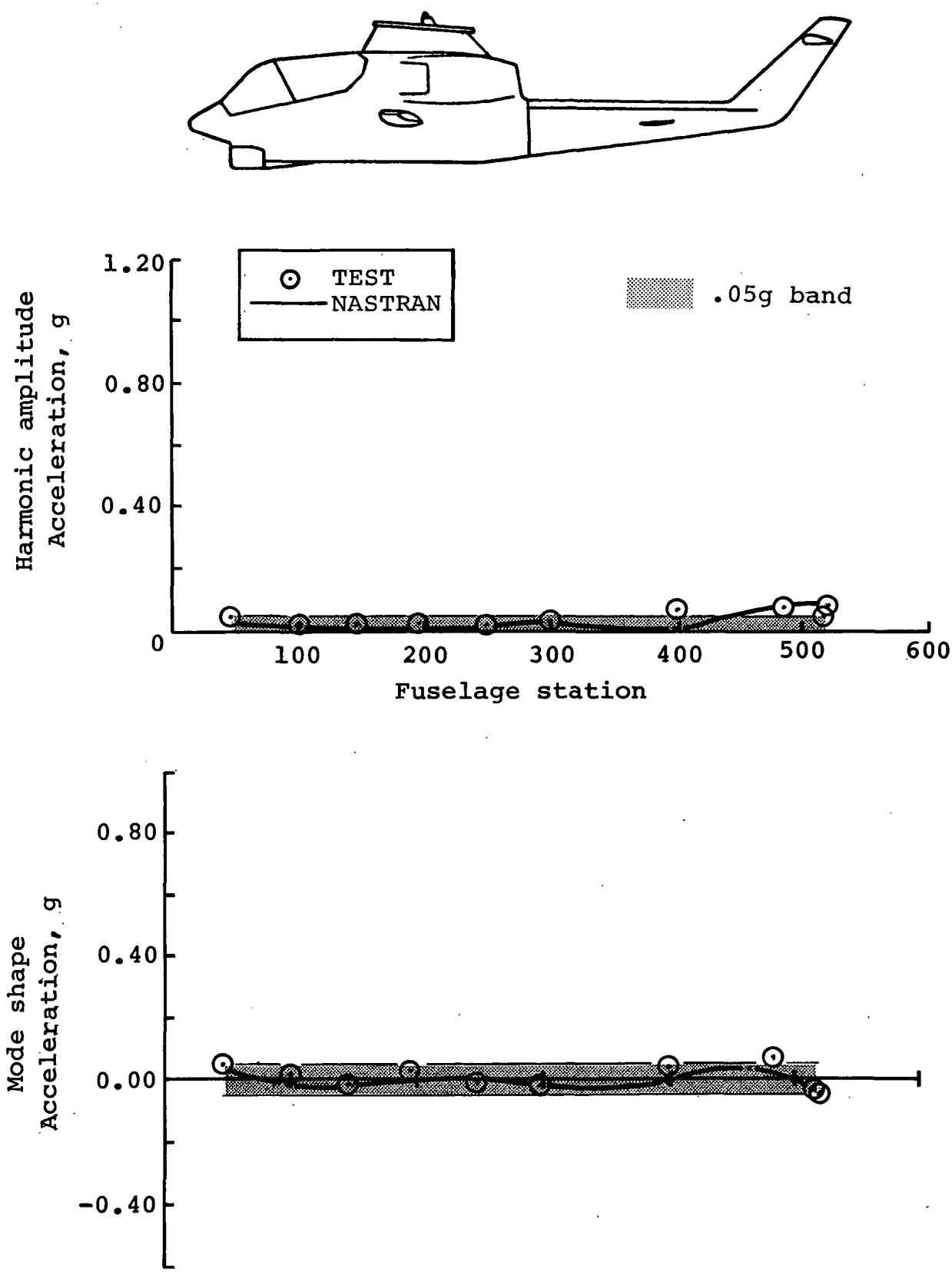

Figure B-59. - Six-per-rev vertical response comparison at 120 knots - wing stores.

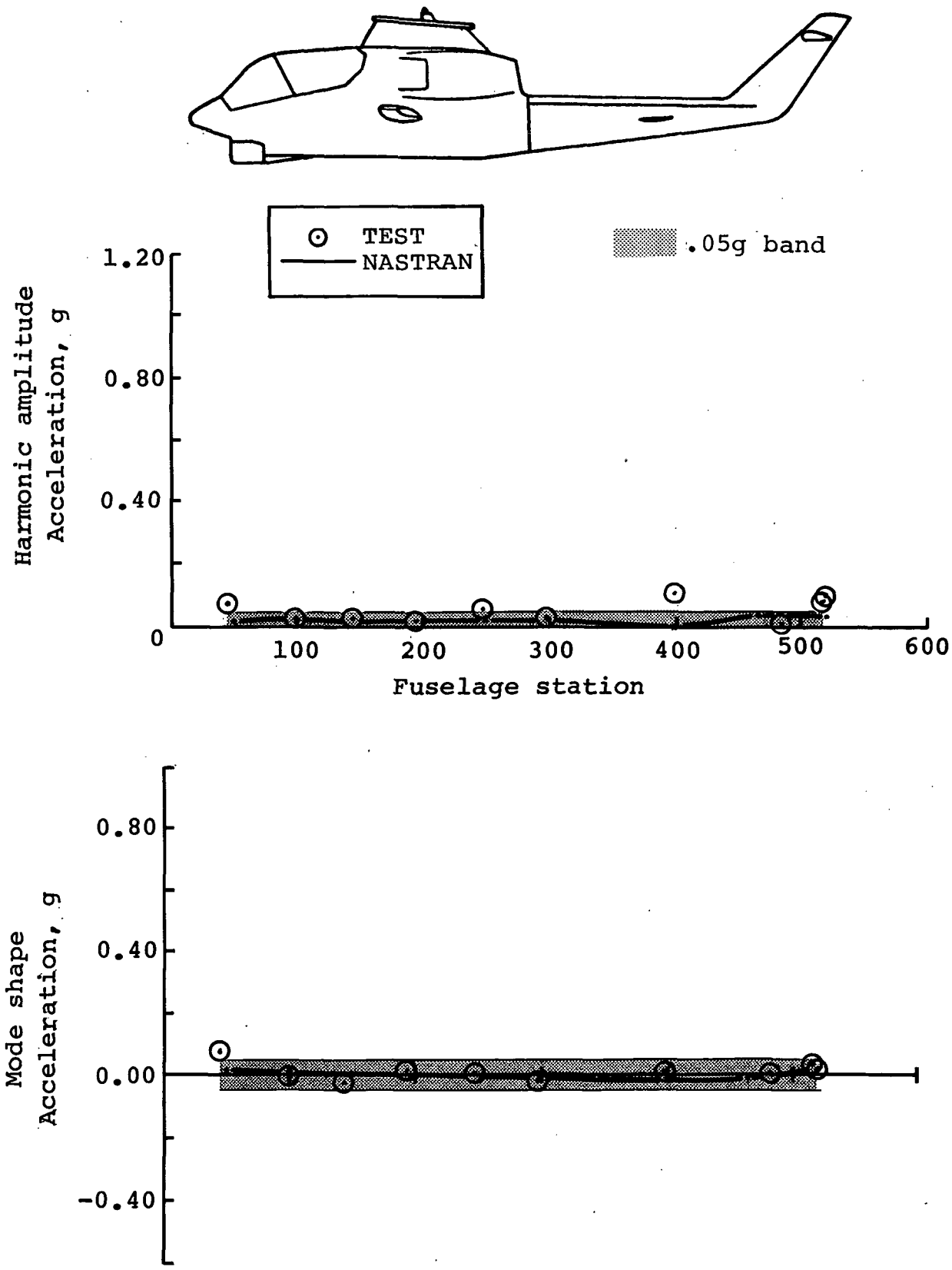

Figure B-60. - Six-per-rev vertical response comparison at 134 knots - wing stores.

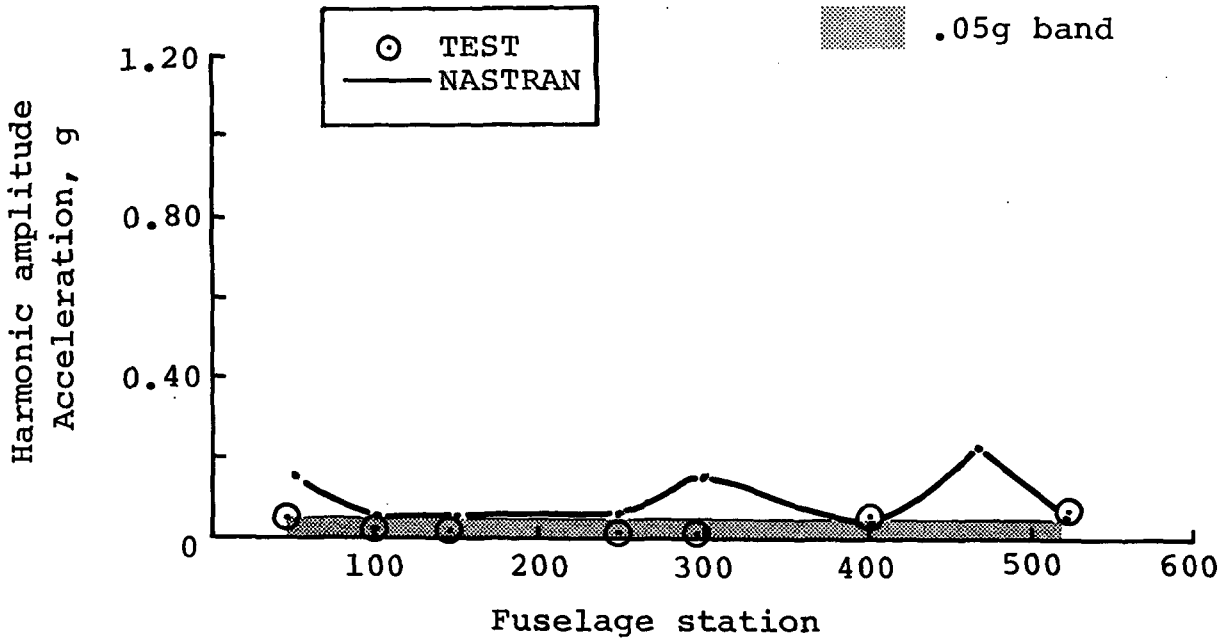

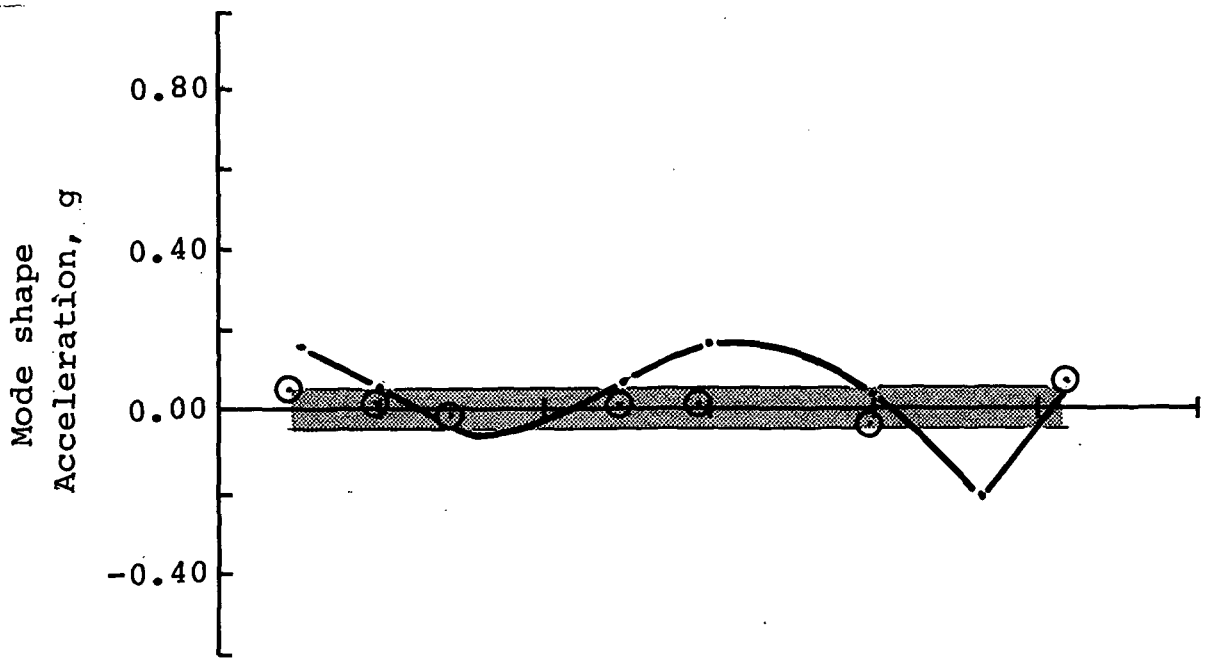

Figure B-61. - Six-per-rev lateral response comparison at 67 knots - clean wing.

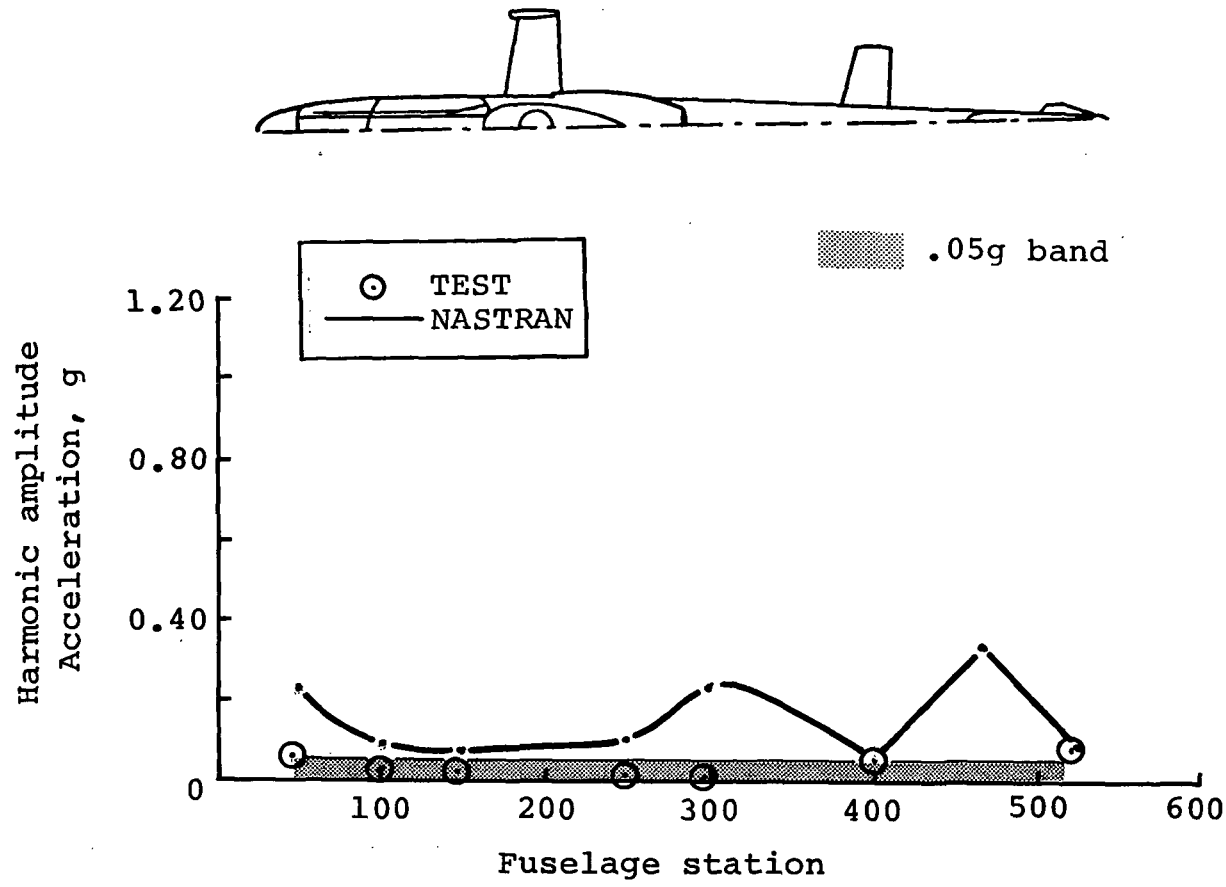

Figure B-62. - Six-per-rev lateral response comparison at 85 knots - clean wing.

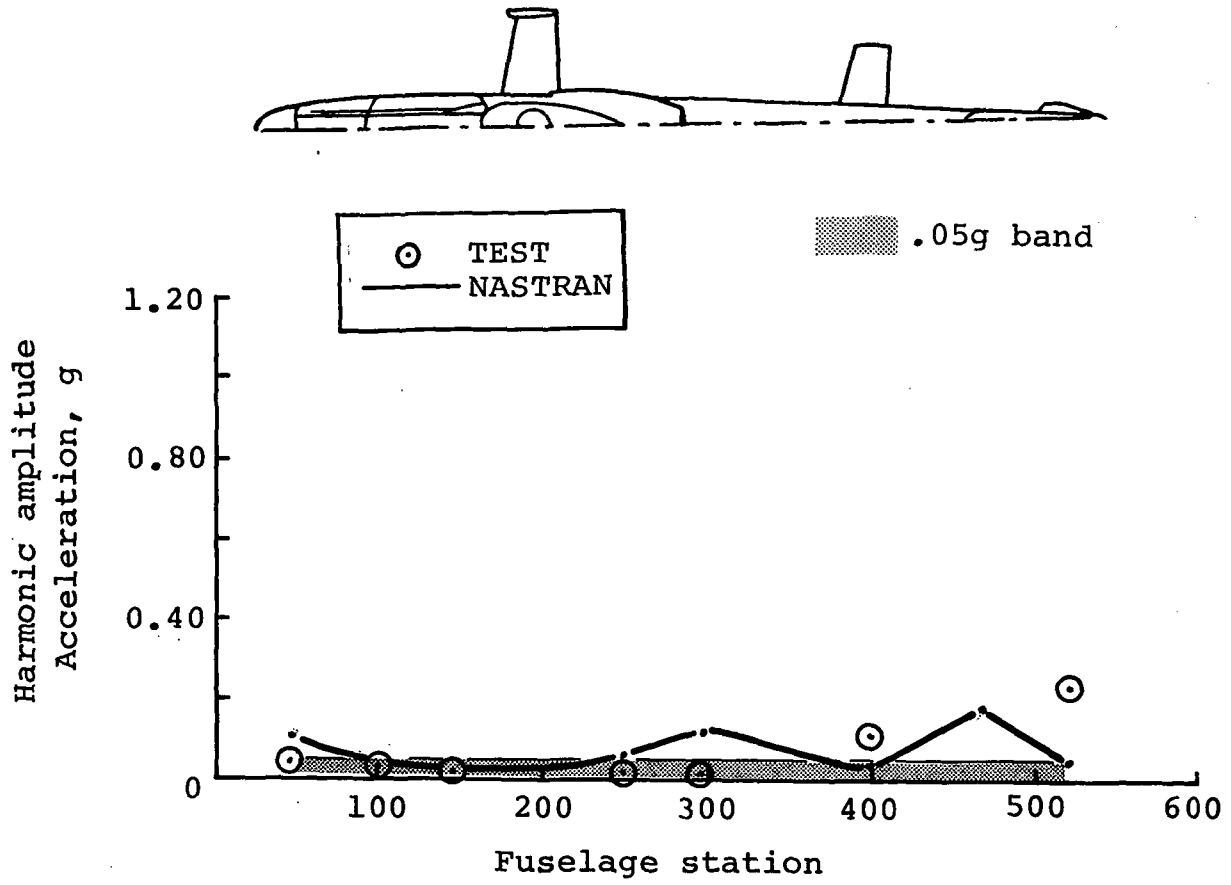

Figure B-63. - Six-per-rev lateral response comparison at 101 knots - clean wing.

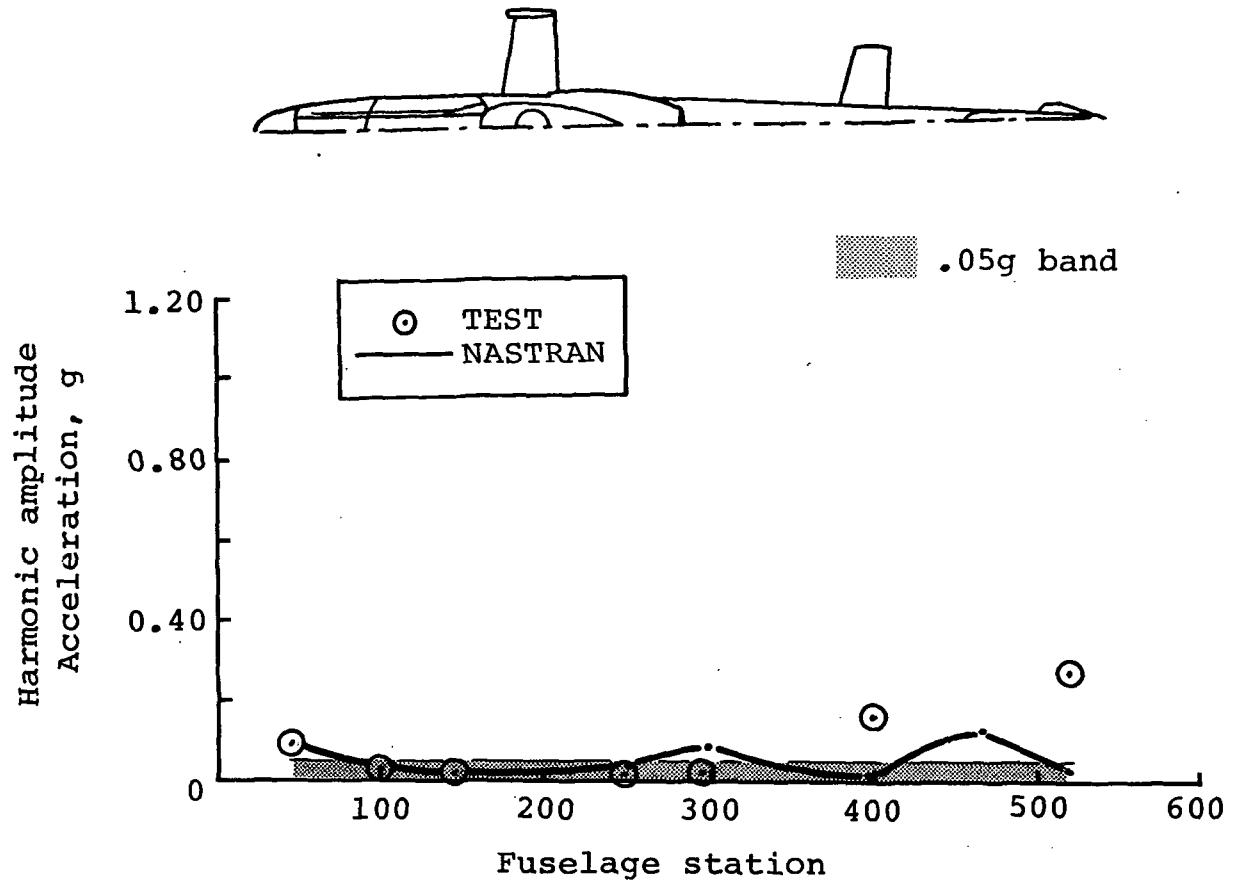

Figure B-64. - Six-per-rev lateral response comparison at 114 knots - clean wing.

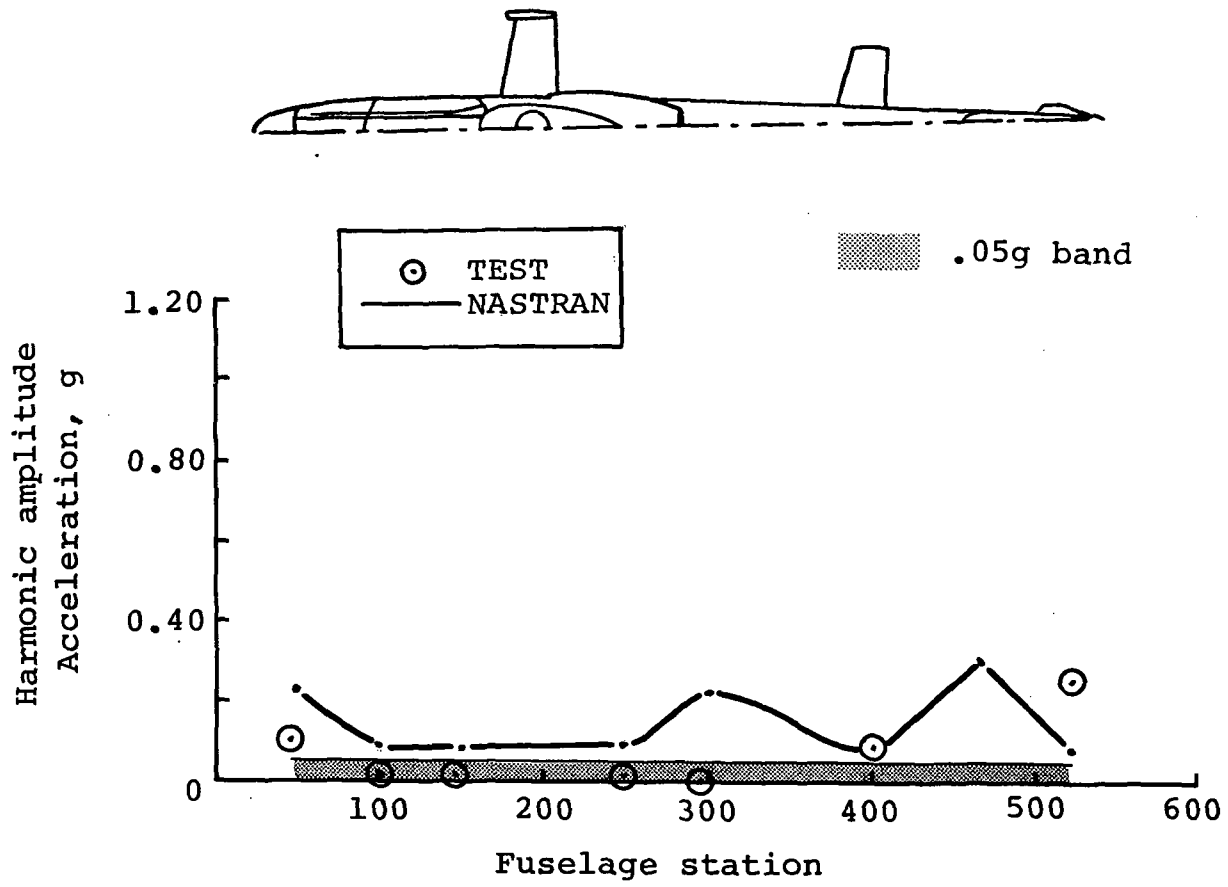

Figure B-65. - Six-per-rev lateral response comparison at 128 knots - clean wing.

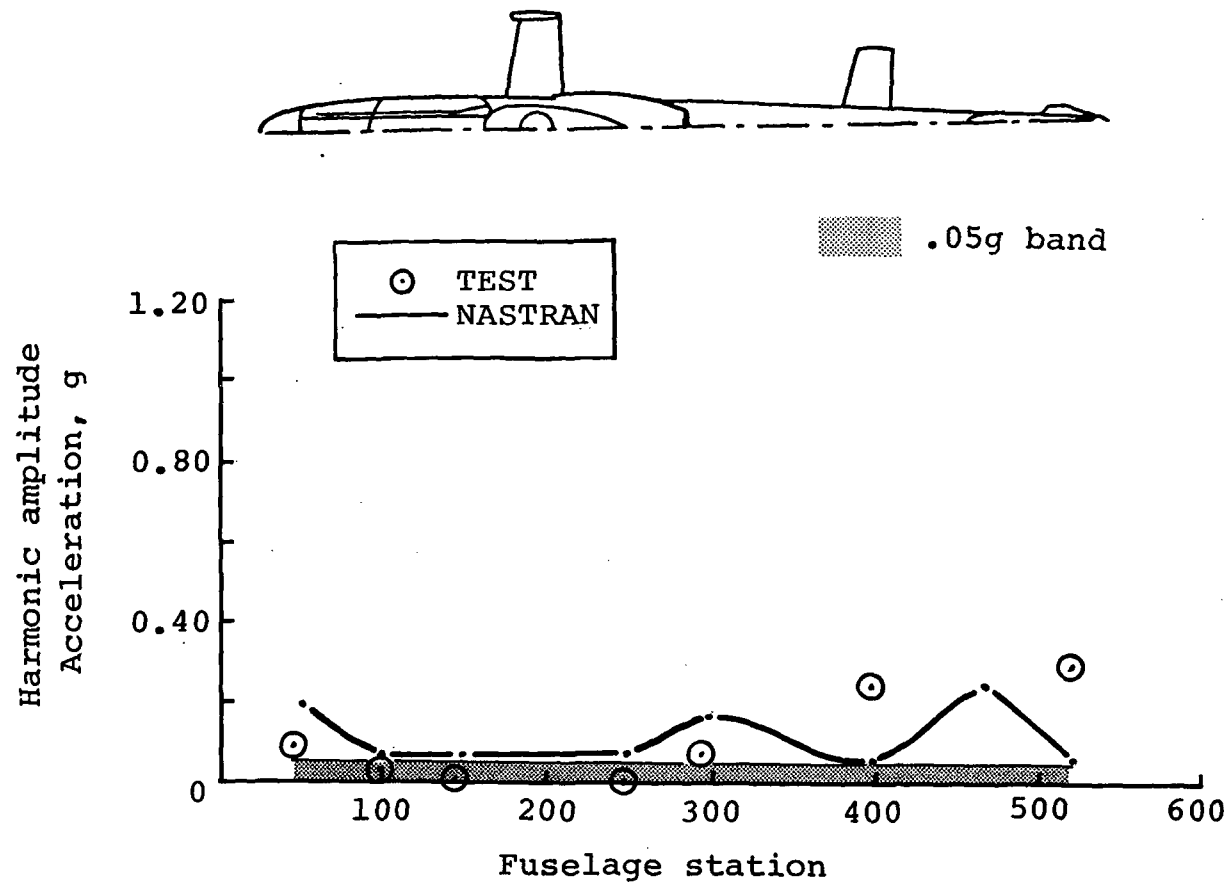

Figure B-66. - Six-per-rev lateral response comparison at 142 knots - clean wing.

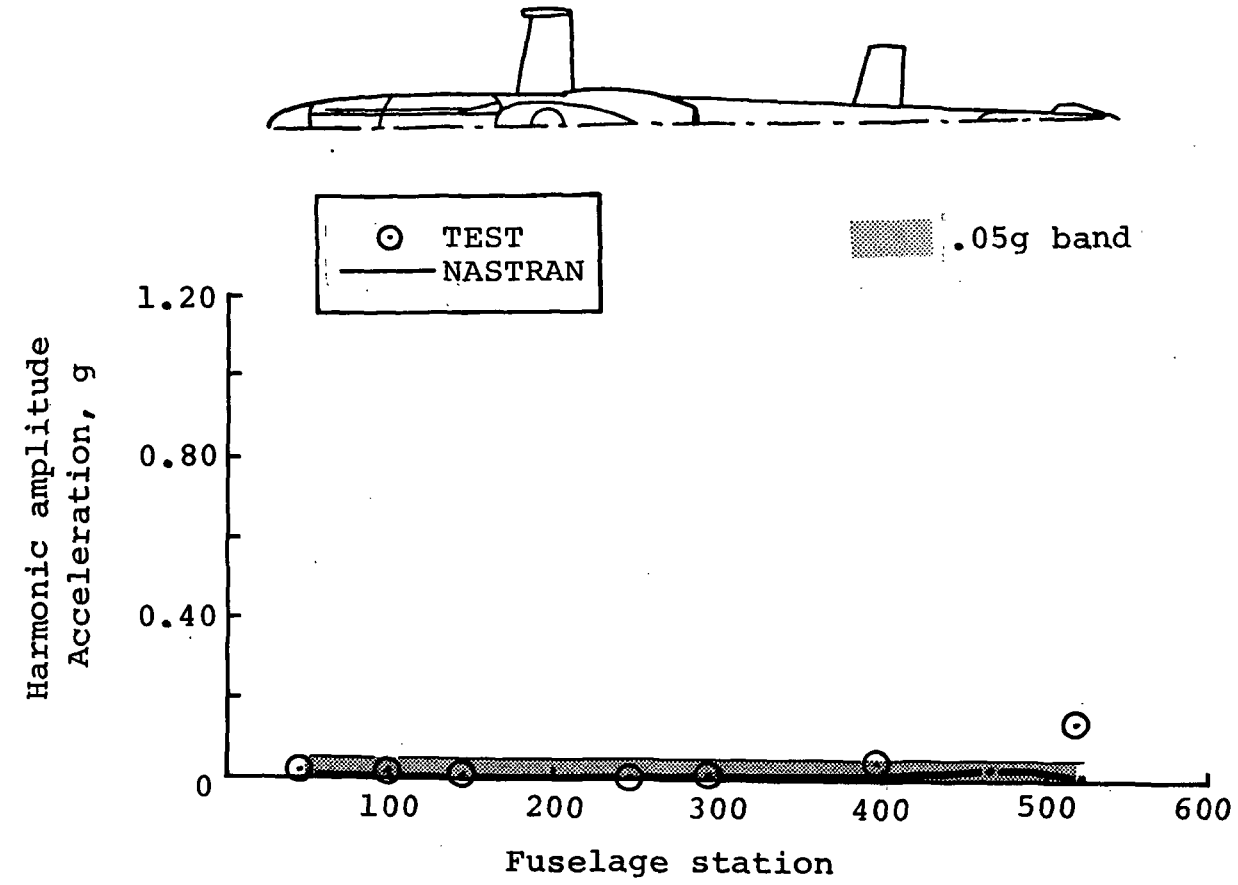

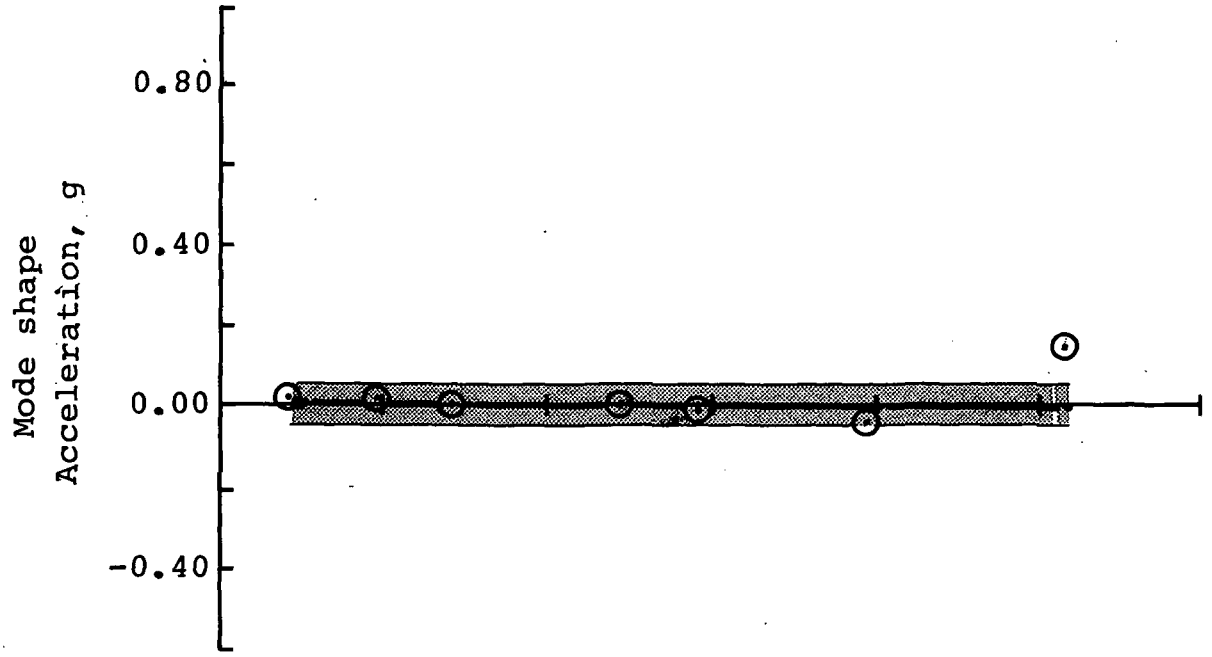

Figure B-67. - Six-per-rev lateral response comparison at 61 knots - wing stores.

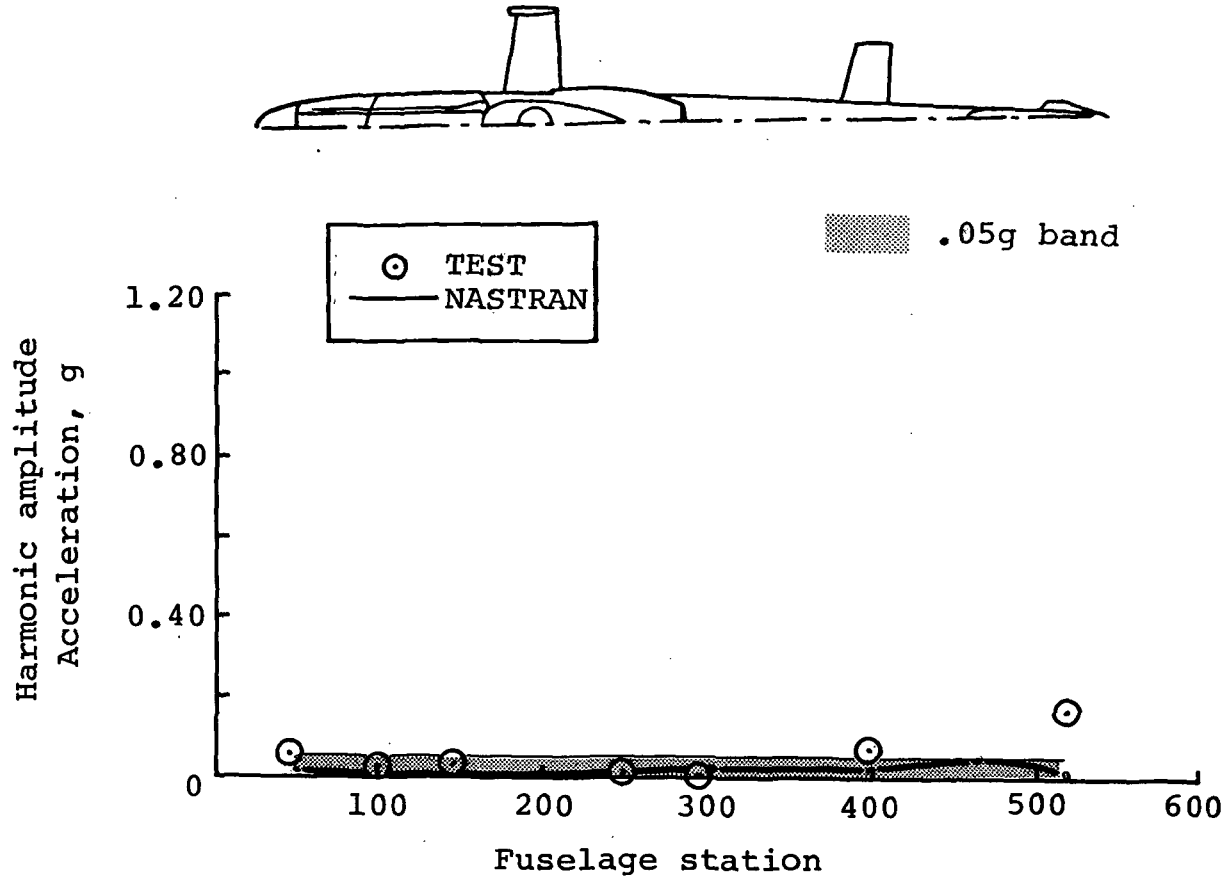

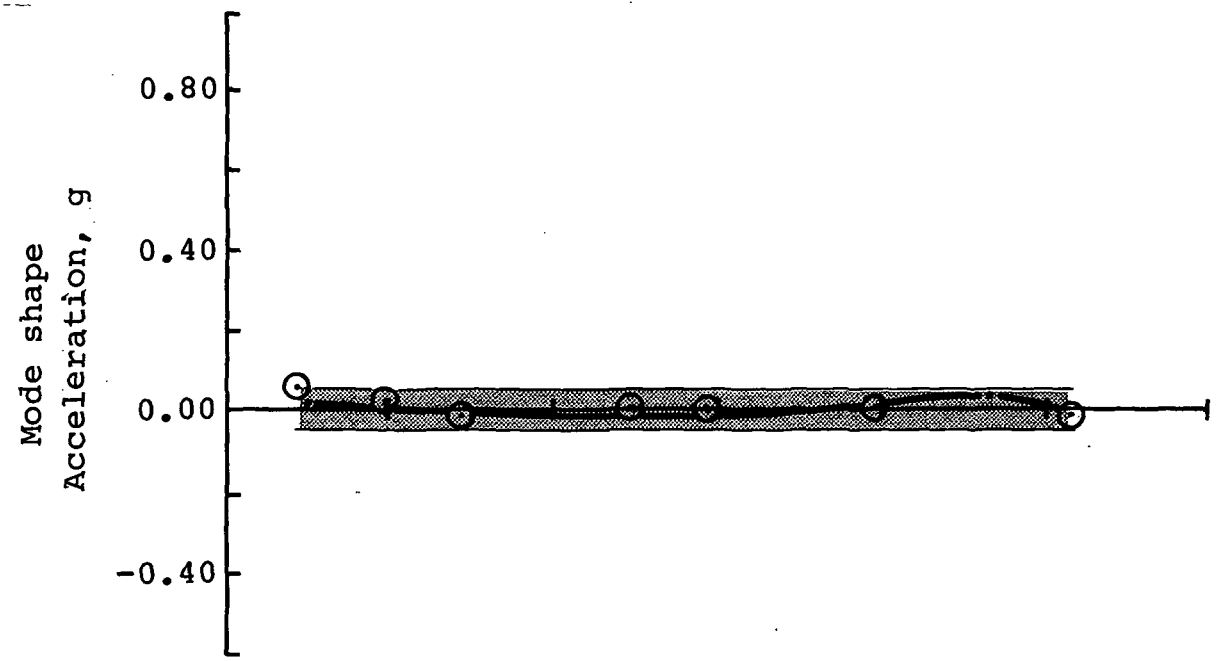

Figure B-68. - Six-per-rev lateral response comparison at 76 knots - wing stores.

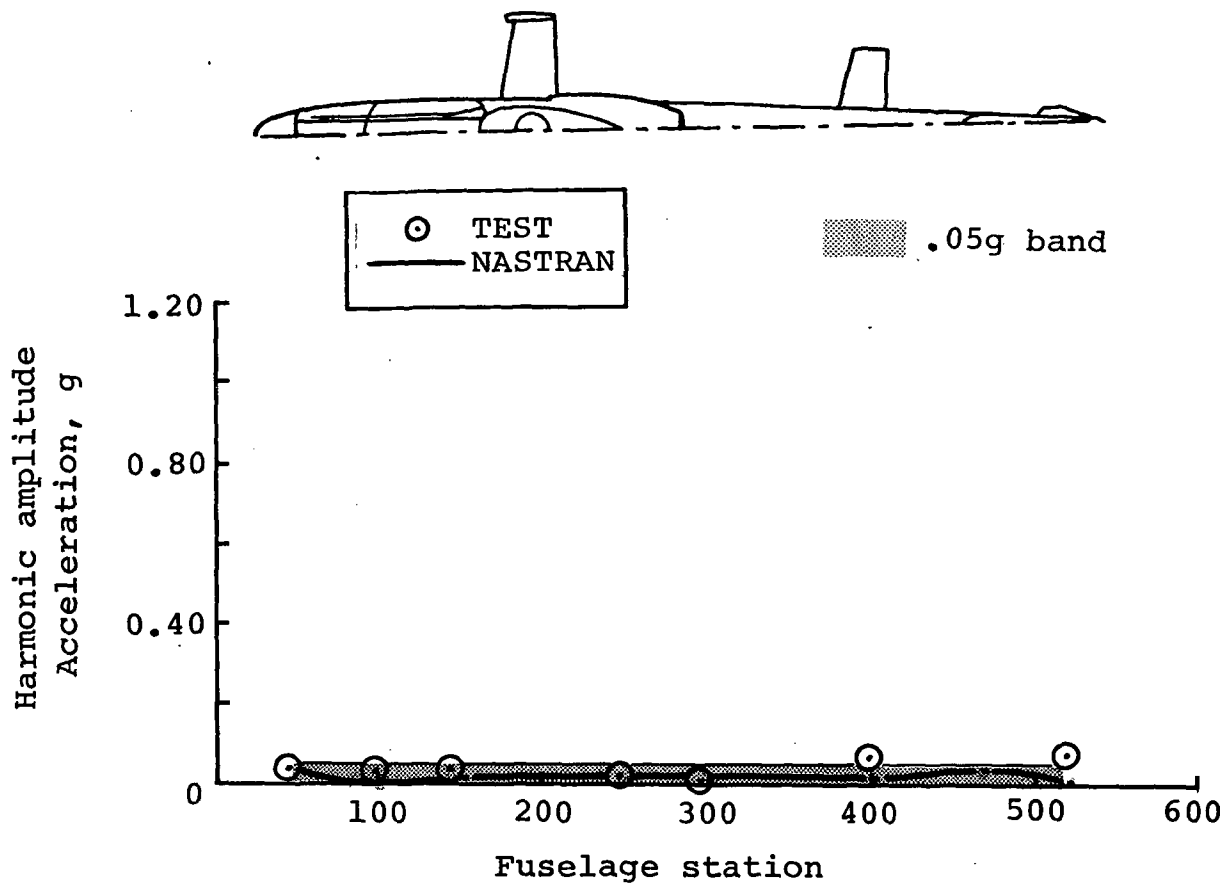

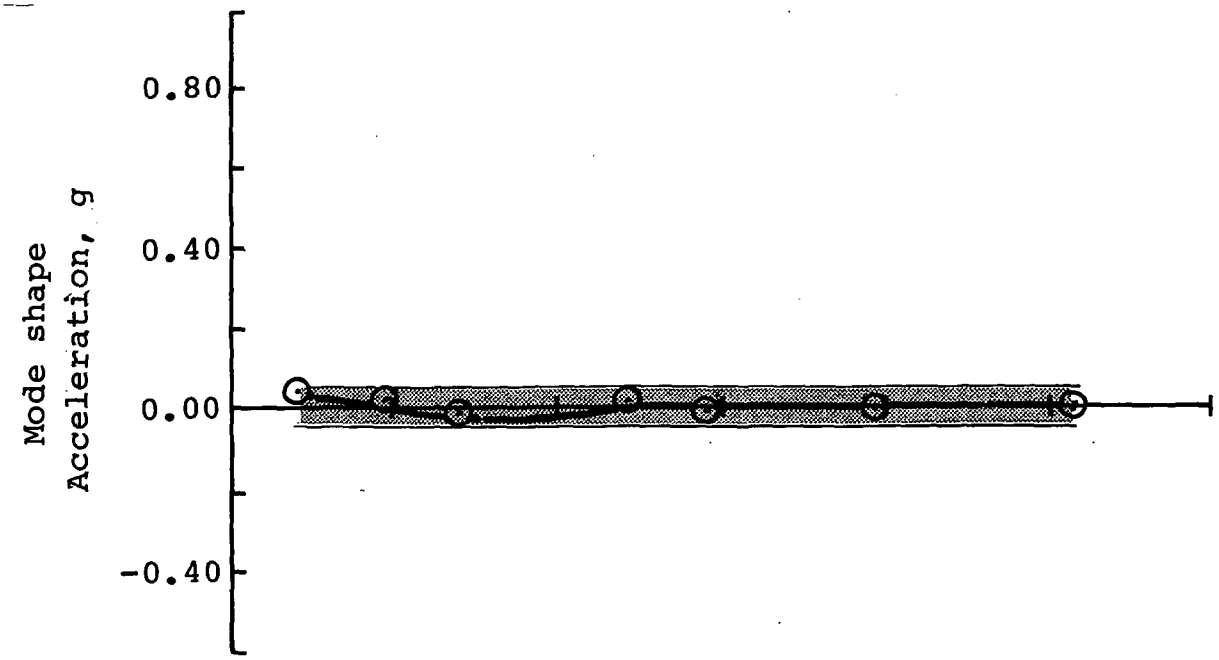

Figure B-69. - Six-per-rev lateral response comparison at 95 knots - wing stores.

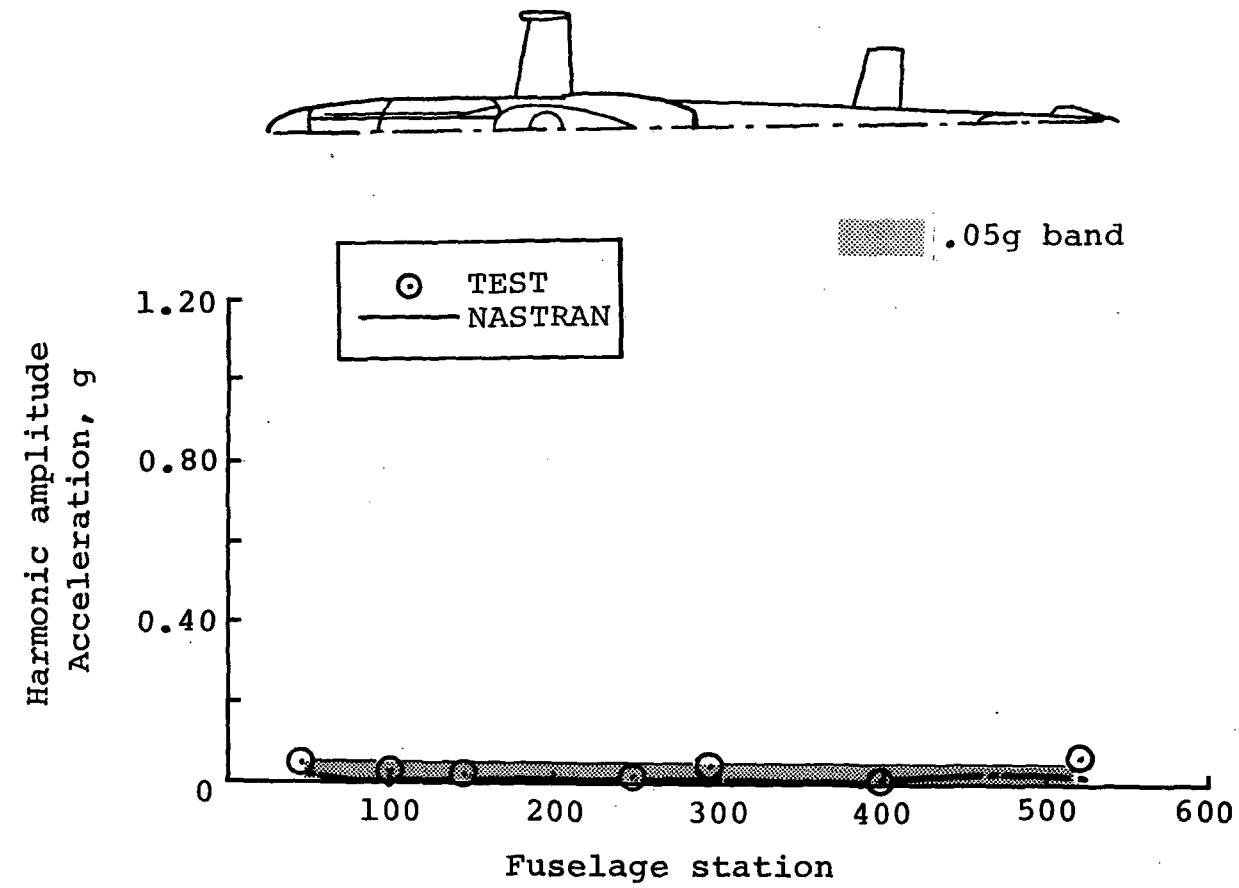

Figure B-70. - Six-per-rev lateral response comparison at 108 knots - wing stores.

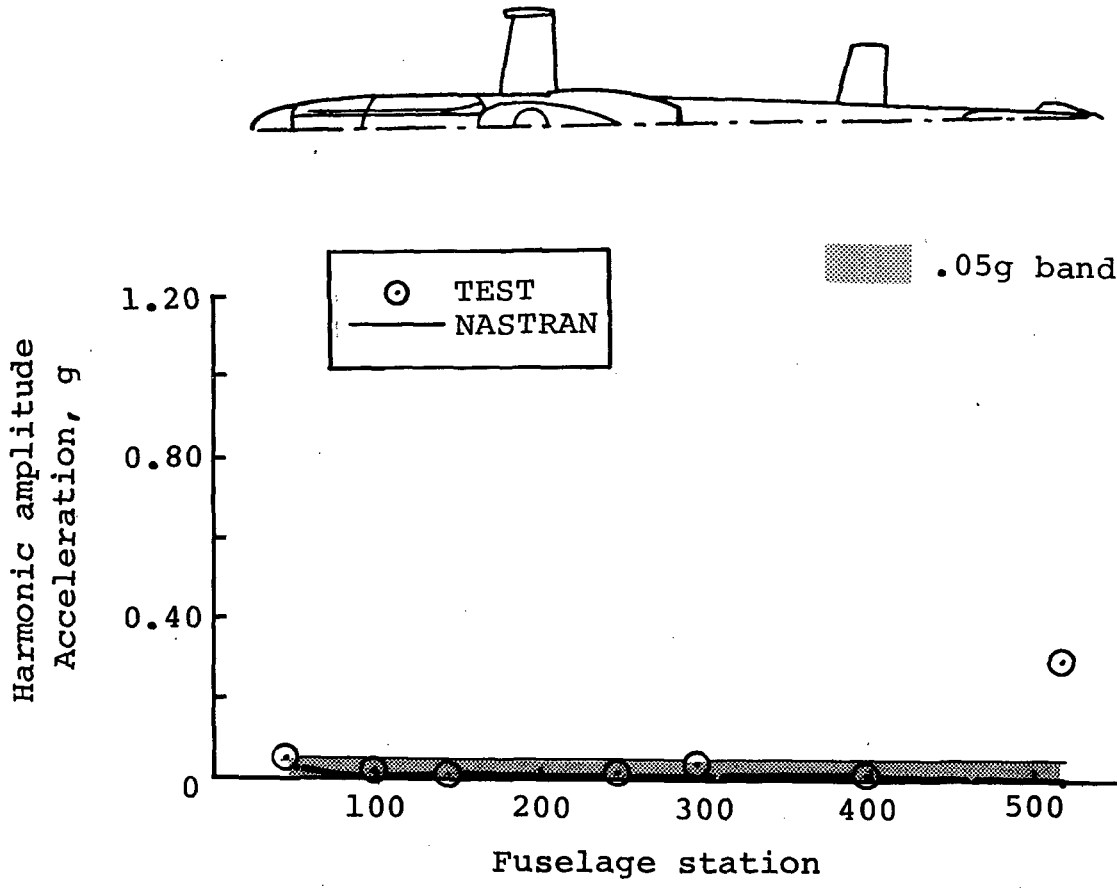

Figure B-71. - Six-per-rev lateral response comparison at 120 knots - wing stores.

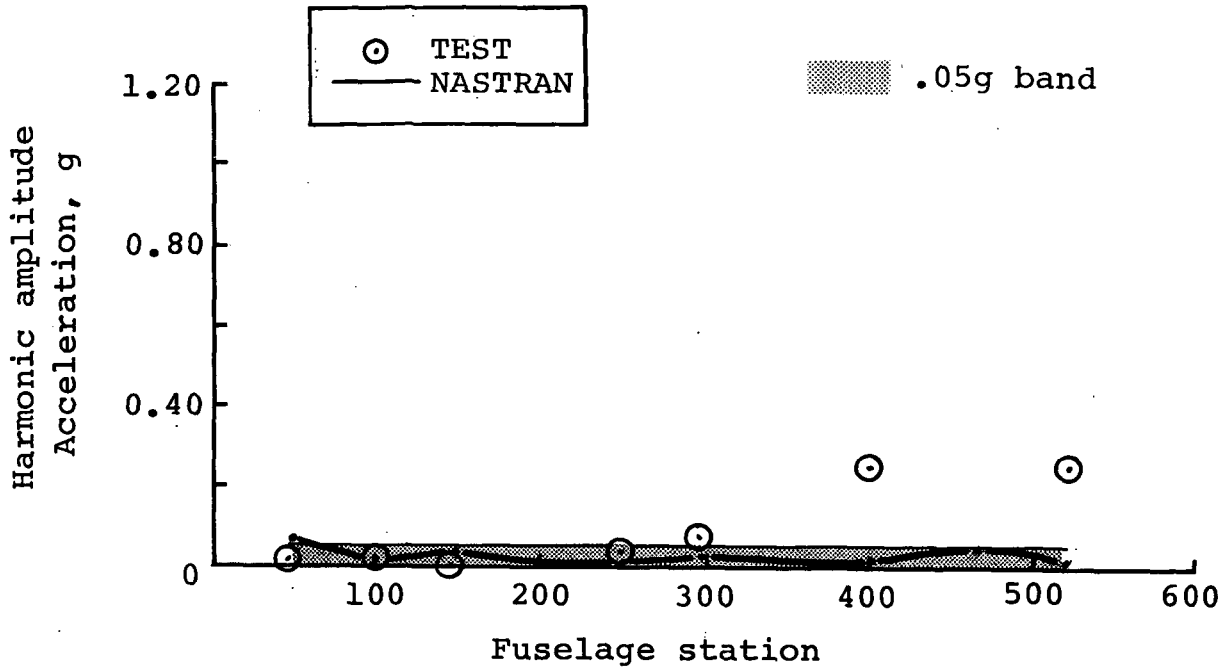

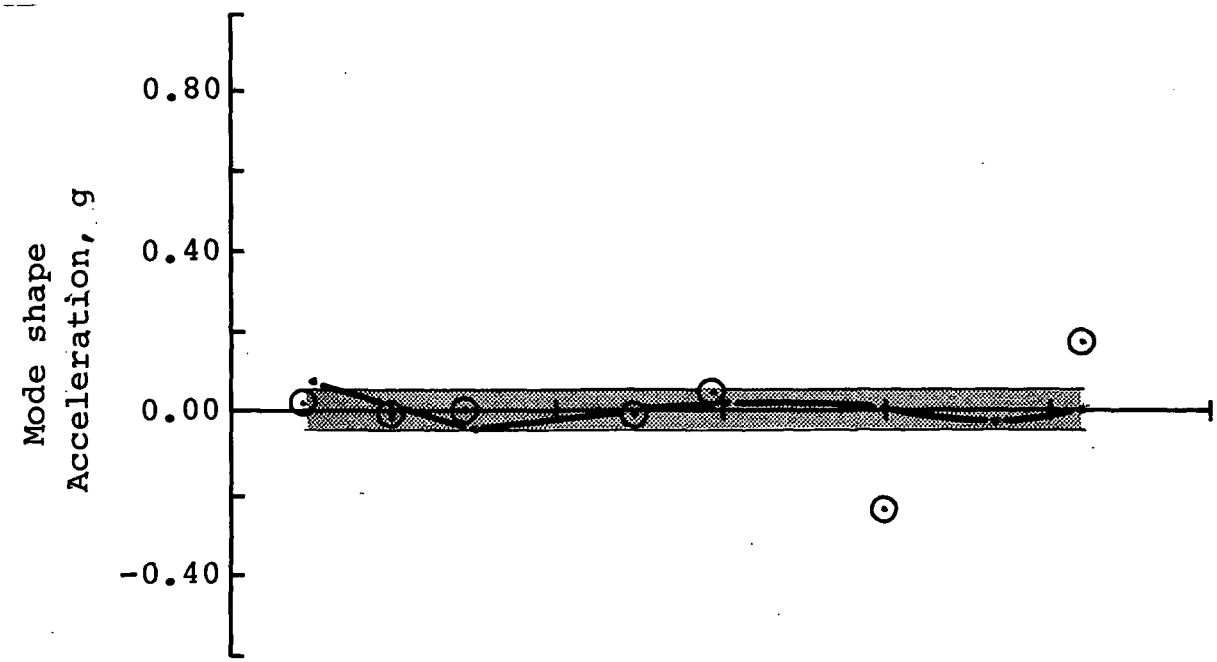

Figure B-72. - Six-per-rev lateral response comparison at 134 knots - wing stores.

APPENDIX C

QUANTITATIVE COMPARISON OF TEST AND ANALYSIS

This appendix contains a quantitative comparison between measured and calculated vibration data using a method suggested by the contract technical monitor from the Army office at Langley, Dr. F. D. Bartlett, Jr.

The relative accuracy between test and analysis is assessed by calculating the average or mean of the differences and standard deviation of the differences for each set of data presented in the figures of Appendix B. These values are ratioed to the mean and standard deviation of the test data as an indication of percentage error and are tabulated in terms of airspeed and main rotor harmonic. The vertical and lateral components of response are presented separately. There is a table for each helicopter configuration. Each data entry in these tables is calculated from the corresponding figure in Appendix B.

The calculations used for determining the mean and standard deviation are given below.

$$\bar{x} = \frac{1}{n} \sum_{i=1}^{n} x_i \,, \qquad \text{where } x_i = \text{value of ith data point}, \quad n = \text{total number of data points}$$

$$\sigma = \sqrt{\frac{n \sum_{i=1}^{n} x_i^2 - \left(\sum_{i=1}^{n} x_i \right)^2}{n(n-1)}}$$

Note that for $\overline{\Delta x}$ and $\sigma_{\Delta x}$, $x = |x_{test} - x_{calculated}|$

TABLES

TABLE C-1. VERTICAL TWO-, FOUR- AND SIX-PER-REV RESPONSE COMPARISON - CLEAN WING CONFIGURATION

Main Rotor Two-per-rev, 10.8 Hz

Airspeed (Knots)	Mean			Standard Deviation		
	$\overline{\Delta x}$	$\overline{x}_{TEST}$	$\overline{\Delta x}/\overline{x}_{TEST}$	$\sigma_{\Delta x}$	σ_{TEST}	$\sigma_{\Delta x}/\sigma_{TEST}$
67	.0360	.1857	.194	.0356	.1726	.206
85	.0229	.1774	.129	.0130	.1500	.087
101	.0605	.2185	.277	.0344	.1630	.211
114	.0998	.2899	.344	.0713	.2177	.328
128	.0753	.3031	.248	.0394	.2138	.184
142	.0854	.3006	.284	.0317	.1619	.196

Main Rotor Four-per-rev, 21.6 Hz

Airspeed (Knots)	Mean			Standard Deviation		
	$\overline{\Delta x}$	$\overline{x}_{TEST}$	$\overline{\Delta x}/\overline{x}_{TEST}$	$\sigma_{\Delta x}$	σ_{TEST}	$\sigma_{\Delta x}/\sigma_{TEST}$
67	.3360	.0925	3.632	.3402	.0714	4.765
85	.0954	.0634	1.505	.0999	.0510	1.959
101	.5207	.0613	8.494	.4806	.0221	21.747
114	.3835	.0712	5.386	.4112	.0221	18.606
128	.8058	.0672	11.991	.8203	.0275	29.829
142	.9868	.0891	11.075	.9162	.0553	16.568

Main Rotor Six-per-rev, 32.4 Hz

Airspeed (Knots)	Mean			Standard Deviation		
	$\overline{\Delta x}$	$\overline{x}_{TEST}$	$\overline{\Delta x}/\overline{x}_{TEST}$	$\sigma_{\Delta x}$	σ_{TEST}	$\sigma_{\Delta x}/\sigma_{TEST}$
67	.0456	.0348	1.310	.0412	.0107	3.850
85	.1016	.0236	4.305	.0574	.0170	3.376
101	.0361	.0582	.620	.0330	.0363	.909
114	.0446	.0753	.592	.0405	.0436	.929
128	.0669	.0580	1.153	.0718	.0192	3.740
142	.0524	.0354	1.480	.0707	.0159	4.447

TABLE C-2. VERTICAL TWO-, FOUR- AND SIX-PER-REV RESPONSE COMPARISON - WING STORES CONFIGURATION

Main Rotor Two-per-rev, 10.8 Hz

Airspeed (Knots)	Mean			Standard Deviation		
	$\overline{\Delta x}$	$\overline{x}_{TEST}$	$\overline{\Delta x}/\overline{x}_{TEST}$	$\sigma_{\Delta x}$	σ_{TEST}	$\sigma_{\Delta x}/\sigma_{TEST}$
61	.0473	.1826	.259	.0301	.1705	.177
76	.0841	.1953	.431	.0344	.1767	.195
95	.0346	.1779	.194	.0141	.1431	.099
108	.0500	.2291	.218	.0344	.1770	.194
120	.0558	.2683	.208	.0139	.2121	.066
134	.0545	.2724	.200	.0528	.1803	.293

Main Rotor Four-per-rev, 21.6 Hz

Airspeed (Knots)	Mean			Standard Deviation		
	$\overline{\Delta x}$	$\overline{x}_{TEST}$	$\overline{\Delta x}/\overline{x}_{TEST}$	$\sigma_{\Delta x}$	σ_{TEST}	$\sigma_{\Delta x}/\sigma_{TEST}$
61	.0688	.0748	.920	.0663	.0422	1.571
76	.0699	.0812	.861	.0486	.0484	1.004
95	.0272	.0421	.646	.0244	.0216	1.130
108	.0579	.0392	1.477	.0748	.0232	3.224
120	.1103	.0296	3.726	.1149	.0164	7.006
134	.1293	.0505	2.560	.1279	.0349	3.665

Main Rotor Six-per-rev, 32.4 Hz

Airspeed (Knots)	Mean			Standard Deviation		
	$\overline{\Delta x}$	$\overline{x}_{TEST}$	$\overline{\Delta x}/\overline{x}_{TEST}$	$\sigma_{\Delta x}$	σ_{TEST}	$\sigma_{\Delta x}/\sigma_{TEST}$
61	.0263	.0426	.617	.0410	.0396	1.035
76	.0411	.0393	1.046	.0286	.0315	.908
95	.0348	.0375	.928	.0204	.0235	.868
108	.0200	.0342	.585	.0253	.0134	1.888
120	.0226	.0393	.575	.0228	.0184	1.239
134	.0414	.0588	.704	.0347	.0319	1.088

TABLE C-3. LATERAL TWO-, FOUR- AND SIX-PER-REV RESPONSE COMPARISON - CLEAN WING CONFIGURATION

Main Rotor Two-per-rev, 10.8 Hz

Airspeed (Knots)	Mean			Standard Deviation		
	$\overline{\Delta x}$	$\overline{x}_{TEST}$	$\overline{\Delta x}/\overline{x}_{TEST}$	$\sigma_{\Delta x}$	σ_{TEST}	$\sigma_{\Delta x}/\sigma_{TEST}$
67	.0469	.0700	.670	.0407	.0519	.784
85	.0639	.0902	.708	.0861	.0961	.896
101	.0500	.0836	.598	.0611	.0639	.956
114	.0824	.1192	.691	.1422	.1395	1.019
128	.1012	.1397	.724	.1781	.1918	.929
142	.2044	.2573	.794	.3329	.3729	.893

Main Rotor Four-per-rev, 21.6 Hz

Airspeed (Knots)	Mean			Standard Deviation		
	$\overline{\Delta x}$	$\overline{x}_{TEST}$	$\overline{\Delta x}/\overline{x}_{TEST}$	$\sigma_{\Delta x}$	σ_{TEST}	$\sigma_{\Delta x}/\sigma_{TEST}$
67	.0317	.0605	.524	.0396	.0515	.769
85	.1395	.0544	2.564	.1200	.0471	2.548
101	.2300	.0422	5.450	.1922	.0354	5.429
114	.0634	.0531	1.194	.0292	.0668	.437
128	.1731	.0282	6.138	.1408	.0234	6.017
142	.2315	.0815	2.840	.1734	.0705	2.460

Main Rotor Six-per-rev, 32.4 Hz

Airspeed (Knots)	Mean			Standard Deviation		
	$\overline{\Delta x}$	$\overline{x}_{TEST}$	$\overline{\Delta x}/\overline{x}_{TEST}$	$\sigma_{\Delta x}$	σ_{TEST}	$\sigma_{\Delta x}/\sigma_{TEST}$
67	.0592	.0360	1.644	.0498	.0241	2.066
85	.0898	.0397	2.262	.0815	.0275	2.964
101	.0741	.0654	1.133	.0589	.0797	.739
114	.0706	.0873	.809	.0912	.0971	.939
128	.1060	.0710	1.493	.0684	.0893	.766
142	.1131	.1097	1.031	.0710	.1154	.615

TABLE C-4. LATERAL TWO-, FOUR- AND SIX-PER-REV RESPONSE COMPARISON - WING STORES CONFIGURATION

Main Rotor Two-per-rev, 10.8 Hz

Airspeed (Knots)	Mean			Standard Deviation		
	$\overline{\Delta x}$	$\overline{x}_{TEST}$	$\overline{\Delta x}/\overline{x}_{TEST}$	$\sigma_{\Delta x}$	σ_{TEST}	$\sigma_{\Delta x}/\sigma_{TEST}$
61	.0642	.0821	.782	.0674	.0744	.906
76	.1097	.1316	.834	.1481	.1560	.949
95	.0775	.1046	.741	.0865	.0989	.875
108	.1077	.1370	.786	.1424	.1546	.921
120	.1153	.1496	.771	.1834	.2002	.916
134	.1404	.1927	.729	.1981	.2429	.816

Main Rotor Four-per-rev, 21.6 Hz

Airspeed (Knots)	Mean			Standard Deviation		
	$\overline{\Delta x}$	$\overline{x}_{TEST}$	$\overline{\Delta x}/\overline{x}_{TEST}$	$\sigma_{\Delta x}$	σ_{TEST}	$\sigma_{\Delta x}/\sigma_{TEST}$
61	.0319	.0380	.839	.0280	.0286	.979
76	.0294	.0518	.568	.0302	.0443	.682
95	.0297	.0475	.625	.0224	.0373	.601
108	.0374	.0438	.854	.0249	.0262	.950
120	.0250	.0368	.679	.0202	.0275	.735
134	.0424	.0752	.564	.0296	.0518	.571

Main Rotor Six-per-rev, 32.4 Hz

Airspeed (Knots)	Mean			Standard Deviation		
	$\overline{\Delta x}$	$\overline{x}_{TEST}$	$\overline{\Delta x}/\overline{x}_{TEST}$	$\sigma_{\Delta x}$	σ_{TEST}	$\sigma_{\Delta x}/\sigma_{TEST}$
61	.0320	.0362	.884	.0477	.0503	.948
76	.0460	.0535	.860	.0512	.0557	.919
95	.0301	.0427	.705	.0243	.0250	.972
108	.0259	.0346	.749	.0198	.0207	.957
120	.0563	.0660	.853	.1072	.1043	1.028
134	.0960	.0951	1.009	.0994	.1094	.909

REFERENCES

1. Cronkhite, J. D., Berry, V. L., and Brunken, J. E.: A NASTRAN Vibration Model of the AH-1G Helicopter Airframe. U. S. Army Armament Command Report No. R-TR-74-045, June 1974.

2. Cronkhite, J. D. and Berry, V. L.: Correlation of AH-1G Airframe Test Data with a NASTRAN Mathematical Model. NASA CR-145119, 1976.

3. Shockey, G. A., Cox, C. R., and Williamson, J. W.: AH-1G Helicopter Aerodynamic and Structural Loads Survey. Bell Helicopter Textron Report No. 699-099-017, May 1976.

4. Shipman, D. P., White, J. A., and Cronkhite, J. D.: Fuselage Nodalization. Presented at the 28th National Forum of the American Helicopter Society, Washington, D. C., May 1972.

5. Perry, D. J.: Aircraft Structures. McGraw-Hill Book Company, 1950.

6. Bruhn, E. F.: Analysis and Design of Flight Vehicle Structures. Tri-State Offset Company, 1965.

7. McCormick, C. W. (Editor): The NASTRAN User's Manaul. NASA SP-222(01), June 1972.

8. Slack, J. R.: Static Load Test of AH-1G Tailboom to Determine Distribution of Internal Stress. Bell Helicopter Textron Report No. 209-095-003, October 1976.

9. Wilson, H. E.: NASTRAN Model Description of AH-1G Tailboom and Fin. Bell Helicopter Textron Report No. 209-099-515, February 1977.

TABLE I. - WEIGHT SUMMARY - CLEAN WING

Item	Weight kg (lb)	Fuselage Station of cg
• Basic ship	2855 (6289)	203.3
• Useful loads		
(1) Fuel	740 (1630)	200.4
(2) Pilot	68 (150)	135.0
(3) Gunner	68 (150)	83.0
(4) Ballast	45 (100)	305.0
• Total	3777 (8319)	200.6

TABLE II. - WEIGHT SUMMARY - WING STORES

Item	Weight kg (lb)	Fuselage Station of cg
• Basic ship	2855 (6289)	203.3
• Useful loads		
(1) Fuel	740 (1630)	200.4
(2) Pilot	68 (150)	135.0
(3) Gunner	68 (150)	83.0
(4) Ballast	23 (50)	40.0
(5) Ballast	68 (150)	75.0
(6) Wing Stores	295 (650)	196.3
• Total	4117 (9068)	196.2

TABLE III. - WEIGHT PARAMETER COMPARISONS

Parameter	Configuration			
	Clean Wing		Wing Stores	
	NASTRAN	Test	NASTRAN	Test
Weight, kg (lb)	3768 (8300)	3777 (8319)	4109 (9059)	4117 (9068)
CG: station	198.34	200.6	194.09	196.2
buttline	-.0349	-	-.0320	-
waterline	72.705	-	70.283	-
Inertia: roll, $kg\text{-}m^2$	3511	-	4044	-
$(in\text{-}in^2)$	(1.1983×10^7)	-	(1.3802×10^7)	-
pitch, $kg\text{-}m^2$	17973	-	18840	-
$(lb\text{-}in^2)$	(6.1342×10^7)		(6.4300×10^7)	
yaw, $kg\text{-}m^2$	14942		15990	
$(lb\text{-}in^2)$	(5.0997×10^7)		(5.4572×10^7)	

TABLE IV - CALCULATED AIRFRAME NATURAL FREQUENCIES

Mode	Natural frequency, hertz	
	3768 kg-clean wing-aft cg	4086 kg-wing stores-mid cg
Main rotor pylon fore-and-aft rocking (pylon pitch)	2.987	2.965
Main rotor pylon lateral rocking (pylon roll)	3.866	3.414
First fuselage lateral bending	7.121	6.927
First fuselage vertical bending	7.969	7.736
Skid	14.572	14.538
First fuselage torsion	16.032	15.622
Second fuselage vertical bending	17.221	17.242
Second fuselage lateral bending	17.783	16.595
Fuselage roll/engine lateral	19.273	18.362
Skid	19.834	19.826
Fuselage torsion/wing yaw	21.879	20.639
Wing asymmetric torsion	-	22.767
Skid	23.431	23.414
Third fuselage vertical bending	25.153	23.720
Main rotor mast lateral bending	25.591	25.522
Third fuselage lateral bending	26.529	24.667
Main rotor mast fore-and-aft bending	27.099	26.609
Wing symmetric torsion	-	28.085
Skid	29.104	28.645
Fourth fuselage vertical bending	32.264	31.315
Fuselage torsion	34.013	31.913

TABLE V - LOCATION OF STRAIN GAGES FOR TAILBOOM STATIC TEST

Gage Channel No.	Item to Which Gage Attached	Location in Tailboom Coordinates		
		W.L.	B.L.	Boom Sta.
1	Stringer	16.26	3.67	69.97
2	Longeron, Upr, RH	11.60	11.53	
3	Stringer	3.94	12.95	
4	Stringer	-3.80	12.98	
5	Longeron, Lwr, RH	-11.56	11.36	
6	Stringer	-16.30	0.0	
7	Longeron, Lwr LH	-11.56	-11.36	
8	Stringer	-3.80	-12.98	
9	Stringer	3.94	-12.95	
10	Longeron, Upr, RH	11.60	-11.56	
11	Stringer	16.26	-3.67	69.97
12	Stringer	14.95	3.67	90.91
13	Longeron, Upr, RH	10.77	10.61	
14	Stringer	3.72	11.92	
15	Stringer	-3.44	11.94	
16	Longeron, Lwr, RH	10.60	10.45	
17	Stringer	-14.99	0.0	
18	Longeron, Lwr, LH	-10.60	-10.45	
19	Stringer	-3.44	-11.94	
20	Door Panel	3.72	-11.92	
21	Longeron, Upr, LH	10.77	-10.61	
22	Stringer	14.95	-3.67	90.91
23	Stringer	13.65	3.67	112.85
24	Longeron, Upr RH	9.93	9.70	
25	Stringer	3.49	10.88	
26	Stringer	-3.08	10.89	
27	Longeron, Lwr, RH	-9.64	9.53	
28	Stringer	-13.67	0.0	
29	Longeron, Lwr, RH	-9.64	-9.53	
30	Stringer	-3.08	-10.89	
31	Stringer	3.49	-10.88	
32	Longeron, Upr, LH	9.93	-9.70	
33	Stringer	13.65	-3.67	112.85
34	Skin Panel	10.32	Right	69.97
35		9.05	Contour	
36		7.77		
37		6.49		
38		5.22		
39		2.65		
40		1.36		
41		.07		
42		-1.22	Right	
43	Skin Panel	-2.51	Contour	69.97

TABLE V (Cont'd)

Gage Channel No.	Item to Which Gage Attached	Location in Tailboom Coordinates		
		W.L.	B.L.	Boom Sta.
44	Skin Panel	3.06	Right	90.91
45		1.56	Contour	
46		0.0		
47		-1.53		
48		-3.06		
49		-4.06		
50		-5.44		
51		-6.75		
52		-8.06	Right	
53	Skin Panel	-9.37	Contour	90.91

Ele. No.		Bay 1 BS 41-BS 60 Initial	Final	Bay 2 BS 60-BS 80 Initial	Final	Bay 3 BS 80-BS 101 Initial	Final	Bay 4 BS 101-BS 122 Initial	Final	Bay 5 BS 122-BS 143 Initial	Final	Bay 6 BS 143-BS 164 Initial	Final	Bay 7 BS 164-BS 185 Initial	Final	Bay 8 BS 185-BS 194 Initial	Final
1	Area	.044	.327	.044	.296	.044	.281	.044	.268	.044	.244	.044	.228	.044	.203	.044	.191
	Load	-102	-238	-106	-427	-37	-3637	-36	-310	-38	-309	-68	-352	-87	-249	-45	92
2	Area	.312	.703	.312	.619	.312	.607	.312	.607	.292	.593	.080	.353	.248	.052	.248	.482
	Load	-3255	-3666	-2172	-2647	-1816	-2254	-1601	-1938	-1555	-1676	-1420	-1359	-1134	-1186	-968	-1304
3	Area	.142	.439	.142	.204	.142	.215	.142	.283	.142	.237	.142	.290	.142	.244	.142	.247
	Load	-724	-583	-1294	-1074	-873	-878	-802	-838	-1085	-979	-998	-987	-779	-791	-666	-656
4	Area	.142	.480	.142	.206	.222	.316	.222	.382	.142	.322	.142	.305	.142	.261	.142	.263
	Load	-548	-497	-1647	-1358	-982	-903	-1003	-1062	-1494	-1494	-962	-1033	-878	-823	-654	-645
5	Area	.510	.865	.431	.673	.332	.616	.312	.611	.312	.658	.312	.661	.312	.636	.312	.601
	Load	-4332	-4051	-3139	-3042	-2141	-2337	-1869	-2041	-2332	-2155	-2253	-2072	-1711	-1610	-1293	-1088
6	Area	.080	.454	.080	.383	.080	.366	.080	.356	.080	.499	.080	.323	.080	.351	.080	.283
	Load	38	-7	55	-37	-7	-84	-48	-100	-44	-60	-33	-15	-26	-8	-31	-27
7	Area	.436	.907	.312	.670	.312	.646	.536	.825	.312	.687	.312	.660	.312	.637	.312	.616
	Load	4216	3955	2892	2842	1926	2268	1718	2136	2232	2215	2186	2056	1654	1592	1252	1100
8	Area	.142	.462	.142	.316	.222	.383	.222	.379	.142	.325	.142	.305	.142	.286	.142	.271
	Load	638	621	1860	1611	1100	1065	1117	1038	1640	1446	1055	1049	958	871	725	709
9	Area	.142	.439	.142	.312	.142	.301	.142	.286	.142	.307	.142	.288	.142	.269	.142	.253
	Load	751	640	1447	1298	1088	1112	1057	974	1380	1129	1229	1059	960	821	826	753
10	Area	.446	.901	.198	.559	.198	.538	.446	.749	.124	.433	.124	.406	.124	.379	.124	.358
	Load	3214	3603	1928	2420	1396	2058	1087	1862	1042	1562	1020	1310	814	1053	669	810
11	Area	.054	.314	.054	.299	.054	.283	.054	.266	.054	.294	.054	.231	.054	.213	.054	.201
	Load	103	223	174	414	190	343	245	2883	255	322	244	344	230	331	186	256

1 pound = 4.448 newton
1 in^2 = 6.452 x 10^{-4} $meters^2$

TABLE VI - 5604 NEWTON LATERAL RIGHT LOAD

Ele. No.		Bay 1 BS 41-BS 60 Initial	Final	Bay 2 BS 60-BS 80 Initial	Final	Bay 3 BS 80-BS 101 Initial	Final	Bay 4 BS 101-BS 122 Initial	Final	Bay 5 BS 122-BS 143 Initial	Final	Bay 6 BS 143-BS 164 Initial	Final	Bay 7 BS 164-BS 185 Initial	Final	Bay 8 BS 185-BS 194 Initial	Final
1	Area	.044	.304	.044	.290	.044	.273	.044	.255	.044	.239	.044	.221	.044	.204	.044	.191
	Load	102	175	106	300	37	225	36	201	38	254	68	315	86	236	51	-84
2	Area	.312	.767	.312	.673	.312	.640	.312	.614	.292	.601	.080	.362	.248	.503	.248	.482
	Load	3255	3523	2172	2491	1817	2118	1601	1865	1556	1619	1420	1345	1135	1176	959	1276
3	Area	.142	.439	.142	.312	.142	.301	.142	.286	.142	.307	.142	.288	.142	.269	.142	.253
	Load	724	626	1294	1235	873	1071	802	977	1085	1108	998	1052	779	813	665	684
4	Area	.142	.462	.142	.316	.222	.394	.222	.379	.142	.325	.142	.305	.142	.286	.142	.271
	Load	548	588	1647	1565	982	1097	1003	1081	1494	1488	962	1044	878	863	656	662
5	Area	.510	.981	.431	.778	.332	.665	.312	.625	.312	.687	.312	.660	.312	.637	.312	.616
	Load	4332	4148	3139	3036	2141	2334	1869	2077	2332	2194	2253	2077	1711	1584	1298	1073
6	Area	.080	.428	.080	.387	.080	.377	.080	.321	.080	.356	.080	.323	.080	.294	.080	.266
	Load	-38	-35	-55	-91	74	-71	48	-8	44	-6	33	-22	26	-6	29	13
7	Area	.436	.832	.312	.599	.312	.589	.536	.836	.312	.673	.312	.657	.312	.660	.312	.617
	Load	-4216	-4141	-2892	-3042	-1926	-2458	-1718	-2348	-2232	-2411	-2186	-2170	-1654	-1646	-1249	-1118
8	Area	.142	.466	.142	.204	.222	.325	.222	.233	.142	.254	.142	.266	.142	.264	.142	.261
	Load	-638	-562	-1860	-1478	-1100	-924	-1117	-733	-1640	-1245	-1055	-939	-958	-817	-723	-677
9	Area	.142	.443	.142	.202	.142	.216	.142	.218	.142	.249	.142	.244	.142	.246	.142	.252
	Load	-751	-658	-1446	-1256	-1088	-922	-1057	-773	-1380	-998	-1228	-947	-960	-760	-826	-736
10	Area	.446	.845	.198	.316	.198	.490	.446	.738	.124	.412	.124	.401	.124	.378	.124	.384
	Load	-3214	-3353	-1928	-2138	-1396	-1933	-1087	-1878	-1042	-1618	-1020	-1365	-813	-1087	-673	-830
11	Area	.054	.328	.054	.289	.054	.291	.054	.268	.054	.253	.054	.234	.054	.215	.054	.224
	Load	-103	-311	-174	-620	-190	-518	-245	-379	-255	-385	-244	-389	-230	-355	-181	-263

1 pound = 4.448 newton
1 in^2 = 6.452 x 10^{-4} $meters^2$

TABLE VII - 5604 NEWTON LATERAL LEFT LOAD

Ele. No.		Bay 1 BS 41-BS 60 Initial	Final	Bay 2 BS 60-BS 80 Initial	Final	Bay 3 BS 80-BS 101 Initial	Final	Bay 4 BS 101-BS 122 Initial	Final	Bay 5 BS 122-BS 143 Initial	Final	Bay 6 BS 143-BS 164 Initial	Final	Bay 7 BS 146-BS 185 Initial	Final	Bay 8 BS 185-BS 194 Initial	Final
1	Area	.044	.305	.044	.289	.044	.273	.044	.255	.044	.239	.044	.221	.044	.204	.044	.191
	Load	289	409	548	905	531	1008	509	958	479	768	426	527	336	527	190	79
2	Area	.312	.767	.312	.673	.312	.640	.312	.614	.292	.601	.080	.362	.248	.503	.248	.482
	Load	3135	2911	2607	2020	2744	1758	2513	1609	2199	1075	1803	922	1396	922	1147	1019
3	Area	.142	.439	.142	.326	.142	.301	.142	.286	.142	.307	.142	.288	.142	.268	.142	.252
	Load	321	240	520	397	467	303	452	259	352	278	355	241	324	241	245	1818
4	Area	.142	.461	.142	.319	.222	.447	.222	.393	.142	.341	.142	.317	.142	.290	.142	.271
	Load	-153	-198	-395	-418	-303	-306	-345	-296	-441	-200	-264	-134	-211	-134	-142	-136
5	Area	.510	.969	.431	.763	.332	.671	.312	.618	.312	.679	.312	.658	.312	.643	.312	.628
	Load	-3440	-3108	-2929	-2323	-2524	-1927	-2287	-1729	-2246	-1457	-2021	-1188	-1596	-1188	-1214	-911
6	Area	.080	.335	.080	.359	.080	.335	.080	.305	.080	.336	.080	.302	.080	.272	.080	.239
	Load	-402	-536	-844	-1210	-853	-1299	-820	-1194	-759	-955	-678	-771	-566	-771	-534	-657
7	Area	.436	.857	.312	.649	.312	.651	.536	.846	.312	.676	.312	.659	.312	.645	.312	.629
	Load	-3023	-2956	-2417	-2200	-2150	-1899	-1985	-1772	-1835	-1437	-1594	-1149	-1301	-1149	-1018	-846
8	Area	.142	.461	.142	.315	.222	.450	.222	.393	.142	.346	.142	.317	.142	.290	.142	.271
	Load	-192	-217	-370	-440	-184	-276	-167	-237	-141	-187	-93	-114	-72	-114	-39	-97
9	Area	.142	.439	.142	.326	.142	.301	.142	.286	.142	.307	.142	.288	.142	.268	.142	.252
	Load	276	231	540	418	597	331	680	269	610	299	509	252	436	252	364	218
10	Area	.446	.901	.189	.559	.198	.526	.446	.749	.124	.433	.124	.406	.124	.379	.124	.358
	Load	2818	2816	2019	1903	1706	1634	1351	1515	1114	1028	971	842	786	841	623	637
11	Area	.054	.315	.054	.299	.054	.283	.054	.266	.054	.249	.054	.231	.054	.214	.054	.201
	Load	323	412	675	954	677	1061	672	984	627	792	537	578	420	578	323	511

1 pound = 4.448 newton
1 in^2 = 6.4516 x 10^{-4} $meters^2$

TABLE VIII - 4448 NEWTON VERTICAL DOWN LOAD

Ele. No.		Bay 1 BS 41-BS 60 Initial	Final	Bay 2 BS 60-BS 80 Initial	Final	Bay 3 BS 80-BS 101 Initial	Final	Bay 4 BS 101-BS 122 Initial	Final	Bay 5 BS 122-BS 143 Initial	Final	Bay 6 BS 143-BS 164 Initial	Final	Bay 7 BS 164-BS 185 Initial	Final	Bay 8 BS 185-BS 194 Initial	Final
1	Area	.044	.259	.044	.266	.044	.267	.044	.167	.044	.240	.044	.224	.044	.205	.044	.191
	Load	-649	-1600	-673	-2940	-236	-2419	-229	-1971	-241	-2354	-431	-2905	-553	-2013	-287	424
2	Area	.312	.615	.312	.560	.312	.575	.312	.566	.292	.555	.080	.317	.248	.476	.248	.465
	Load	-20666	-23411	-13788	-17144	-11534	-14981	-10163	-13449	-9876	-11835	-9018	-9590	-7202	-8169	-6147	-8618
3	Area	.142	.248	.142	.166	.142	.166	.142	.168	.142	.181	.142	.181	.142	.185	.142	.191
	Load	-4600	-3504	-8216	-6358	-5546	-4441	-5091	-3902	-6892	-5417	-6337	-5285	-4948	-4082	-4227	-3805
4	Area	.142	.262	.142	.165	.222	.253	.222	.441	.142	.178	.142	.186	.142	.190	.142	.201
	Load	-3479	-2818	-10454	-7895	-6236	-5036	-6370	-6967	-9488	-7261	-6107	-4663	-5576	-4387	-4153	-3483
5	Area	.510	.748	.431	.657	.332	.561	.312	.551	.312	.600	.312	.558	.312	.600	.312	.593
	Load	-27507	-26046	-19929	-19936	-13596	-15046	-11869	-13337	-14807	-15069	-14303	-14376	-10865	-10865	-8208	-7368
6	Area	.080	.392	.080	.302	.080	.331	.080	.321	.080	.395	.080	.377	.080	.294	.080	.266
	Load	244	-60	347	-359	-46	-883	-307	-11878	-277	-1060	-210	-805	-162	-477	-195	-301
7	Area	.436	.907	.312	.625	.312	.646	.536	.849	.312	.687	.312	.660	.312	.637	.312	.616
	Load	26770	25056	18346	17895	12232	14352	10907	13695	14175	14303	13881	13285	10501	10191	7948	6977
8	Area	.142	.462	.142	.316	.222	.383	.222	.379	.142	.325	.142	.305	.142	.286	.142	.271
	Load	4053	4033	11807	10481	6986	6846	7091	6733	10411	9347	6701	6819	6085	5641	4606	4561
9	Area	.142	.439	.142	.312	.142	.301	.142	.286	.142	.307	.142	.288	.142	.269	.142	.253
	Load	4769	4107	9183	8347	6906	7174	6710	6299	8761	7307	7801	6860	6095	5337	5247	4849
10	Area	.446	.901	.198	.559	.198	.538	.446	.749	.124	.433	.124	.406	.124	.379	.124	.358
	Load	20405	22901	12244	15441	8865	13182	6900	11918	6619	9926	6473	8456	5170	6837	4234	5172
11	Area	.054	.314	.054	.299	.054	.283	.054	.266	.054	.354	.054	.231	.054	.214	.054	.201
	Load	655	1338	1104	2467	1207	1918	1558	1606	1621	2117	1552	2206	1458	1989	1182	1591

1 pound = 4.448 newton
1 in^2 = 6.452 x 10^{-4} $meters^2$

TABLE IX - 35584 NEWTON LATERAL RIGHT LOAD

TABLE X - COMPARISON BETWEEN THE AVERAGE TEST STRESSES AND THE STRESSES CALCULATED USING NASTRAN LOADS

Tailboom Bay	Ele. No.	5604 N Rt. Load TEST	5604 N Rt. Load NASTRAN	5604 N Lft Load Test	5604 N Lft Load NASTRAN	4448 N Down Load Test	4448 N Down Load NASTRAN
2	1	-1936	-1443	1448	1036	3331	3131
	2	-2969	-4276	3424	3702	1949	3002
	3	-5281	-5269	5063	3958	968	1217
	4	-5432	-6590	4280	4953	-1086	-1311
	5	-4984	-4520	3220	3902	-2548	-3045
	6	211	- 96	53	- 236	-5458	-3371
	7	4839	4242	-3792	-5079	-3516	-3391
	8	5682	5099	-5471	-7247	-1541	-1397
	9	3127	4159	-3555	-6220	948	1284
	10	4957	4329	-7038	-6768	4128	3404
	11	599	1383	-2061	-2147	4187	3191
3	1	-1291	-1294	1613	827	3904	3694
	2	-3516	-3713	4734	3310	2759	2747
	3	-3983	-4084	4707	3556	777	1007
	4	-4075	-2856	3661	2786	- 790	- 685
	5	-5511	-3795	3615	3510	-3035	-2872
	6	20	- 228	59	-1895	-3817	-3877
	7	4957	3511	-3753	-4174	-3681	-2917
	8	3838	2780	-3160	-2843	- 704	- 614
	9	2772	3695	-2791	-4267	626	1100
	10	3575	3826	-4312	-4114	2752	3107
	11	1752	1212	-2679	-1780	4029	3750
4	1	-1185	-1158	1237	787	4319	3757
	2	-3760	-3192	3786	3037	2679	2621
	3	-4470	-2962	4372	3418	790	905
	4	-4300	-2783	3937	2852	- 955	- 754
	5	-3872	-3340	3351	3323	-2904	-2798
	6	- 53	- 281	- 13	- 25	-3141	-3916
	7	3917	2589	-3476	-2808	-2963	-2094
	8	2746	2740	-2607	-3148	- 580	- 603
	9	3193	3404	-2949	-3544	770	943
	10	3970	2486	-4378	-2545	3127	2022
	11	2021	1084	-2568	-1415	4168	3700

1 pound = 4.448 newton
1 PSI = 6895 N/m^2

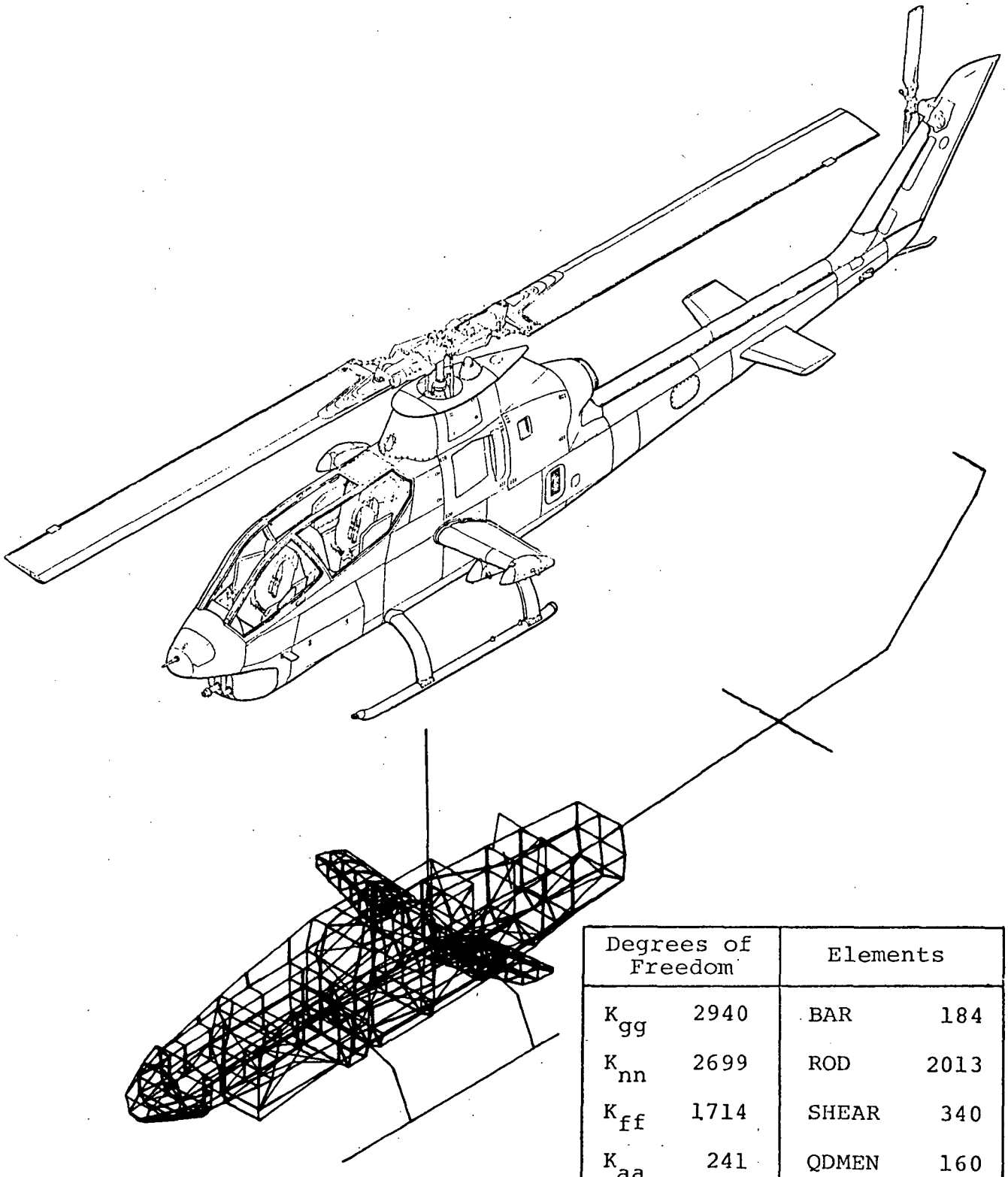

Degrees of Freedom		Elements	
K_{gg}	2940	BAR	184
K_{nn}	2699	ROD	2013
K_{ff}	1714	SHEAR	340
K_{aa}	241	QDMEN	160
K_{ll}	235	TRMEM	243

Figure 1. NASTRAN model of AH-1G helicopter airframe.

Figure 2. AH-1G helicopter used for flight tests.

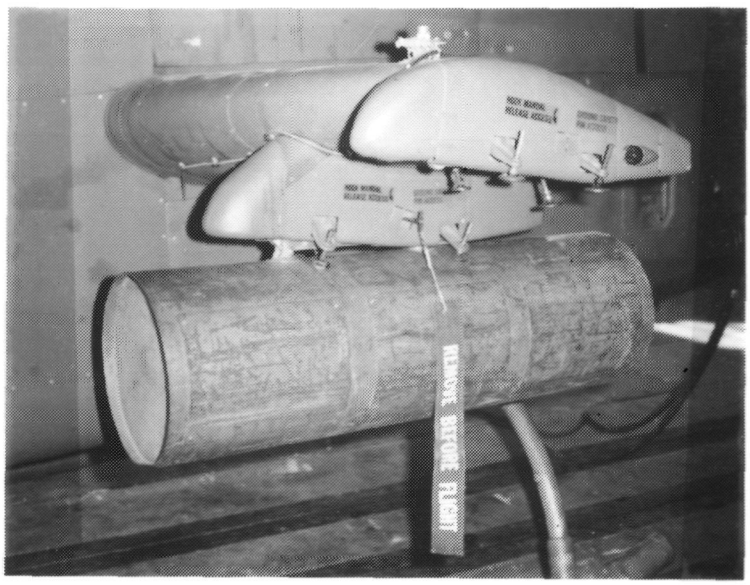

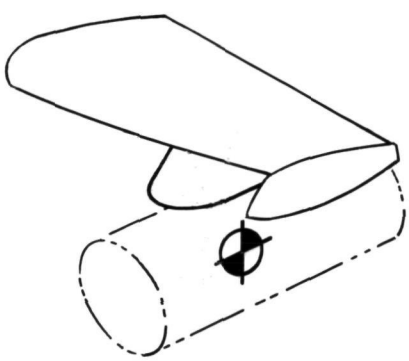

WEIGHT = 148 kg (325 lb) per side

CG: STA 196.25
BL ±42.50
WL 43.41

INERTIAS = ROLL = 5.859 kg-m^2 (19995 lb-in^2)
PITCH = 17.912 kg-m^2 (61132 lb-in^2)
YAW = 17.912 kg-m^2 (61132 lb-in^2)

Figure 3. Wing store.

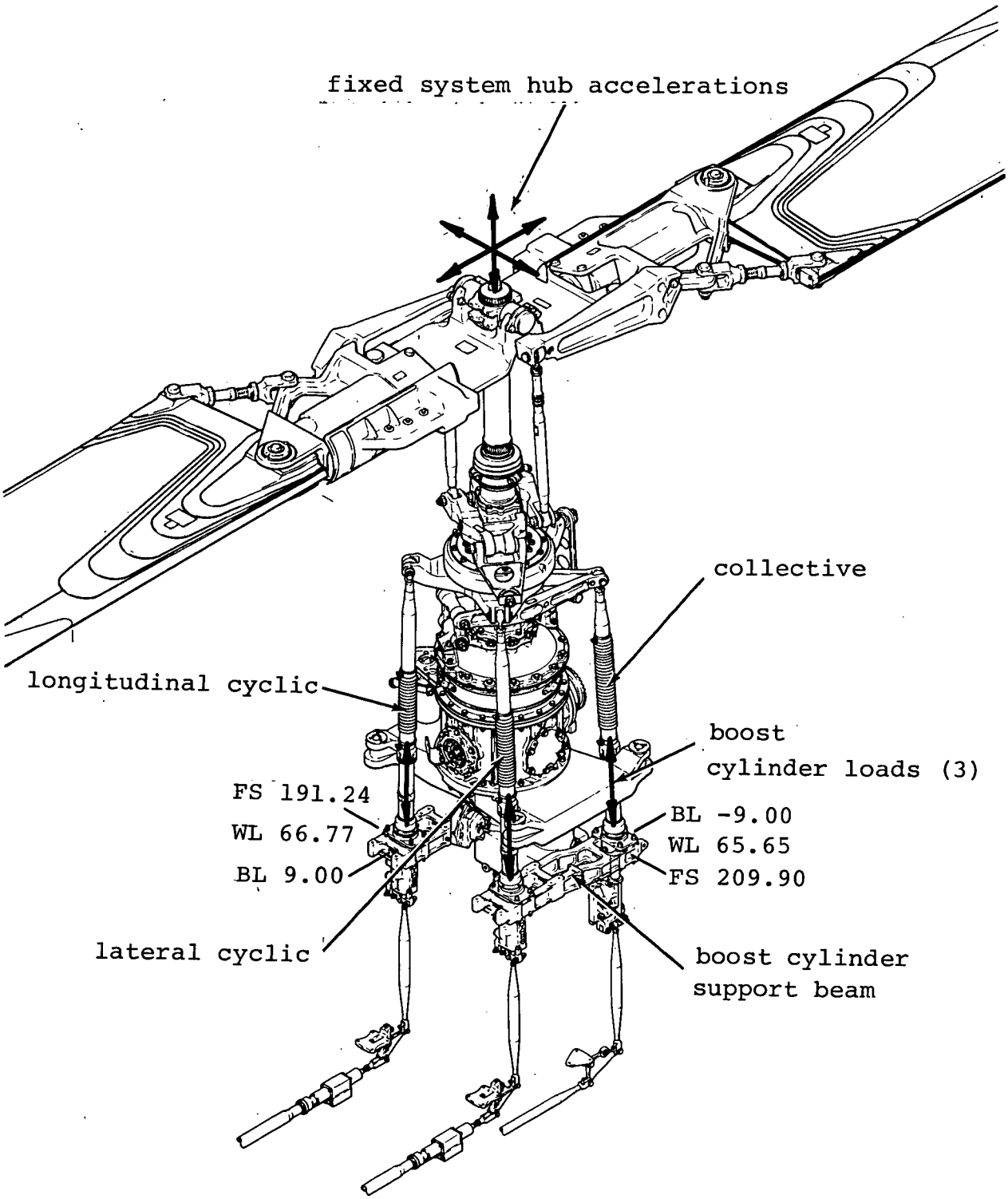

Figure 4. Main rotor excitation to airframe.

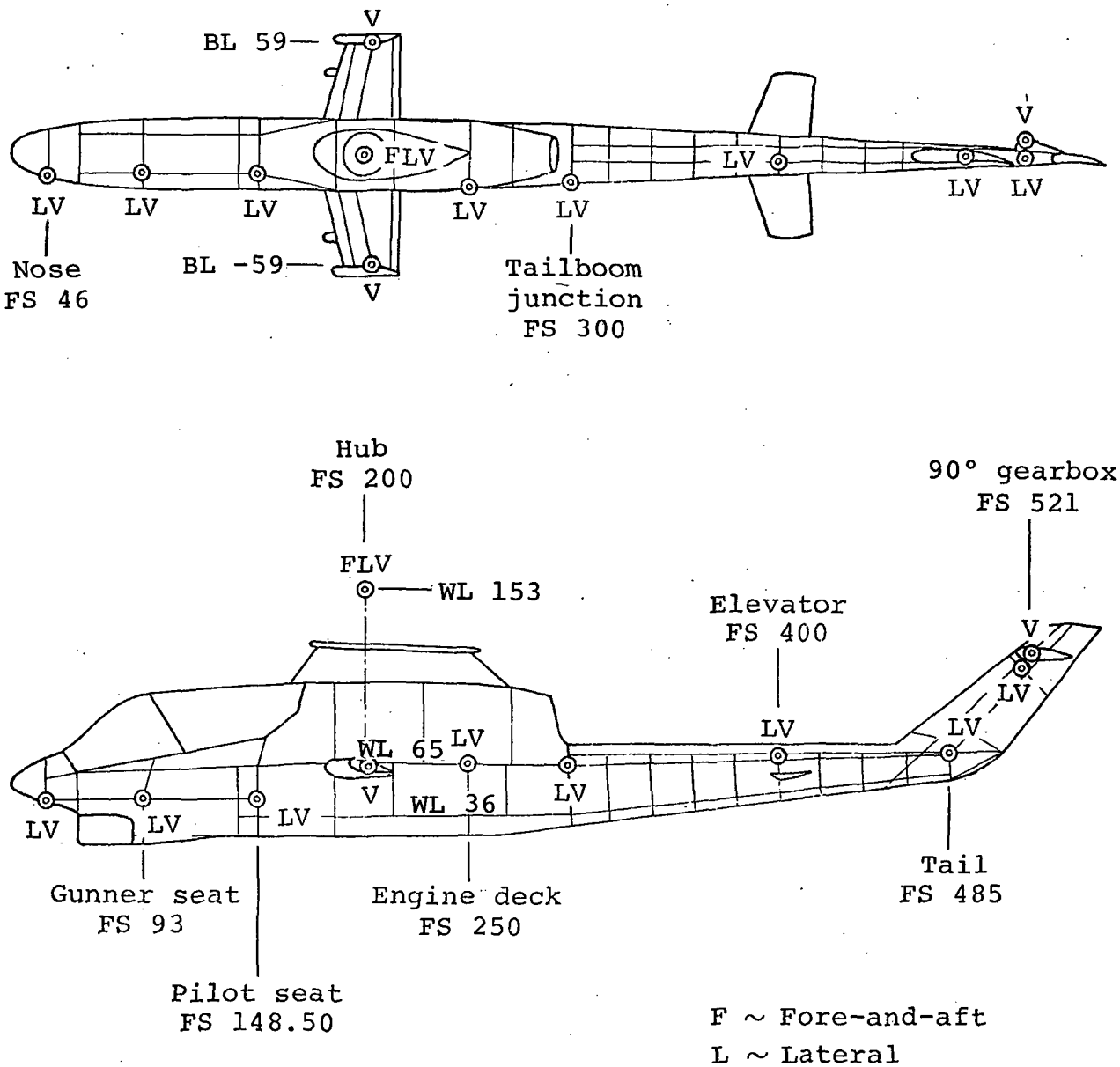

F ~ Fore-and-aft
L ~ Lateral
V ~ Vertical
FS ~ Fuselage station
WL ~ Waterline
BL ~ Buttline

Figure 5. Accelerometer locations for flight tests.

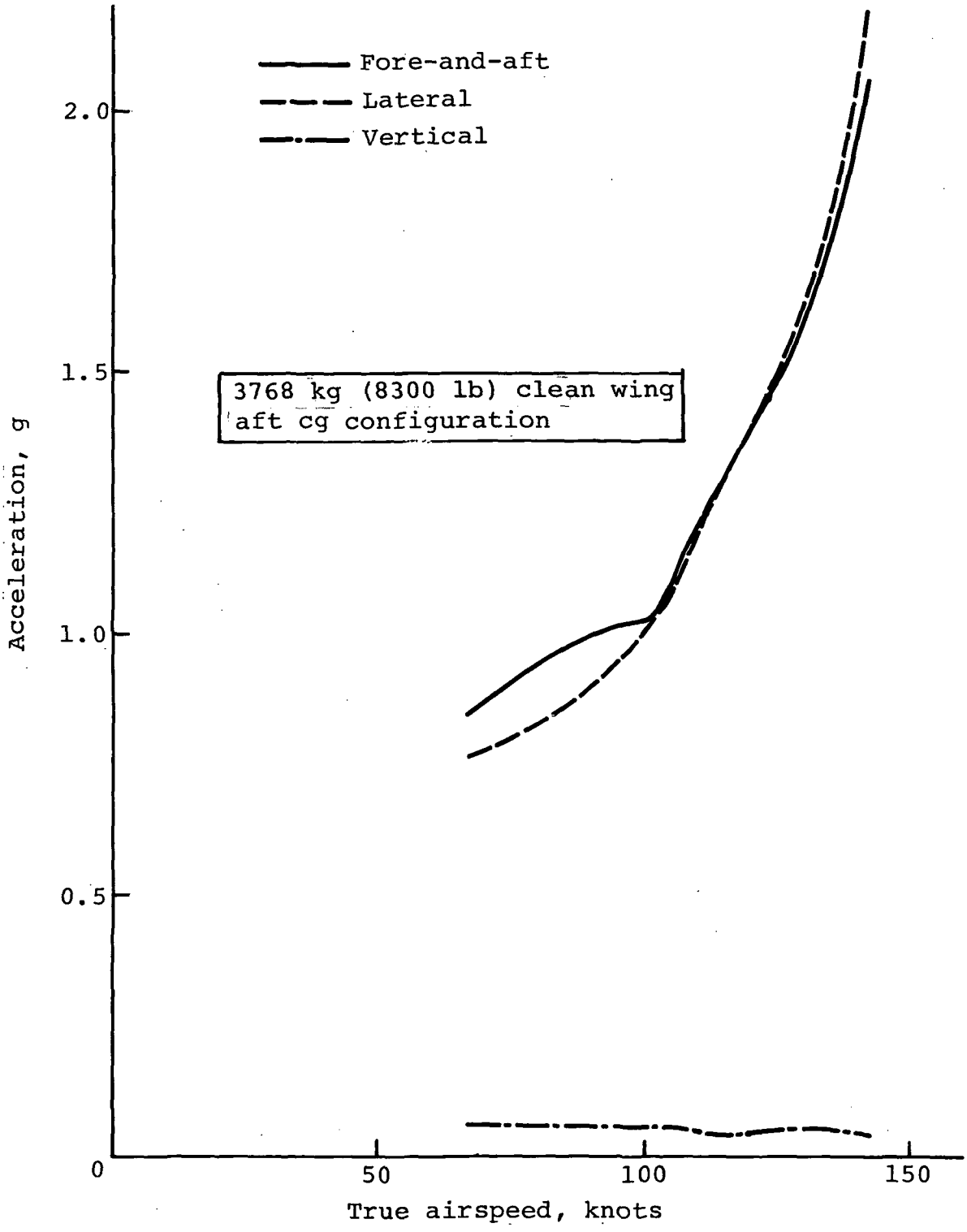

Figure 6. Two-per-rev hub accelerations versus airspeed.

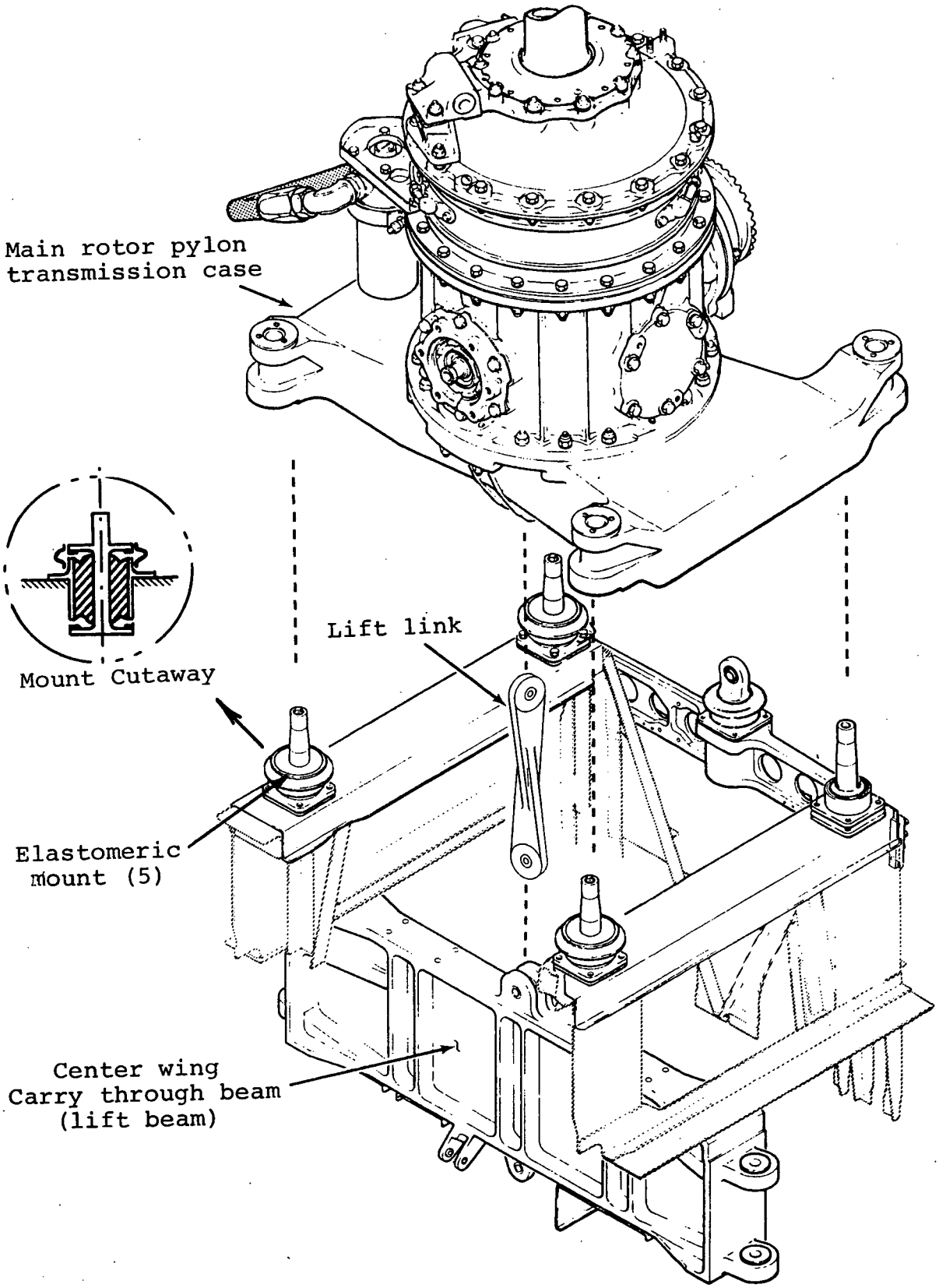

Figure 7. Main rotor pylon mounting.

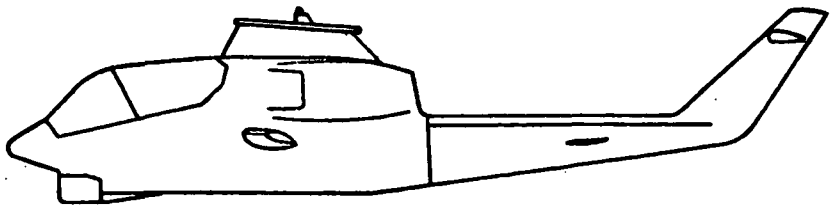

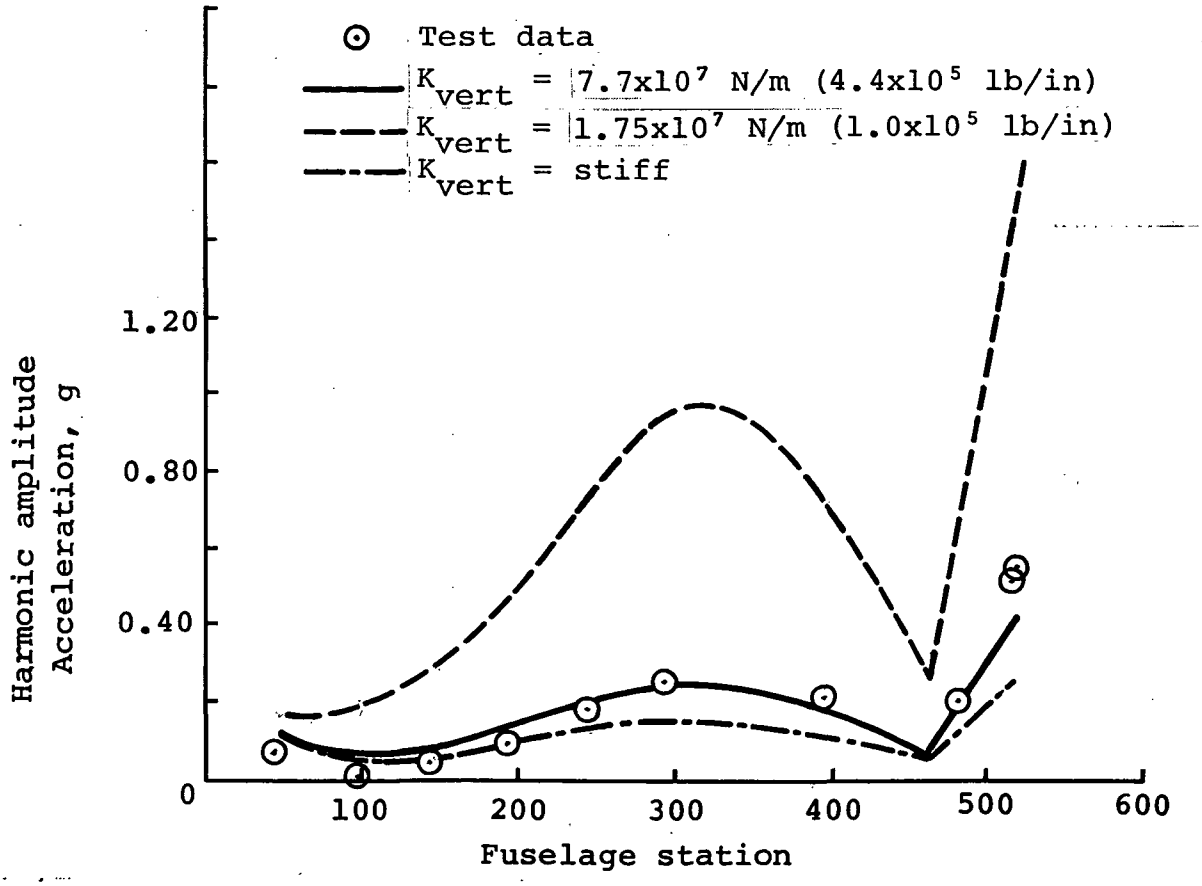

Figure 8. Effect of vertical pylon stiffness on vertical two-per-rev response.

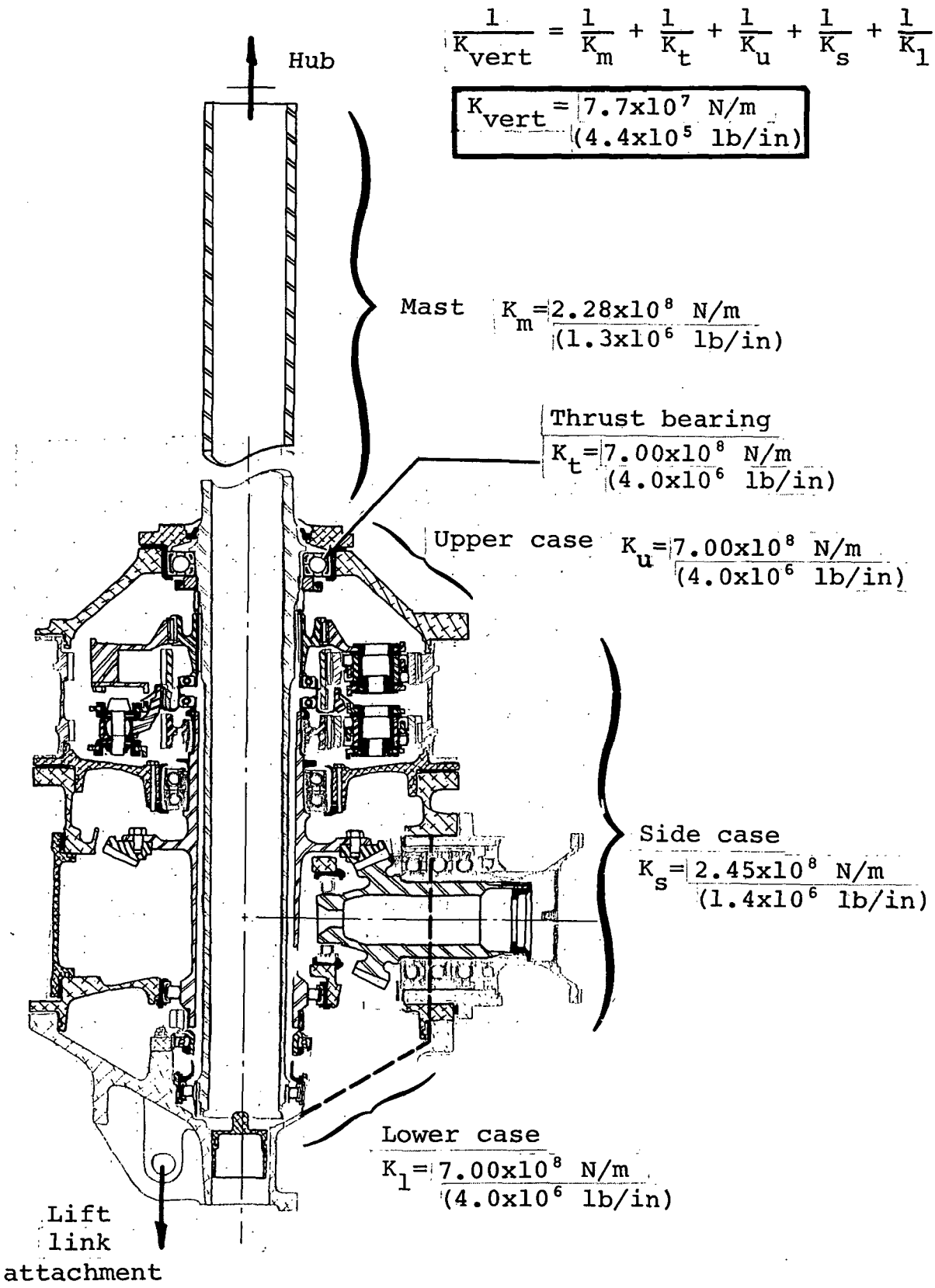

Transmission and mast cutaway

Figure 9. Vertical stiffness of main rotor pylon.

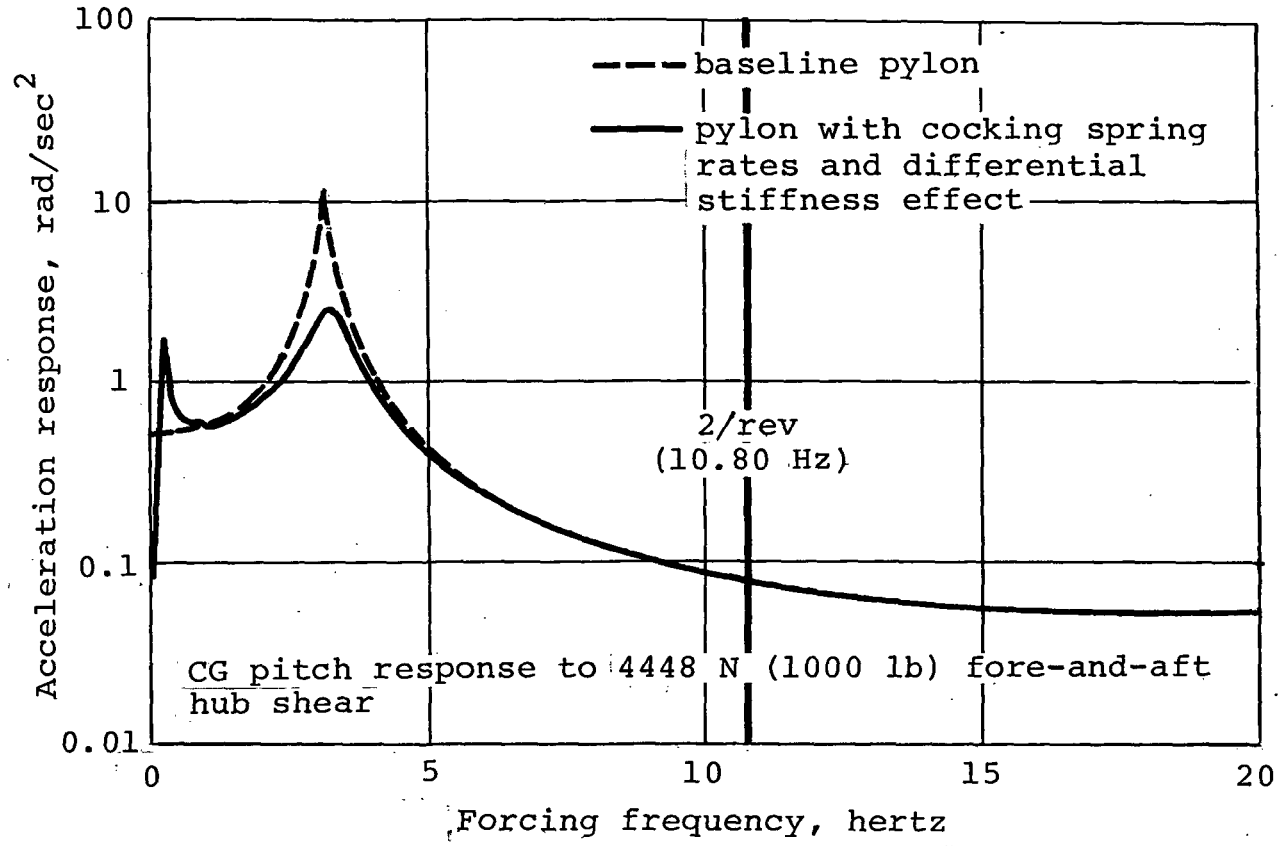

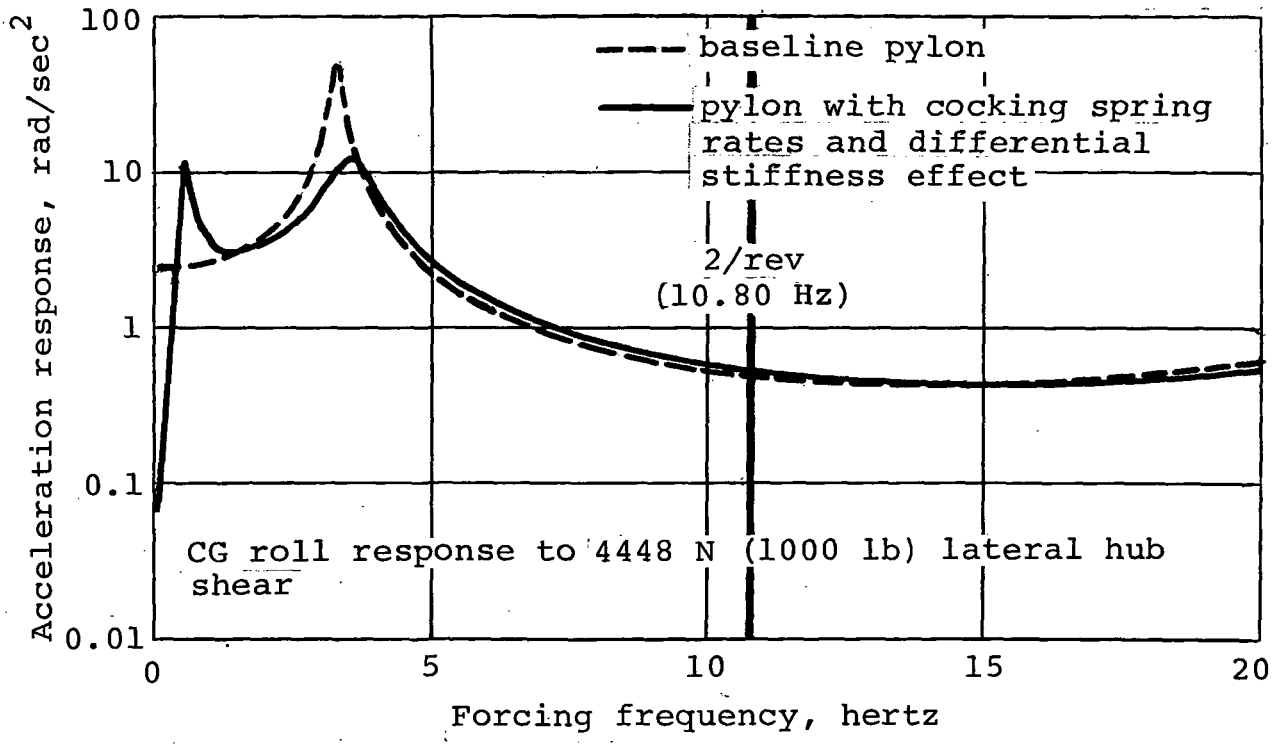

Figure 10. Effect of pylon stiffening and damping on two-per-rev isolation.

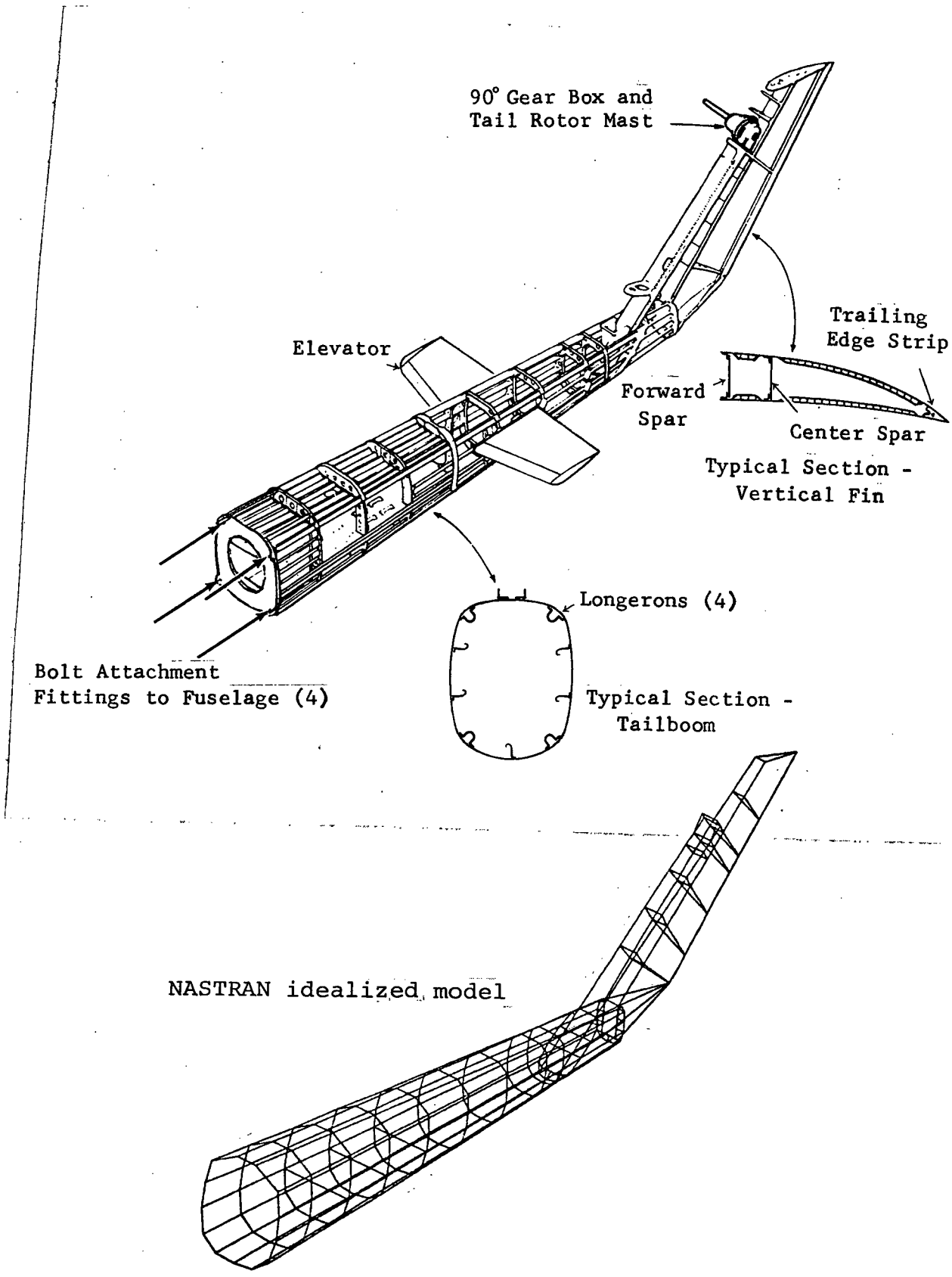

Figure 11 - Tailboom and fin.

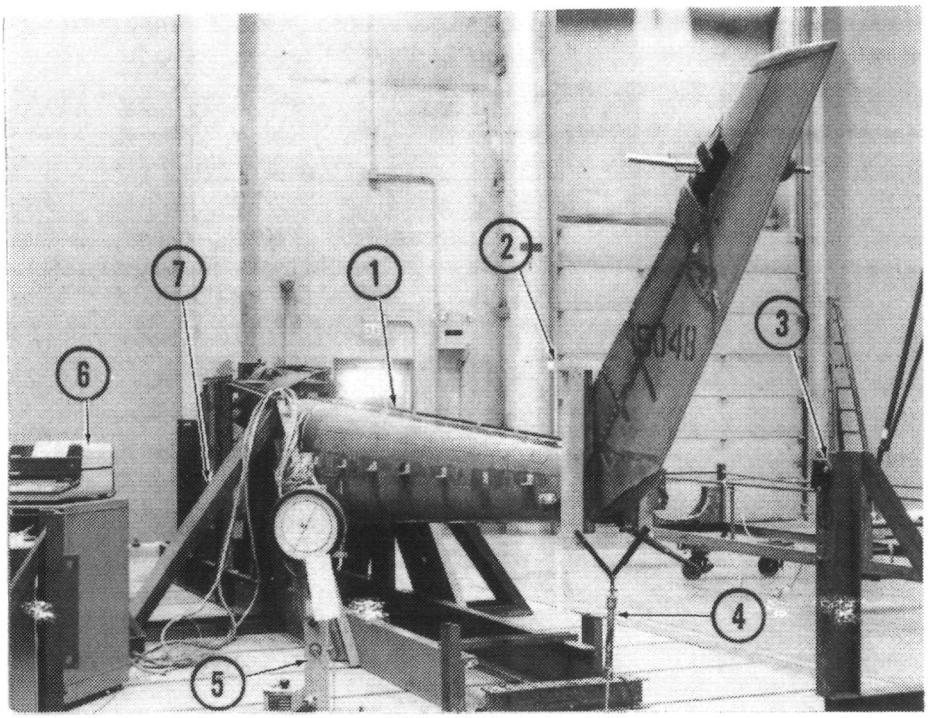

Figure 12. Test setup for tailboom static load versus internal stress.

Arrows indicate:

1. AH-1G tailboom test specimen
2. Contour frame for load application
3. Fixture for attaching hydraulic cylinder for lateral right load
4. Hydraulic cylinder for applying vertical down load
5. Hand pump with calibrated pressure gage
6. HP9830A data acquisition system
7. Tailboom mounting fixture

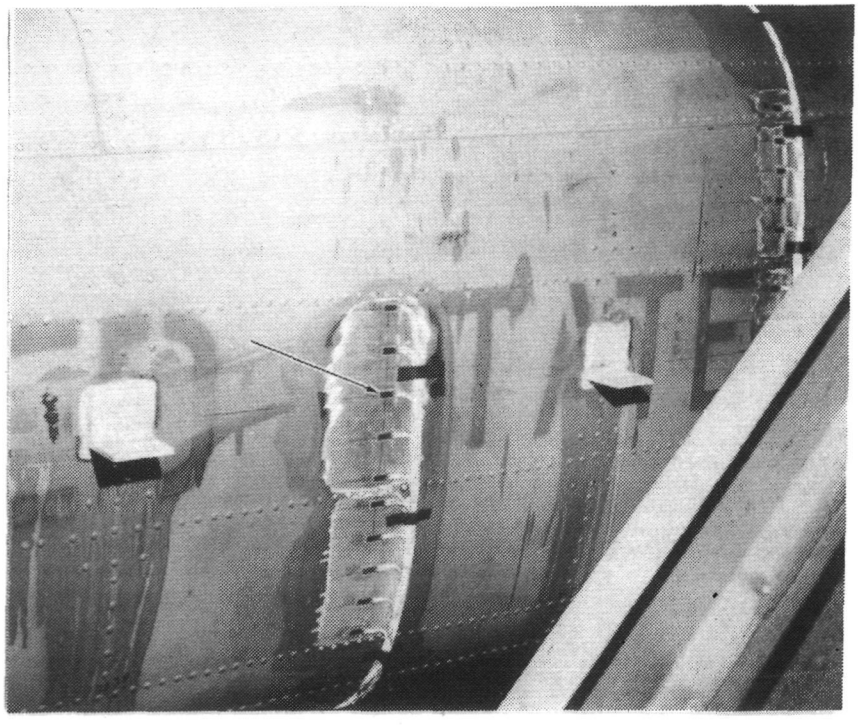

Figure 13. Skin panel gage installations for AH-1G tailboom static load test.

A typical single active arm gage is indicated by the arrow. The angle brackets were used in a previous test.

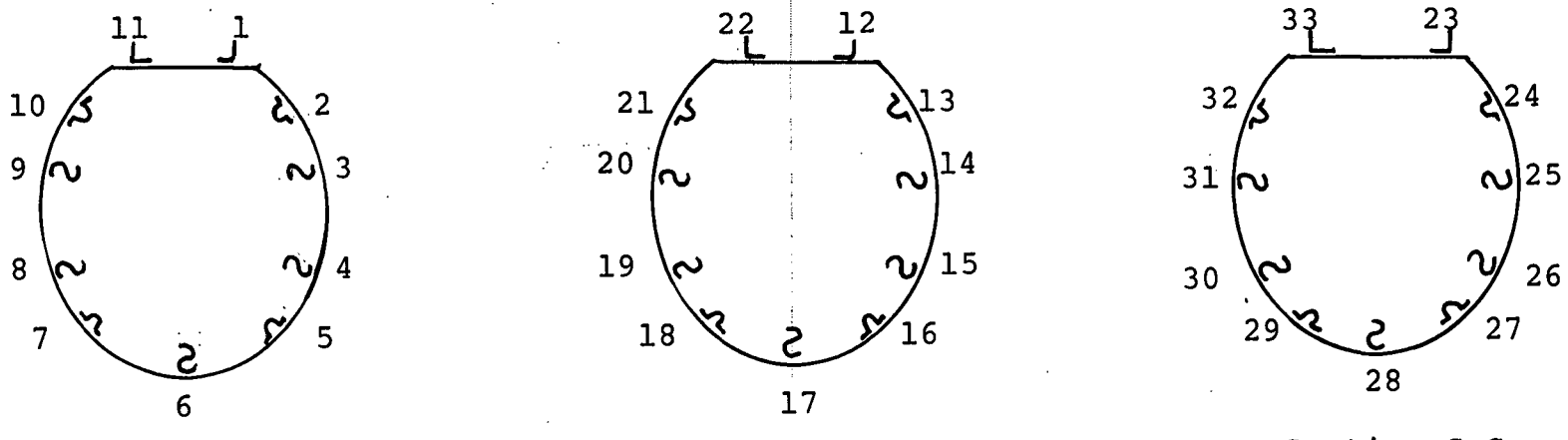

Section A-A
B.S. 69.97

Section B-B
B.S. 90.91

Section C-C
B.S. 118.85

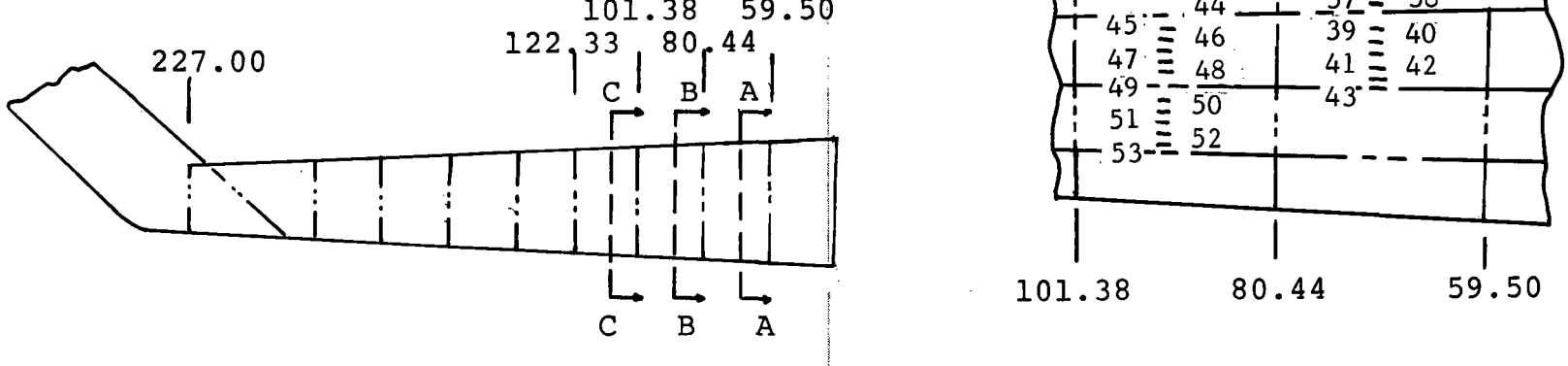

Figure 14 - Illustration of strain gage location for AH-1G static test.

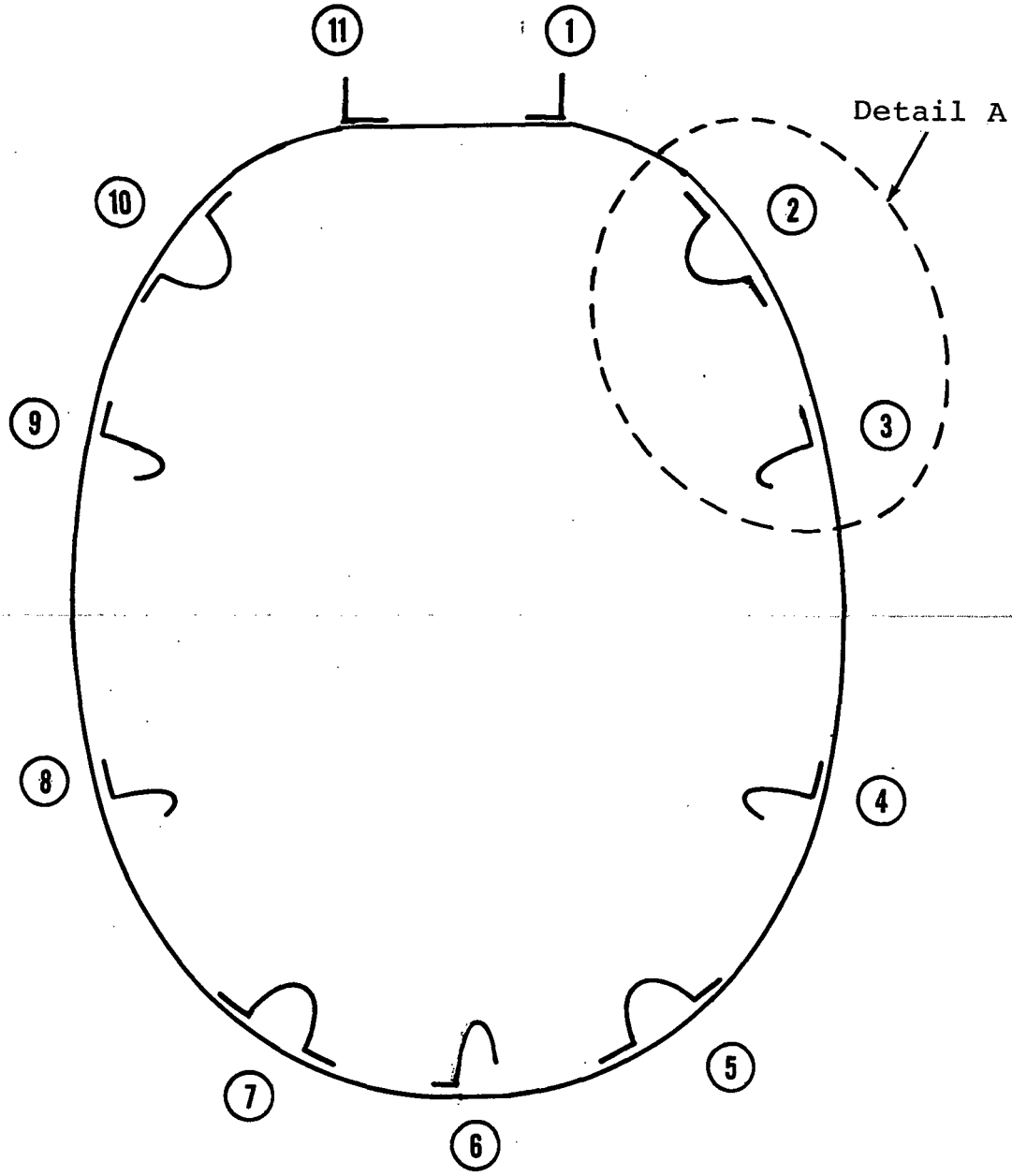

Figure 15 - Typical tailboom cross section and element numbering convention.

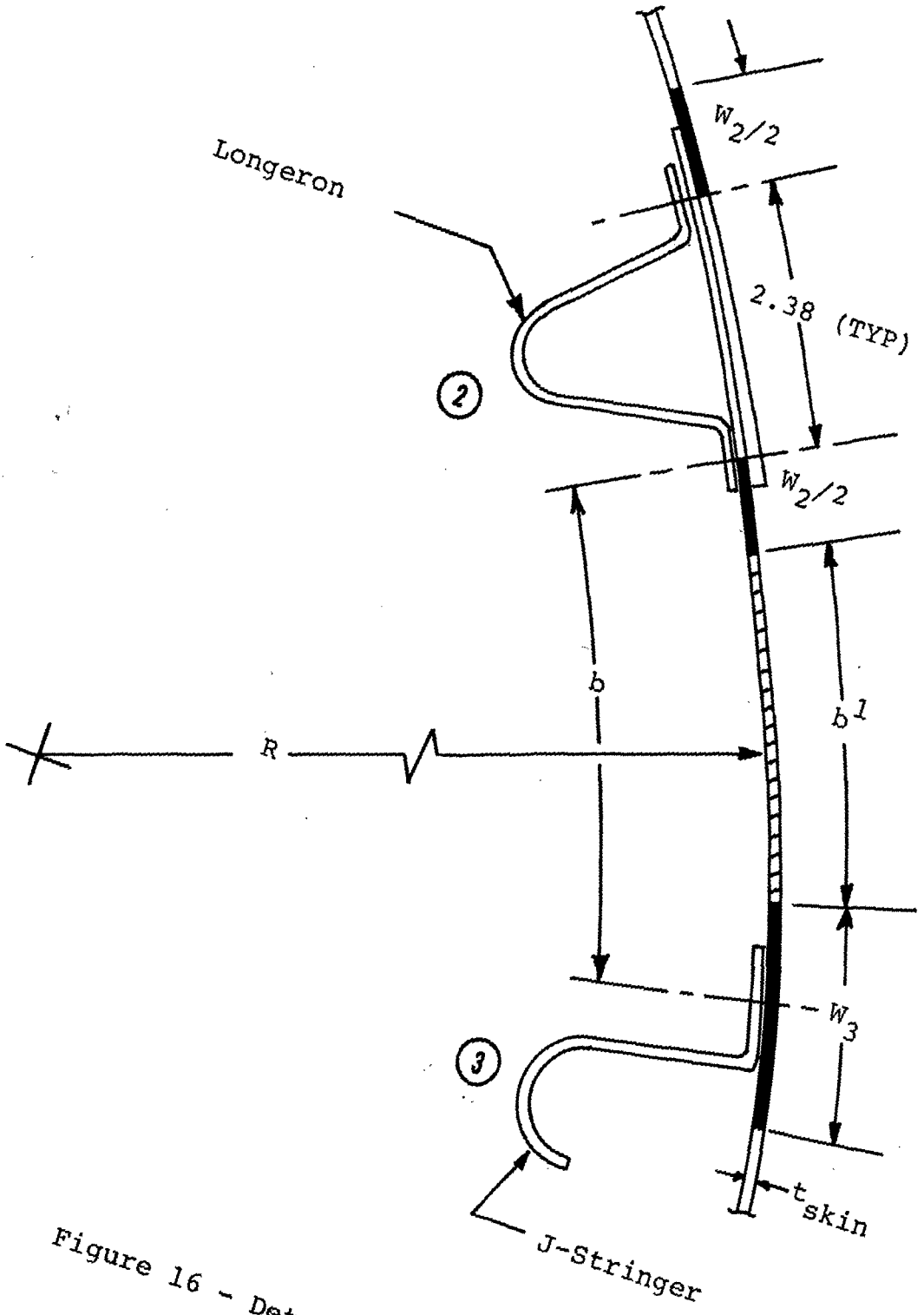

Figure 16 - Detail A from Figure 15.

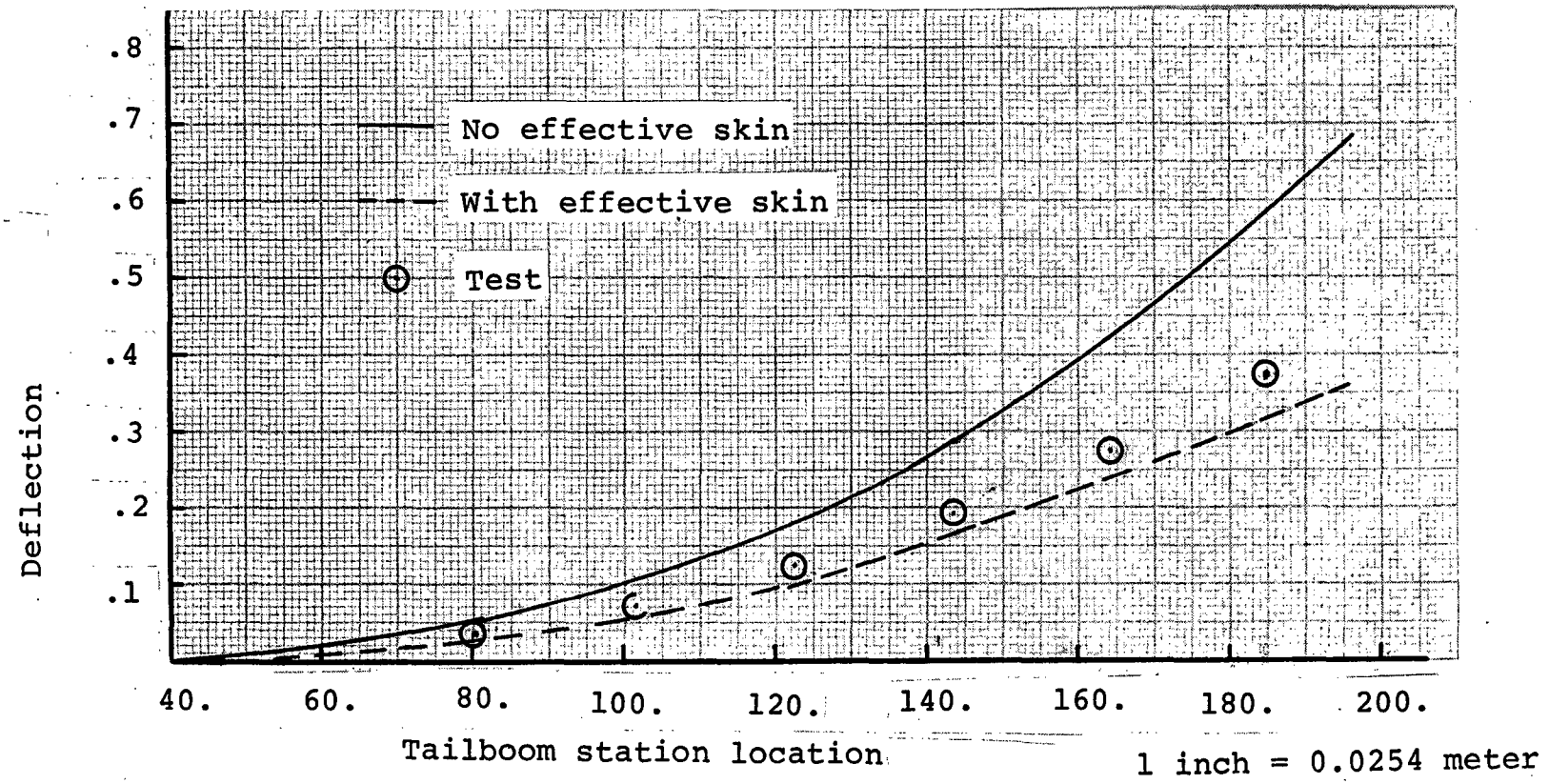

Figure 17 - Lateral deflection for 4448 newton side load.

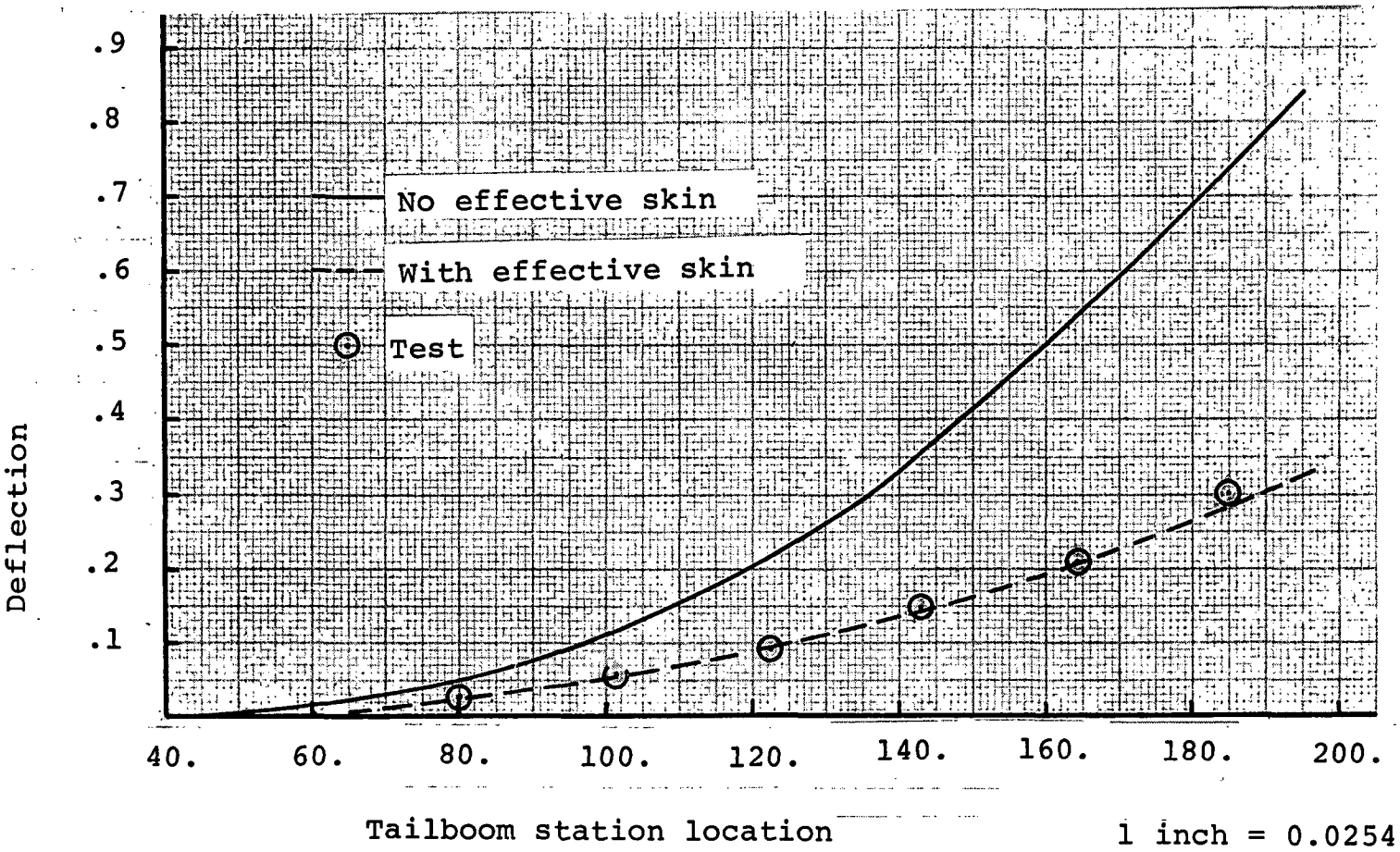

Figure 18 - Vertical deflection for 4448 newton down load.

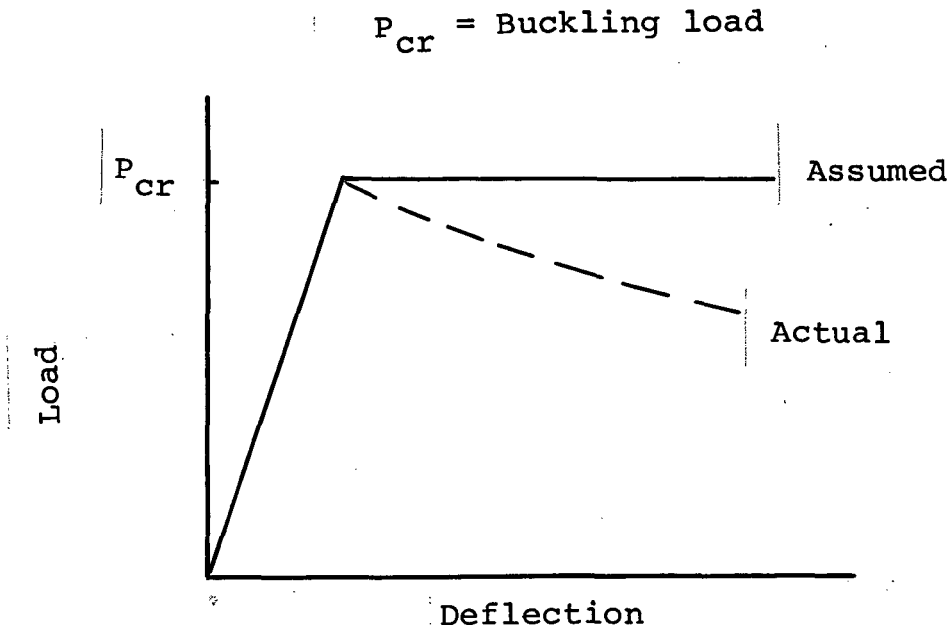

Figure 19 - Skin buckling behavior.